PREDICTION OF DEFORMATIONS IN POST-TENSIONED PRESTRESSED SUSPENDED SLABS IN TALL BUILDINGS

Thomas J. Vincent
B.E. Civil Engineering (Hons.)

A thesis submitted in fulfilment
of the requirements for the degree of
Master of Engineering

at

The University of Adelaide
(Faculty of Engineering)

July 2008

1. INTRODUCTION

1.1.   *The research topic*

Partially Prestressed Suspended (PPS) slabs are a very common form of construction, particularly for multistorey buildings. The main benefits of PPS slabs are their ability to increase construction speed, reduce slab thickness and maintain minimal to no slab deflections. Due to these benefits PPS slabs have become a very popular and familiar form of construction for multistorey buildings.

When quick erection and deflection control are essential requirements, designers frequently rely on PPS slabs as an effective solution. However, accurately predicting outcomes such as the erection time (or cycle time, which is the erection time of each floor) and the resulting deflections are challenging. There are many factors that affect these two outcomes, including concrete properties, stressing time(s), prop movement, construction loading and atmospheric conditions. This combination of factors is unique for each individual building site and hence predicting cycle time and slab deflections constantly involves some level of uncertainty.

The current method for predicting cycle time and slab deflection relies heavily on monitoring concrete compressive strength gain. It is the concrete compressive strength gain which is the logical limiting factor for many construction and design requirements such as slab strength, stressing time(s), prop movement and access to the slab. For example; the concrete supplier may be required to supply concrete with a characteristic compressive strength (f'_c) of 32 MPa, which will also produce a compressive strength of at least 24 MPa after 7 days so the slab can be successfully stressed ready to withstand the construction load of the neighbouring upper slab. The concrete compressive strength gain shown in Figure 1-1(a) is a good example of concrete that passes this example requirement. However, if mix designs or atmospheric conditions hinder the strength gain of the concrete, a graph such as the one shown in Figure 1-1 (b) may be produced.

As can be seen in Figure 1-1(b), at 7 days stressing of the slab can not be achieved safely and in fact 24 MPa is not reached until 3-4 days later. On a construction site, such as the one utilised in this research (where there are 7 slabs which are each poured in 2 stages), an extra 3-4 days per pour becomes a significant problem and can equate to nearly 2 months additional construction time for the project. This extra construction time not only means delays in the client accessing their building, but more importantly can translate to extra hundreds of thousands of dollars spent on site costs for the project, simply due to a slight change in concrete properties.
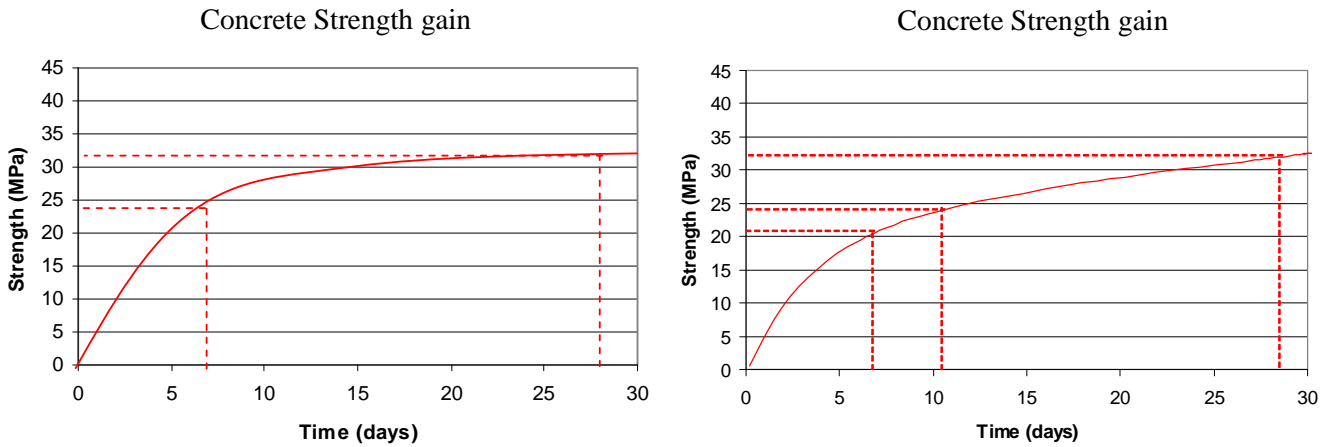
Figure 1-1 *Examples of concrete compressive strength gain*
(a) Adequate Concrete Compressive Strength gain.   *(b) Inadequate Concrete Compressive Strength gain*

Long term strength values (after 28days) of both of these strength gain curves remain approximately the same. The value of concrete strength at 28days is a dominant value in concrete supply and structural strength design. Hence this small change in concrete strength gain at low age usually receives minimal focus. Many designers and concrete suppliers remain confident when long term concrete performance is adequate. This situation gives rise to the need for research focus on the early age material property developments.

Knowing the exact strength within the slab is another major issue. Samples from the concrete pour can be taken and cured under conditions similar to the slab, but realistically knowing the true strength of the concrete and its spatial variation is difficult. The standard method of measuring concrete compressive strength is via cylinder samples, as per AS 1012.9 (1999). These cylinders are typically stored in a standard curing bath, which best represents the curing condition experienced by concrete at a typical construction site. However, a problem arises when using a standard curing bath. The bath is designed to maintain a constant temperature of 23 ºC, which is the curing temperature that concrete experiences due to its natural insulation properties in the majority of concrete pours, such as typical beams, slabs and foundations. PPS slabs however, are much thinner than typical concrete members and hence curing concrete samples at 23 ºC may hydrate the cement at a faster rate than that experienced in the slab and hence produce inaccurate material properties such as a higher compressive strength. To overcome this problem many concrete suppliers air cure extra test cylinders in an attempt to obtain recorded material properties that better simulate what is occurring in the thin slabs. Which curing method is more appropriate for PPS slabs remains unresolved.

Concrete compressive strength gain may be the limiting factor for outcomes such as slab strength, prestressing times, prop movement and access to the slab. But for maintaining accurate deflections, strength (which is an ultimate state) should not be of importance when predicting a serviceability state. Stress-strain relationships, values of modulus of elasticity (E_c), tensile strength (plus associated cracking) and long term effects such as creep and shrinkage are more relevant characteristics. One of the current problems with predicting deflections in the design stages is that the modulus of elasticity of concrete mixes is not monitored regularly. Hence, when deflections are crucial in design, concrete suppliers can not accurately mix and supply concrete based on reaching a specified value of elastic modulus.

Unlike values of concrete compressive strength, site specific values of deflection can be recorded. Over the years, many local surveys of suspended slabs in Adelaide, Australia have yielded values of deflection that do not accurately relate to the predicted values. This gives rise to the problem that there may be inaccuracies with the methods used to predict PPS slab deflections.

In summary, this research addresses multiple linking problems summarised above. These problems are best simplified and explained by noting the three main candidates which benefit from this research; the structural designer, the construction manager and the concrete supplier:

- The key issue that emerges from the structural designer's perspective is not being able to confidently and accurately design for minimal deflections. For this issue, obtaining accurate concrete material properties as well as accuracy of models and relationships incorporating material properties and deflections are of key interest.
- The key issue from the construction manager's viewpoint is not being able to predict cycle times accurately, which affects site rental costs. For this issue accurate concrete properties and efficient construction practise, such as prop movement techniques, are of interest.
- Both of the above issues then link to the concrete supplier, who is unsure how to design a concrete mix to meet requirements and how to accurately monitor the compressive strength (and other material properties) gain over time of this supplied concrete. Accordingly, mix designs and concrete performance are of interest.

This research aims to tackle each of these issues and ultimately provide the structural designers, concrete suppliers and construction crew with accurate outcomes of what is realistically achievable on site. Due to the natural uncertainty due to each construction site being unique, a large emphasis of this research has been placed on the statistical confidence associated with behaviour prediction.

1.2.   Research methodology

This section describes the development and progression of the studies performed for this research. This overview outlines an explanation of the steps taken in this research to arrive at the final conclusions.

The progress of this research began with data collection from the provided construction site, 151 Pirie. The data collection stage of the research was a significant stage and lasted as long as the construction timeline of the slabs, which was over 6 months. The aim of this data collection stage was to collect material property data as well as site specific data such as ambient and concrete temperatures. The main focus of the research at this stage was to take the opportunity to collect as much on-site data as possible whilst the construction site was available.

Following the data collection stage was the review of the current literature relating to the topic of deformations of PPS slabs. Once an understanding of the current literature was established, a comparison of the material property models and deformation prediction models were performed. In the comparison of deformation prediction models, emphasis was placed on the model inputs and associated assumptions of each model. During this comparison attention was drawn to how altering the concrete material property inputs effects slab deformations and construction time. At this point of the research it was decided that it would be beneficial to establish a statistical output of predicted deformation. The typical approach to deformation prediction does not include a statistical output, only a single value of member deformation. It was decided that a statistical output could be produced from the statistical distribution of concrete material property inputs with the use of a Monte Carlo simulation.

A Monte Carlo simulation program was created in Microsoft Excel which allowed a statistical distribution of member deformation to be produced from the statistical distribution of concrete material properties. Once the results of this program had been established and the output analysed, it was discovered that the program was producing unexpected output. After a closer examination of these inaccuracies it was concluded that the errors were due to inaccurate assumptions within the application of the models. Therefore steps were taken to produce a second program where the emphasis of this program was removing these assumptions. Removing the inaccurate assumptions, as well as utilising the statistical distribution of the inputs, allowed this research to produce a statistical prediction of on site slab deformations. These statistical predictions of slab deformations were then compared to surveyed values.

In summary, this project commenced with the aims of providing concrete designers, suppliers and builders with confident predictions of partially prestressed concrete slab behaviour. These aims were met by initially performing an extensive on site experimental program to record on site concrete data and construction time. The data collected supplied this research with an understanding of how the supplied concrete performs on site. Two new deformation prediction methods were then produced which utilise the on site data to produce a statistical prediction of slab deformation from the statistical distribution of on site material properties. These programs help provide concrete designers, suppliers and builders with a more detailed understanding of the behaviour of partially prestressed concrete slabs. This detailed understanding of the behaviour of the slabs leads to higher confidence in design of PPS slabs.

1.3.   Structure of thesis

Initially the *Introduction* establishes the problem statement and outlines the areas of research required to address this problem statement. The second chapter, the *Literature Review*, examines and compares the current knowledge associated with this form of deformation prediction. Following this, the *Experimental Program* describes each of the experiments performed, as well as all the data obtained for this project. The *Prediction of Slab Deflections* chapter details each of the processes developed and performed to supply designers with confident slab deflection predictions and the associated accuracies. Finally the *Conclusion and Recommendations* summarises the outcomes of the research, highlights the potential future work on this topic and states concluding remarks.

2. LITERATURE REVIEW

2.1. Introduction

This literature review critically discusses the current knowledge associated with predicting slab deflections in post tensioned suspended slabs. A detailed examination of the background of prestressing, including development in deflection calculations, is initially discussed. Following this is an analysis on the many factors which affect deflections and cycle times, namely concrete material properties including maturity. The prediction of the influence of construction methods on slab deflections is then presented. Finally, an examination of relevant engineering statistics and statistical simulations has been addressed.

2.2. History of Prestressing

To appreciate the current methods used on construction sites utilising PPS slabs, it is worth discussing the relevant history of how these methods have evolved and developed over time. Discussed in this section is how the changing demands in construction over the years, as well as changes in technology have led to current prestressing methods.

It was the 1880s when the earliest suggestions of prestressing concrete surfaced in San Francisco by P H Jackson. However, Jackson's practical attempts were unsuccessful due to the creep and shrinkage strains in the concrete being so large that a complete loss of prestress occurred within a short period of time. R H Dill in the 1920's then recognised that high-strength wire could provide a much higher initial prestrain which would maintain a steady prestress within the member. This theory was then first commercially used in construction of circular water tanks. In the 1930's the Preload Corporation developed techniques of winding wires around cast-in-place circular concrete walls. This technique is a variation on the age old technique of prestressing wine barrels by heating metal tension bands. The precompression achieved when the bands cool prevents leaks (Warner et al. 1998).

Eugene Freyssinet is accredited with the first practical and successful designs of prestressing concrete in bridges and buildings. Freyssinet not only agreed with the idea of using high strength wire to overcome the creep and shrinkage, but also introduced the idea of using higher strength concrete. Shortly after the Second World War, Freyssinet designed a number of highly successful bridges in France, which led to wide acceptance of prestressed concrete (Collins and Mitchell 1997).

In 1956, the construction of the first high rise building to utilise post-tensioned slabs began, namely, the Diamond Head Apartments in Honolulu, Hawaii. This structure was 14 storeys high with replicated floor plans for each level. It was evident, even in this initial development in post-tensioned slabs, that this scenario was where post-tensioned slabs had a significant advantage. The cycle of propping, pouring, stressing and back propping was simply repeated at each level, with building services ensuing. Prop movement was simplified, with props simply elevated each time they were required. The labour intensive and potentially complex stage of stressing (timing and quantity of stressing) became more efficient as a familiar construction routine emerged with time.

After these initial designs in the early 50's the popularity of prestressed concrete grew rapidly, with more and more positive research helping this growth in popularity. Figure 2-1 highlights this popularity, showing the exponential growth of the prestressed concrete industry in United States and Canada.

NOTE:
This figure is included on page 7 of the print copy of
the thesis held in the University of Adelaide Library.

Figure 2-1 Growth of prestressed concrete industry in United States and Canada.
Data from Prestressed Concrete Institute (Collins and Mitchell, 1997).

Partially prestressing emerged in the 1940's as a very similar, but slightly different way of using prestressed concrete. In 1939 Austrian H. von Emperger made the suggestion that limiting the amount of prestressed wires, so as to allow minimal cracks to occur had benefits. Allowing cracking under full design working load allowed sufficient control over deflection and crack widths and hence achieved good service load behaviour. This led to the use of the terms *full prestressing* and *partial prestressing*, to distinguish between structures which respectively are not designed to crack, and structures allowed limited cracking which gives greater deflection control (Warner et al. 1998).

2.3.   Deflection and camber control of slabs

2.3.1. Past

In the early years of prestressing slabs, deflection control was not a major focal point. Crack control, minimising slab thickness and ultimate design were the dominant benefits. Hence the initial idea of using prestressed concrete, or partially prestressed concrete, to design for deflection control was ignored by most engineers.

It wasn't until the 1960s when simplified design techniques of prestressed members developed. Prior to this, design methods evolved chiefly from experience in the field and intuition rather than on established theories. Guyon in the early 1950s was the first to realise that slabs prestressed in two directions behaved analogously to the two-way arch action of thin shell structures (Nasser, 1969). Specific focus on deflection control, and its importance in designing prestressed lift slabs, first arose from Rice and Kulka in 1960. Shortly after this, research was performed by T. Y. Lin, in 1963, on the load balancing method. It was then made apparent that the tendon profiles could be designed so that upward cable force could neutralise downward loads and hence provide reliable deflection control.

2.3.2. Present

Currently the methods of deflection control use calculations which rely heavily on slab dimensions, concrete properties and applied loadings. Table 2-1 shows examples of slab deflection prediction calculations that rely on these three key factors. As can be seen the main factors that these equations rely on are;

1) Slab Dimensions; such as length (l) and slab depth (h),
2) Concrete properties; mainly modulus of elasticity (E_c) and
3) Applied loadings; such as uniformly distributed loading [UDL] (w).

This research is concerned with the accuracy of measuring and monitoring each of these inputs. This can be achieved accurately by physical measurements, material property testing and known applied loads. Slab dimensions can be measured on site by accurate surveying and is typically a predictable variable. Concrete properties can be laboratory tested and applied loads can be determined by the building's category of application. The main uncertainty of these three types of inputs is the concrete properties due to the material's natural variance in performance on site. This variance is due to naturally occurring factors such as ambient temperature, ambient humidity and

compaction. Compared to concrete properties, slab dimensions and applied loadings are considered predictable variables.

It is worth noting that slab curvature (Φ) is typically generated by simple geometric equations incorporating basic inputs from the discussed categories (slab dimensions, concrete properties and applied loadings).

Table 2-1 Expressions for predicting slab deflections exposed to UDL loadings.

Researcher	Deflection calculation	Comment
Chang and Hwang (1996)	$\Delta_{b1} = \dfrac{1}{384}\dfrac{(wl_2)l_{n1}{}^4}{EI_{b1}}$ $\Delta_{b2} = \dfrac{1}{384}\dfrac{(wl_2)l_{n2}{}^4}{EI_{b2}}$	- Sub scripts 1 & 2 denote the x & y direction. - Column strip deflection prediction, or combine to obtain mid panel deflection
Hwang and Chang (1996)	$\Delta = \dfrac{0.00128wl^4}{D}$ **where** $D = \dfrac{E_c h^3}{12}(1-v^2)$	- Mid panel deflection prediction only. - Intended for use with continuous supports.
Collins and Mitchell (1997)	$\Delta = \dfrac{2.60}{384}\dfrac{wl^4}{EI}$	- Column strip deflection predictions only. - Use with continuous supports only.
Collins and Mitchell (1997)	$\Delta = 0.163\dfrac{wl^4}{Eh^3}$	- Mid panel deflection prediction only. - Requires equal 90° spans - Use with continuous supports only.
Collins and Mitchell (1997)	$\Delta = \displaystyle\int_0^{0.5l}\Phi x\,dx$	- Intended for column strip deflection predictions.
Ghali (1986)	$\Delta = \dfrac{l^2}{96}(\Phi_1 + 10\Phi_2 + \Phi_3)$	- Sub scripts 1, 2 & 3 denote the left, middle and right curvatures. - Intended for column strip deflection predictions.
Naaman (1983)	$\Delta = \dfrac{5}{384}\dfrac{wl^4}{EI}$	- Intended for use with column strip deflection predictions. - Intended for use with pinned supports.
Naaman (1983)	$\Delta = \Phi_1\dfrac{5l^2}{48}$	- Intended for use with column strip deflection predictions. - Intended for use with pinned supports.
Warner et al. (1998)	$\Delta = K_1 K_2\dfrac{(w+k_{cs}w_s)}{7E_c}I\left(\dfrac{L_n}{d}\right)^3$	- K1 and K2 are constants that account for slab location. - Mid panel deflection prediction only.

Table 2-1 displays sample deflection prediction equations for both column strip deflections and mid panel deflections. It is important to note that there exists two main different approaches for predicting mid panel deflections. The first method simply involves combining two adjacent orthogonal column strip deflections to obtain the mid panel deflection. The second method involves utilising a deflection prediction method that is designed specifically for mid panel analysis only. An example of the differing approaches is highlighted in Figure 2-2.

NOTE:
This figure is included on page 10
of the print copy of the thesis held in
the University of Adelaide Library.
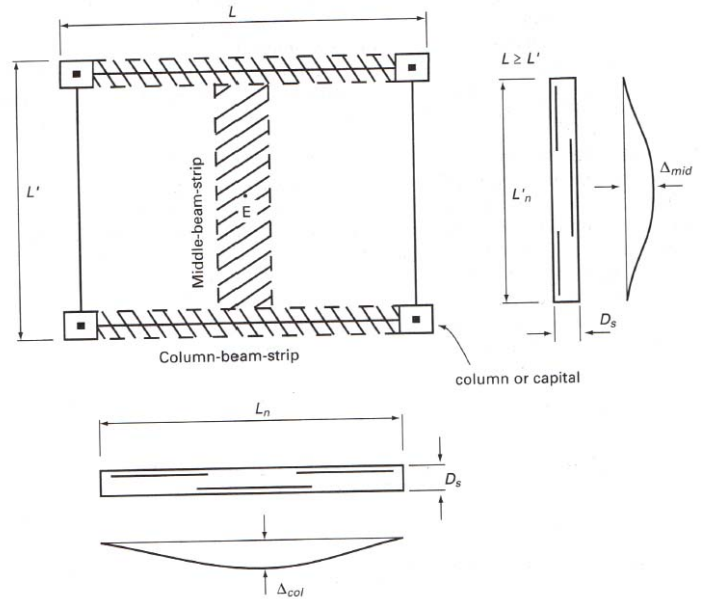
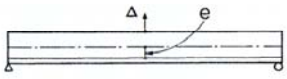$$\Delta = K_1 K_2 \frac{(w + k_{cs} w_s)}{7E_c} l \left(\frac{L_n}{d}\right)^3$$
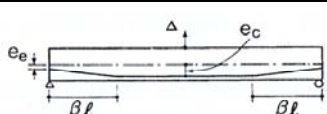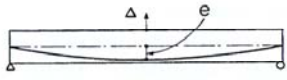
Figure 2-2 *Mid panel deflection prediction methods*

(a)
Predicting mid panel deflection as a sum of deflections of adjacent beam strips in 2 orthogonal directions.
(Collins and Mitchell, 1997)

(b)
Approximating mid panel deflection utilising methods derived specifically for mid panel analysis only.
(Warner et al. 1998)

Accurately predicting total slab deformation in PPS slabs incorporates accurate camber calculations. These calculations consider the effect prestressing has on serviceability performance, which is a significant effect for PPS slabs. Camber calculations not only depend on the same factors stated above, but also depend significantly on tendon profile. Table 2-2 shows an array of camber calculations, which vary depending on tendon profile chosen in design.

***Table 2-2** Expressions for predicting slab camber.*

	Collins and Mitchell (1997)	Namaan (1983)	Comment
Constant eccentricity	$\Delta = \dfrac{1}{8}\dfrac{Pel^2}{EI}$	$\Delta = \dfrac{1}{8}\dfrac{Pel^2}{EI} = \Phi\dfrac{l^2}{8}$	
Single harping point	$\Delta = \dfrac{2e_c+e_e}{24}\dfrac{Pl^2}{EI}$	n/a	
Double harping point	$\Delta = \left[\dfrac{e_c}{8} - \dfrac{\beta^2}{6}(e_c-e_e)\right]\dfrac{Pl^2}{EI}$	$\Delta = \dfrac{Pl^2}{8EI}\left[e_c + (e_c - e_e)\dfrac{4a^2}{3l^3}\right]$ $= \phi_1\dfrac{l^2}{8} + (\Phi_2 - \Phi_1)\dfrac{a^2}{6}$	where a = βl
Parabolic profile	$\Delta = \dfrac{5}{48}\dfrac{Pel^2}{EI}$	$\Delta = \dfrac{Pl^2}{8EI}\left[e_2 + \dfrac{5}{6}(e_1-e_2)\right]$ $= \phi_1\dfrac{l^2}{8} + (\Phi_2 - \Phi_1)\dfrac{l^2}{48}$	

Note: E_c relates to the modulus of elasticity at the time of stress transfer, which can be assumed to be 7 days.

Hwang and Chang (1996) state a very important point in their research on deflection calculations. It states "Concentrating on important parameters as well as ignoring those that have relatively small effects are essential in order to progress towards a solution of a real problem in design". This helps highlight the real problem that this research is aiming to solve. Many deflection equations include very complicated, lengthy equations with many variables (An example of such equation is outlined in Appendix A). These lengthy equations can help increase accuracy when the time is taken to use these equations meticulously. However, the added complexity inevitably has a tendance to lead to designers blindly trusting their own incorrect input.

Computer programs that predict deflections of prestressed slabs can be beneficial for many reasons. Firstly, due to automated calculations computer programs can incorporate a large number of variables from both material properties and construction procedure. Another beneficial trend is that scenarios where the peak deflection is not in the centre point of the slab, the location of the peak deflection can be calculated. Hence, deflection plots can be utilised to calculate deflections for the entire slab. An example of a computer program that predicts deflections is Ram Conce*pt* which is a commonly available computer package used for designing PPS slabs. This computer package is of extra significance to this research as it was used in designing the slabs on a construction site monitored in this research. Even with computer packages that can accommodate many variables and

equations, ultimately material properties remain the dominant fundamental factors which the equations rely on, due to their significant effect on slab performance.

In conclusion it can be seen in Table 2-3 a summary of the factors which effect deflections for PPS slabs and their associated category. Although theoretical calculations can range from simple deterministic equations to finite element computer programs, the raw input values (which all these calculations rely on) are the main concern for this research. A comparison of each equation and its associated accuracy will be presented but focus is drawn to the accuracy of the input. The main input factors to theoretically compare are material properties and applied loadings. The construction method is another major factor affecting slab deformation due to its ability to affect applied loadings, which is covered in more detail in Section 2.6. Each of the factors affecting slab deflection shown in Table 2-3 are is discussed further in sections 2.4, 2.5 and 2.6.

Table 2-3 *Factors which affect deflections in PPS Slabs*

Factors affecting slab deflection	Category
Compressive strength (f'$_c$)	Material Property
Tensile Strength (f'$_t$)	Material Property
Modulus of elasticity (E$_c$)	Material Property
Creep	Material Property
Shrinkage	Material Property
Applied live load (quantity and timing)	Applied loadings
Dead load	Applied loadings
Prestressing (quantity, timing and sequence)	Applied loadings
Propping time	Construction method
Propping sequence	Construction method
Reinforcement (placement and amount)	Construction method
Concrete casting/finishing	Slab dimensions
Moment of Inertia	Slab dimensions
Slab length and depth	Slab dimensions
Cracking	Slab dimensions

2.4.   Material properties of concrete

Material properties such as compressive strength (f$_c$), modulus of elasticity (E$_c$), tensile strength (f$_t$), shrinkage and creep are all major material properties that affect the performance of a concrete structure. Deflection and camber equations, previously summarised in Table 2-1 and Table 2-2, depend significantly on these values. Therefore, when predicting deflections, designers need to be assured that the models that predict material properties are accurate.

2.4.1. Compressive Strength (f_c)

The strength of concrete in uniaxial compression is the material property most frequently used in structural design calculations (Warner et al. 1998). Hence, compressive strength gain of concrete poured on site is rigorously tested and monitored in the lab as it can be the limiting factor for construction sequences as well as the obvious requirement for ultimate strength design. Predicting compressive strength gain is very complicated and concrete suppliers generally rely on testing history from previous mix designs and field experience to supply concrete aimed for a required compressive strength.

Due to this frequency of testing for compressive strength it is convenient to relate the remaining concrete material properties (E_c, f_t, creep and shrinkage) to compressive strength, where appropriate. However the accuracy of these relationships to compressive strength is seldom verified.

It is worth clarifying the difference between compressive strength (f_c) and characteristic compressive strength (f'_c). f_c is a single measured value of strength whereas f'_c is a statistical threshold for a population of strengths, for example the strength attained by 95% of the concrete. This concept applies to compressive strengths as well as tensile strengths.

2.4.2. Modulus of Elasticity (E_c)

The modulus of elasticity (E_c) is one of the most important mechanical properties of concrete and provides a bridge between stress and corresponding strain (Rashid et al. 2002). This relationship assists significantly with predicting serviceability behaviour such as deformations. Table 2-4 illustrates a range of equations available for predicting E_c. As can be seen in this table, all expressions for predicting E_c rely on f'_c. This constant trend is simply due to frequency of testing for f'_c, as stated previously. Other variables considered include density (ρ) and the constants α_E and C_{ca}. These constants are variables which change depending on the type of coarse aggregate selected in the mix design.

Kliszczewicz and Ajdukiewicz (2002) conducted experiments on different types of coarse aggregate and found that this has a significant effect on the value of E_c. The most commonly used aggregates in Adelaide are dolomite and limestone, which are not ideal aggregate for concrete due to their low strength performance. The research by Kliszczewicz and Ajdukiewicz (2002), combined with infrequent industry testing, highlights that there may prove to be a large variance between theoretically derived values and values recorded on Adelaide construction sites. With E_c being one

of the most important mechanical properties of concrete for building performance, it requires a large amount of focus in this research.

Table 2-4 *Expressions for Modulus of Elasticity (E_c)*

Code of Practice/ Researcher(s)	Expression for Ec (MPa)	Range of Concrete Compressive Strength (f'_c)
ACI (1995)	$4,730\sqrt{f'_c}$	No specified strength range
ACI (1992)	$3,320\sqrt{f'_c}+6900$	$21 < f'_c < 83$
Ahmad and Shah (1985)	$8,800(f'_c)^{0.325}$	$f'_c < 84$
CEB-FIB (1993)	$21,500\alpha_E(f'_c/10)^{1/3}$	$f'_c < 80$
Iravani (1996)	$4,700C_{ca}\sqrt{f'_c}$	$55 < f'_c < 125$
Norges (1992)	$9,500(f'_c)^{0.3}$	$25 < f'_c < 85$
AS 3600 (2001)	$\rho^{1.5}0.043\sqrt{f'_c}$	$f'_c < 50$

Note:

Units of f'_c are MPa in all expressions

ρ = density of concrete (kg/m^3)

α_E = 1.2 for basalt, dense limestone aggregates; 1.0 for quartzitic aggregates; 0.9 for limestone aggregates; 0.7 for sandstone aggregates.

C_{ca} = 0.97 for quartzite and traprock aggregates; 0.92 for limestone and dolomite aggregates; 0.90 for diabase aggregates; 0.82 for granite aggregates; 0.76 for siliceous gravel aggregates; 0.71 for sandstone gravel aggregates; 0.61 for sandstone aggregates.

It is important to highlight that each expression displayed in Table 2.4 is coupled with a range of concrete compressive strength. With the acceptation of ACI (1995), each code of practise/researcher(s) states that their expression of E_c is only accurate within certain bounds. This research deals with the scenario of low age material properties which intern equate to low values of compressive strengths and therefore these limitations become important boundaries to abide by.

Table 2-4 is presented graphically in Figure 2-3 and it can be seen that in the commonly accepted regions of concrete compressive strength (approximately 20 MPa to 40 MPa) there is minimal difference between the models. The main notable difference between the models occurs at compressive strengths higher than values experienced in this research. However, the difference in the models at low values of compressive strength (less than 20 MPa) may prove to become a significant focal point due to the expected focus on precision of low age concrete behaviour in this research.

The uncertainty and discrepancies between models may be attributed to the different types of aggregate used in concrete mixes when creating these models. Therefore accurate modelling of E_c for concrete supplied in Adelaide will be investigated in this research through experimental testing, with particular emphasis on whether one of the current models is sufficiently accurate or a new model will need to be developed.
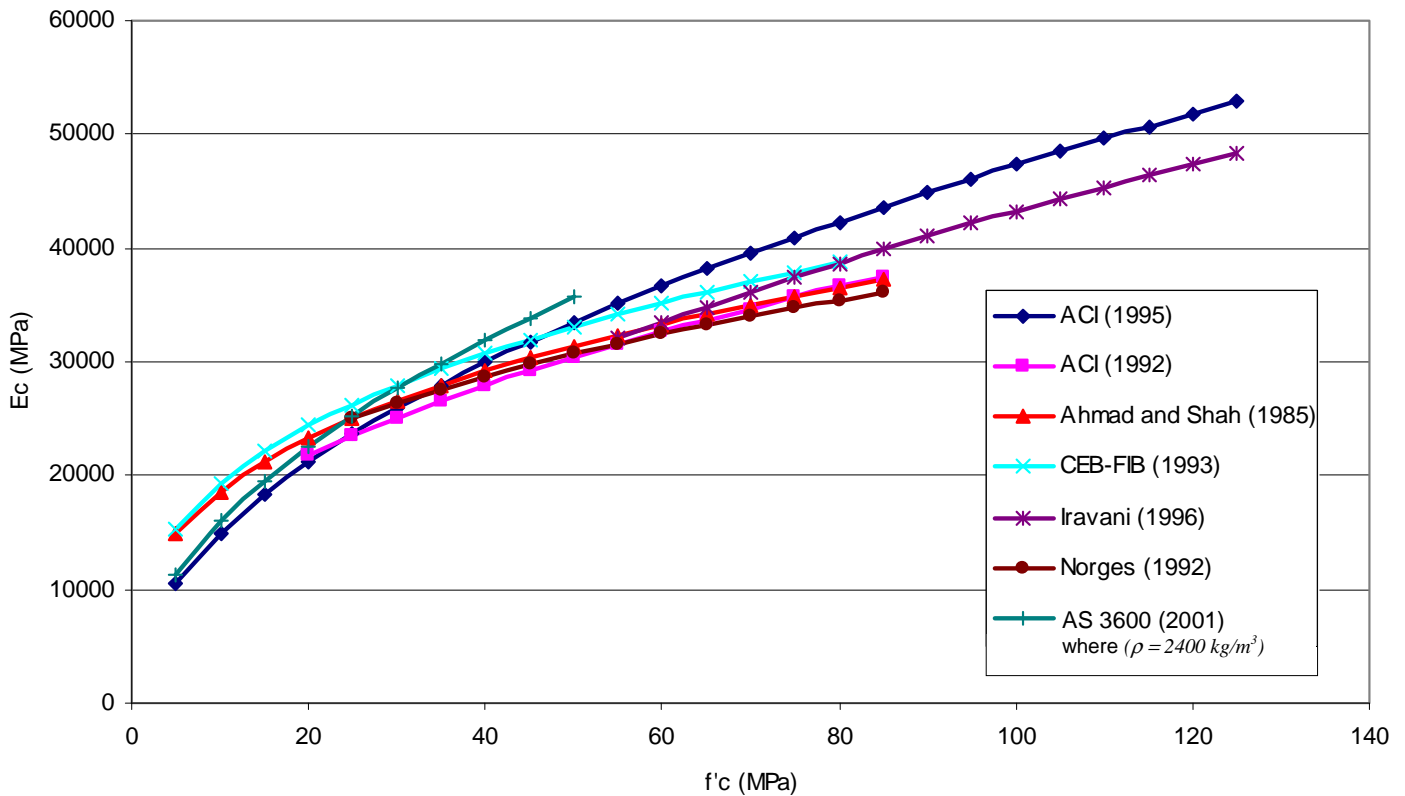
Figure 2-3 *Comparison of Modulus of Elasticity (E_c) Models.*

Table 2-4 and Figure 2-2 show examples of models obtaining instantaneous values of E_c from a given f'$_c$. Instantaneous, or short term, loading of a concrete member will result in a stress strain relationship, and corresponding value of E_c, displayed in Figure 2-4. However, a building's deformation behaviour is rarely dominated by instantaneous loading, it is the sustained stress on the concrete that produces the largest deformation. This is due to a phenomenon called concrete creep which is reviewed in more detail in Section 2.4.5. In this section it is worth noting that maintained levels of stress within a concrete member over time result in a reduction of the value of E_c in the member, which is extremely important for accurate deflection prediction. This sustained stress effect, called concrete creep, is highlighted in Figure 2-5. Figure 2-5 demonstrates the stress strain response when an initial stress is applied, shown by loading line AB. This constant stress is then maintained and the response is an increase in strain along the line BC. It is worth noting that both the magnitude of the stress as well as the length of time of applied stress (loading history) are pivotal for obtaining an accurate long term stress strain relationship, or effectively, a accurate long term value of E_c (Warner et al. 1998).
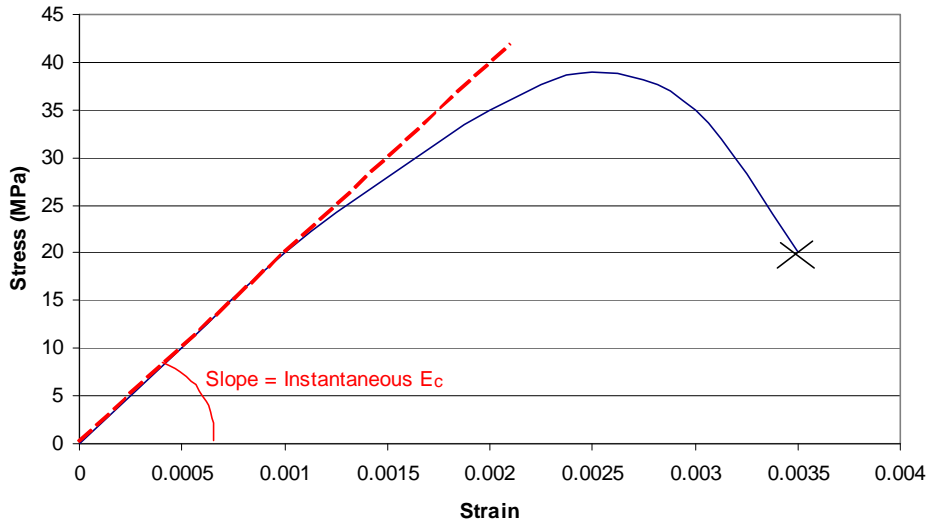
Figure 2-4 *Typical instantaneous stress strain response and associated slope, E_c.*
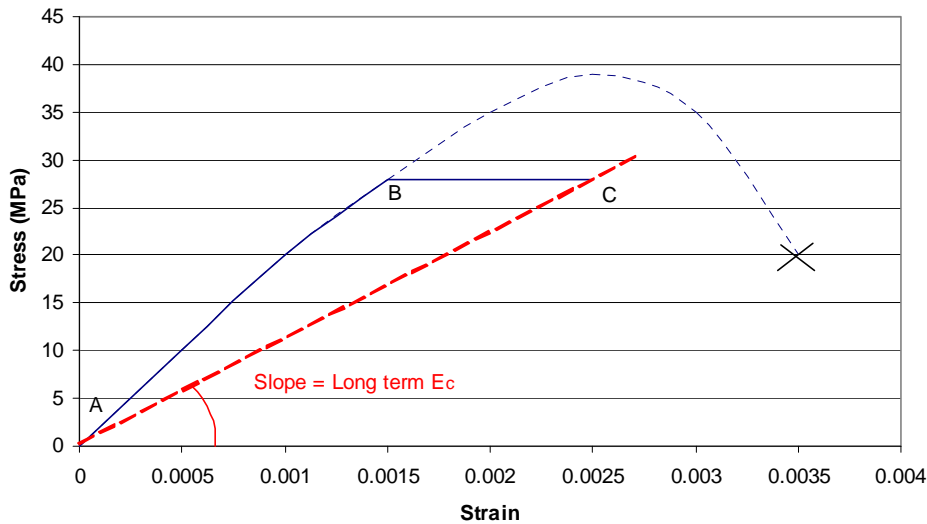
Figure 2-5 *Typical long term stress strain response and associated slope, E_c.*

2.4.3. Tensile Strength (f_t)

Tensile strength in fully prestressed structures receives little to no monitoring as the concrete does not experiences tensile stresses under service loadings. However, for partially prestressed structures, where tensile stresses are expected, tensile strength is pivotal as it determines whether cracking has occurred, which has a significant effect on long term deflections via changes to sectional properties. Table 2-5 displays an array of equations available for modelling f_t from f'_c and the associated ranges of f_c where these models maintain accuracy.

Tensile strength can not be experimentally tested directly and hence indirect methods of recording tensile strength are used in the concrete industry. The two most commonly accepted methods, as per AS 1012.9 (1999), are; the Splitting Tensile Strength (STS) test (commonly referred to as the Brazilian test) and the Flexural Tensile Strength (FTS) test.

Table 2-5 Expressions for Tensile Strength

Code of Practice/Researcher	STS (MPa)	FTS (MPa)	Range of Concrete Compressive Strength
Larrard and Malier (1992)	$0.6 + 0.06f'_c$		no limits given
Zain et al. (2002)	$0.59\sqrt{f'_c}(t/t_{28})^{0.04}$		$f'_c < 120$
Iravani (1996)	$0.57\sqrt{f'_c}$		$50 < f'_c < 100$
ACI (1992)	$0.59\sqrt{f'_c}$	$0.94\sqrt{f'_c}$	$21 < f'_c < 83$
ACI (1995)		$0.62\sqrt{f'_c}$	no limits given
Ahmad and Shah (1985)	$0.46(f'_c)^{0.55}$	$0.44(f'_c)^{2/3}$	$f'_c < 84$
AS 3600 (2001)	$0.4\sqrt{f'_c}$	$0.6\sqrt{f'_c}$	$f'_c < 50$

Note: Units of f'_c are MPa in all expressions

Rashid et al. (2002) state in their research "although the tensile strength generally increases with compressive strength, the increase is not directly proportional to the compressive strength". An earlier study by Larrard and Malier (1992) postulate a linear model for STS, hence, even without experimental results for comparison, it is clear from the literature that sufficient differences in models is evident

It is worth emphasising that Zain et al. (2002) includes a parameter that incorporates the change in tensile strength with respect to time $[(t/t_{28})^{0.04}]$. This allows f_t to be calculated at all stages of curing, including crucial early stages when stressing is occurring, not just long term strength (usually denoted by 28 days). For this research this adjustment to the material property could prove to be useful in increasing accuracy for crucial early age material properties, and a similar adjustment maybe required to E_c.

Table 2-5 is presented graphically in Figure 2-6 and Figure 2-7 for the STS and FTS models respectively. It is clear that significant differences can be seen between the models. It is worth highlighting again that this research anticipates values of f_c to be less than approximately 45 MPa, which are typical concrete compressive strengths associated with PPS slabs. Absolute values of tensile strength are not of concern in this research, the main concern is determining whether cracking has occurred or not, on specific sections of the structure. Therefore a conservative model proving that cracking has not occurred will suffice. FTS tests are more relevant for this research due to flexural loading nature experienced in PPS slabs. However, more time, preparation and quantity of concrete is required to achieve this style of tensile strength testing. STS tests are more common, require minimal preparation and require less concrete to be achieved. Hence this research will aim to monitor f_t via STS tests. An accurate relationship between the two forms of tensile strength testing needs to be reviewed.
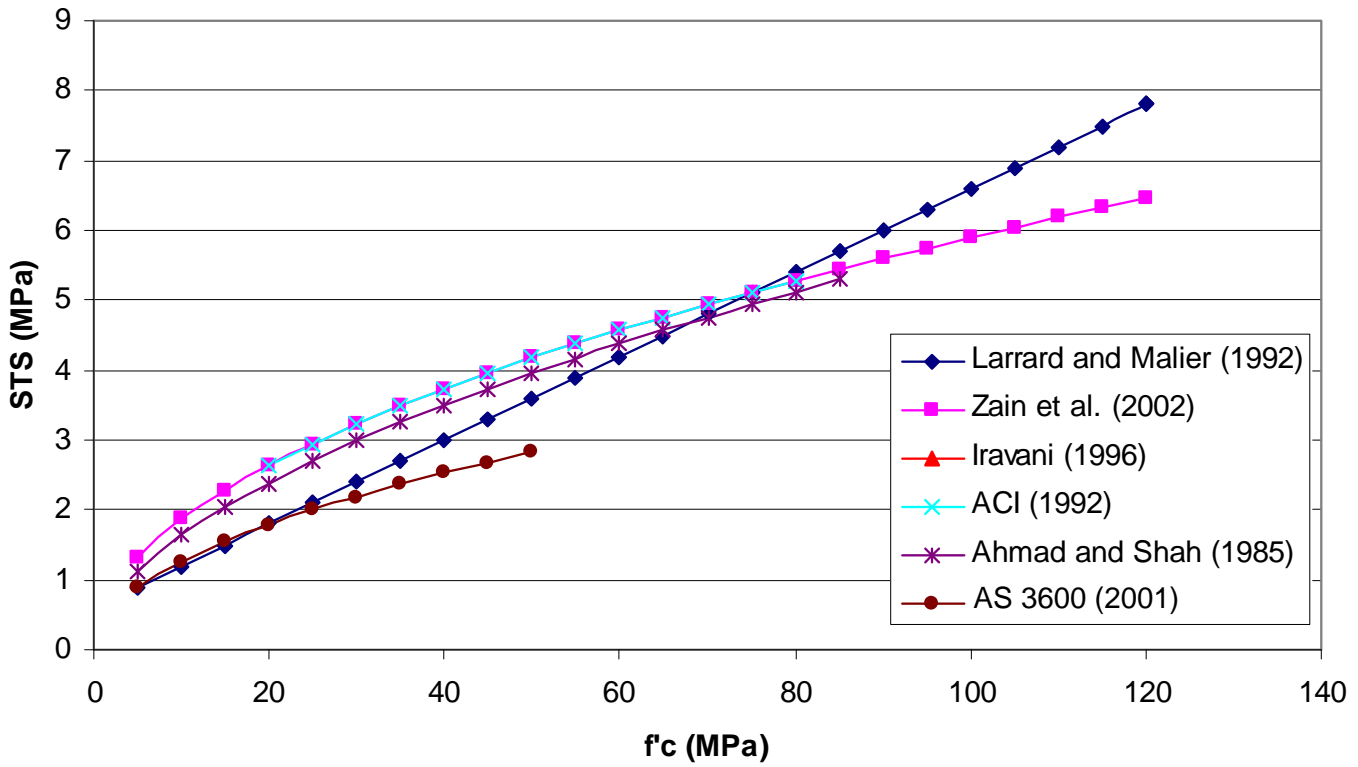
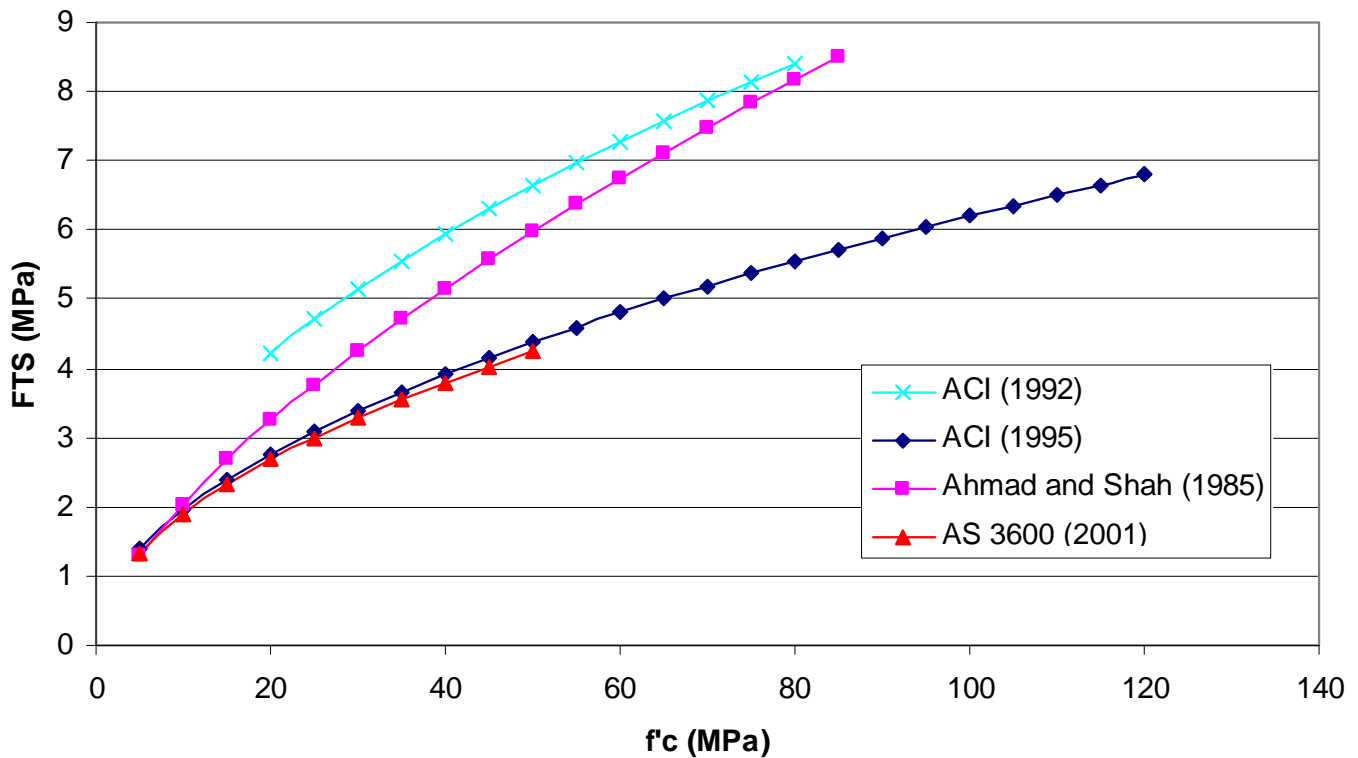*Figure 2-6* Comparison of Splitting Tensile Strength Models

Figure 2-7 Comparison of Flexural Tensile Strength Models

Note:
For this graphical comparison t is assumed to equal t_{28} for the model proposed by Zain et al. (2002)

Equations by ACI (1992) and AS 3600 (2001) in Table 2-5 allude to a linear relationship between STS and FTS however, the coupled equations by Ahmad and Shah (1985) suggests this may not be the case. Extensive research on tensile strength and specific relationships between STS and FTS by Narrow and Ullberg (1963) concluded that "the flexural to tensile splitting strength ratio is not a single value, but varies inversely with the strength of the concrete". However, Narrow and Ullberg (1963) test results suggest that a linear model provides sufficient accuracy for typical tensile strengths experienced in PPS slabs (typically normal strength concrete [NSC] with a lab tested STS of between 2 MPa to 5 MPa). A summary of Narrow and Ullberg's (1963) experimental data and model, along with associated degree of correlation, is displayed in Figure 2-8.

NOTE:
This figure is included on page 19 of the print copy of the thesis held in the University of Adelaide Library.

Figure 2-8 Relationship between STS and FTS for NSC (Narrow and Ullberg, 1963)

Therefore it can be concluded that Equation 2-1 determines an accurate correlation between values of STS and FTS for values of STS between approximately 2 and 4.5 MPa.

$$FTS = 1.0171 \times STS + 1.674$$

Equation 2-1

Where units of FTS and STS are MPa.

2.4.4. Shrinkage.

Shrinkage is related to the drying process which involves the evaporation of absorbed water from the capillary pores of the cement paste (Warner et al. 1998). Shrinkage associated with typical concrete supplied for use in PPS slabs is regularly laboratory tested and monitored by concrete suppliers. Shrinkage strains vary minimally from typical industry supplied values unless large quantities of admixtures (such as superplasticisers, silica fume or fly ash) is added, or large water to cement ratios (w/c) are used (Warner et al. 1998). Concrete mixtures associated with this research

will not contain these constituents, hence, for this research supplied shrinkage strains from the concrete supplier will provide adequate accuracy. Therefore a comparison of shrinkage strain prediction models is not necessary.

Concrete shrinkage can lead to significant deformations in beams and slabs. If a beam or slab contains equal amounts of compressive and tensile reinforcement then uniform shortening of the member occurs. However, the area of tensile reinforcement is usually larger than that of the compressive steel, which, for typical slabs, creates a downward buckling or warping which contributes to slab deflection (Warner et al. 1998).

Table 2-6 displays current models and limitations for calculating shrinkage-induced curvatures. These curvatures are then converted to a member deflection by Equation 2-2.

Table 2-6 Expressions for Curvature caused due to Shrinkage

Code of Practice/Researcher	Shrinkage-induced Curvature	Comments
Warner et al. (1998)	$\Phi(t) = \dfrac{\varepsilon_{sh}(t) - \varepsilon_s(t)}{(e - y)}$	- Intended for non cracked sections.
Warner et al. (1998)	$\Phi(t) = 1.15 \dfrac{\varepsilon_{sh}(t)}{d} \left[1 - \dfrac{A_{sc}}{A_{st}} \right]$	- Intended for cracked sections.
Branson (1968)	$\Phi(t) = 3.2 \dfrac{\varepsilon_{sh}(t)}{D} (p - p_c)^{0.33} \left[\dfrac{p - p_c}{p} \right]^{0.5}$	- Intended for use when; $(p - p_c) \le 0.03$
Branson (1968)	$\Phi(t) = \dfrac{\varepsilon_{sh}(t)}{D}$	- Intended for use when; $(p - p_c) > 0.03$

Where:

   $\varepsilon_{sh}(t)$ = *Shrinkage strain at time t.*
   $\varepsilon_s(t)$ = *Compressive strain in the steel.*
   e = *eccentricity of the reinforcement measured from the centroid of the concrete.*
   y = *distance from neutral axis down to the member centroid.*
   d = *depth to tensile steel.*
   D = *overall sectional depth.*
   p = *tensile reinforcement ratio (A_{st}/bd)*
   p_c = *compressive reinforcement ratio(A_{sc}/bd)*

$$\Delta_{sh} = \beta_{sh} \Phi_{sh}(t) L_{ef}^{\,2}$$ **Equation 2-2**

Where:

   β_{sh} = *a factor representing the support conditions of the beam/slab (0.5 for cantilevers, 0.125 for simple beams, 0.086 for continuous at one end only, 0.063 for continuous at both ends)*
   L_{ef} = *effective span.*

2.4.5. Creep.

Creep is commonly defined as the increase in strain under a sustained stress (Neville 1986). This concept has been discussed and introduced in Section 2.4.2, due to the significant effect creep has on E_c. Neville (1986) suggests that although the effect of shrinkage on creep is to increase the magnitude of creep, they are often added by superposition for ease of calculation, and hence, creep is taken as a deformation in excess of shrinkage.

Creep and shrinkage are vital in determining long term effects such as long term deflection. While shrinkage begins as soon as the concrete is placed, creep does not commence until a load is applied. Figure 2-9 shows the effect that creep and shrinkage have on concrete members when a constant load is applied.
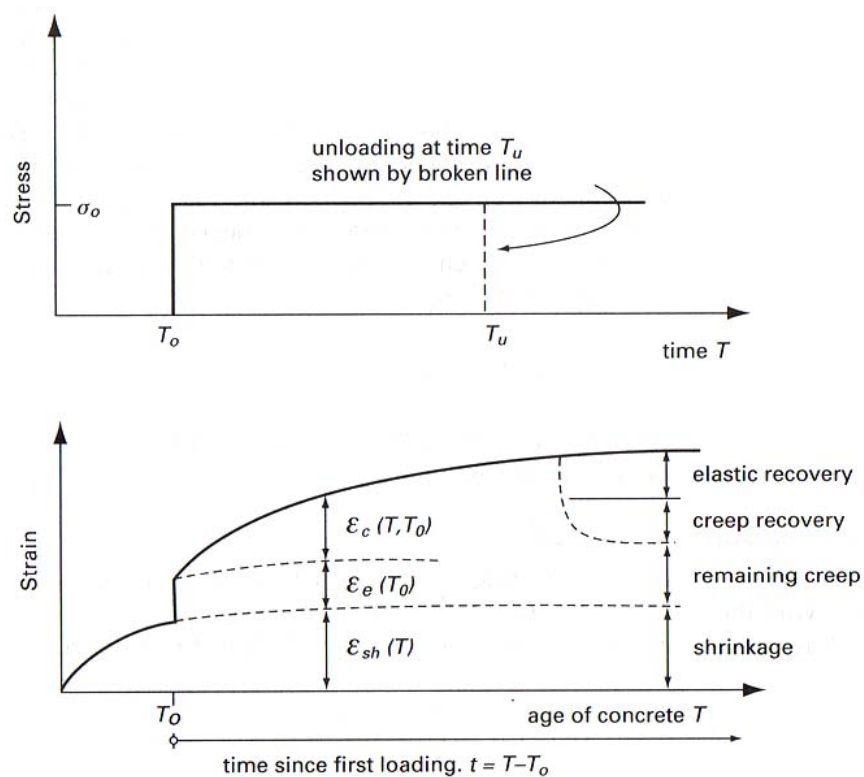
Figure 2-9 *Creep and shrinkage effects under constant sustained stress (Warner et al. 1998).*

Where:
 $\varepsilon_c(T,T_o)$ = Creep strain at time T, with loading applied at time T_o.
 $\varepsilon_e(T_o)$ = Elastic strain due to load applied at T_o.
 $\varepsilon_{sh}(T)$ = Shrinkage strain at time T.

Similar to shrinkage, creep behaviour of typical concrete mixes is regularly tested and monitored by concrete suppliers and hence, can be accurately quoted when concrete is supplied. Therefore, creep strain prediction models do not need to be reviewed. Instead attention is drawn to reviewing the effect a certain degree of creep will have on a member's behaviour, particularly deformations.

Within the usual working stress range, creep strain is approximately proportional to the applied stress σ_o. The initial elastic strain $\varepsilon_e(T_o)$ is also proportion to the applied stress. Dividing the creep strain at time T by the initial strain we therefore obtain a coefficient that is independent of stress $\Phi(T, T_o)$, which is referred to as the creep coefficient. This creep coefficient can be employed to calculate effective E_c values when the long term effects of creep and shrinkage have occurred (Warner et al, 1998). To calculate this effective E_c, Equation 2-3 may be used

$$E_c = \frac{E_{28}}{1 + \Phi(T, T_o)}$$

Equation 2-3

The creep coefficient, $\Phi(T, T_o)$, is usually obtained via laboratory testing and analysis. However Collins and Mitchell (1997) recommend in lieu of data for the specific concrete, the following simplified expression of the creep coefficient, Equation 2-4, be used.

$$\Phi(T, T_o) = 3.5 k_c k_f \left(1.58 - \frac{H}{120}\right) t_i^{-0.118} \frac{(t - t_i)^{0.6}}{10 + (t - t_i)^{0.6}}$$

Equation 2-4

Where the following equation and table are also utilised and;

H = relative humidity in percent.

kc is a factor which accounts for volume-to-surface ratio

kf is a factor which accounts for lower creep of higher strength concretes
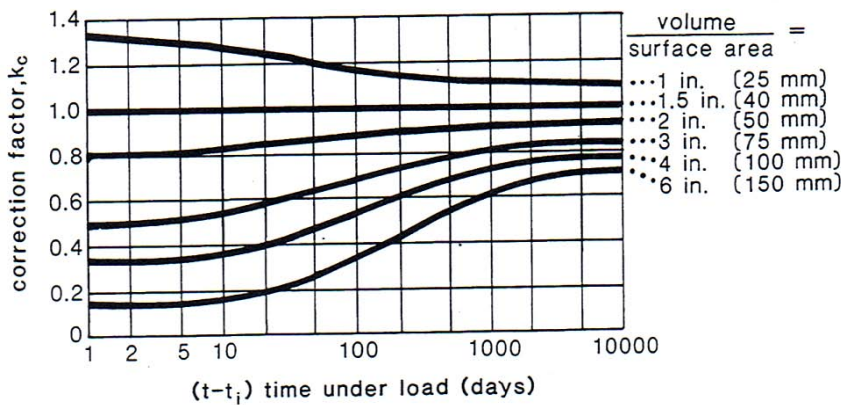
Monitoring long term effects such as shrinkage and creep are crucial for accurately predicting long term deflections. However, it is worth noting that a large proportion of this research draws focus to early age concrete performance and the effects early age factors have on short term as well as long term deflections. Hence, standard creep and shrinkage values from the concrete supplier will be used in analyses, with Equation 2-4 used for comparison due to its specific accuracy for PPS slabs.

2.5.   *Maturity of concrete*

The hydration of cement within concrete is the main reaction that determines the rate of gain of material properties such as compressive strength and stiffness gain. Similar to most chemical reactions, heat can drastically affect the rate at which the hydration, and material property gain occurs. Hence when determining compressive strength gain in respect to time, which is crucial for accurate cycle times, heat is a significant factor.

Maturity of concrete is a technique utilised in the concrete industry which helps predict in situ concrete properties, mainly compressive strength, by monitoring temperature. The maturity method converts the actual temperature-time history into a maturity factor that is used to estimate in situ concrete slab strength based upon previously established strength-maturity functions obtained through known thermal curing (Choong J, 2003).

Figure 2-10 shows an expected temperature-time graph experienced inside a concrete member. Saul (1951) proposed Equation 2-5 as a simple maturity equation to be used with a temperature-time graph. The temperature-time factor at some age *t**, equals the area below the temperature curve and above the datum temperature which is usually valued at -10 ˚C (Choong J, 2003).
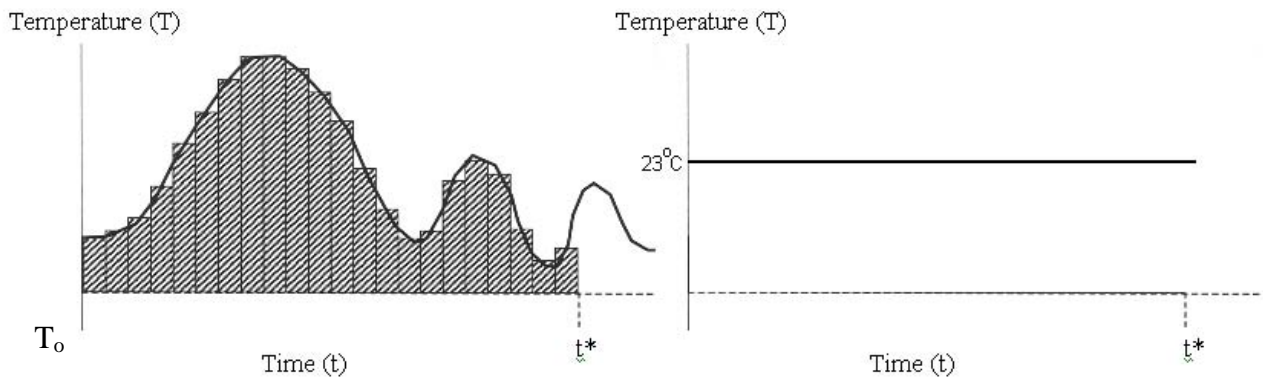
Figure 2-10 *Time-Temperature relationships of curing concrete*

a)	*b)*
Typical time-temperature graph for in situ concrete	*Typical time-temperature graph for laboratory cured concrete.*

$$M = \sum_{0}^{t} (T - T_0)\Delta t$$ **Equation 2-5**

where
M   =   maturity index (˚C hours)
T   =   average concrete temperature (˚C) during time interval Δt
T₀   =   datum temperature
Δt   =   time interval (hours)

Concrete cured under the constant 23 Deg C (which is standard laboratory curing, shown graphically in Figure 2-10(b)) can be tested and using the maturity index of the two separate conditions, an accurate concrete strength for the in situ concrete can be determined.

Saul (1951) also introduced the 'maturity rule' principle, i.e., concrete of the same mix at the same maturity (reckoned in temperature-time) has approximately the same strength regardless of the combination of temperature and time to make up that maturity (Choong J, 2003).

The material properties stated in Section 2.4 can be tested in a laboratory but the argument always occurs whether or not values recorded in a laboratory accurately represent in situ properties. The maturity method is the method adopted by this research to attempt to reduce the uncertainty associated between comparing laboratory conditions and on-site conditions. This is achieved by accounting for the effects temperature and humidity have on curing. The biggest benefit this has is accurately determining cycle times. Cycle times depend significantly on the strength, or maturity, of the in situ concrete. If cycle times are incorrectly predicted, stressing failures can occur. Dead end failure, which is a typical stressing failure, is shown below in Figure 2-11. Repairing these failures can add extra days or weeks to a construction cycle.

<div style="border:1px solid black; padding:1em; text-align:center;">
NOTE:
This figure is included on page 24 of the print copy of
the thesis held in the University of Adelaide Library.
</div>

Figure 2-11 *Dead end Failure in a prestressed slab (Choong J, 2003).*

2.6.   Effect of Construction methods on deflections

On construction sites a number of additional factors affect the deflections of the slabs and for this research these factors could become key contributors into explaining the difference between theoretically predicted deflections and surveyed values. The three main construction methods that will be investigated are premature stressing of the tendons, premature or incorrect formwork movement and initial casting/levelling techniques of the concrete slab.

Premature stressing of tendons is a well known cause of structural failure through mechanisms such as dead end or live end failure, as shown in Figure 2-11 and covered by Stivaros and Halvorsen (1990). To ensure this mechanism of failure does not occur designers specify that a required level of compressive strength must be obtained so stressing of the member can be performed without failure. For this research, where deformations are the main interest not strength, inadequate camber of the slab due to inadequate E_c at stressing times will be examined. In current practise there is no specified value of E_c that is required to be obtained for acceptable stressing of the member. Compressive strength is the only material property gain that is a limitation on the time of prestress application.

Formwork movement is closely related to the stressing time/technique of prestressed slabs. Formwork and props are typically removed directly after the slab receives stressing which is adequate to hold the dead load of the slab and construction loads. These loads may exceed the designed strength of the building's structure or produce early cracking of the floor, which can adversely affect its service conditions (J.F.M.A. Prado et al, 2003). Few international codes provide guidelines of this crucial procedure, The ACI Formwork of Concrete (1989) recommends only the method described by Grundy and Kabaila (1963), referred to as the "simplified method". J.F.M.A. Prado et al (2003) continued research on this method and produced accurate practical load factors (k) for each step of the construction process. Appendix B highlights this process. This research aims to draw a link between these load factors and the effect this method can have on deflections.

When multistorey construction includes the use of a construction joint, such as the construction site utilised in this research, continuity between the slabs at this joint during the construction stages is crucial for maintaining adequate structural strength and performance. Designers supply construction crew with a required one or two bay over-lap of formwork at these construction joints. Previous research into this requirement, and how significant this effect is on deflections, has received little to no consideration.

The initial stages of casting and levelling of concrete slabs are prime instances in the construction process when inaccurate deflections can be introduced. Theoretical equations assume that the slabs are perfectly flat, realistically this is impossible to achieve on site due to the magnitude of typical multistorey concrete slab pours (regularly in excess of 5m by 5m). For prestressed slabs, where eventual deflections are designed to be at an absolute minimum this effect is amplified. For example, partially prestressed slab deflection equations can produce predicted deflection values of 2-3 mm but if there is an initial varying deformation introduced at the casting stage of ± 5 mm, deflection equations are effectively meaningless.

2.7.   Applied Loads.

Service loads on PPS slabs include sustained loads and temporary loads. Self weight and dead loads are both sustained over the life of the structure and are considered sustained loads. Live loads, which act in relatively short periods of time, are considered temporary loads. Separating these applied loads is crucial as only the sustained loads contribute to long term effects such as creep, covered in Section 2.4.5 (Warner et al,. 1998).

For a flexural member with prestressed steel, the self weight of the member usually acts at the same time that the prestressing force is introduced. Therefore, the initial upward deflection due to camber is usually somewhat larger than the downward deflection due to the self weight. A typical loading history and associated deflection history is given in Figure 2-12.

Prestressing loads are accurately monitored on site and current prestress jacking techniques allows an adequate level of accuracy of these values for this research. The same can not be said for applied dead loads and live loads. Due to the nature of dead and live loads, it is rather complicated to use accurate values in slab deformation prediction equations. Warner et al. (1998) suggests the use of live load reduction factors for serviceability design, given in AS 1170.1 (2002). Even though these factors have a history of yielding relatively accurate loading values, each construction site (and structural member on that site) is unique. An exact loading on each section of the structure will always contain a degree of uncertainty.

It is worth highlighting that this research is involved with predicting deflections associated with serviceability loadings. Hence typical loadings due to everyday serviceability are of interest, full design loadings or peak deflections due to ultimate state analysis are not of interest.
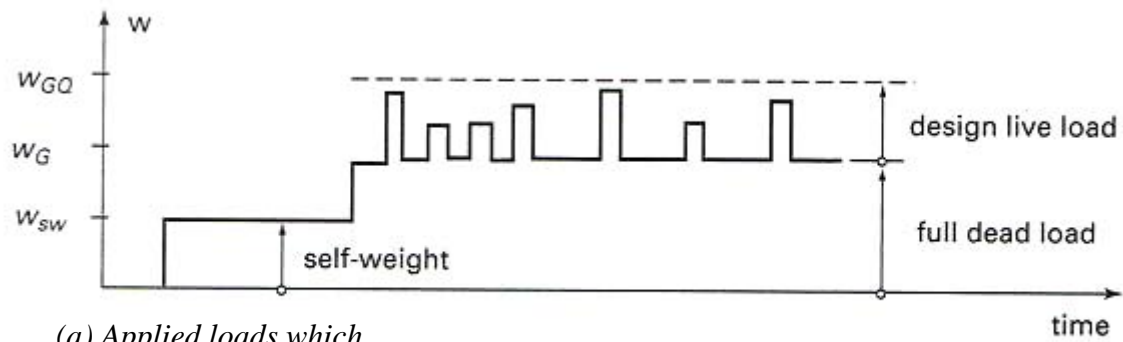
(a) Applied loads which cause downward deflection (Live loads and Dead loads)
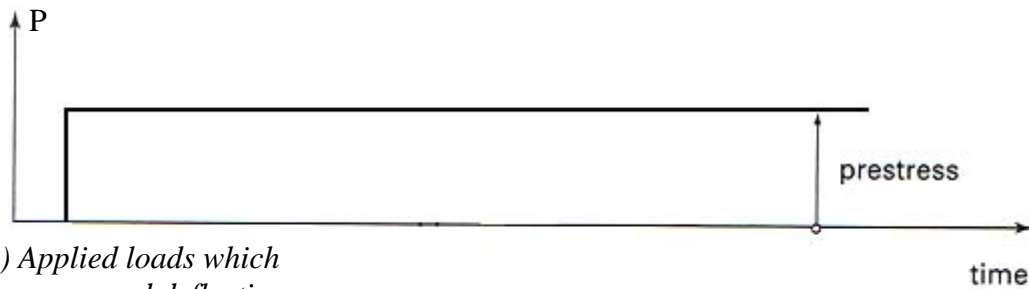
(b) Applied loads which cause upward deflection (Prestressing force)

(c) Typical deflection history of a partially prestressed member

Figure 2-12 *Load and deflection histories for partially prestressed members (Warner et al, 1998)*

2.8.   Conclusion

This literature review has introduced the main topics and issues that affect the serviceability performance of partially prestressed concrete slabs. An overview of the past and current deflection prediction methods has been displayed and discussed. The material properties, that the deflection equations rely on, have been summarised. The concept of maturity and the effect this has on material properties and the accuracy of predicting material properties has been examined. Finally, the realistic effect construction methods and applied loadings have on deflections on site has been summarised.

It has been shown that there are simple equations that only consider inputs such as span, f'_c, E_c and slab depth, other equations consider each effect of curing, time, shrinkage, load timing, load quantity and other factors effecting serviceability history. However, there is no definite method of combining each of these equations into a method specifically for PPS slabs that has justified confidence and accuracy.

It has been proven that each input for predicting deflections has the ability to affect other inputs, for example loading behaviour can affect the member's effective stiffness via creep. It has also been proven that each construction site is unique, this opens up a large array of potential variances between predicted outcomes and measured outcomes. Therefore, some form of confidence or statistical analysis needs to be employed to draw a justified link between theoretical predictions and what is occurring on site.

To accurately examine the deflections of prestressed concrete slabs this project will investigate not only the deflection equations and their associated accuracy for Adelaide's conditions, but also the natural variance in the factors and variables which effect deflections on site. A large testing program is performed to accurately monitor each factor and its associated variation experienced due to realistic onsite factors. This experimental program, including the analysed construction site is covered in detail in Chapter 3. Following this Literature Review is Chapter 3 where the methodology behind this research is explained.

3. EXPERIMENTAL PROGRAM

3.1.　　Introduction

This chapter of the research presents the processes employed to obtain a large database of site specific experimental data. Initially the site specific details of the chosen site for this research are presented. Details of the unique construction process and associated design requirements are also explained in this section. Following this, the results of the concrete material property laboratory experiments are presented. The results from this section are not unique to this construction site and can effectively be applied to any Adelaide supplied N32 or N40 concrete mix. Once the material property results have been presented, a data analysis of the concrete is performed. This data analysis contains a significant statistical element to clarify the confidence associated with the performance of N32 and N40 concrete. Finally the outcomes that are specific to the analysed construction site are examined. These outcomes include the construction process utilised and the surveyed deflections, which are documented and summarised.

3.2.　　Site Specific Details

3.2.1. The Site

Due to the strong industry support for this research, access to a construction site incorporating PPS slabs was supplied at the commencement of the research. This allowed the experimental component of this research to test and measure a wide range of variables on site. The construction site chosen was a multi storey office block in Adelaide's Central Business District (CBD) initially called Admiral House. Near completion, the client renamed this building 151 Pirie. Therefore, it should be noted in this research that reference to this building is primarily 151 Pirie, but in the instances where the name Admiral House is unavoidable due to the timing of the reference, the reference still refers to the same building and/or construction site. Seven out of the ten slabs being poured at 151 Pirie utilised an identical two-way PPS slab arrangement. Due to the large size of the slabs, each of the seven slabs were poured in two sections. This gave the research fourteen opportunities to collect concrete samples directly from the construction site at the time of pouring.

151 Pirie was designed in late 2004 to early 2005, with the construction beginning early May 2005. The site is located on the corner of Pultney and Pirie St, Figure 3-1 and Figure 3-2 show images of this building during construction stages and final state, respectively.

Figure 3-1 *151 Pirie Construction (mid 2005)*

Figure 3-2 *151 Pirie Completed (June 2006)*

3.2.2. 151 Pirie Slab Detailing

The PPS slabs at 151 Pirie are all flat slabs incorporating drop panels. The typical dimensions of each internal bay were 9.6 m by 8.4 m. Drop panels were either 3 m x 2.4 m x 350 mm deep or 2.4 m x 2.4 m x 350 mm deep, depending on the location. Slab thickness was 200 mm with 25 mm of cover. Concrete compressive strength was rated at 32 MPa in a standard mixture called N32. The concrete mix was changed mid construction to 40 MPa, with a mix called N40, explained further in Section 3.2.3.

Steel reinforcement was N12 (12mm diameter deformed bars with 500 MPa tensile strength) spaced at 400 mm for both directions, with 400 mm laps. Edge beams were 900 mm wide by 650 mm deep,

or 900 mm wide by 550 mm deep, depending on location. The post tensioning tendons consisted of 12.7 mm nominal diameter 7 wire stress relieved super grade low relaxation strands, as per AS 1311 (1987) with a minimum breaking load of 184 kN. Prestressing drapes were parabolic in both directions, concrete cover to all ducts was at least 25 mm. Structural plans detailing the above information can be found in Appendix C.

3.2.3. Strength Specifications

The post-tensioning tendons at 151 Pirie were prestressed to 25% of the final jacking force after 24 hours. For this stressing stage to be achieved safely (without structural damage, such as that shown in Figure 2-11), the PPS slab's concrete compressive strength (f_c) was required to be above 6 MPa. After 7 days, 100% of the jacking force was applied, which was 156 kN, or 85% of the Ultimate Tensile Strength (UTS). For this second stage to be completed successfully the PPS slab's compressive strength was required to be above 24 MPa. The compressive strength limitation of 24 MPa was the only limiting factor for final prestressing, therefore if 24 MPa was proven to be achieved earlier, or later, than 7 days, prestressing could only occur at that time.

The construction of 151 Pirie was based on a limited timeline and this limitation of final prestressing at $f_c > 24$ MPa became a focal point. If final prestressing occurred as low as 5 or even 4 days then over the course of 14 slab pours approximately 2 months could have be save on construction time (compared to final prestressing at 7 to 9 days). The concrete compressive strength gain shown in Figure 3-3(a) is a good example of concrete that passes the 7 day strength requirement. However, if mix designs or atmospheric conditions delayed the strength gain of the concrete, a graph such as the one shown in Figure 3-3(b) may have be produced. As can be seen in Figure 3-3(b), stressing of the slab could not be achieved safely at 7 days and in fact 24 MPa is not reached until 3-4 days later.
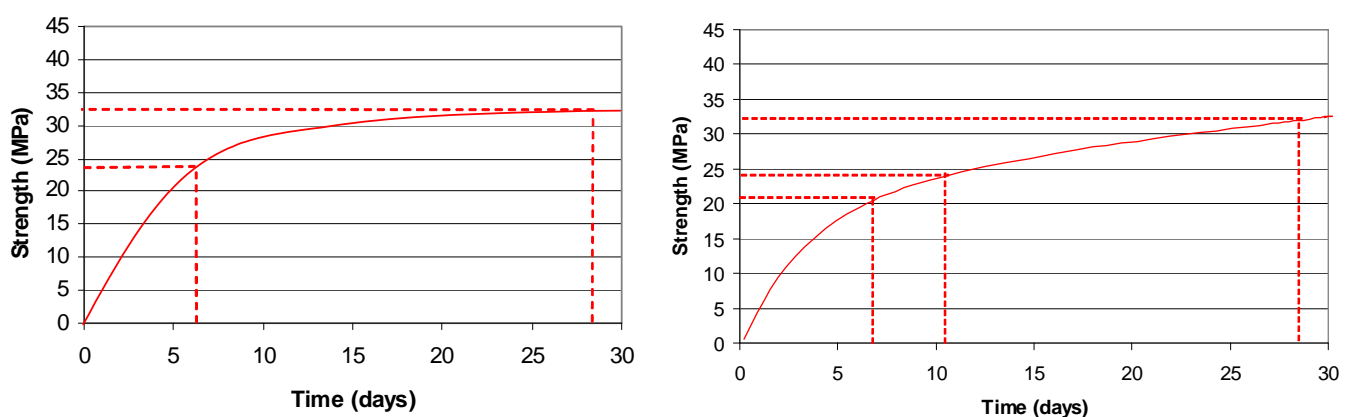
Figure 3-3 Examples of concrete compressive strength gain

(a) Adequate Concrete Compressive Strength gain. (b) Inadequate Concrete Compressive Strength gain

The possibility of upgrading the specification of the concrete mix to achieve higher early age strengths was discussed during the design stages of 151 Pirie. The most feasible outcome was to use a slightly higher grade of concrete such as concrete rated with a compressive strength of 40 MPa (N40). The possibility of including High Early-Strength (HE) cement in the current mix (N32) was considered risky on a project with such strict time line, due to potential negative outcomes such as large surface cracks from excessive shrinkage at later dates.

Figure 3-4 shows an example of typical compressive strength performance of the N40 mix versus the N32 mix, it can be seen at 28 days each mix comfortably passes its required compressive strength. It is worth noting that each strength gain curve depends significantly on site specific conditions such as temperature and humidity. As stated in the Literature Review chapter, typically low temperature equates to low strength. Therefore, as highlighted in Figure 3-4, when a slight variance of strength gain is kept in mind the strength gain has the potential to threaten construction time.
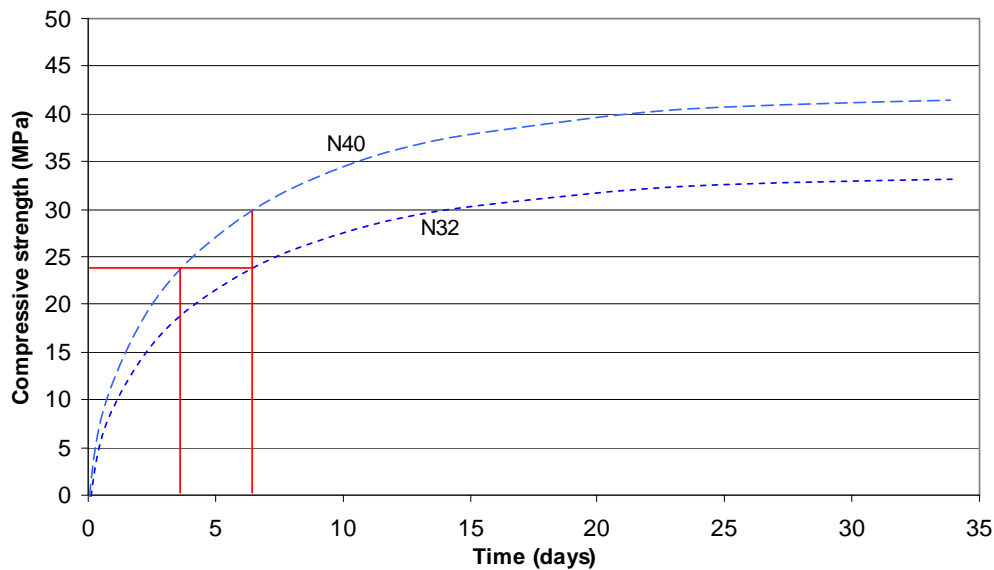
Figure 3-4 Compressive strength gain of N32 and N40 concrete mixes

3.2.4. Concrete Mixes and Materials

Both the N32 and N40 mixes were batched at the Readymix Brompton batching plant. Both mixes used materials in accordance with AS 3972 (1997) for cement, AS 3582.1 (1998) for supplementary cementitious materials, AS 2758.1 (1998) for aggregates and AS 1478.1 (2000) for admixtures. The mixes were designed to fully comply with AS 3600 (2001) and AS 1379 (1997).

Concrete property testing on site, such as temperature tests and slump tests, were performed by Readymix's NATA certified testers according to AS 1012.3.1 (1998) and AS 1012.8.1 (2000). Sampling and placement of the concrete cylinder samples was performed and managed by this research and the procedure is explained in more detail in Secion 3.2.6. Tabulated summary of both the N32 and the N40 concrete mixes, and concrete supply details, can be found in Table 3-1. Specific detail on each concrete mix and pour can be found in Appendix D.

Table 3-1 Concrete mix details

N32 mix (f'c rating of 32 MPa at 28 days)		
Constituent	Type	Detail
Cement	GB Cement	
Admixtures	Superplasticiser	Accelerator - dosed at approximately 1 L/m^3
	Fly Ash	Approximately 15-20%
Aggregate	Dolomite	Max aggregate size of 20mm

N40 mix (f'c rating of 40 MPa at 28 days)		
Constituent	Type	Detail
Cement	GB Cement	
Admixtures	Superplasticiser	Accelerator - dosed at approximately 1 to 2 L/m^3
	Fly Ash	Approximately 15-20%
Aggregate	Dolomite	Max aggregate size of 20mm

3.2.5. Concrete Placement and Levelling

The concrete delivery for the PPS slabs at 151 Pirie was achieved by concrete delivery trucks with capacities between 5.2m^3 and 10m^3. The trucks were filled with the N32 or N40 concrete at the Readymix Brompton Concrete batching plant approximately 6 kms away. Concrete placement to the slabs was achieved via the use of a Putzmeister concrete pumping truck. Levelling of the slabs was achieved with a concrete trowlling machine commonly referred to as a concrete helicopter. Each PPS slab was poured in two halves, the first pour being approximately 60% of the total slab and the second pour was the final 40%. Samples of concrete taken for this research for testing material properties was done from the concrete truck prior to concrete pumping. Examples of the placement and levelling techniques used can be viewed in Figure 3-5.
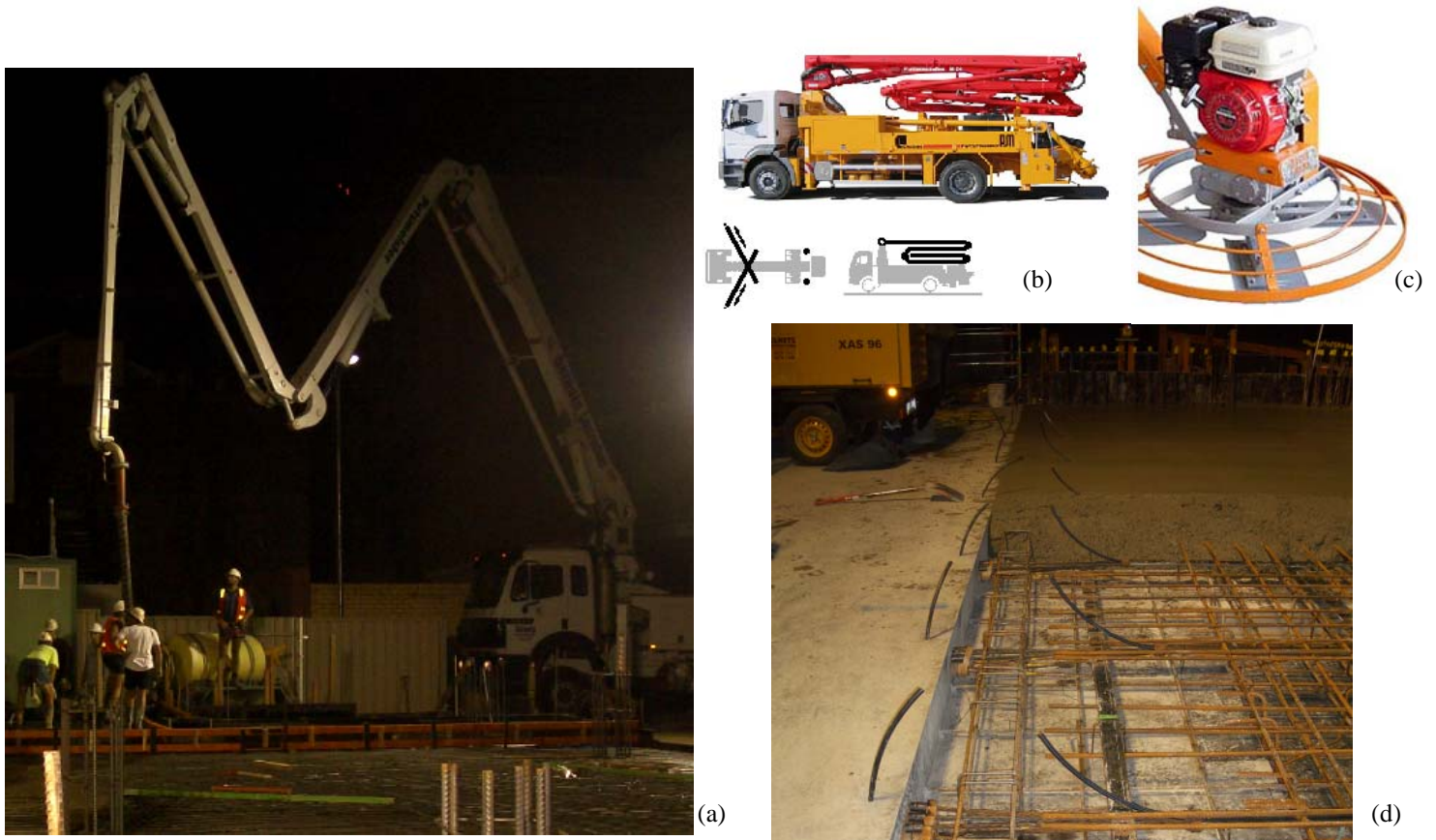
Figure 3-5 *Concrete placement and finishing techniques used for the PPS slabs at 151 Pirie*
- a) & b) Examples of Putzmeister concrete pump, c) concrete trowelling machine/helicopter, d) construction joint.

3.2.6. Experimental Testing Program

The experimental testing program was planned very early in the timing of this research. This was due to the construction of 151 Pirie commencing approximately at the same time as the research. Therefore, without having enough time to research the most suitable material properties for this research, the experimental testing program was designed to cover a significant selection of the most commonly tested concrete material properties.

It was decided that the experimental testing was to be completed and managed entirely by this research and not outsourced. This method was chosen to gain an understanding and appreciation of the testing methods performed by the concrete technicians on site. It was also chosen to ensure that each test was monitored and completed at the correct time without confusion or disruption to mandatory testing sequence performed by the concrete suppliers.

The experimental testing program selected included a total of 30 concrete cylinder samples for each concrete pour. This was chosen based on the number of material properties monitored for

deflections, available testing equipment and timeline. However, the number of testing cylinders varied slightly for each concrete slab pour. The reason for this was realistic limitations on site such as the availability of concrete molds, available space, quantity of concrete for testing and/or time restraints. These 30 or so cylinders consisted of samples used for obtaining values of the following: ultimate compressive strength (f_c), modulus of elasticity (E_c), tensile strength (f_t) and Creep. These key concrete values were necessary to record as they each affect deflection.

All molds used were standard cylindrical molds made from steel, 100 mm diameter by 200 mm high. All cylinders were cast on site and left overnight under insulating sheets to minimise moisture loss. All concrete cylinders poured as part of this research were done separately to mandatory cylinder tests poured by Readymix. As per AS 1012.9 (1999) Readymix was required to monitor the concrete compressive strength gain by pouring 3 cylinders samples to be testing for every 50 m^3 or part thereof. One cylinder was to be tested at 7 days and 2 cylinders were to be tested at 28 days, where all 3 cylinders were cured in a standard lime bath. Readymix tested their cylinders at the Readymix testing laboratory at Brompton. Cylinders tested as part of this research were tested at the University of Adelaide's Engineering North Annex laboratory. Each concrete cylinders test was performed in accordance with AS 1012.9 (1999).

As stated previously in Section 2.5 the material properties of concrete can be noticeably affected by changing the method of curing, hence it was decided to cure half of the 30 cylinders in a standard lime curing bath, at 23 deg C, at Readymix Brompton (standard concrete construction practice as per AS 1012.9 (1999)), and half of the cylinders on site subjected to ambient temperatures, commonly referred to as air cured. The air cured method was included as it is a more realistic replica of the curing environment experienced by the thin PPS slabs. Concrete cylinders were 100 mm diameter, 200 mm high, the PPS slabs at 151 Pirie were 170 mm thick so natural insulation, which traps temperature and humidity for curing, was at a minimum for both scenarios. Both sets of cylinders were intended to be as identical as possible, hence both samples were obtained at the same time, from the same truck, with the same on site properties such as slump and concrete temperature. Both sets of cylinders were cured for the first 24 to hours (plus or minus 6 hours) in identical molds and demolded at the same time. An example of the curing conditions that was selected can be seen in Figure 3-6 and an arrangement of the 30 concrete cylinder samples is highlighted in Table 3-2. It should be noted that each cylinder tested for E_c can be reused for testing f_c due to tests for E_c being non-destructive. Due to the initial 24 hour curing requirement of all cylinders, all tests performed at 1 day have identical curing methods. This curing method is neither considered lab nor site curing and appropriately is considered separate to lab and site curing.

Figure 3-6 *Curing conditions of concrete cylinders*
a) Curing conditions on site   *b) Curing conditions in the laboratory.*

Table 3-2 Summary of testing cylinders for each pour.

Laboratory Cured Cylinders		
#	age	Test(s)
1	3 days	f_c
2	3 days	E_c and f_c
3	3 days	f_t
4	7 days	f_c
5	7 days	f_c
6	7 days	E_c and f_c
7	7 days	f_t
8	14 days	f_c
9	14 days	E_c and f_c
10	28 days	f_c
11	28 days	f_c
12	28 days	E_c and f_c
13	28 days	f_t

Site Cured Cylinders		
#	age	Test(s)
1	3 days	f_c
2	3 days	E_c and f_c
3	3 days	f_t
4	7 days	f_c
5	7 days	f_c
6	7 days	E_c and f_c
7	7 days	f_t
8	14 days	f_c
9	14 days	E_c and f_c
10	28 days	f_c
11	28 days	f_c
12	28 days	E_c and f_c
13	28 days	f_t

1 day samples		
#	age	Test(s)
1	1 day	f_c
2	1 day	E_c and f_c

Note: Four additional cylinders were poured to monitor creep at two of the fourteen concrete slab pours. Concrete shrinkage molds were poured and tested by Readymix.

In summary it was planned that at each day of testing (ages of 1, 3, 7, 14 and 28 days), f_c tests were performed on 2 cylinders. E_c was tested at least 3 times on the same cylinder and f_t tests were completed when necessary (approximately 2 to 3 times for each pour). Initially f_t tests were not considered a focal point as the slabs were prestressed and hence not expected to develop significant tensile stresses. However, tensile tests were still completed to obtain and monitor as much data as possible about the slabs. Two separate creep rigs were set up and loaded, at separate times, to monitor creep values for the concrete. Measurements of shrinkage were managed at the concrete laboratories at Readymix. This arrangement allowed a thorough database to be created and repeated tests allow an adequate level of confidence in the results obtained.

To monitor the maturity of the concrete, the use of thermocouples was incorporated into this project. As stated previously, the curing conditions of concrete can have a considerable affect the material properties of the concrete. The use of thermocouples allowed monitoring of the temperature of the curing concrete, which has a direct relationship to strength gain and other concrete material property gains over time. Temperature data was recorded within the in situ slab as well as concrete cylinder. The concrete cylinder time-temperature relationship, coupled with the outcomes of laboratory strength tests would be used to calibrate the maturity model, explained in Section 2.5.

Due to the time taken to prepare the thermocouples, it was decided to attempt only a few thermocouple readings at 151 Pirie. The time taken to prepare thermocouples left little time to be allocated to sampling concrete cylinders for the same pour. Considering that monitoring material properties was the major factor for this research, thermocouple readings were considered a second priority. Slab depth and arrangement did not vary for 151 Pirie, so it was considered a safe assumption that a single temperature-time history recorded for a slab would be accurate for all subsequent slabs, for the same concrete mix.

3.2.7. Surveying Plan

Surveying of the PPS slabs was a delicate procedure that required considerable experience to gain accuracy. Due to this, the surveying of the PPS slab deformations at 151 Pirie was performed and managed by Engineering Surveys Pty Ltd. For this research the peak deflection values were of interest, to ensure that these points were surveyed the initial design deflection predictions from the computer program RAM Conce*pt* were used to locate the peak deflection points. The confidence of the magnitude of the predicted values was questionable, but from surveying experience supplied by Engineering Surveys Pty Ltd the location of the peak deflections remained accurate. Based on the long term deflection prediction contour plot shown in Figure 3-7 the surveying grid shown in Figure 3-8 was selected. It is worth noting that in addition to the peak deflection values, a two-bay grid was also chosen to be monitored very closely. The location of this grid was chosen due to expected minimal traffic or obstructions during the construction stages, which allowed access to accurate surveying when required.
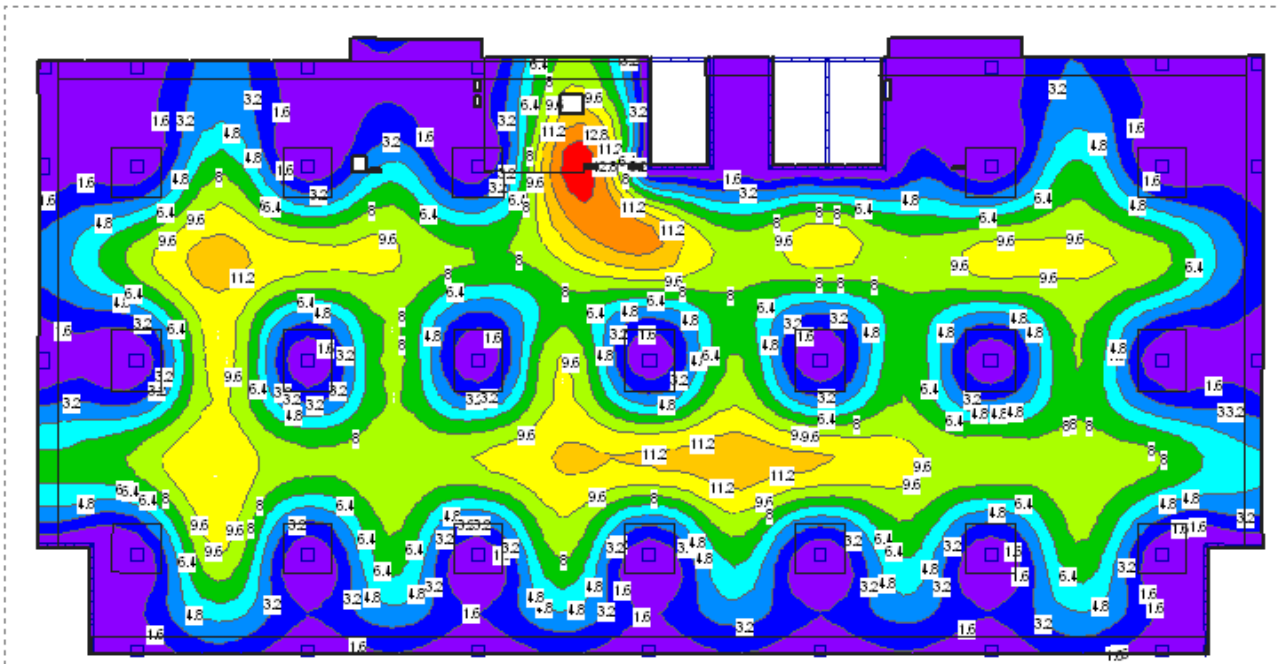
Vertical Deflection Plot (mm)

Figure 3-7 Long Term Deflection Prediction Plot from Initial Design Stages using RAM Concept
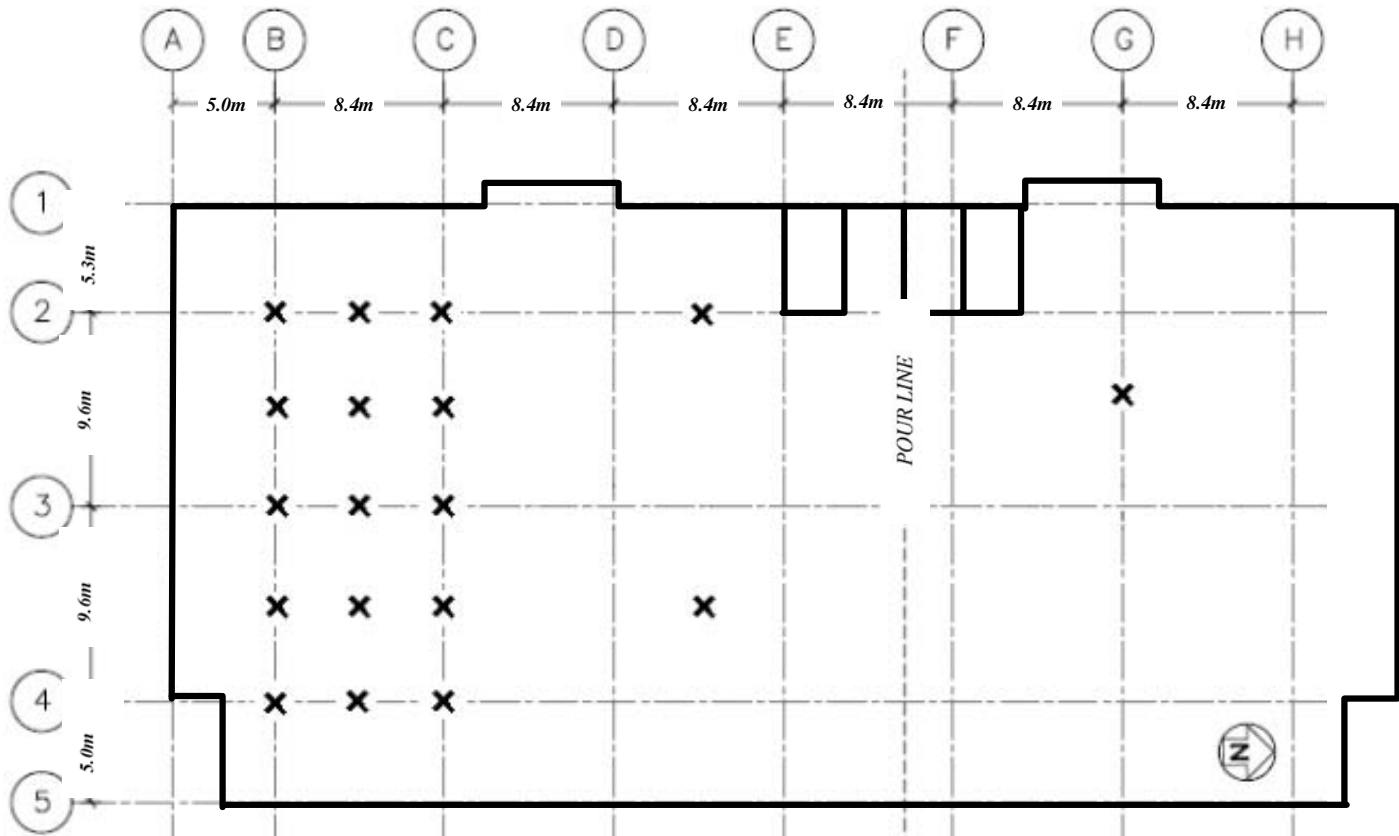

Figure 3-8 Surveying Grid Established based on Long Term Deflection Predictions

The surveying plan shown in Figure 3-8 resulted in a total of 18 deflection readings for each floor (7 floors) which was considered sufficient for this research. The surveying method included deflection readings sampled at day 1 as the zero readings, then surveyed again after the initial stressing, to monitor the camber of the slabs. The final surveying readings were then taken just prior to the laying of the carpet. To allow long term deflection readings, the surveying method included deflection readings on the underside of the slab so surveying could be achieved well into the future without effecting floor coverings.

3.3. Concrete Material Properties Results

3.3.1. Compressive Strength (f_c)

The cured cylinders, shown previously in Figure 3-6, were collected from the construction site and lime curing bath at Brompton then taken to the testing laboratory at the University of Adelaide at the required day of testing. Prior to testing the cylinders, each lime bath cured cylinder was washed and dried to ensure excess dried lime did not effect measurements such as weight. Each cylinder's height and diameter was then recorded along with weight. From this combination of results density of the concrete mixture could be determined, along with accurate conversions from recorded force to resisted compressive pressure. The laboratory equipment used to test the concrete cylinders for f_c was a manually operated hydraulic compression rig (Seidner D 7940 Riedlingen) with a spherical seated top plate. This arrangement is displayed in Figure 3-9.

Figure 3-9 Experimental testing apparatus at the University of Adelaide Annex Laboratory.

Initially each cylinder was prepared for compressive testing with a standard compressive testing rubber cap. After a few initial compressive tests it was discovered that rubber capping was causing premature failure of cylinders at low ages (up to 3 days). This was due to the top edge of the

cylinders shearing when the rubber cap compressed and expanded. This was not an issue for normal strength cylinder testing (f_c greater than approximately 15 MPa) but considering the focus of this research lies on early age compressive strength gain a new type of cap, which did not cause premature failure, was required. Dental paste was employed as a capping method that was adequate for all ranges of compressive strength. Dental paste caps helped confine the top of the concrete testing cylinder as well as supplying an adequately flat surface for symmetrical and consistent compression testing.

Figure 3-10 shows the rubber caps, including evidence of the expanding rubber being crushed against the inside edge of the metal casing. Figure 3-10 also shows examples of a cylinder tested with a rubber cap and the associated premature failure, along with a cylinder prepared with a dental paste cap and the uniform crushing at ultimate load.

(a)   (b)   (c)

Figure 3-10 *Premature failure of early age concrete compression tests.*
- a) Rubber cap with crushed rubber edge, b) Prematurely failed specimen due to rubber cap, c) failed specimen under uniform compression with dental paste cap.

The possibility of non uniform crushing due to eccentric loading was another problem with concrete cylinder testing. As stated earlier the testing apparatus uses a spherical seat to ensure that the top plate sits firmly against the top of the sample being tested. This type of seat maintains a vertical load for situations where the cylinder cap is not completely horizontal. Due to the explosive nature of compressive failure of concrete cylinders, failed specimen dust can cause this spherical seat to gain unwanted friction and become jammed when being operated. This results in an eccentric load being applied to the specimen, which transfers into premature shear failure. Premature failure due to eccentric loading is highlighted in Figure 3-11.
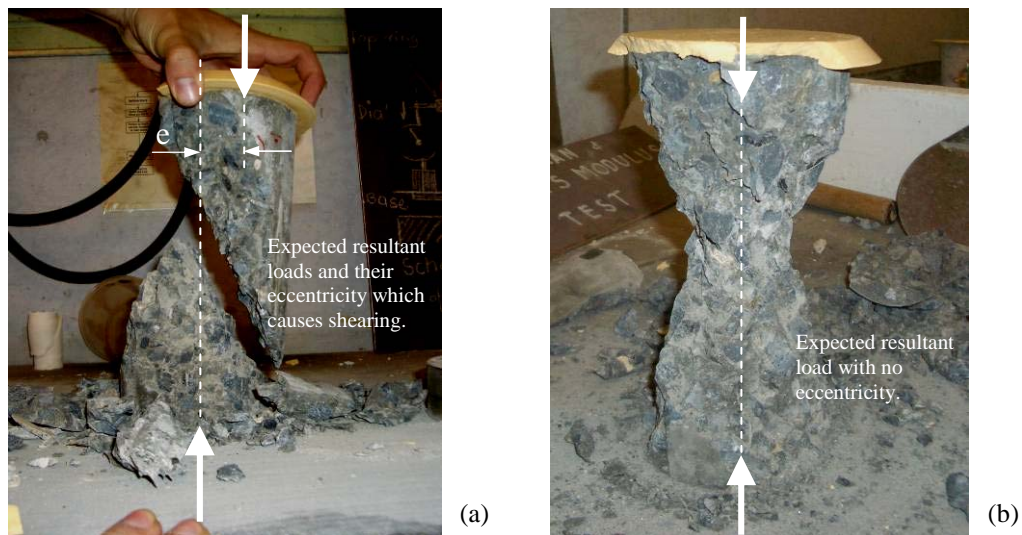
Figure 3-11 *Premature failure due to eccentric loading*
a) Diagonal shearing of the concrete cylinder due to eccentric loading,
b) Failed specimen under uniform compression [with excess loose concrete removed].

Where premature failure was evident in the compressive strength tests, the resulting data was ignored and did not contribute to the final conclusions. In occurrences where only small signs of premature failure were evident, the value(s) obtained were compared to other identical tests and the data was either included or ignored based on an educated interpretation and examined crack formation. For all tests every attempt was made to exclude premature failure, performing multiple tests at a certain age (as outlined in Table 3-2) allowed this to occur successfully.

The testing schedule highlighted in Table 3-2 was achieved by testing all cylinders at The University of Adelaide's laboratory. In addition to these tests, mandatory testing was done at Readymix's laboratory, with the cylinders cured in the standard curing bath (3 compressive strength tests in total, one at 7 days and two at 28 days). A comparison was made between the results produced at these two laboratories to rule out any inconsistencies associated with differing testing equipment. Figure *3-12* displays an example of this comparison. As can be seen there is minimal statistical difference in the strengths recorded from different laboratories when cylinders have identical curing. So we can conclude that there is insignificant difference between the testing procedures of the two different laboratories.
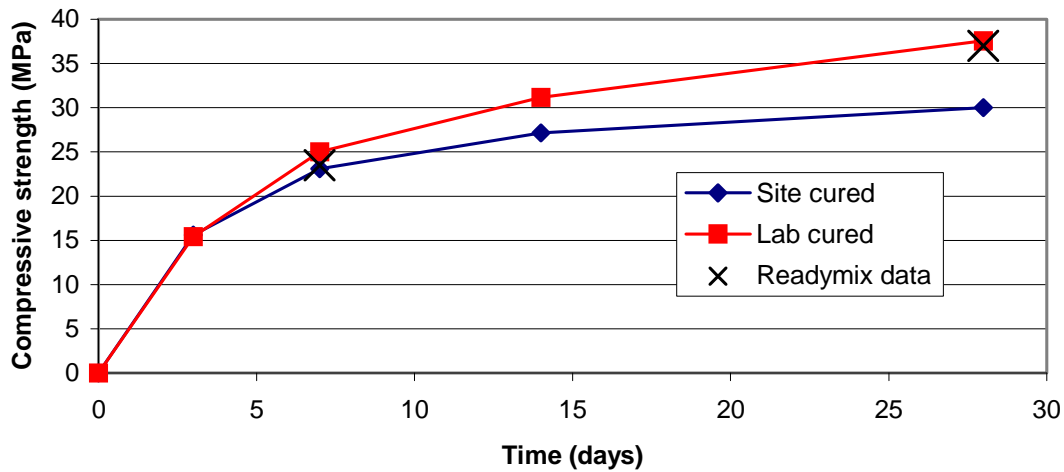
Figure 3-12 *Comparison of Strength results from Readymix and Adelaide University laboratories.*

From the testing procedure, graphs of compressive strength gain were produced for each slab pour. One of the main reasons these strength gain graphs were of such interest is due to the strength specification of $f_c > 24$ MPa at 7 days, as explained in Section 3.2.3. N32 concrete was the concrete specified for the slabs due to satisfactory long term strength. Furthermore, at 7 days, 24 MPa was considered achievable during typical Adelaide weather. However, as shown in the recorded strength gain of the N32 mix in Figure 3-12, 24 MPa was only marginally achievable at 7days, even for cylinders cured in the laboratory under ideal conditions. Due to this marginal difference between required strength limits and tested laboratory strengths, the timing of early age strength gain became an issue. The most probable reason for this lack of early age strength gain is due to the concrete pouring occurring during the colder winter months, where the predicted strength gain was based on an average ambient temperature of the whole year. Compounding this problem was the selected pouring times of the concrete for the slabs. Due to the construction site's location (high traffic area of the CBD) the only time to achieve the slab pours was between 2 am and 6 am. Therefore, during the most crucial concrete curing time the ambient temperature is an absolute minimum (as low as 6 ${}^oC$).

The air cured cylinders contained significantly lower early age strength than the laboratory cured cylinders. This suggests that the slab may not have contained sufficient compressive strength to be stressed at the expected 7 days. To overcome this problem the mix design was altered mid-way through the project to N40 concrete. This change in mix design not only increased the final strength of the concrete mix, but significantly increased the early age strength (to comply with the 7 day compressive strength target). Figure 3-13 highlights the difference between concrete strength performance of the N32 mix and the N40 mix.
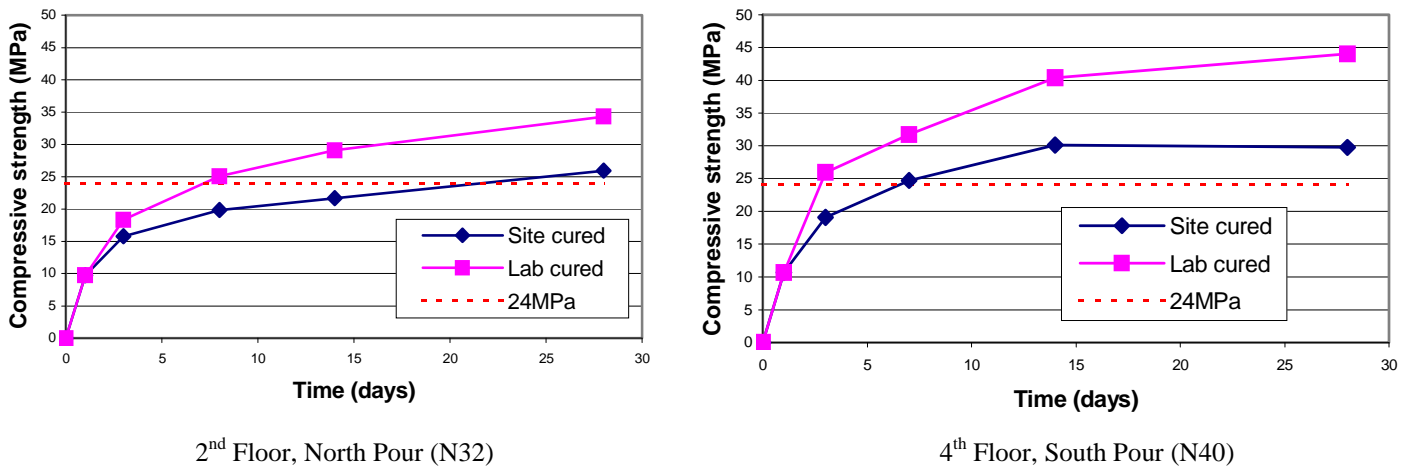
2nd Floor, North Pour (N32)   4th Floor, South Pour (N40)

Figure 3-13 Example f'c gain for differently cured N32 and N40 concrete.

As can be seen in Figure 3-13 the lab cured cylinders outperformed the site cured cylinders at all ages for both the N32 and the N40 mix. It is also noticeable in this comparative graph that the 24 MPa threshold for strength is achieved at a wide range of times. This threshold was reached as early as 3 days for the N40 mix cured in the laboratory, but took up to approximately 22 days to reach the same strength for the site cured N32 mix. This time difference has considerable potential to drastically affect the construction time of the multistorey building.

For statistical reasons it is worth highlighting that the data points displayed in Figure 3-13 were obtained by testing for compressive strength on at least 2 separate cylinders, with the displayed value being the average. Figure 3-14 details a summary of the recorded concrete strength gain from each of the slabs sampled at 151 Pirie. Figure 3-15 displays a comparative summary of the f_c data, with the N32 and the N40 data displayed separately.

Throughout the months of compressive strength testing a few interruptions to the testing schedule occurred. Missing data points occured due to uncontrollable situations such as testing malfunctions, damaged cylinders on site or limited access to site. There were a few situations where Readymix required some research cylinders for their own laboratory analysis to help confirm the slab's strength. This led to some of the data points not being obtained at the times outlined in Table 3-2. In situations where testing times required altering, the next most appropriate testing time to sustain a smooth strength gain graph was selected. Concrete samples were unable to be taken for three out of the fourteen slab pours. This was due to time restraints associated with setting up thermocouples. Appendix E contains specific recorded details and comments about each test for f_c.
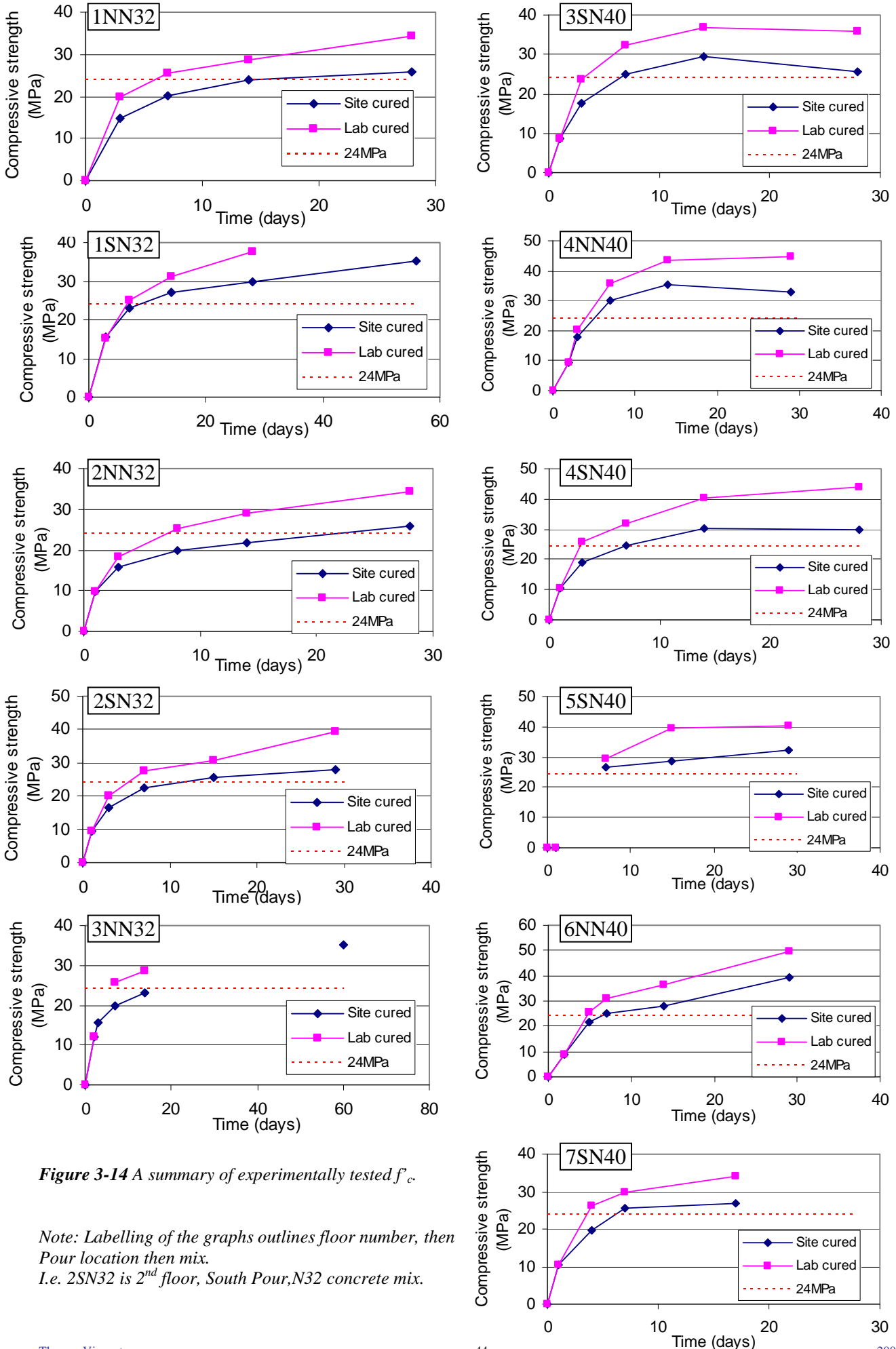
Figure 3-14 *A summary of experimentally tested f'$_c$.*

Note: Labelling of the graphs outlines floor number, then Pour location then mix.
I.e. 2SN32 is 2nd floor, South Pour,N32 concrete mix.
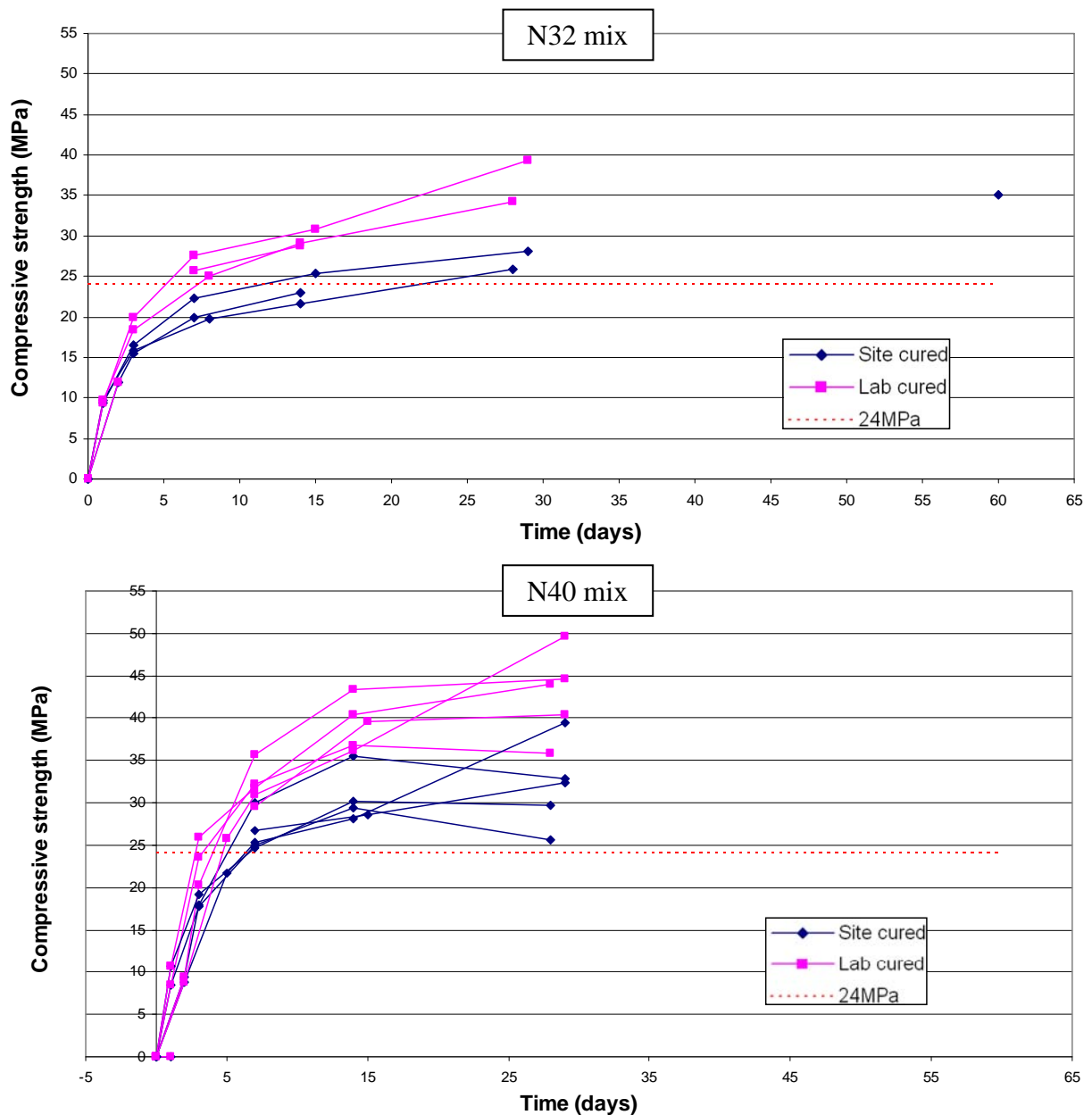
Figure 3-15 *Compressive strength performance of the N32 and N40 mixes.*

Data from Readymix's mandatory monitoring of f_c, which is independent of the cylinders poured for this research, supplied this research with additional data for lab cured cylinders tested at 7 and 28 days. These cylinders were not managed or handled by this research and although there may be some slight differences, such as demolding time and testing times, the data obtained by Readymix remains relevant to this research.

The concrete sampled for this research was 30 cylinders for each slab pour, taken from one concrete truck. The mandatory concrete sampling by Readymix required a frequency of 3 cylinders for every $50m^3$ or part thereof. Considering that the concrete slab pours are in the order of $100m^3$ to $200m^3$ this requirement supplied this research with 3 to 5 extra sets of concrete data. In total this equated to

9 to 15 extra lab cured data points for each pour, or approximately 150 extra data points in total. These strength gain graphs are displayed in Figure 3-16.
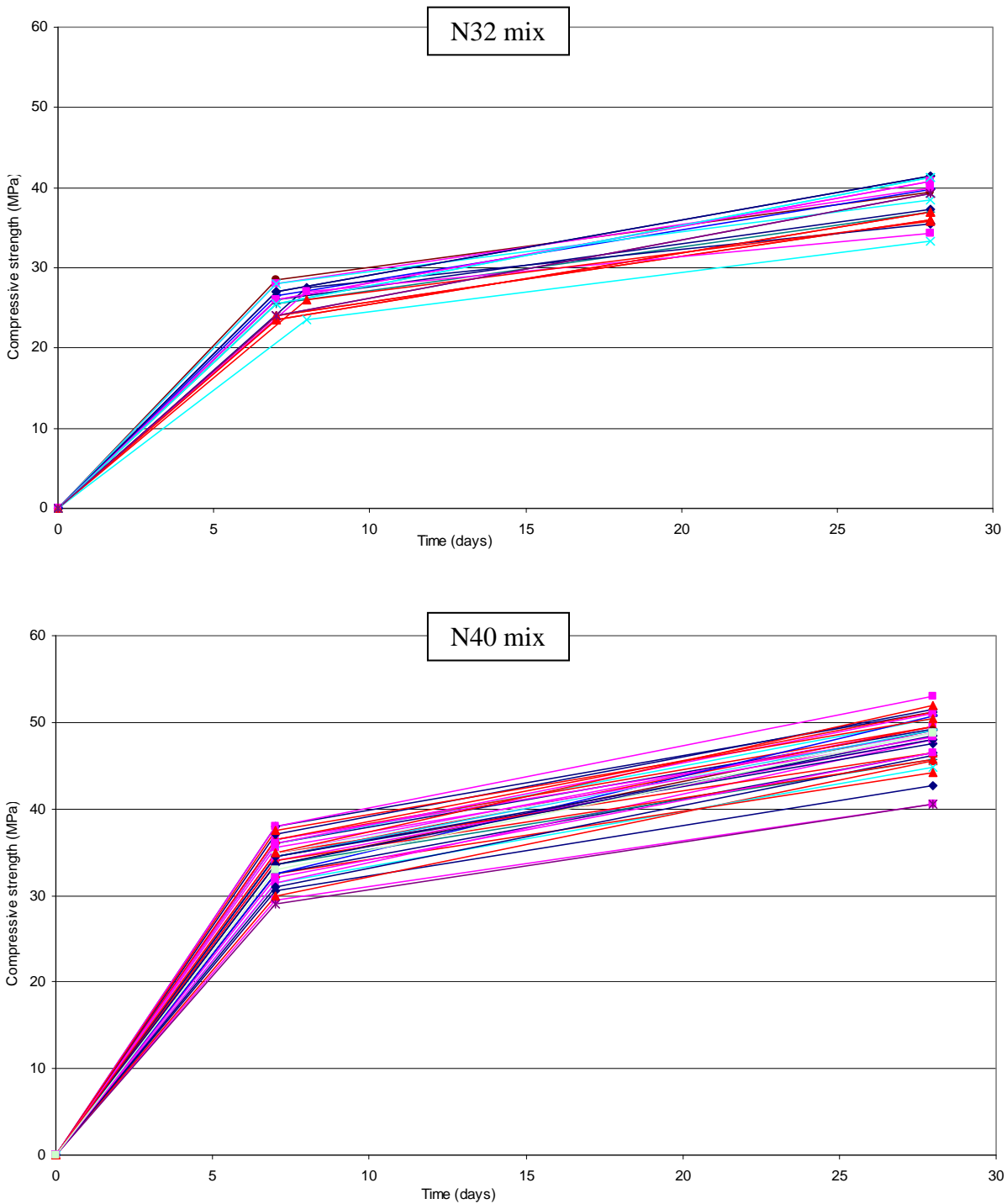
Figure 3-16 *f_c performance of the N32 and N40 mixes for Readymix's samples.*

More detail on the data analysis of the experimental results of f_c can be found in Section 3.4. Compressive strength is almost always the most commonly tested material property in the concrete industry. However, the material property that has the most affect on serviceability behaviour is the relationship between applied stress and experienced strain, namely the modulus of elasticity (E_c).

3.3.2. Modulus of Elasticity (E_c)

Modulus of elasticity (E_c) of the concrete for the slab pours was measured using the standard two-ring rig, as specified in AS 1012.17 (1997). This set up allows a transducer to record the vertical deflection of the cylinder whilst under a steadily increasing compressive stress. The compressive stress was recorded by an internal load cell in the compression rig. To monitor the data acquisition the computer program *Visual Designer* was utilised. Figure 3-17 shows an example of the standard two-ring rig experimental apparatus.

Figure 3-17 Modulus of elasticity two ring test rig.

Australian Standards (AS 1012.7, 1997) states that E_c can only be tested within the compressive stress range of less than 40% of f_c. So for this research it was logical to first undertake a destructive test for f_c, to obtain f_c and the E_c test threshold, then perform the E_c test on a separate, equivalent cylinder. If loads of only less than $0.4f_c$ were applied to the cylinder then that same cylinder could be used again for an accurate f_c test, without premature failure. This method of testing reinforces the reason for the arrangement of the testing schedule proposed in Table 3-2, where a single cylinder can be tested for both f_c and E_c.

Due to the non–destructive nature of the E_c experiments, numerous tests could be performed on the same cylinder. In this research testing for E_c three times on the same cylinder, and taking an average, was considered an adequate amount statistically whilst also achievable within time restraints. Figure 3-18 displays the process of obtaining the value of E_c utilised in this research, including example data. It is worth highlighting, for statistical purposes, a final value of f_c is obtained from testing three separate cylinders, whilst a final value of E_c is obtained from testing one cylinder three separate times.

Cylinder Testing Sequence

#1   #2   #3

Test number	1	2	3	4	5	6
Material property tested	f_{c1}	E_{c1}	E_{c2}	E_{c3}	f_{c2}	f_{c3}
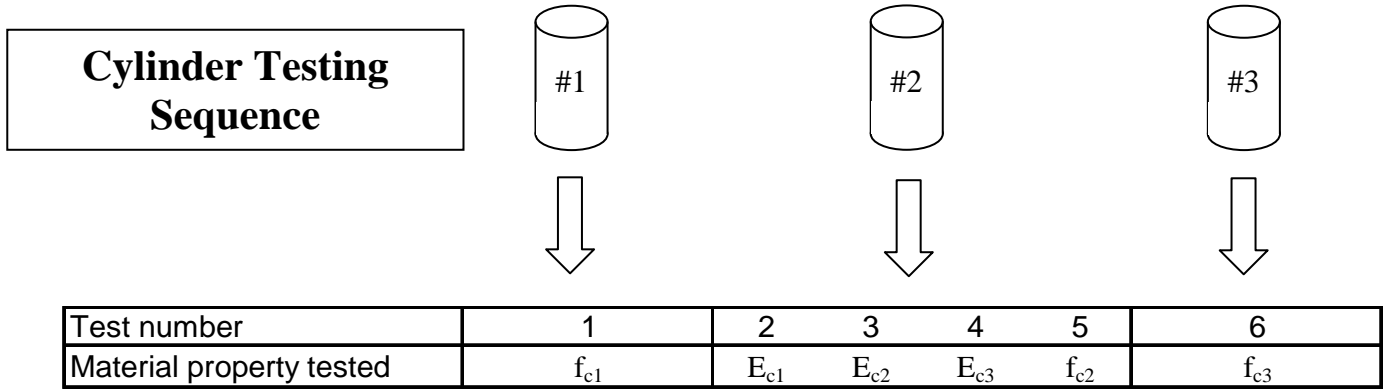
Example Data

Test 1:

f_{c1}=15.58 MPa

(40% of f_{c1}= 6.23 MPa
Notice that tests for E_c do not pass this threshold)

Test 2:

$y = 21017x - 0.6073$

E_{c1}

Test 3:

$y = 20432x + 0.1387$

E_{c2}

Test 4:

$y = 21092x - 0.0227$

E_{c3}
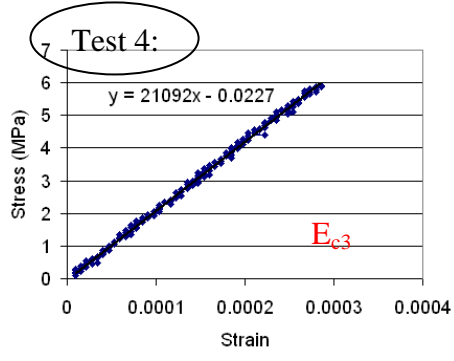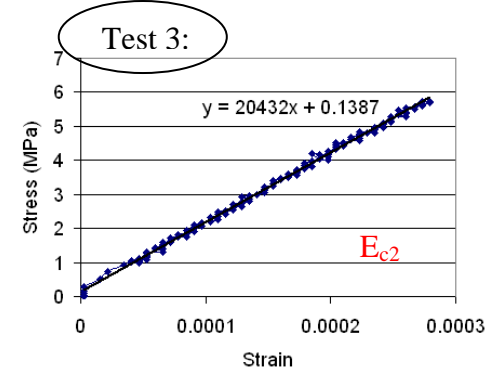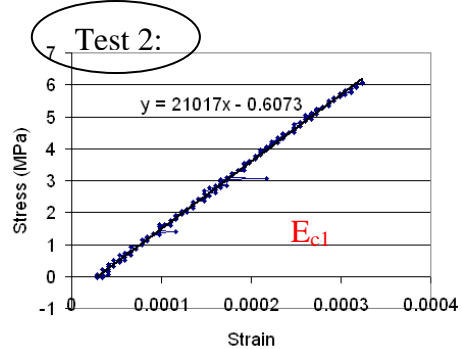
Test 5:

f_{c2}=15.83 MPa

Test 6:

f_{c3}=15.9 MPa

CONCLUSIVE DATA SET:

$\mathbf{f_c}$ = average (15.58,15.83,15.9)
       = **15.77 MPa.**
$\mathbf{E_c}$ = average (21017, 20432, 21092)
       = **20847 MPa**

Figure 3-18 Data acquisition process for fc and E_c

The compressive strength requirement outlined in Figure 3-13, which caused the concrete mix upgrade from N32 to N40, also caused an increase in E_c in the slab. This change of E_c was of minimal to no significance for the construction timing, but was of large significance to serviceability behaviour such as deflection predictions. Figure 3-19 shows an example of the different E_c values recorded from the lab and site cured cylinders for the N32 and N40 mixes.

2nd Floor, North Pour (N32)   4th Floor, South Pour (N40)
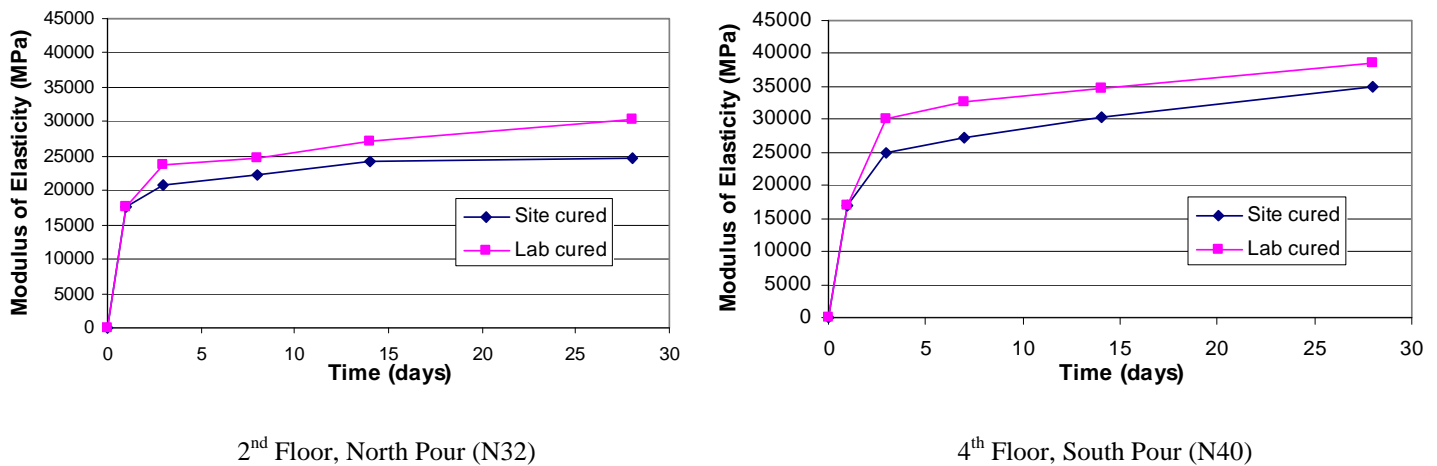
Figure 3-19 *Example E_c gain for differently cured N32 and N40 concrete.*

Similar to the f_c results, it can be seen that the lab cured cylinders out performed the site cured cylinders at all ages for each mix. It was also evident that a significant increase in E_c performance was noticed when increasing the mix from N32 to N40. Unlike the increase in f_c, which relates to an increase in ultimate behaviour, an increase in performance of serviceability behaviour (E_c) was of more importance when predicting deformations. A summary of all of the E_c data recorded from the concrete samples taken from 151 Pirie can be found in Figure 3-20. Figure 3-21 displays a comparative summary of the E_c data, with the N32 and the N40 data displayed separately.
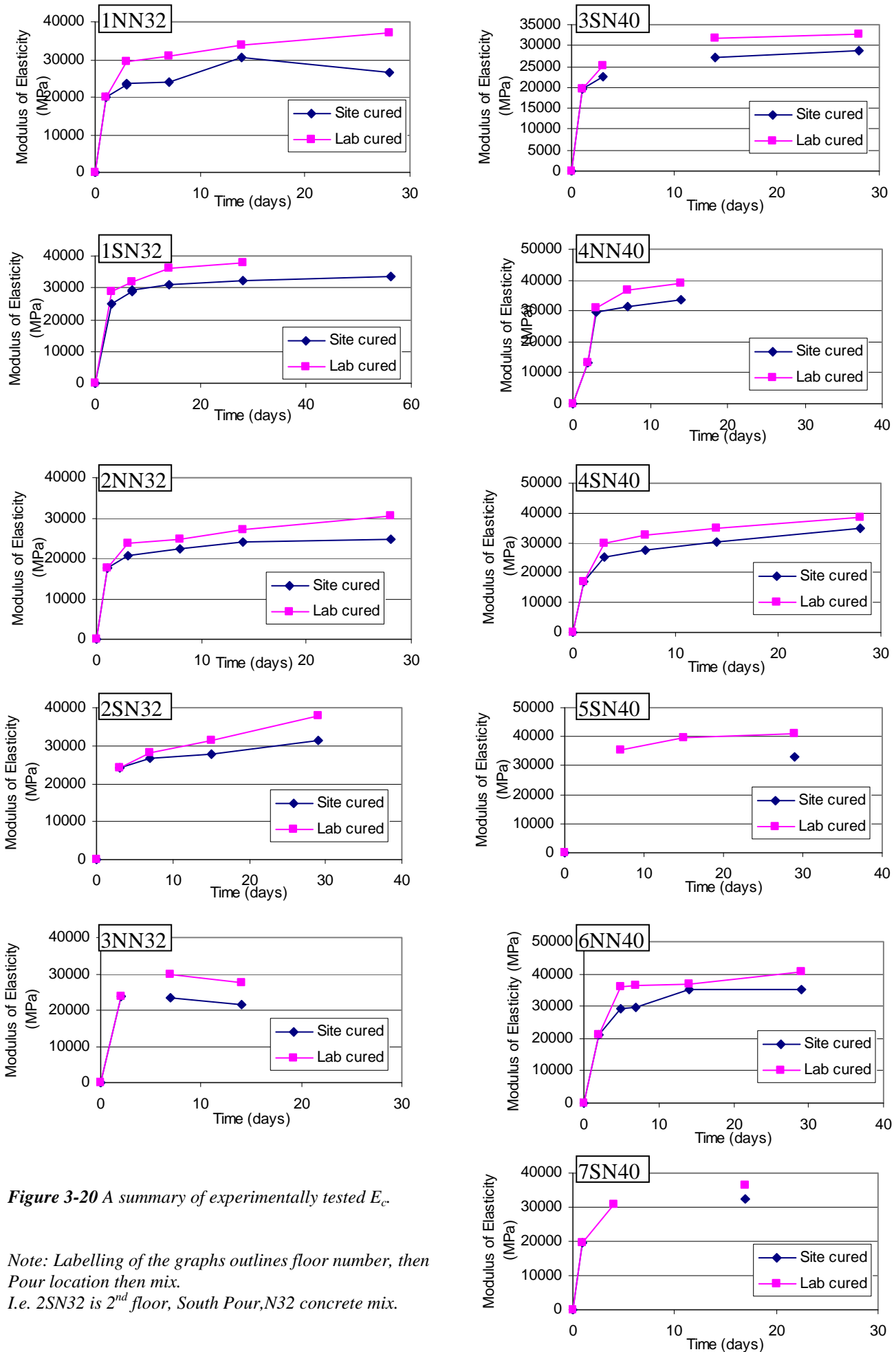
Figure 3-20 *A summary of experimentally tested E_c.*

Note: Labelling of the graphs outlines floor number, then Pour location then mix.
I.e. 2SN32 is 2nd floor, South Pour,N32 concrete mix.
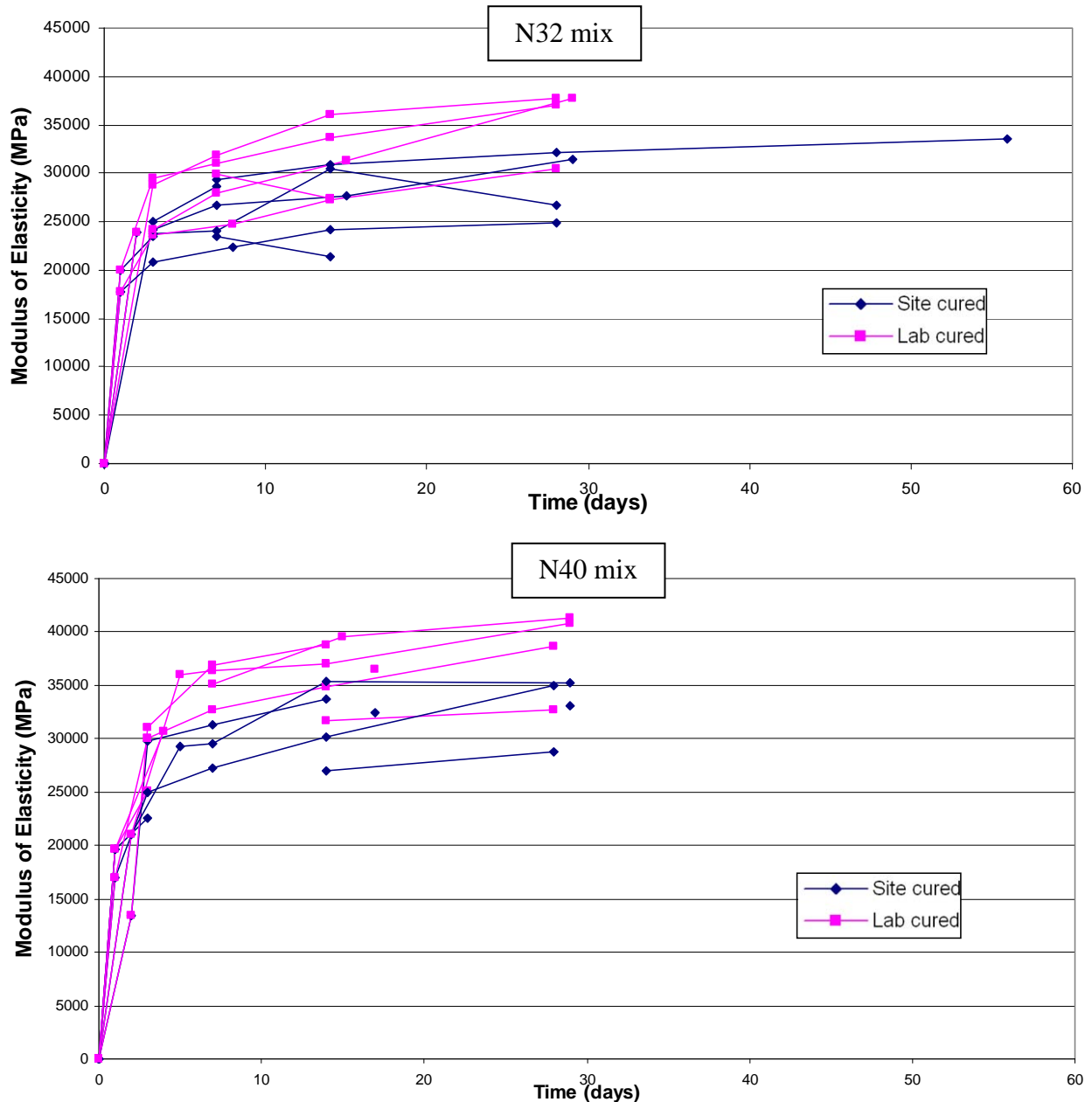
Figure 3-21 Modulus of Elasticity performance of the N32 and N40 mixes.

A noticeable outcome from the E_c gain results was that there are multiple sections where E_c reduces over time, which was not an expected outcome. The reasoning for this was hard to pinpoint for each situation but was potentially due to natural differences between each concrete cylinder. A slight difference between individual cylinders can give the appearance that the concrete mix was gaining and losing E_c sporadically over time. This was not considered to be the case for these concrete mixes. Every step was taken to attempt to create identical concrete cylinder samples, with identical compaction. However, considering each data point was taken from a different cylinder, each cylinder may not be gaining E_c uniformly (due to slightly different concrete sampling, curing conditions, compaction or laboratory handling) and hence this scatter graphically appears as though

concrete can lose E_c over time. The potential for concrete to lose E_c over time is not considered a conclusive outcome in this research.

More details on the experimental results and data analysis for the material property E_c can be found in Section 3.4. Recorded data for each individual E_c test, including the manual tests achieved without the electronic transducer, can be found in Appendix F.

3.3.3. Tensile Strength (f_t)

Section 2.4.3 of this research explains the different methods of experimentally testing for tensile strength (f_t). It was concluded that the splitting tensile strength (STS) test would be utilised in this research and the data from these tests would be converted into f_t values which relate to flexural tensile strength (FTS). FTS is more appropriately applicable for this research due to the nature of the flexural loading on the PPS slabs.

3.3.3.1. Splitting Tensile Strength (STS) test results

Tensile strength (f_t) of the concrete supplied to 151 Pirie was experimentally tested via the splitting tensile strength (STS) test. This material property test, commonly referred to as the Brazilian test, is displayed in Figure 3-22. The STS tests performed in this research involved a standard concrete sample cylinder (200 mm by 100 mm diameter) loaded laterally with an increasing compressive stress until the cylinder splits cleanly in two. To ensure that the cylinder was loaded symmetrically (to reduce eccentricity or any other unwanted factors that will cause premature failure) a steel testing rig is utilised and can be seen in Figure 3-22. A sample of a failed specimen can be viewed in Figure 3-23.
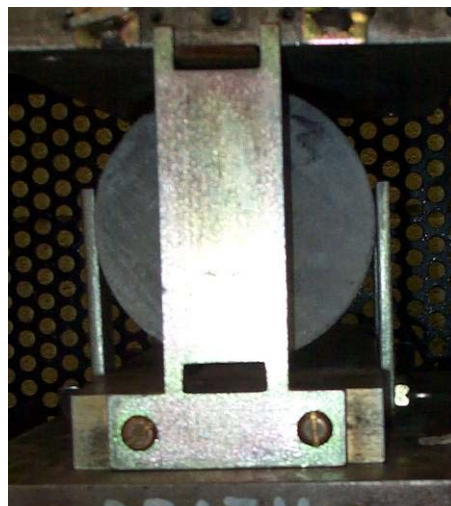
Figure 3-22 The Splitting Tensile Strength (STS) testing rig

Figure 3-23 *An example of a failed specimen from the STS test.*

The STS test required the application of an increasing compressive stress to the concrete cylinder and the peak compressive stress resisted by the specimen was documented. In accordance with the Australian Standards (AS 1012.10, 1985) this peak compressive stress was converted into an equivalent splitting stress experienced by the cylinder at 90° to the compressive stress. Equation 3-1 was used to obtain the peak splitting stress. Figure 3-24 is the testing requirement given by AS 1012.10 (1985) to obtain f_t for the STS test. The testing requirement was adjusted slightly to accommodate for the 100 mm by 200 mm diameter cylinders, instead of the expected 150 mm by 300 mm cylinders. This adjustment was a simple geometric adjustment which had no affect on the load application process.

$$T = \frac{2000P}{\pi LD}$$

Equation 3-1

Where:
T = Indirect tensile strength, in MPa.
P = Max applied force indicated by the testing machine, in kN.
L = Length, in mm.
D = Diameter, in mm.

NOTE:
This figure is included on page 53 of the print copy of the thesis held in the University of Adelaide Library.

Figure 3-24 *Australian Standards testing rig requirement for obtaining STS (AS 1012.10, 1985)*

Initially f_t was a material property that was intentionally omitted from the testing schedule for 151 Pirie. This was due to the expected insignificance of tensile strength in the deflection behaviour of PPS slabs. Due to the applied prestressing the slabs were only expected to crack near ultimate loading, therefore f_t was considered insignificant for the prediction of serviceability behaviour addressed in this research. After the initial f_c test results yielded lower than expected values for the air cured cylinders, incorporating f_t in the testing schedule was arranged. Reasons for this were mainly to confirm the expected lack of cracking, rather than concerns of member ultimate strength or potential damage when applying prestressing.

If cracking of the PPS slabs was experienced under serviceability loading, assumptions within deflection prediction equations would yield incorrect deflection values. Many of the deflection prediction equations are based on the assumption of linear elastic theory. This is incorrect for occurrences of member cracking, even in situations where prestressing significantly reduces the effects of cracking. In summary it can be said that only a minor analysis to confirm that f_t values are above the required threshold for cracking was considered sufficient for this research. Exact values of f_t were not of concern for this research. Adequate tensile strength and the direct relation it has to member cracking was the only concern.

Results of the experimental tests for f_t are displayed in Figure 3-25. Reasons for missing data points were due to the influence on the project from natural incidents on site, which were explain earlier for the material properties f_c and E_c. It was also noticeable that recordings for f_t did not begin until the second pour of the second storey slab. This was the time when the inclusion of the f_t tests was decided upon. For statistical reasons it is worth stating that each data point in Figure 3-25 is obtained by testing only 1 concrete cylinder.

It is evident in Figure 3-25 that the tensile strength performance of concrete cylinders cured in laboratory conditions outperformed the cylinders air cured at all ages. This trend was noticeable for each material property experimentally tested (f_c, E_c and f_t). This agrees with the concept of the 'maturity rule' principle explained in Section 2.5. This rule is typically only applied directly to f_c, but considering the experimental outcomes and the relationships between f_c and other material properties it was evident that this concept holds true for each material property.

Figure 3-25 *A summary of experimentally tested STS values.*

Note: Labelling of the graphs outlines floor number, then
Pour location then mix.
I.e. 2SN32 is 2nd floor, South Pour,N32 concrete mix.

3.3.3.2. Flexural Tensile Strength (FTS) conversion results

As stated previously a conversion from STS to FTS was required for this research as FTS was more applicable to the loading scenario experienced in PPS slabs. Explained previously in the Literature Review is Narrow and Ullberg's (1963) extensive research on this specific topic. Their research covers the specific relationship between STS and FTS. From their experimental data, which has been displayed previously in Figure 2-8, a conversion equation was created and utilised to convert the STS values recorded in this research into FTS values. This equation, Equation 2-1, has been presented in the Literature Review.

Figure 2-8 proves that Equation 2-1 remains significantly accurate for values of STS between approximately 2.0 MPa and 4.7 MPa. It can be seen in Figure 2-8 that all of the data for this research, except one point, lie between these boundaries. Therefore, with the exception of the stated data point, the STS data has been converted into FTS data and is displayed in Figure 3-26. Further discussion and analysis of the STS and FTS experimental results can be found in Section 3.4.4
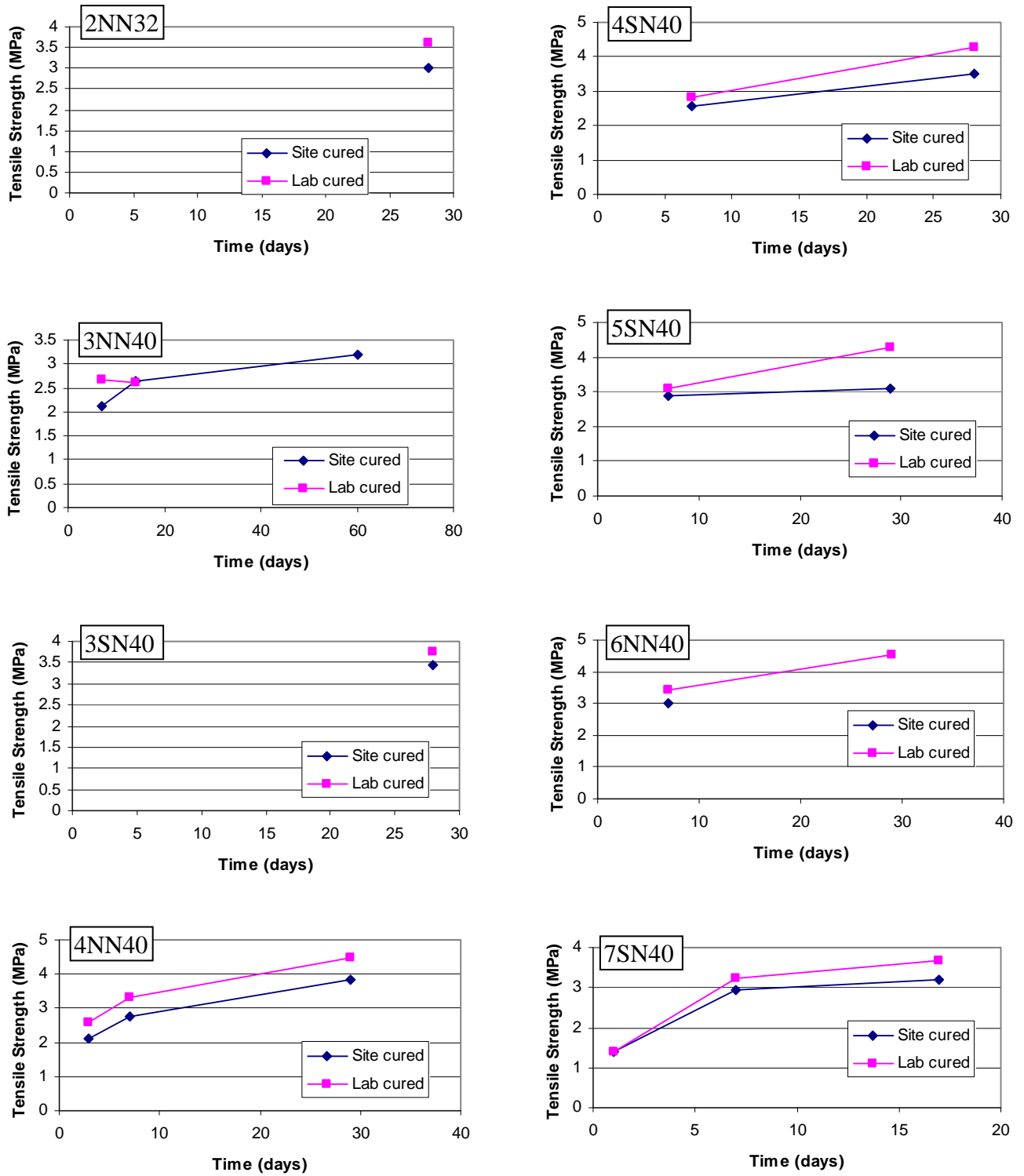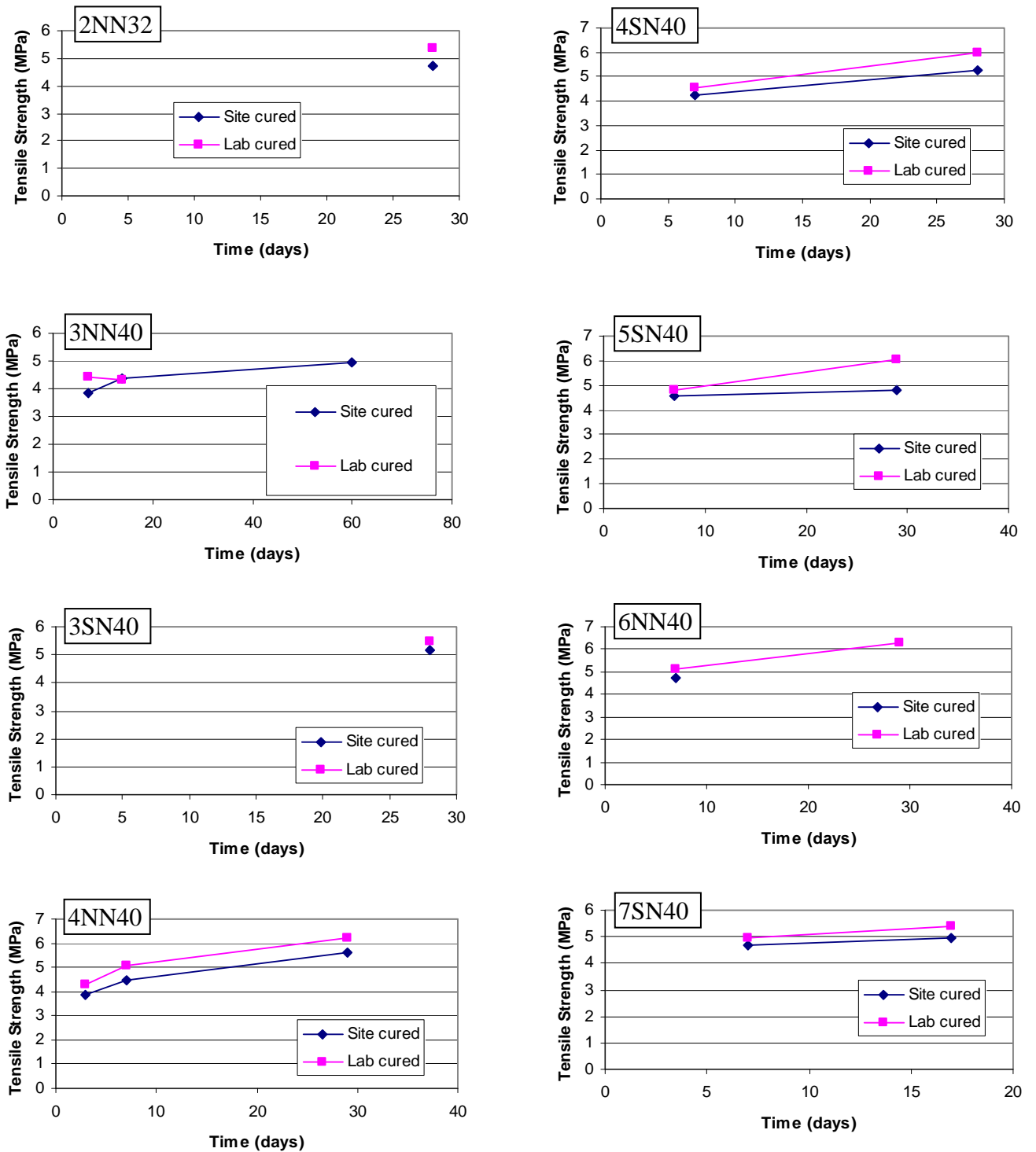
Figure 3-26 A summary of experimentally tested FTS values.

Note: Labelling of the graphs outlines floor number, then Pour location then mix.
I.e. 2SN32 is 2nd floor, South Pour,N32 concrete mix.

3.3.4. Creep

Creep characteristics of the N32 and N40 concrete were experimentally recorded by this research. To determine the creep strains, four cylinders from each mix were placed in standard creep rigs (as specified in AS 1012.16 (1996)), along with two control specimens, and all were placed in a temperature controlled room in the Chapman Laboratory of the University of Adelaide. To ensure that applied load on the four cylinders was maintained at 40% of the 28 day ultimate load, each rig was monitored by strain gauging the bars of the rig. Figure 3-27(a) shows the creep rig set utilised. Shortening of the individual cylinders was measured by the use of 4 inch demountable mechanic strain gauges (DEMEC strain gauges). The DEMEC targets were placed at 3 locations on the surface of each cylinder; an example of this can be seen in Figure 3-27(b).

(a)   (b)
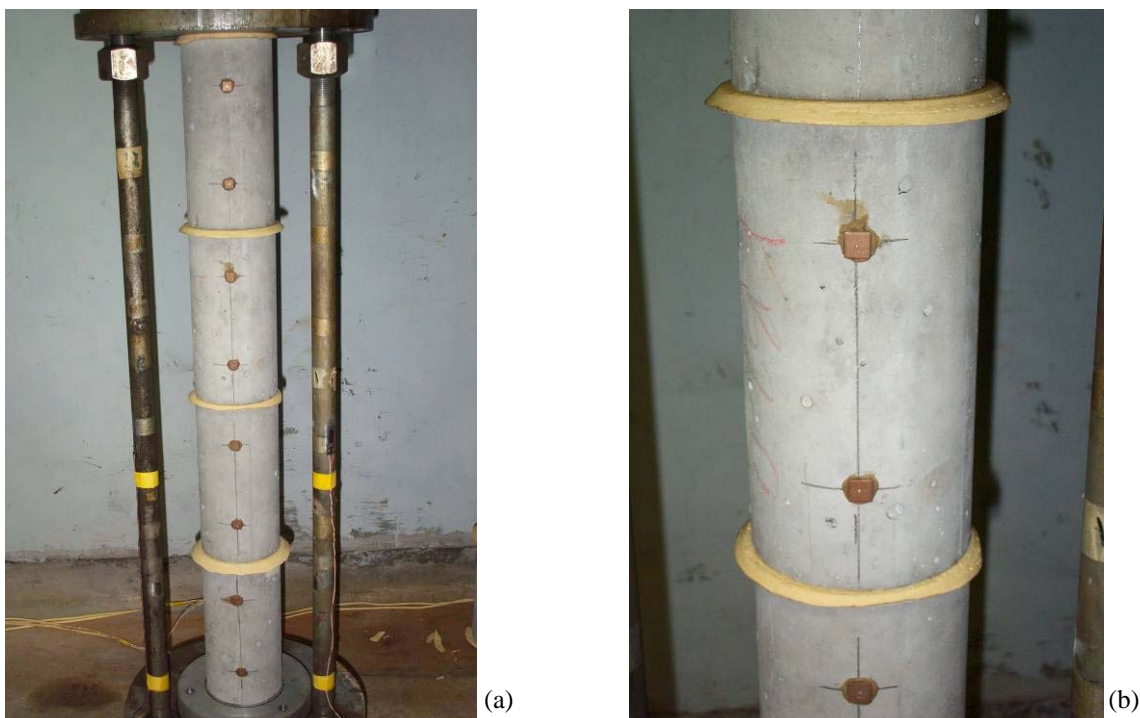
Figure 3-27 *Creep rig arrangement*
a) Creep rig including strain gauges on steel bars, b)4 inch DEMEC gauges

Unfortunately during the initial load application stages, the hydraulic jack used to apply the compressive stress (40% of f_c) contained questionable calibration for both the N32 cylinders and the N40 cylinders. This resulted in an applied stress that was below the required 40% of f_c. DEMEC gauge readings were taken for the weeks following the initial load application. Once the incorrect calibration was discovered it was decided not to repeat the creep rig tests. The concrete mixes utilised for this project (N32 and N40) are concrete mixes that Readymix have tested for creep numerous times. The creep strain results that the Readymix laboratory have obtained over years of research would supply significant confidence for use with this research. It was advised by Readymix that a creep factor of $\Phi = 2.6$ is accurate for both the N32 and N40 mixes.

3.3.5. Shrinkage

Shrinkage tests were performed and monitored entirely by the Laboratory at Readymix Brompton due to specific equipment required. Shrinkage molds were cast for each mix at least 3 separate times and an average was taken. The shrinkage results for both the N32 and N40 mixes produced shrinkage strains within the typical region of $\varepsilon_{sh} = 400$ microstrain. Due to the minimal affect shrinkage has on very thin concrete members, specific values of shrinkage were not a major focal points. Therefore, for deflection prediction calculations in this research it can be confidently concluded that $\varepsilon_{sh} = 400$ microstrain.

3.3.6. Summary of Acquired Material Property Data

The summary of the material property testing schedule that was performed as part of this research is shown in Figure 3-28 and continued in Figure 3-29. It can be seen that the testing times (1 day, 3 days, 7 days, 14 days, 28 days) are conveniently achievable with in the construction timeline, whilst still maintaining sufficiently smooth material property gain graphs. Figure 3-28 and Figure 3-29 also highlight the final cycle times that were an outcome at 151 Pirie. The site specific outcome of cycle times is discussed and analysed in detail in Section 3.5.

Acquiring material property data from an actual construction site such as 151 Pirie is a crucial step in this research. Obtaining material property data from concrete samples that have been exposed to realistic conditions on site, such as ambient temperatures, is crucial. Utilising this on site data in deformation prediction models allows a true justification of the deflection prediction methods without potential inaccuracies from utilising laboratory performance data.

The material property data from 151 Pirie can be considered to fall into one of two categories; 1) Primary material properties (f_c, E_c and f_t) due to their direct effect on member behaviour and 2) Secondary material properties (Creep and shrinkage) due to their indirect, long term effect on member behaviour. Primary material properties are of more concern for this research due to their dependence on ambient temperatures and curing methods.

Testing Diary

Floor / concrete grade / column key:
- 1st floor: N32 (1S), N32 (1N)
- 2nd floor: N32 (2S), N32 (2N)
- 3rd floor: N40 (3S), N32 (3N)
- 4th floor: N40 (4S), N40 (4N)
- 5th floor: N40 (5S), N40 (5N)
- 6th floor: N40 (6S), N40 (6N)
- 7th floor: N40 (7S), N40 (7N)

Date	1S	1N	2S	2N	3S	3N	4S	4N	5S	5N	6S	6N	7S	7N	Cycle time	COMMENTS
11/5/05	pour															
12/5/05	dm/1d															
13/5/05																
14/5/05	3d															
15/5/05																
16/5/05															*9day cycle time*	
17/5/05																
18/5/05	7d															
19/5/05																
20/5/05		pour														
21/5/05		dm/1d														
22/5/05																
23/5/05		3d														
24/5/05																
25/5/05	14d														*10day cycle time*	
26/5/05																
27/5/05		7d														
28/5/05																
29/5/05																
30/5/05			pour													
31/5/05			dm/1d													
1/6/05																
2/6/05			3d													
3/6/05		14d													*7day cycle time*	
4/6/05																
5/6/05																
6/6/05			7d	pour												
7/6/05				dm/1d												
8/6/05	28d															
9/6/05	creep			3d												
10/6/05	creep															
11/6/05	creep															
12/6/05															*11day cycle time*	
13/6/05	creep		14d	7d												
14/6/05																
15/6/05	creep															
16/6/05																
17/6/05		28d			pour											
18/6/05	creep				dm/1d											
19/6/05																
20/6/05				14d	3d											
21/6/05															*8day cycle time*	
22/6/05	creep															
23/6/05																
24/6/05					7d											7 day Ec cylinder damaged (for 3S)
25/6/05						pour										
26/6/05																Testing could not be performed at day 1 due to computer malfunctions, next opportunity, day 2, is taken (3N).
27/6/05			28d			dm/2d										
28/6/05						3d										
29/6/05	creep															
30/6/05															*11day cycle time*	
1/7/05					14d											Ec tests are now performed manually due to computer malfunction.
2/7/05						7d										
3/7/05																
4/7/05				28d												Computer malfunction rectified.
5/7/05	creep															
6/7/05	56d						pour									
7/7/05							dm/1d									
8/7/05																
9/7/05						14d	3d								*7day cycle time*	
10/7/05																
11/7/05																
12/7/05																
13/7/05						7d	pour									
14/7/05							dm/1d									

Figure 3-28 Material Property testing schedule for 151 Pirie

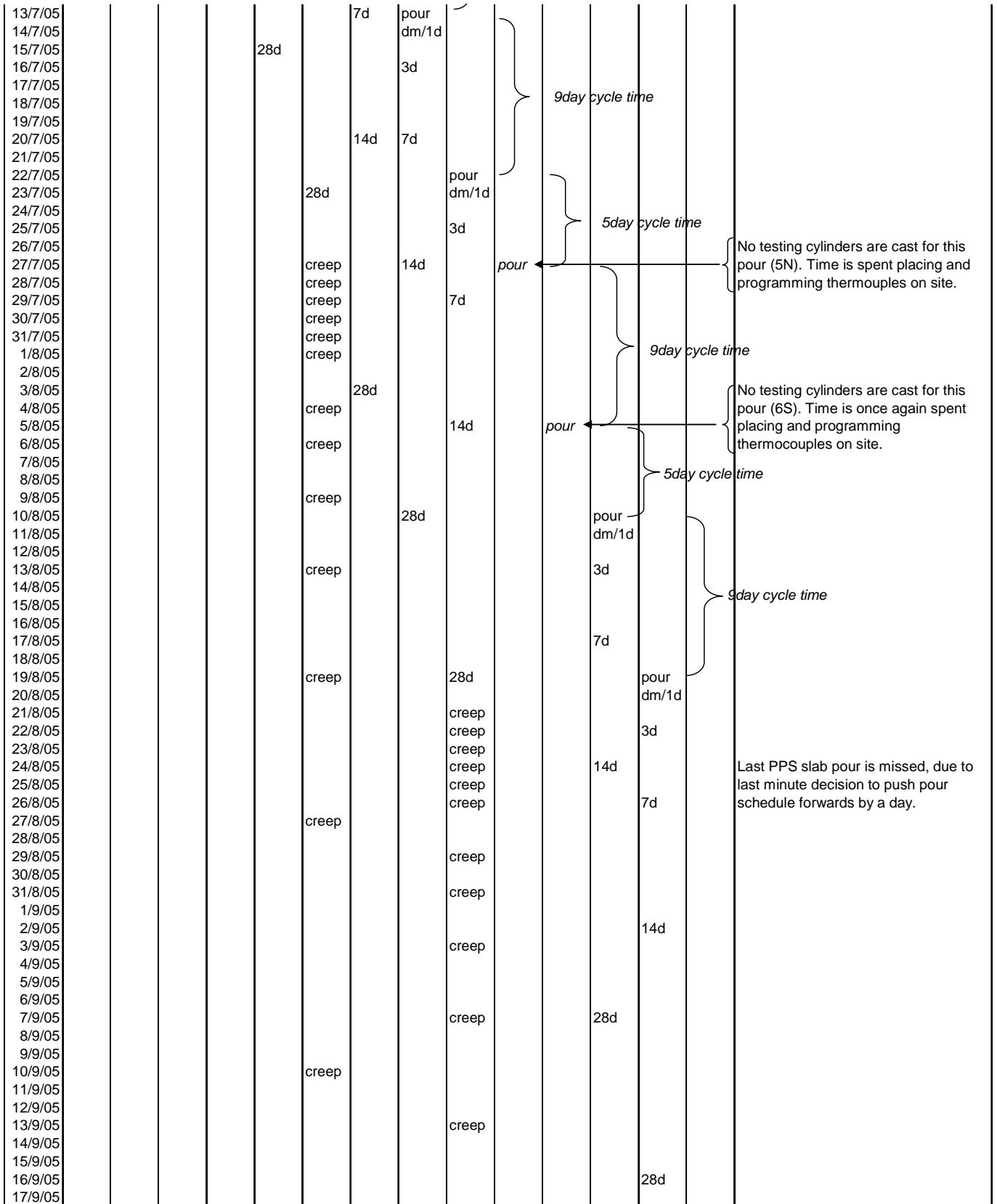| Date												
13/7/05						7d	pour dm/1d					
14/7/05												
15/7/05				28d								
16/7/05							3d					
17/7/05								9day cycle time				
18/7/05												
19/7/05												
20/7/05						14d	7d					
21/7/05												
22/7/05							pour dm/1d					
23/7/05					28d							
24/7/05								5day cycle time				
25/7/05							3d					
26/7/05										No testing cylinders are cast for this pour (5N). Time is spent placing and programming thermouples on site.		
27/7/05					creep		14d	pour				
28/7/05					creep							
29/7/05					creep		7d					
30/7/05					creep							
31/7/05					creep							
1/8/05					creep							
2/8/05								9day cycle time				
3/8/05						28d				No testing cylinders are cast for this pour (6S). Time is once again spent placing and programming thermocouples on site.		
4/8/05					creep							
5/8/05							14d	pour				
6/8/05					creep							
7/8/05												
8/8/05								5day cycle time				
9/8/05					creep							
10/8/05						28d		pour dm/1d				
11/8/05												
12/8/05												
13/8/05					creep		3d					
14/8/05								9day cycle time				
15/8/05												
16/8/05												
17/8/05							7d					
18/8/05												
19/8/05					creep		28d	pour dm/1d				
20/8/05												
21/8/05							creep					
22/8/05							creep	3d				
23/8/05							creep					
24/8/05							creep	14d	Last PPS slab pour is missed, due to last minute decision to push pour schedule forwards by a day.			
25/8/05							creep					
26/8/05							creep	7d				
27/8/05					creep							
28/8/05												
29/8/05							creep					
30/8/05												
31/8/05							creep					
1/9/05												
2/9/05								14d				
3/9/05							creep					
4/9/05												
5/9/05												
6/9/05												
7/9/05							creep	28d				
8/9/05												
9/9/05												
10/9/05					creep							
11/9/05												
12/9/05												
13/9/05							creep					
14/9/05												
15/9/05												
16/9/05								28d				
17/9/05												

Figure 3-29 *Material Property testing schedule for 151 Pirie continued.*

The primary material property testing schedule, outlined and discussed earlier in this chapter, was completed successfully with a sufficient degree of detail. In summary over 300 concrete cylinders were tested to monitor the primary material properties. Each daily f_c record contained an average of at least 2 separate cylinders tested under identical conditions and age. Each E_c data point recorded was an average of 3 separate tests on the same cylinder. Each f_t data point recorded was simply the individual recorded value for that test. The secondary material property tests were performed by Readymix. The quantity of material property values recorded on site now allows a significant data analysis of concrete material properties to be completed.

3.4. Analysis of Concrete Material Properties

3.4.1. Introduction

The experimental program carried out on the concrete material properties at 151 Pirie allowed this research to perform a significant analysis of the collected data. This analysis applied material property models, introduced previously in Section 2.4, and compared the outcomes of these models with the recorded data. The accuracy of each material property model was then determined.

Independent of the material property model analysis was the statistical variation that each material property contained at a certain time. The statistical variations of inputs, such as Ec, have a direct effect on the outputs, i.e. deflections. Quantifying the variation of each material property was the first step in producing statistically confident slab deformation predictions. This data analysis section contains analysis of the primary material properties; f_c, E_c and f_t.

3.4.2. Compressive strength (f_c)

The experimental program outlined in the previous chapter presented f_c gain over multiple days (1 day, 3 days, 7 days, 14 days, and 28 days). This gain in material property was of interest only for determining accurate cycle times in the construction stages. For predictions of deformations the data that was of interest was only the 7 day and 28 day f_c values. These two values are the primary two values utilised in design to represent the mean age at which stress transfer occurs (7 days) and the age at which a material property has adequate maturity (28 days). 7 day material properties were crucial inputs for accurate camber calculations (displayed earlier in Table 2-2). 28 day material properties were relevant for all deflection prediction equations. Therefore this section of research focuses primarily on the data obtain only at 7 and 28 days.

The individual 7 day f_c values, for both concrete mixes and both curing conditions, were collated for this analysis. Included in this analysis is data obtained from managing cylinders at both the University of Adelaide as well as the laboratory at Readymix Brompton. Considering laboratory testing times were frequently altered, depending on experimental delays, data from plus or minus 24 hours has been included which is in accordance with AS 1012.9 (1999). The mean (μ) and standard deviation (σ) of each data set was calculated and has been displayed in Table 3-3.

Table 3-3 *Statistical arrangement of 7 day f_c from separate laboratories.*

| | | Readymix's data | | Adelaide Uni data | | | |
| | | Lab cured | | Site cured | | Lab cured | |
		N32 mix	N40 mix	N32 mix	N40 mix	N32 mix	N40 mix
7 day compressive strength (MPa)	no. of data	47	37	5	6	5	6
	mean (MPa)	24.87	32.36	21.02	26.15	25.76	31.66
	standard deviation (MPa)	2.30	3.75	1.56	2.01	1.05	2.23

Considering both sets of lab cured data, from Adelaide University and Readymix, have been proven to contain accurate correlation (Section 3.3.1), these two sets of data have been combined to create a single statistical distribution of lab cured data. This result is presented in Table 3-4.

Table 3-4 *Summary of statistical arrangement of 7 day f_c values.*

| | | Lab cured | | Site cured | |
		N32 mix	N40 mix	N32 mix	N40 mix
7 day compressive strength (MPa)	no. of data	52	43	5	6
	mean (MPa)	24.96	32.27	21.02	26.15
	standard deviation (MPa)	2.22	3.56	1.56	2.01

The individual 28 day f_c values were extracted and subjected to a similar statistical data analysis. Similar to the 7 day f_c values, data from plus or minus 24 hours was included in each statistical distribution. The results of the separate laboratory test results are displayed in Table 3-5. Once again the two sets of lab cured data have been combined into the one data set and displayed in Table 3-6.

Table 3-5 *Statistical arrangement of 28 day f_c from separate laboratories.*

| | | Readymix's data | | Adelaide Uni data | | | |
| | | Lab cured | | Site cured | | Lab cured | |
		N32 mix	N40 mix	N32 mix	N40 mix	N32 mix	N40 mix
28 day compressive strength (MPa)	no. of data	43	54	11	10	11	8
	mean (MPa)	37.51	47.57	28.70	31.92	36.11	43.18
	standard deviation (MPa)	2.41	3.53	3.82	5.05	2.78	4.64

Table 3-6 *Summary of statistical arrangement of 28 day f_c values.*

| | | Lab cured | | Site cured | |
		N32 mix	N40 mix	N32 mix	N40 mix
28 day compressive strength (MPa)	no. of data	54	62	11	10
	mean (MPa)	37.23	47.01	28.70	31.92
	standard deviation (MPa)	2.52	3.94	3.82	5.05

It can be seen in Table 3-6 that the mean values of f_c for lab cured cylinders are sufficiently above the quoted compressive strength for their mix. AS 3600 (2001) requires that the quoted characteristic strength of concrete in compression is defined as the strength attained at 28 days by 95 per cent of the concrete, as assessed by standard tests. Figure 3-30 highlights this compressive strength requirement, where f_{cm} is defined as the mean compressive strength of the population (AS 3600, 2002).

NOTE:
This figure is included on page 65 of the print copy of
the thesis held in the University of Adelaide Library.

Figure 3-30– *Compressive strength variability (Warner et al. 1998).*

The following calculations highlight how the concrete tested in this research compares to this statistical requirement:

Assuming a normal distribution, the probability distribution function is given by Equation 3-2.

$$f(x) = \frac{1}{\sigma\sqrt{2\pi}} \exp\left(-\frac{(x-\mu)^2}{2\sigma^2}\right)$$

Equation 3-2

Therefore;

Lab Cured N32 Concrete;
$x = 32.00$, $\mu = 37.23$, $\sigma = 2.52$
$f(x)_{N32} = 98.1\%$

Site Cured N32 Concrete;
$x = 32.00$, $\mu = 28.70$, $\sigma = 3.82$
$f(x)_{N32} = 20.4\%$

Lab Cured N40 Concrete;
$x = 40.00$, $\mu = 47.01$, $\sigma = 3.94$
$f(x)_{N40} = 96.2\%$

Site Cured N40 Concrete;
$x = 40.00$, $\mu = 31.92$, $\sigma = 5.05$
$f(x)_{N40} = 5.48\%$

An important comparison has been made between the values of standard deviation for the lab cured data and the site cured data, presented in Table 3-4 and Table 3-6. Due to the constant curing temperature present in the laboratory, it was expected that the σ for lab cured cylinders would be less than the σ for site cured cylinders. This trend is notice for the 28 day data but not for the 7 day data. The reason this trend was not noticed for the 7 day data is expected to be due to a low sample

of data. Only 5 and 6 data points were considered for the 7 day data, where 11 and 10 data points were considered for the 28 day data. If the number of samples were increased for the 7 day data, it would be expected that the σ would be higher for the site cured cylinders.

In summary it can be stated that both the N32 and N40 lab cured concrete passed the characteristic strength requirement stated in AS 3600 (2001). However, a significant portion of the site cured cylinders failed this requirement, with only 20.4% and 5.48% passing for the N32 and N40 mixes respectively. It is worth noting that there is no such requirement for characteristic strength at other ages or curing conditions.

It is worth drawing focus to the number of samples tested to obtain the data displayed in the summary tables, Table 3-4 and Table 3-6. For each mix the number of tests performed on laboratory cured cylinders drastically outweighs the number of tests performed on the site cured cylinders. This was simply due to Readymix specifically targeting these two days for all of their compressive strength testing. Therefore there was an extra degree of confidence with the laboratory cured results. The magnitude of confidence (or inversely the associated error) is discussed in further detail, for each step of the analysis process, in Section 4.5.

3.4.3. Modulus of Elasticity (E_c)

Modulus of elasticity (E_c) is a concrete material property that is typically modelled from f'$_c$. An example of these models is displayed in Table 3-7. These models are designed to be used only for concrete material properties at 28 days.

Table 3-7 *Models for obtaining E_c from 28 day values of compressive strength.*

Code of Practice/Researcher	Modulus of Elasticity (MPa)
Eurocode 2 (2001)	$9500(f_{ck}+8)^{1/3}$
CEB-FIP MC90 (1993)	$10000(f_{ck}+8)^{1/3}$
ACI 318-99 (1999)	$4730\sqrt{f'_c}$
ACI 363-92 (1994)	$3320\sqrt{f'_c}+6900$
AS3600 (2001)	$5050\sqrt{f'_c}$

where; f_{ck} is the European characteristic compressive strength and is assumed to be f_{cm} – 8 MPa independent of the grade of concrete (Eurocode 2, 2001).

The intentional coupling of f$_c$ tests with E_c tests, during the experimental program, allowed this research to conduct a direct comparison of accuracy of models that predict E_c from f$_c$. The E_c models displayed in Table 3-7 were compared to the E_c data recorded. However, as stated

previously this comparison could only be performed for data at 28 days. The comparison of this 28 day data is displayed in Table 3-8.

Table 3-8 *Modelling 28 day values of E_c from f'_c*

	f'c (MPa)	Modelled value of Ec (MPa)					Laboratory tested Ec (MPa)			
		Eurocode 2 (2001)	CEB FIP MC90 (1993)	ACI 318-99 (1999)	ACI 363-92 (1994)	AS3600 (2001)	Lab cured		Site cured	
							μ	σ	μ	σ
N32 mix	32	32490	34200	26757	25681	28567	35709	3525	29750	3780
N40 mix	40	34525	36342	29915	27898	31939	38350	3921	33320	2673

It can be seen in Table 3-8 that the models displayed are producing conservative results of E_c for a given f'_c. The reason for this could be due to numerous factors. The concrete mix proportions may have been adjusted slightly, for 151 Pirie, to help maintain satisfactory setting times in the cold ambient temperatures. The performance of the local aggregates, which are unique for each geographical location, may be the reason for the difference between measured values and modelled values. Hence, steps were required to be taken to develop a more suitable model for values of E_c in this research.

Microsoft Excel was employed to construct the most accurate model of E_c from a given f_c. Data from all ages was utilised in this analysis. Relationships directly between f_c and E_c were contemplated. However, considering the prior research on E_c relationships discussed in the Literature Review and displayed in Table 2-4, a relationship between $\sqrt{f_c}$ and E_c would yield more simplistic result. The linear trends produced by Excel for both scenarios, with corresponding accuracy (R^2), are presented in Figure 3-31. Linear trends were selected due to containing a high degree of accuracy combined with ease of application.
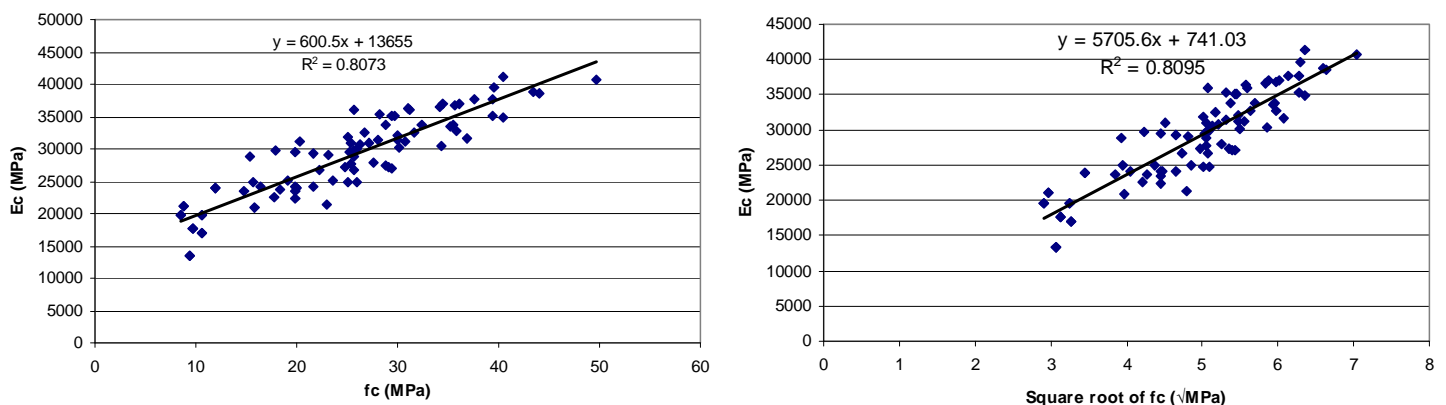
Figure 3-31 *Modelling E_c from experimental values of compressive strength.*

The most appropriate model to select from the two options displayed in Figure 3-31 is the model relating $\sqrt{f_c}$ to E_c. This model passes closely by the origin so it is logical that this trend line is more accurate for a wider range of f_c values. In fact if the trend line is shifted to include the origin the value of R^2 reduces minimally for the added benefit of an easier to apply model. This simplified model which still maintains accuracy is produced and displayed in Figure 3-32. The model produced by AS 3600 (2001) has been included in Figure 3-32 to highlight its conservative prediction of E_c. The model produced by AS 3600 (2001) was selected due to its frequent local use in Australia. It should be noted that the model produced by AS 3600 (2001) is only relevant to 28 day material properties, hence is not applicable to all values in Figure 3-32, only the 28 day data.
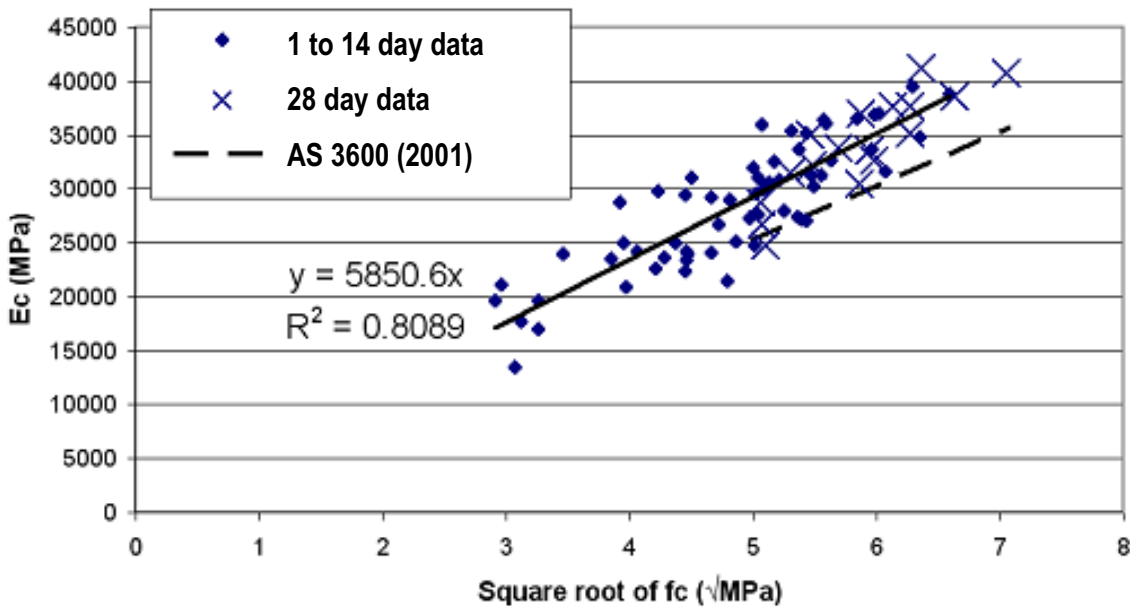
Figure 3-32 *Simplified E_c Model.*

The statistical variance of the data points from the accurate model displayed in Figure 3-32 is a crucial focal point for this research. It was necessary to quantify and record this variation so statistically accurate deflection prediction simulations could be produced. To quantify the variation, the scatter of the data from the model was graphed and the standard deviation recorded. The scatter of the data from the model is shown in Figure 3-33. The scatter was then divided by $\sqrt{f_c}$ and a separate graph produced and scrutinised. The reason for this was to determine if the variance of the data from the model depended on the value of f_c, or more appropriately for this scenario, $\sqrt{f_c}$. The graph of $\sqrt{f_c}$ versus $(E_c*-E_c)/\sqrt{f_c}$ is displayed in Figure 3-34. Ec* is the term representing the value of modulus of elasticity produced by the model $E_c = 5850.6\sqrt{f_c}$.
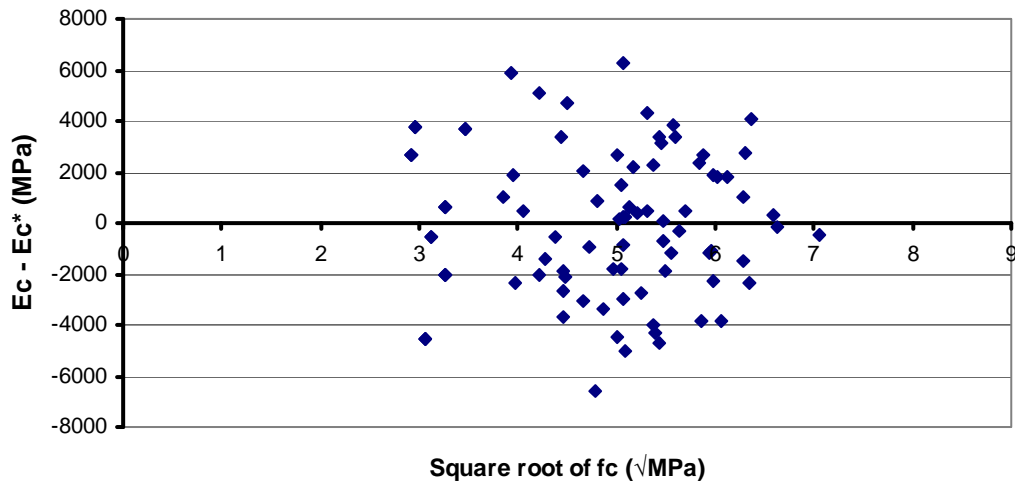
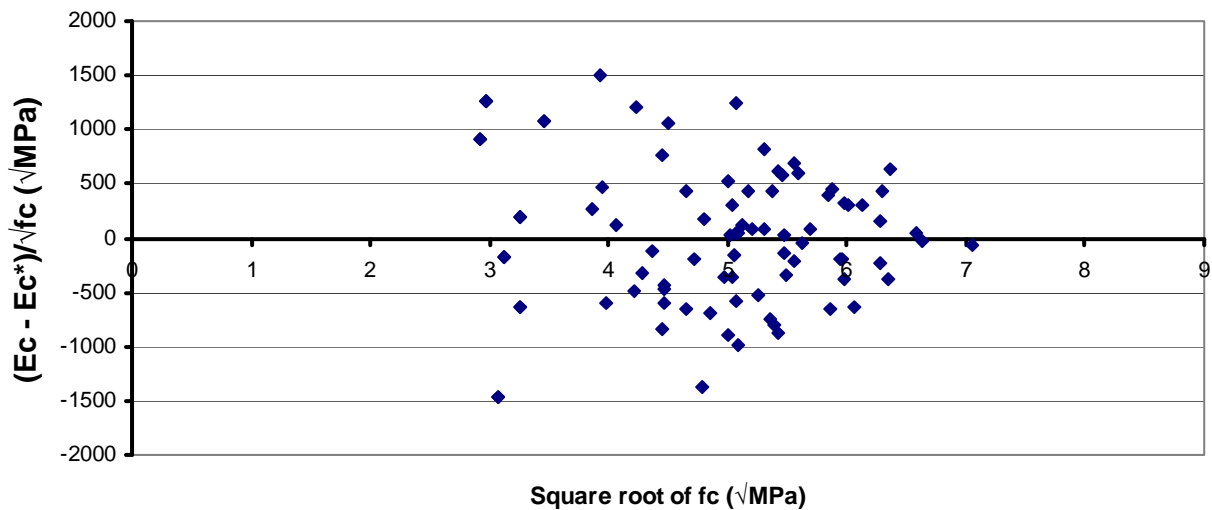*Figure 3-33* Scatter of E_c values from the obtained model

Figure 3-34 Determination of E_c model's dependence on f_c

Upon examination of the scatter patterns produced in Figure 3-33 and Figure 3-34, it was clear that the variation of individual E_c values from the model were random and did not depend on the magnitude of $\sqrt{f_c}$ for the data range of values used. The standard deviation of the data displayed in Figure 3-33 was then determined which was accurate for the entire range of f_c displayed. This standard deviation was derived under the assumption that the data was normally distributed.

The process of analysis of modelling E_c from f_c was repeated for the separate data of lab cured and site cured cylinders. Altering curing conditions could have an effect on the relationship between these two material properties, which requires examination. Concrete mix was another factor that

required examination, so the data was also separated according to mix. Upon completion of the multiple repeated processes it was evident that the models remained relatively similar for each scenario. It was also evident, from examining the scatter that in each situation E_c remained independent of the magnitude of $\sqrt{f_c}$. Table 3-9 summarises these findings. More detail on this analysis process and outcomes can be found in Appendix G.

Table 3-9 *Final Outcomes of Modelling E_c from f'_c*

Both N32 and N40			
	Site Cured	Lab cured	Both
Linear equation	5725.4sqrt(fc)	5944.5sqrt(fc)	5850.6sqrt(fc)
Standard deviation	2629.5	2968.5	2846.824

N40			
	Site Cured	Lab cured	Both
Linear equation	5863.7sqrt(fc)	5999.8sqrt(fc)	5944.2sqrt(fc)
Standard deviation	2714.8	2893.1	2801.3

N32			
	Site Cured	Lab cured	Both
Linear equation	5571.3sqrt(fc)	5870.2sqrt(fc)	5734.3sqrt(fc)
Standard deviation	2402.2	3089.0	2830.2

Due to the similar nature of each of the models (similar equations and magnitude of standard deviations) it was considered unnecessary to apply separate models depending on curing conditions and concrete mixture. For simplicity and ease of application the preferred model was the model which considers all data points, i.e. $E_c = 5850.6\sqrt{f_c}$, $\sigma = 2846.8$ MPa. This model considers all data points so it is also preferred due to lack of bias.

It can be concluded that a thorough examination of a wide range of data allowed a detailed analysis of E_c data. This range of data incorporated different curing methods, different curing times and different concrete mixes. The outcome of this analysis was that the relationship between f_c and E_c for concrete in Adelaide contains an easily applicable model that was independent of concrete mix and curing time or curing method and was applicable for all typical values of f_c for NSC (up to approximately 45 MPa).

3.4.4. Tensile Strength (f_t)

Monitoring of tensile strength (f_t) in this research was considered a secondary priority to the monitoring of f_c and E_c. The reason behind this priority was made clear in Section 2.4.3 of the Literature Review as well as Section 3.3.3 where a reduced experimental program for monitoring f_t was performed. The material properties f_c and E_c require close examination because these material

properties have a direct effect on the deflection prediction models. The values of f_t do not have a direct effect on deflection prediction models. The values of f_t act as a threshold, when this threshold is surpassed, member cracking occurs which affects the sectional properties of the member. If the f_t threshold is not surpassed, cracking does not occur and the sectional properties of the concrete member are maintained as gross sectional properties. So if the f_t threshold was not surpassed, behaviour of the concrete member could be considered unaffected.

Tensile strength data recorded in the experimental program has been compared to the models introduced in the Literature Review in Section 2.4.3. In this comparison modelled values of STS are directly compared to the tested values of STS. The modelled values of FTS were however, only able to be compared to the STS data which has been converted into FTS data via Equation 2-1. This comparison is presented in Table 3-10 and Table 3-11.

Table 3-10 *A comparison of modelled values of STS to measured values.*

	f'c (MPa)	Modelled value of STS (MPa)					Laboratory tested STS (MPa)			
		Larrard and Malier (1992)	Zain et al. (2002)	ACI (1992)	Ahmad and Shah (1985)	AS 3600 (2001)	Lab cured		Site cured	
							μ	σ	μ	σ
N32 mix	32	2.52	3.34	3.34	3.09	2.26	3.61	N/A	3.14	0.12
N40 mix	40	3.00	3.73	3.73	3.50	2.53	4.27	0.29	3.48	0.31

Table 3-11 *A comparison of modelled values of FTS to converted values of FTS from STS values.*

	f'c (MPa)	Modelled value of FTS (MPa)				Laboratory determined FTS (MPa)			
		ACI (1992)	ACI (1995)	Ahmad and Shah (1985)	AS 3600 (2001)	Lab cured		Site cured	
						μ	σ	μ	σ
N32 mix	32	5.32	3.51	4.43	3.39	5.35	N/A	4.86	0.12
N40 mix	40	5.95	3.92	5.15	3.79	6.02	0.30	5.21	0.31

In Table 3-10 and Table 3-11 it can be seen that the models generally underestimate the values of both STS and FTS, with the exception of the model developed by ACI (1992) for predicting FTS. The reason for this was similar to the conservative nature discovered when examining the E_c models displayed in Table 3-8.

Due to the conservative nature of the models presented for analysis, construction of an accurate model for the concrete analysed in this research was required. The steps taken to construct this model were similar in concept to the steps taken to construct the model for E_c. Microsoft excel was again utilised to construct linear trend lines to the f_t vs f_c data pairs recorded. The most appropriate model was then selected based on ease of application and accuracy. The two most suited models

have been displayed in Figure 3-35 where f_t has been graphed against $\sqrt{f_c}$. The first model is linear in nature with an R^2 of 0.8735 the second model is a power trend line with an R^2 of 0.9025.
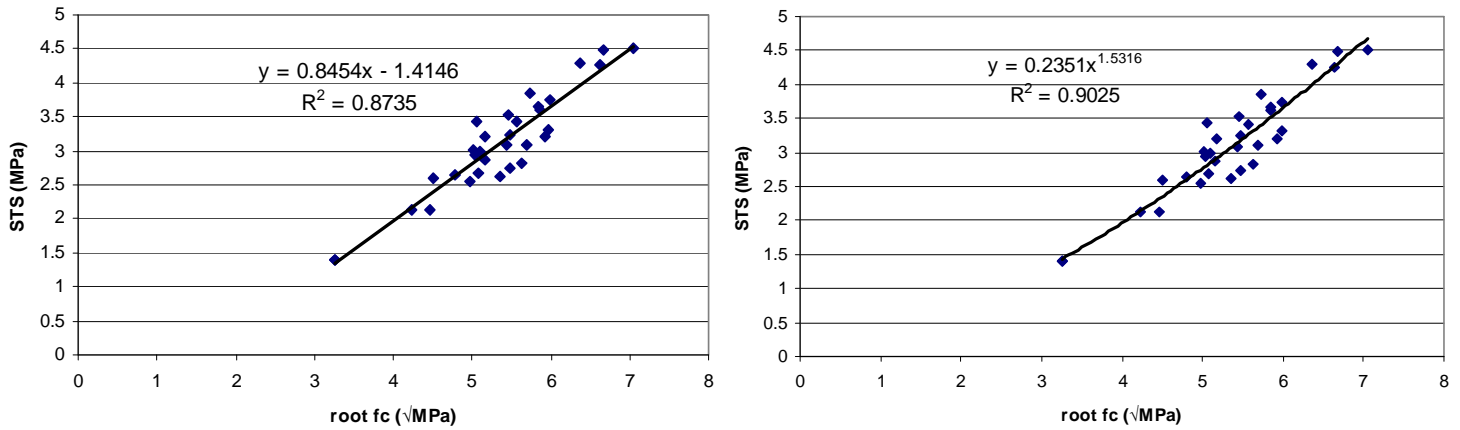

Figure 3-35 *f_t modelling from the experimental data.*

For this situation, where one model contains the benefit of a slightly higher degree of accuracy whilst the other model contains a higher degree of ease of application, the power model with a higher degree of accuracy is considered the preferred model. The linear model fails to pass through the origin which was not considered a favourable characteristic. If the linear model was adjusted to pass through the origin accuracy decreased significantly. The benefit of ease of application was considered minimal for further automated calculations achieved by computer programming in this research. However, this first model would be potentially beneficial for structural designers who perform many of their calculations by hand, ensuring that the range of 3 MPa $< \sqrt{f_c} <$ 7 MPa is adhered to. Similar to the models for E_c, the selected f_t model's scatter was analysed for potential trends, as well as dependency on the magnitude of f_c. Figure 3-36 and Figure 3-37 display the outcomes of this graphical examination and it was once again clear that due to the random scatter in both graphs that f_t contains no obvious trends and the variance of individual values from this model did not depend on the magnitude of f_c.
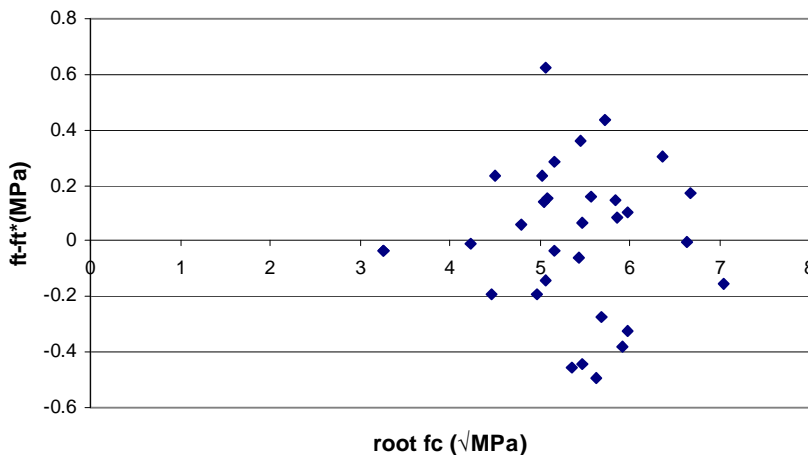
Figure 3-36 *Scatter of f_t values from the obtained model*
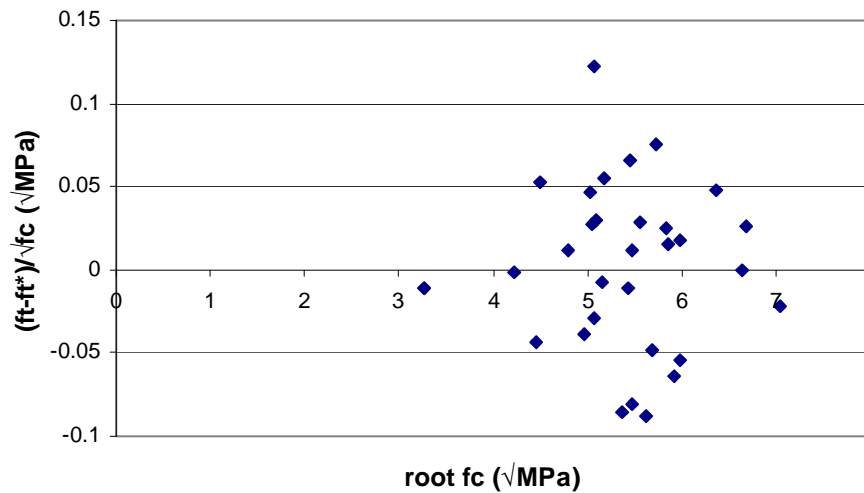
Figure 3-37 Determination of the STS prediction model's dependence on f_c

This process of data analysis was repeated for the separate mixes and curing conditions similar to the process achieved in the E_c data analysis. The separated f_t data, however, contain significantly less data points to perform this data analysis with confidence. Nonetheless, this was still achieved and the final outcomes have been posted in Table 3-12.

Table 3-12 Final outcomes from modelling f_t from f_c

	N32 and N40		
	Site Cured	Lab cured	Both
Linear equation	0.8096sqrt(f'c) - 1.2168	0.8781sqrt(f'c) - 1.6168	0.8454sqrt(f'c) - 1.4146
Standard deviation	0.294	0.257	0.270
Power equation	0.2258sqrt(f'c)^1.5638	0.2244sqrt(f'c)^1.5522	0.2351sqrt(f'c)^1.5316
Standard deviation	0.301	0.238	0.269

	N40		
	Site Cured	Lab cured	Both
Linear equation	0.8441sqrt(f'c) -1.3438	0.8542sqrt(f'c)-1.4387	0.842sqrt(f'c) - 1.3516
Standard deviation	0.308	0.243	0.267
Power equation	0.2132sqrt(f'c)^1.6083	0.2377sqrt(f'c)^1.5259	0.2386sqrt(f'c)^1.5303
Standard deviation	0.312	0.235	0.269

	N32		
	Site Cured	Lab cured	Both
Linear equation	0.6793sqrt(f'c) -.6965	1.2689sqrt(f'c) -3.9189	0.7799sqrt(f'c) -1.231
Standard deviation	0.200	0.232	0.231
Power equation	0.3082sqrt(f'c)^1.345	0.0707sqrt(f'c)^2.2055	0.2564sqrt(f'c)^1.4519
Standard deviation	0.209	0.222	0.232

It can be seen in Table 3-12 that the modelling equations as well as the associated standard deviations remain similar when altering curing conditions and mix. Due to this, it can be concluded that the power equation acquired from both mixes, $f_t = 0.2351\sqrt{f_c}^{1.5316}$, or $f_t = 0.2351*f_c^{0.7658}$ was the

most accurate method for modelling f_t from f_c. This model was appropriate for all curing conditions and concrete mixes and remains accurate for the range of f_c between approximately 20 and 50 MPa.

The question of member cracking due to insignificant FTS was still a topic that requires attention. This topic, along with other site specific outcomes for 151 Pirie, is discussed in further detail in Section 3.5.

3.5.   Site Specific Recorded Data

The data recorded and analysed in the previous sections; Section 4.3 and 4.4, were general material properties of concrete that can be supplied to any construction site. This section addresses the site specific factors which affect PPS slab deflections that were monitored specifically at 151 Pirie. The main topics of interest to discuss are the cycle times achieved on site, the member behaviour due to concrete properties, the monitored concrete and ambient temperatures and the slab deflections.

3.5.1. Cycle Time Monitoring

The time taken for a construction crew to complete the construction requirements of one floor of a multi storey building is considered one cycle time. In one cycle time each of the following processes needs to occur in the following order:

- Propping of formwork
- Place reinforcement
- Place prestressing tendons
- Pour and level and concrete
- Initial Prestress (at approximately 1 day after pouring concrete)
- Prop removal
- Install back propping
- Final Prestress (at approximately 7 days after pouring concrete)

One of the main aims for this project was to find what the lowest cycle times that could be achieved for 151 Pirie. The testing diary recorded for this project gives a record of the cycle times achieved at 151 Pirie. From this record, which was shown previously in Figure 3-28 and Figure 3-29, it was evident that cycle times from each slab pour varied from 5 to 11 days. This outcome is displayed in Figure 3-38.
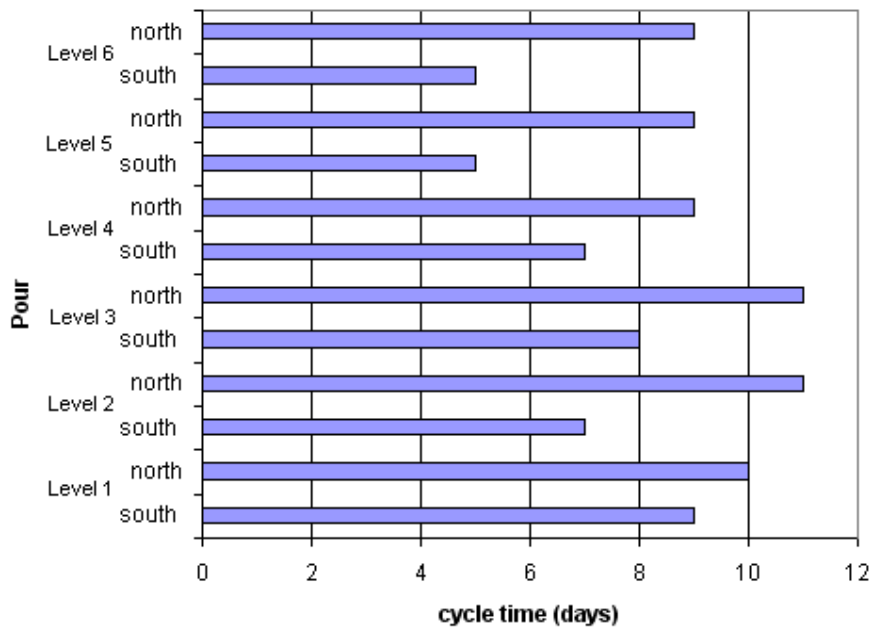
Figure 3-38 *Cycle times experienced at 151 Pirie*

It is worth noting that 151 Pirie was constructed with two concrete pours for each PPS slab, separated by a construction joint. Therefore, a cycle time for this instance was classified as either; the time taken from the pouring of the first half of the slab to the second half, or the time taken from the pouring of the second half of the slab to the first half of the next higher slab. Naturally the later cycle time was a longer cycle time considering the extra time taken to begin constructing formwork, scaffolding and other temporary structures such as lift access for the next level. To attempt to lessen the effects of this extra construction effort required for the second cycle time, the second slab pour was significantly less area than the first pour. For 151 Pirie the south pour related to the first pour, the second pour related to the north pour.

It has been stated earlier, in Section 3.3, that the concrete compressive strength requirements were not passing comfortably at early stages of construction. This resulted in adding extra days to the early cycle times to ensure that the process of final prestressing could occur safely. Mid way through the construction of 151 Pirie the mix was changed to N40 concrete to make certain that this delay was minimised. The change from N32 to N40 concrete occurred between the 3rd and 4th floor. It was decided that the 3rd floor north pour would contain N32 whilst the 3rd floor south contained N40. Slabs lower than the 3rd floor contained N32 whilst slabs higher contained N40. In Figure 3-38 it is clear that cycle times containing N40 concrete were significantly reduced compared to cycle times with N32 concrete. The lowest cycle times produced for the north and south slabs were 9 and 5 days respectively. It is worth noting that the concrete performance was not the only factor determining cycle times, bad weather, public holidays, rostered days off and general construction delays can each contribute to longer cycle times.

3.5.2. The Effect of Concrete Performance on Member Performance

During the construction stages of 151 Pirie unwanted member performance, associated with the pouring of the concrete slabs, could be separated into one of two categories; member failure during prestress stages and member cracking due to insignificant tensile strength. Failure of the member during the prestressing stages (and subsequent repair) had the potential to effect cycle times, whilst member cracking had the potential to effect slab deflections.

Member failure during the prestressing stages, such as localised concrete crushing due to premature prestressing or dead end pullouts, did not occur at 151 Pirie. The 24 MPa compressive strength requirement imposed by the structural engineer was admitted to be a conservative strength requirement.

Prestress application and prop movement are two construction procedures that were required to be synchronised to ensure unwanted deflections or member failure did not occur. 151 Pirie contained a construction joint and it was a structural requirement that at least 1 bay of props remained when adjusting adjacent props to maintain continuity at this construction joint. This was not monitored closely by this research. However, the recorded outcome was that potential issues surrounding prestressing timing and prop movement did not have a negative effect on the construction or cycle times.

Cracking of a concrete member due to insignificant tensile strength is a difficult quantity to monitor. Tests to monitor the degree of cracking in the concrete slabs were not performed, however the tensile strengths in the experimental program performed well above the required level that would indicate cracking. The computer software package RAM Conce*pt* was utilised, along with the experimental data, to simulate the potential for cracking to occur. Material properties were altered in RAM Conce*pt* so a conservative simulation was created and the outcome analysed. Figure 3-39 indicates the tensile strengths that RAM Conce*pt* utilised as well as the tensile strengths recorded in the experimental program. When simulating the potential for member cracking with RAM Conce*pt*'s conservative inputs, no member cracking was evident. Therefore with significantly higher tensile strengths, seen in Figure 3-39 it can be concluded that member cracking is highly unlikely for the PPS slabs at 151 Pirie.
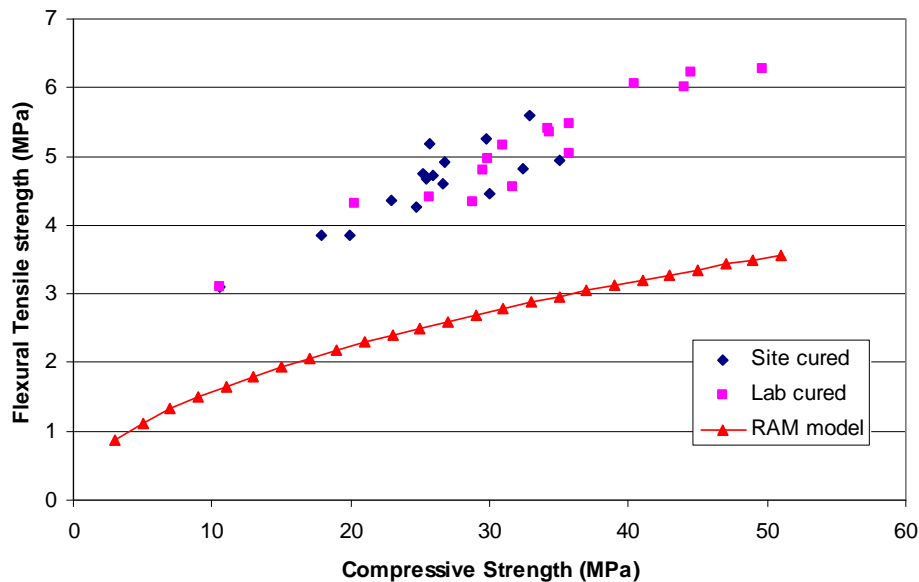
Figure 3-39 RAM Concept's model of tensile strength

In conclusion, this research observed that no prestress failures due to prestressing the tendons or any other member failures occurred during the construction of 151 Pirie.

3.5.3. Temperature Monitoring

Temperature monitoring was performed on the PPS slabs at 151 Pirie in an attempt to accurately record material properties via the maturity method. The temperature recording system consisted of a DT600 battery operated Datataker unit, with multiple channels connected to T-type thermocouples. Thermocouples were attached to the reinforcement before pouring of the concrete. Several thermocouple locations for temperature recording were chosen which happened to be close to the edge of the slab so the data taker could rest on the nearby crane tower. Not only were multiple locations chosen for recording data but also multiple depths of the slab to verify the expected temperature profile of the slab. In total there were 9 sets of temperature data recorded by the DT600. Three were at location A at low, mid and high locations in the slab. Two more were located inside the PPS slab at mid height locations of B and C. The next three temperature records were from inside typical concrete cylinder molds. The final time-temperature data recorded was the ambient temperature.

The software loaded onto the DT600 was *Delogger* software. To help reduce damage to the DT600 an esky was utilised to maintain a water tight seal whilst recording data on site. The setup used in this research, including the DT600 and thermocouple placement, can be seen in Figure 3-40. It is worth noting that steps were taken to ensure that the time-temperature records obtained from inside

the PPS slab were a good representative of the average temperature across the whole slab. These steps included heat shielding the thermocouples to ensure minimal disturbance from the steel reinforcement. Locations of at least 1m from the edge were selected for the thermocouples to ensure the same insulating properties for the rest of the slab were simulated.
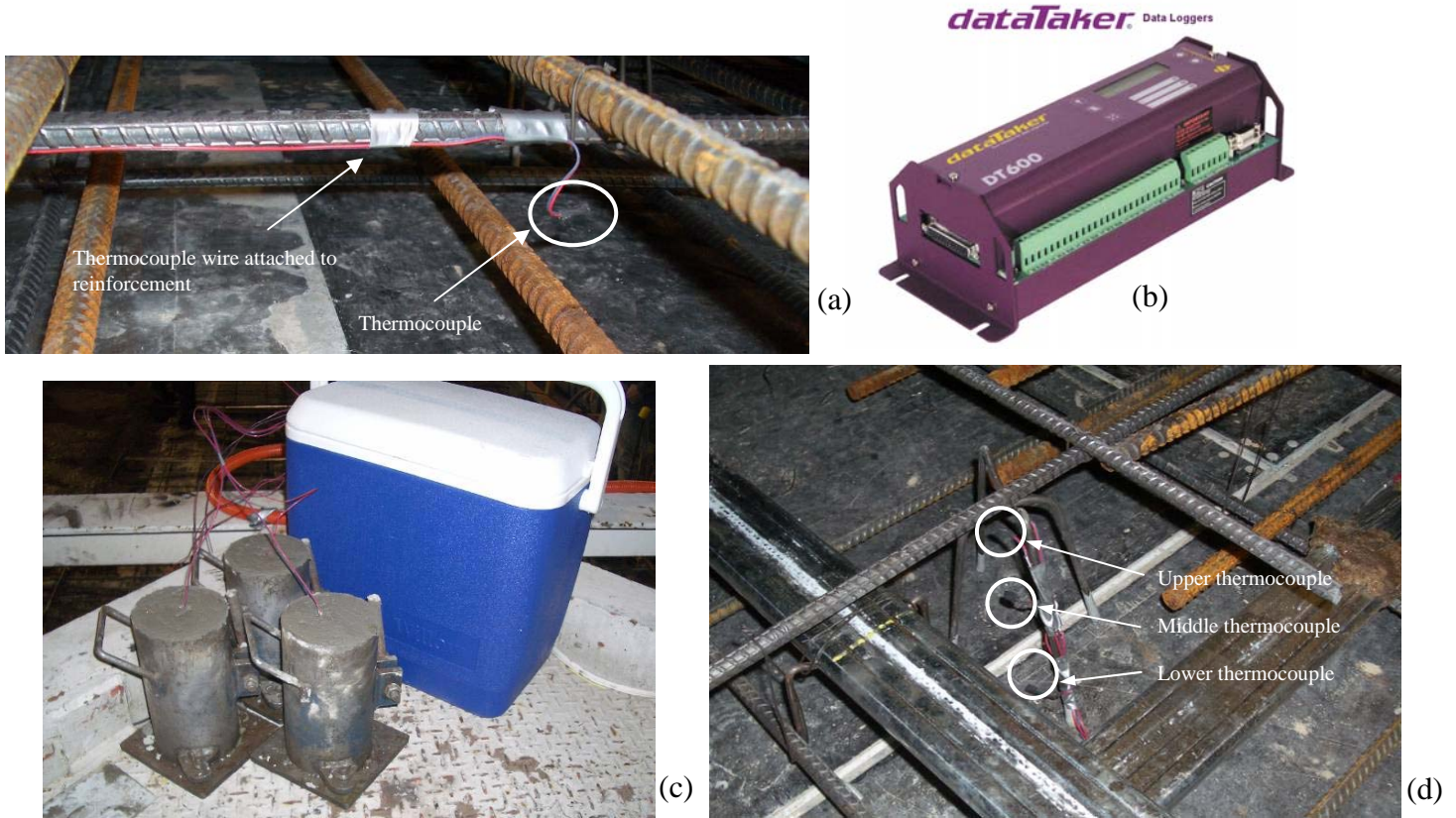

Figure 3-40 *Thermocouple equipment and arrangement on site*
- a) Example of thermocouple wiring, b) DT600, c) Thermocouples attached to concrete cylinders,
d) Example of recording layered temperature profile.

The data recorded from the thermocouple arrangement was unfortunately subjected to a noticeable degree of interference on site. Examination of the data revealed that the data spikes up and down outside the region of expected temperatures (approximately 5 – 80 deg C). After consulting a thermocouple technician it was advised that these spikes were usually associated with interference with some form of radio or mobile phone signals. It was suggested that the reinforcement within the slab was acting as a large antenna and these frequencies cwere affect the recording of temperatures from this thermocouple set up. Upon further discussions it was decided that rectifying this problem would cost time and affect the demanding concrete cylinder testing schedule. Therefore the decision was made to discontinue the data collection of temperature at 151 Pirie. This decision was made partly due to Readymix undertaking separate temperature tests on the same concrete mixes with similar member profiles. The results from these tests could be applied to the maturity calculations in this research.

A sample of the corrupted data obtained from the datataker is displayed in Figure 3-41 where the ambient temperature is compared to the temperature recorded from two of the molds. In Figure 3-41 it can be seen that realistic data is obtained for each channel up until the moment of concrete pouring. At the moment of concrete pouring the data points sporadically spike to positive and negative infinity whilst also recording unrealistic temperatures outside the range of approximately 5 to 80 deg C. However, there is evidence of a few of the channels maintaining realistic temperature readings for the initial few hours. The data records within these few hours indicate that the temperature within the molds vary little from the ambient temperature. This indicates that there is little to no insulating properties of such thin sections of concrete.
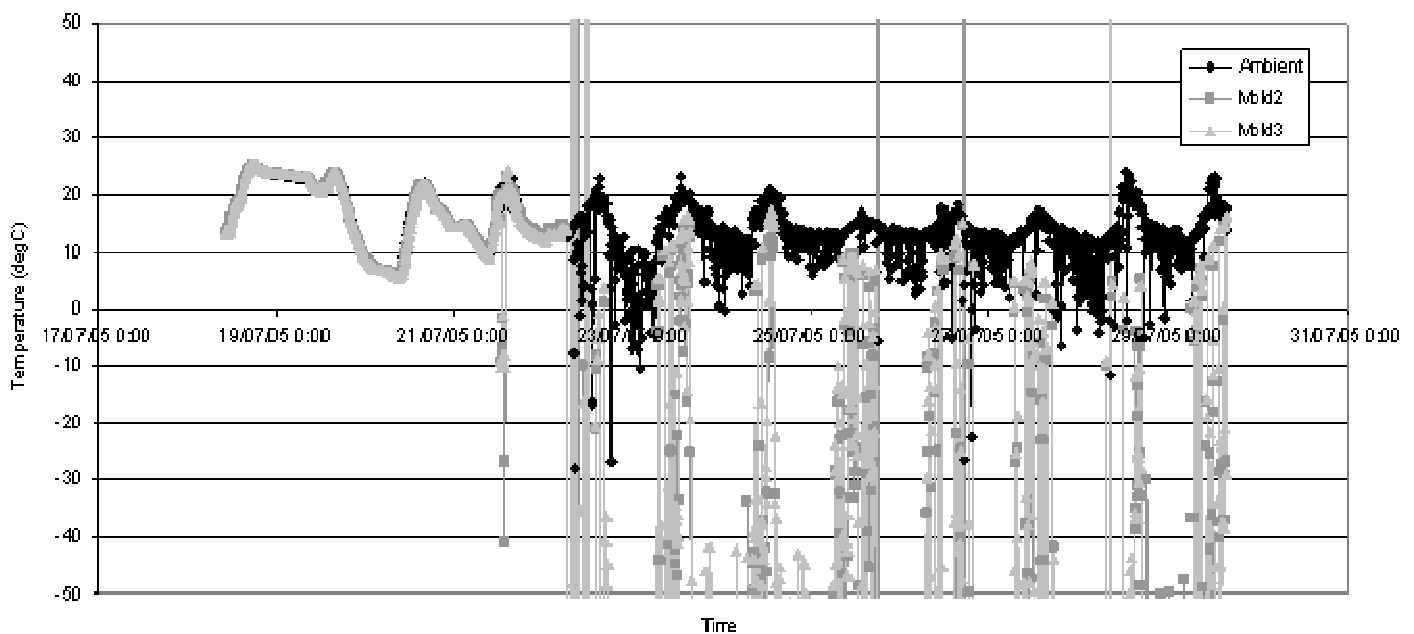
Figure 3-41 *Thermocouple readings obtained from 151 Pirie.*

Independent research into the heat of hydration of thin PPS slabs, performed by Readymix's laboratory at Brompton, indicates that N32 and N40 concretes contain minimal insulating properties for extremely thin slabs. This internal research also concluded the effect of heat of hydration lasts for, at most, approximately 12hrs. Due to this experimental outcome on identical concrete, this research will conclude that there is very minor error in assuming that the air cured cylinders are an accurate replica of the material properties experienced inside the thin PPS slabs (Peter Carson Readymix (2007, pers. comm., Jan)).

3.5.4. Slab Deformation Surveying

Engineering Surveys Pty Ltd managed the data acquisition of the slab deformations. The data that was supplied by them has allowed a comparison between predicted deformations produced from the initial stages of design using RAM Conce*pt* and actual deformations. It was apparent early in the research that single deformation readings would not be useful if not accompanied by adjacent column measurements. Adjacent column measurements allow for independent column settling to be accounted for. This resulted in disregarding survey measurements that were not in the 2 bay grid established in Figure 3-8. A summary of the surveyed grid is given in Figure 3-42. Differences in column heights, due to column settling were accounted for by applying equations that account for the difference between initial and final measured deformations of a particular point, whilst negating the average column settlement of adjacent columns. An example of these equations is shown in Equation 3-3 and Equation 3-4 where two adjacent columns for column strip deformations are considered in Equation 3-3 and four adjacent columns for mid panel deformations are considered for Equation 3-4. Subscripts i and f denote initial and final deformations respectively. Table 3-13 displays an example of the comparison between surveyed values and predicted values.
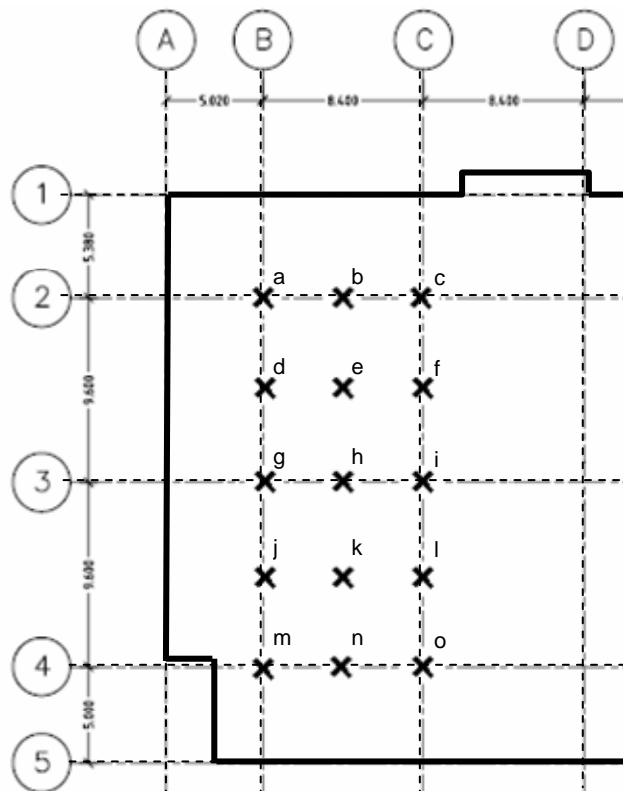

Figure 3-42 *Surveyed grid on each slab.*

$$\Delta_b = \left(b_f - \frac{a_f + c_f}{2} \right) - \left(b_i - \frac{a_i + c_i}{2} \right)$$
<div align="right">**Equation 3-3**</div>

$$\Delta_e = \left(e_f - \frac{a_f + c_f + g_f + l_f}{4} \right) - \left(e_i - \frac{a_i + c_i + g_i + l_i}{4} \right)$$
<div align="right">**Equation 3-4**</div>

Table 3-13 Comparison of survey deformations to initially prediction deformations.

	DEFORMATIONS AT LEVEL 5					
	Day 36			Day 138		
Grid Point	Survey	RAM (Dead and Balance)	difference	Survey	RAM	difference
b	0.0	-1.2	**1.2**	-3.5	-8.0	**4.5**
d	-1.0	-1.2	**0.2**	-2.5	-8.0	**5.5**
e	-1.3	-1.4	**0.2**	3.3	-11.5	**14.8**
f	-1.5	-1.2	**0.3**	0.0	-10.0	**10.0**
h	n/a	-2.0	**n/a**	-4.0	-10.0	**6.0**
j	-1.5	-1.2	**0.3**	-2.5	-8.0	**5.5**
k	-2.5	-1.2	**1.3**	-0.3	-11.0	**10.8**
l	-2.5	-1.0	**1.5**	-3.0	-8.5	**5.5**
n	-3.5	-1.6	**1.9**	-3.5	-9.6	**6.1**

As can be seen the RAM Conce*pt* predicted deformations are larger than the measured deformations in all cases. The average difference is approximately 5 to 6 mm for column strips and 10 to 15 mm for middle strips, with the exception of point 'f'. Reasons for this difference are considered to be due to insignificant time for long-term effects to occur plus due to the floors being vacant at the time of surveying minimal to no loadings existing on the slabs.

Inaccurate casting and levelling of the concrete has the potential to introduce significant initial deformations. Each of the column points was included as a surveying point and hence a summary was made on how accurate the casting and levelling of the concrete is. Theoretically column points are expected to maintain a relative 0 mm deformation over time, but as Table 3-14 shows this is not the case. Table 3-14 shows the average column point reading over time, as well as the maximum difference between column points on a given floor. As can be seen this maximum difference can be significantly large, up to 10.2 mm, which was approximately the same amount as the recorded deformations for middle strip deformations.

Table 3-14 *Surveyed deformation values at column points*

Average deformation reading over time						
floor						
Column point	2	3	4	5	6	7
a	-3.5	-0.3	4.7	-0.3	-6.5	0.3
c	4.5	-2.0	8.3	7.3	3.7	8.3
g	0.5	5.7	3.3	-2.7	-2.3	6.0
i	1.5	3.3	7.7	5.3	-4.0	2.0
m	0.0	4.7	4.7	5.0	-2.3	5.0
o	3.0	5.7	1.7	3.0	0.7	0.7
Maximum Difference	8.0	7.7	6.7	10.0	10.2	8.0

In conclusion of the surveying performed on 151 Pirie, deformation monitoring was performed for the short term deformations (up to approximately 4 to 6 months, depending on location) on the grid outlined previously in Figure 3-7 and Figure 3-8. Long term deformations are yet to be performed due to insignificant time, but can be performed when required due to surveying arranged on the underside of the slab. On initial analysis, short term readings are below the expected long term readings which were predicted within the design stages. This outcome is logically expected due to insufficient time for long term effects and full working loads to completely develop. More detail on deformation readings and deformation prediction is covered in Chapter 5, where a significant analysis is undertaken.

3.6.   Summary

The experimental program outlined in Section 3.2.6 was undertaken successfully. Primary material properties (f_c, E_c and f_t) were each monitored over the time periods of 1, 3, 7, 14 and 28 days. This monitoring occurred for laboratory and site curing conditions for both the N32 and N40 concrete mixes. Secondary material properties were obtained from independent testing performed by Readymix. A statistical data analysis yielded the statistical array of primary material properties for Readymix's N32 and N40 concretes in Adelaide. Adequate deformation surveying was performed by Engineering Surveys Pty Ltd. Thermocouple readings for this research were not sufficiently accurate, however, the inclusion of site cured cylinders allowed material property adjustments due to thermal differences to be made successfully. No member damage, such as dead end pull outs, occurred during the prestressing stages of 151 Pirie.

The experimental program has successfully supplied this research with adequate data points for a statistical approach for the prediction of the slab deformations. This statistical approach will help supply designers and construction managers with not only a predicted mean deformation, but an associated confidence of certain deformation limits. The process of performing this statistical analysis and essential outcomes are presented in Chapter 4.

4. PREDICTION OF SLAB DEFORMATIONS

4.1.   Introduction

This chapter of the research investigates the relevance and accuracy of the inputs, methods and assumptions associated with the deflection and camber prediction methods detailed in the Literature Review. These deflection and camber prediction models are employed to predict the deformations experienced at the PPS slabs at 151 Pirie.

Initially, accurate inputs for the deflection and camber prediction models are calculated and presented. These inputs included summarising the previously calculated material properties as well as presenting other inputs that have received less focus such as prestressing forces and applied loads. Following the analysis on the inputs is the investigation into the methods of predicting deflections and camber. In this section three main categories of prediction methods are investigated. Initially, the large array of current numerical equations are presented and analysed. Following this is the analysis combining the statistical distribution of material properties with the numerical equations in a Monte Carlo simulation. Finally, in an attempt to reduce the assumptions associated with deflection and camber models, a finite element prediction method is created from first principles. Once the deflections and cambers have been calculated from the three applied methods, a comparison is made between the predicted final deformations and the surveyed values. Following this comparison is the explanation of the limitations of accuracy associated with each method. To avoid confusion of terminology in this chapter, the term "deflection" has been used to relate to downward slab deformation due to applied dead and live loadings. The term "camber" relates to the upward slab deformation due to the applied prestressing force. The term "final deformation" relates to the superimposed combination of member camber and deflection. A downward deflection, an upward camber and an upward final deformation are all considered positive unless stated otherwise.

Throughout this chapter frequent references are made to the surveyed 2 bay grid at 151 Pirie. For this grid the deformation points of interest have been labelled (from *a* to *o*) as per Figure *4-1*. This arrangement is the same arrangement shown previously in Figure 4.44. Due to the common usage of strip analysis in predicting cambers and deflections, Figure 4-1 also displays the labelling system used for each of the column strips (labelled *1* to *7*) and middle strips (labelled *8* to *11*).
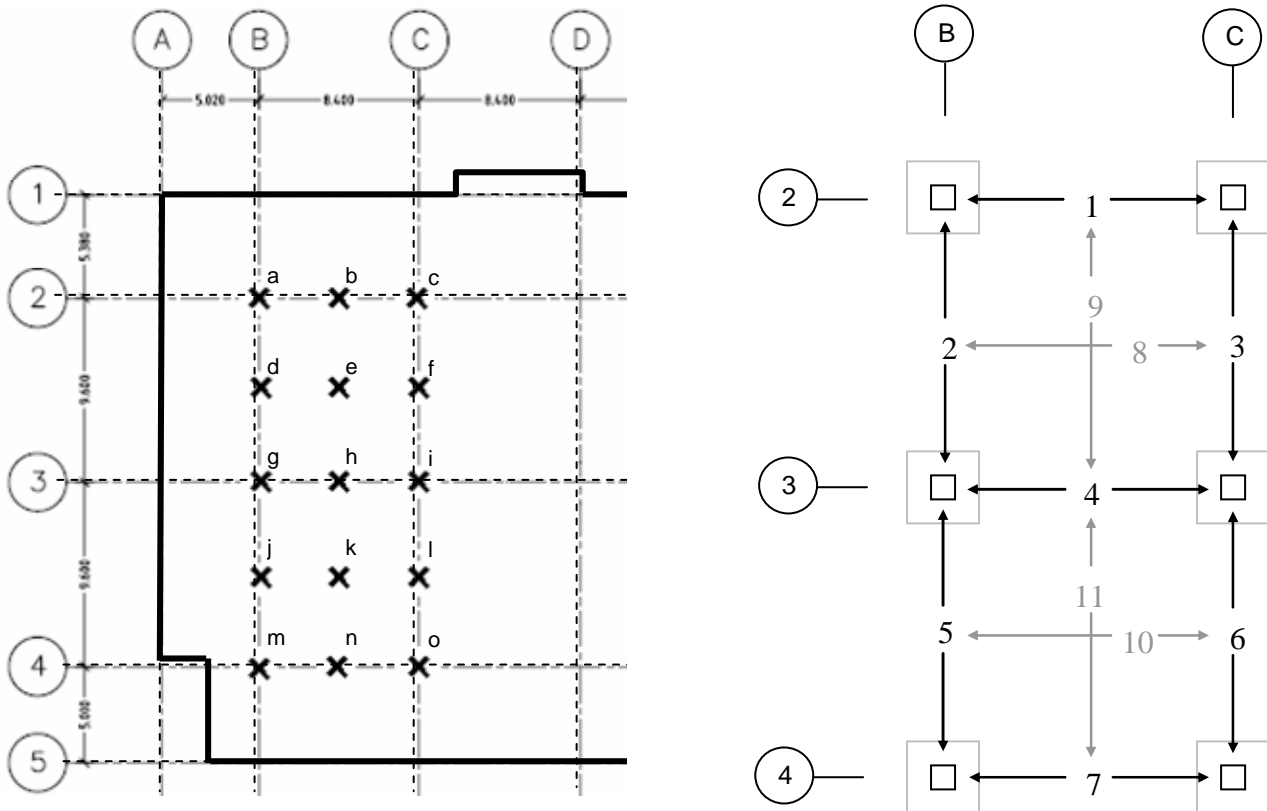
Figure 4-1 *Labelling of the 2 bay grid points as well as the mid and column strips.*

This section of the research presents a summary of the outcomes and crucial findings on the topic of deformation prediction methods. Details of each selected input, applied method and final outcome are supplied in Appendix H.

4.2.   *Determination of Accurate Inputs for Deflection Prediction*

To ensure that the final predicted deflection and camber values are relevant to the building under analysis, inputs are required to be used as accurately as possible. Chapter 4 has discussed in detail the steps taken to ensure that accurate concrete material properties have been determined for 151 Pirie. The findings of this analysis have been summarised in Table 4-1 where typical design values (extracted from RAM Conce*pt*) are contrasted with the statistically determined values. The remaining inputs, namely the applied loadings and factors relating to slab dimensions, are investigated in this section.

The three factors that require the most attention in this section are post-tensioned tendon force calculations, applied load determination (live and dead loads) and effective width of the column and middle strips. Factors such as length and slab depth do not require the same level of attention due to their values being easily determined and accurately maintained on site.

Table 4-1 *Summary of Accurate Material Properties*

			Design values		Statistically determined values			
			7day	28day	7day		28day	
					mean	standard deviation	mean	standard deviation
fc (MPa)	lab	N32	20	32	24.96	2.22	37.23	2.52
		N40	20	40	32.27	3.56	47.01	3.94
	site	N32	20	32	21.02	1.56	28.7	3.82
		N40	20	40	26.15	2.01	31.92	5.05
Ec (MPa)		N32	25000	31000	5850.6 √fc	2846.8	5850.6 √fc	2846.8
		N40	25000	34000				

The comparison of accurately determined inputs to commonly used design values is achieved for each of these three categories of inputs. Accurately determined inputs require significant time to determine, so in typical design stages it is more feasible to use commonly used design values as inputs. However, these commonly used design values contain many assumptions. This section highlights the differences between commonly used design values and accurately determined inputs. Details on how the difference in inputs and related assumptions affects serviceability prediction are covered later in Section 4.4.

4.2.1. Post-tensioned Tendon Force Calculations

The average prestressing force in each tendon in the analysed two bay grid was achieved accurately by accounting for losses along each duct. These losses include friction due to the parabolic tendon profile as well as losses due to the draw in effect. Figure 4-2 displays the two bay tendon arrangement including dead end and live end locations.

It was found in this analysis that the tendons positioned in the North-South direction were only affected by friction losses. The draw in effect, which effects only the prestressing force towards the live end, did not proceed far enough towards the two bays under analysis. A summary of the calculated prestressing force in each strand along the North-South direction is displayed in Figure 4-3. In this figure it can be seen that the average stress between the column lines B and C is 1484.5 MPa.

The tendons positioned in the East West direction were found to be affected by both friction and the draw in effect. A summary of the calculated prestressing stress in each strand along the East-West direction is displayed in Figure 4-4. The average stress due to applied prestressing in between column lines 2-3 and 3-4 are 1533.5 MPa and 1541.8 MPa respectively.
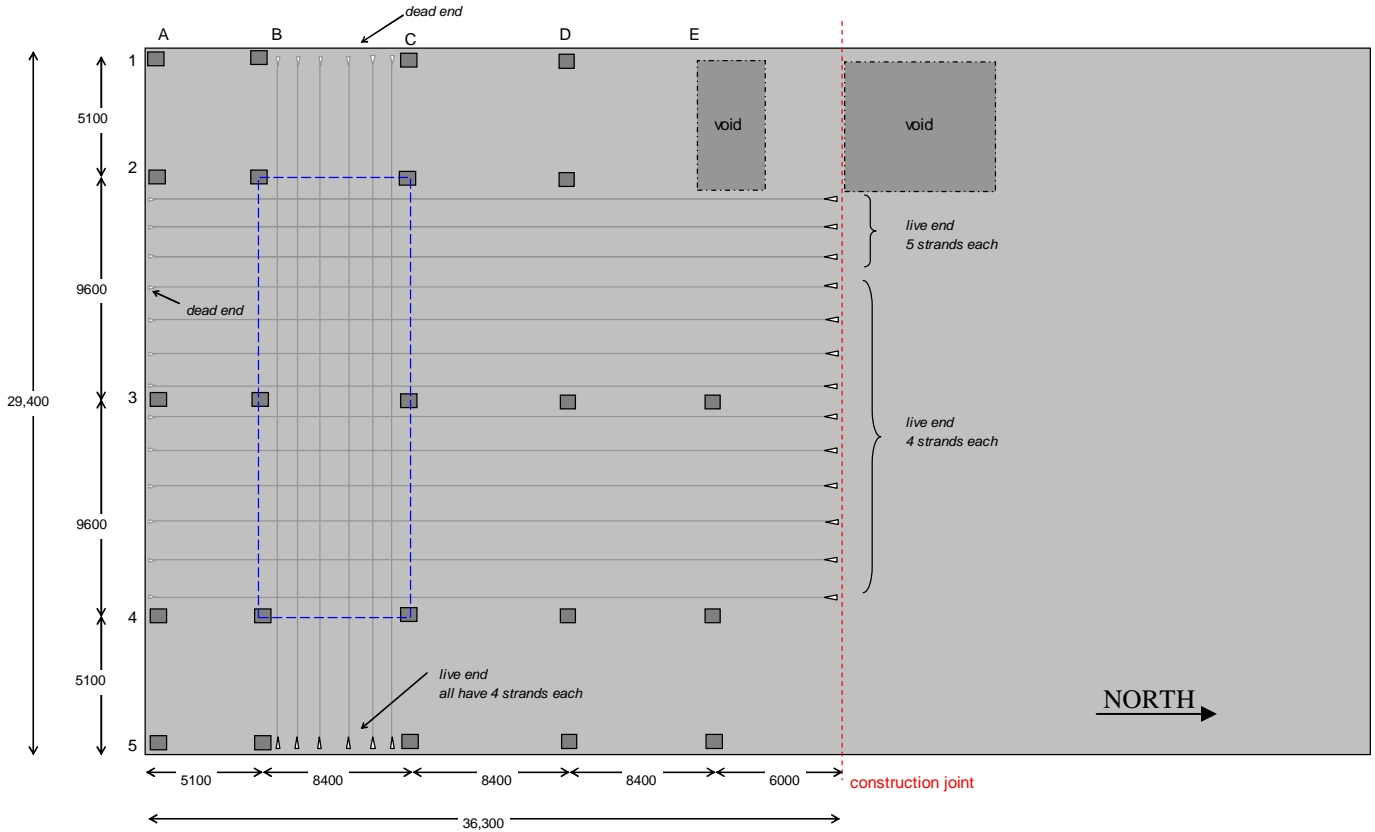
Figure 4-2 *Prestressing arrangement under analysis for the 2 bay grid (measurements are in mm)*
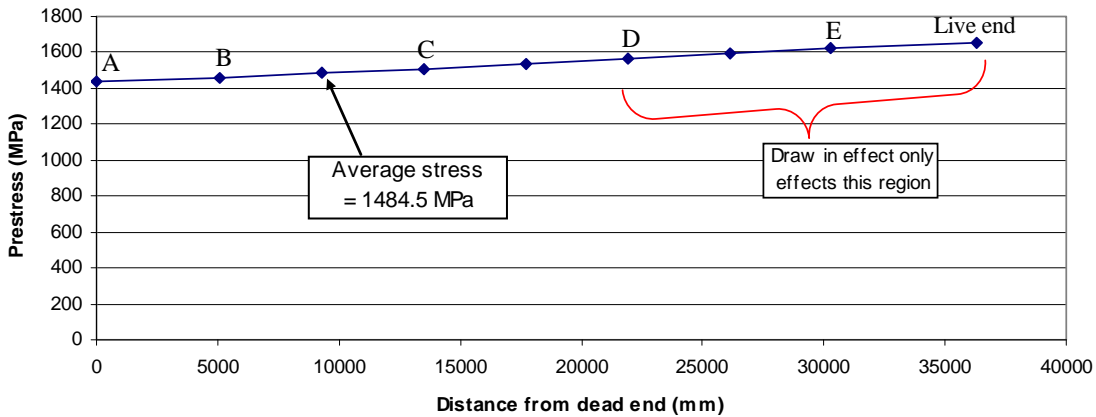

Figure 4-3 *Prestressing stress for each strand in tendons situated in North-South direction*
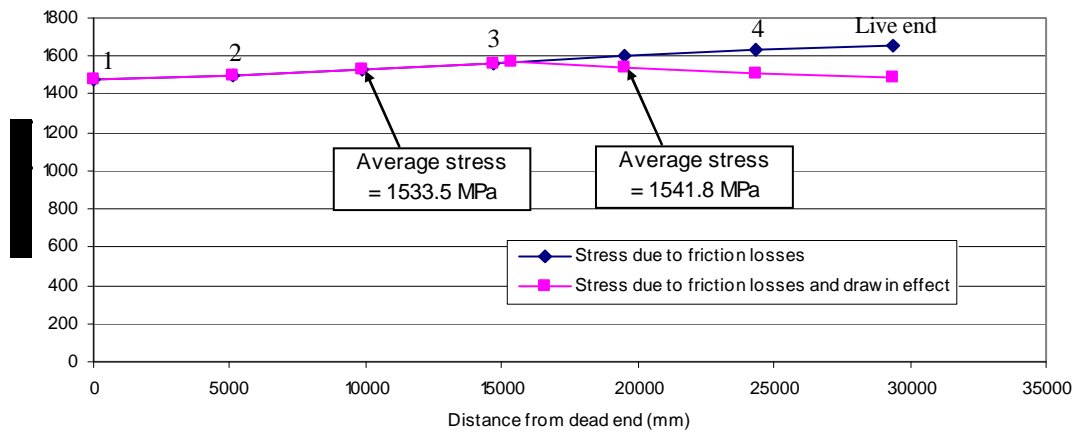

Figure 4-4 *Prestressing stress for each strand in tendons situated in East-West direction*

Prestressing stresses shown in Figure 4-3 and Figure 4-4 are for each strand in the ducts. To determine the total prestressing load applied to a column strip or middle strip these stresses are logically multiplied by the number of strands in the associated strip. Table 4-2 displays the determination of the number of strands in each strip, labelled as per Figure *4-1*, as well as the final prestressing forces determined after all losses including long term effects of concrete shrinkage. For comparison, it is worth noting that the values of prestressing used in the computer package RAM Conce*pt* are kept at a constant 1100 MPa without adjustments for friction or long term effects.

Table 4-2 *Prestressing summary for each column strip and middle strip*

Location	Total # of strands	cs area mm^2	Total cs area mm^2	Applied stress (MPa)	Prestress loss (MPa)	Final prestress	Applied P (kN)	**Final P (kN)**	*%loss*
1	28	94.3	2640.4	1484.5	80	1404.5	3919.7	**3708**	*5.39*
2	20	94.3	1886	1533.5	80	1453.5	2892.2	**2741**	*5.22*
3	26	94.3	2451.8	1533.5	80	1453.5	3759.8	**3564**	*5.22*
4	26	94.3	2451.8	1484.5	80	1404.5	3639.7	**3444**	*5.39*
5	20	94.3	1886	1541.8	80	1461.8	2907.8	**2757**	*5.19*
6	24	94.3	2263.2	1541.8	80	1461.8	3489.4	**3308**	*5.19*
7	20	94.3	1886	1484.5	80	1404.5	2799.8	**2649**	*5.39*
8	27	94.3	2546.1	1484.5	80	1404.5	3779.7	**3576**	*5.39*
9	24	94.3	2263.2	1533.5	80	1453.5	3470.6	**3290**	*5.22*
10	24	94.3	2263.2	1484.5	80	1404.5	3359.7	**3179**	*5.39*
11	24	94.3	2263.2	1541.8	80	1461.8	3489.4	**3308**	*5.19*

Note: *(cs=cross sectional)*

In summary, it can be seen in Table 4-2 that accurately calculated values contain a final prestress of approximately 1405 to 1460 MPa. These calculated values, which include accurate losses, are considerably higher that the assumed value of 1100 MPa due to the assumed losses. The effect of this inaccurate design assumption on deformation prediction will be quantified in later sections.

4.2.2. Applied Loads Calculations

Obtaining specifically accurate dead and live loads for each slab, along with the time of application, is logistically unfeasible. Due to this level of complexity for each specific slab it was determined that standard serviceability load factors would be incorporated in predicting deformations. AS 1170.1 (2002) states the short-term and long-term factors for live load application in a typical office space as 0.7 and 0.4, respectively. Self weight of the slab was determined using the density of the concrete, a value which was experimentally confirmed. Sustained loading due to permanent fixtures was supplied by the structural design engineer. Table 4-3 details the applied loads that were utilised in this research. It is worth noting in this section that the computer program RAM Conce*pt* utilises its own loading factors, which differ slightly from AS 1170.1 (2002). RAM conce*pt*'s loading factors are also displayed in Table 4-3.

Table 4-3 *Applied Loads utilised in 151 Pirie's deformation analysis*

	AS1170.1 (2002)	RAM Concept
Design Live Load (kPa)	3.0	3.0
Instantaneous Live Load reduction factor	0.4	0.25
Long Term Live Load reduction factor	0.7	0.65
Dead Load (kPa)	slab depth * density	slab depth * density
Extra Dead Load (kPa)	1.4	1.4

The difference between the two methods of determining applied loads is minimal. The only major difference that exists is the difference in instantaneous loading where AS 1170.1 (2002) recommends a factor of 0.4 where RAM Conce*pt* recommends 0.25. Instantaneous loadings have a significantly less effect on the maximum deformations experienced by the slab. Sustained loadings, which are the major contributor to maximum deformations remained quite similar.

4.2.3. Determining Accurate Moment of Inertia

Accurate values for moment of inertia are complicated to determine for slabs. Unlike columns and beams, slabs require the employment of effective widths, as practical values of widths do not exist for each strip. Many of the deformation prediction methods, summarised in Section 2.3.2, suggest a recommended width to use for calculations of moment of inertia. However, there remains a number of these deformation prediction methods which do not specify this input precisely. Of the specified values for width (w_{eff}), the following equations are recommended – w_{eff} = whole span, w_{eff} = 0.4 * span or w_{eff} = drop panel width.

The determination of effective width can also be calculated by methods presented by Eurocode 4 (1994) and Ansourian (1975) which are commonly used for composite slabs. For application of effective width in this research it is worth noting that the method suggested by AS 3600 (2001) is identical to the Eurocode 4 (1994) method. The two methods have been highlighted in Equation 4-1 and Equation 4-2, with reference to Figure 4-5 and Figure 4-6 (Oehlers & Bradford, 1999).

Eurocode 4 (1994) recommendation -

$$w_{eff} = 0.25 L_c$$

Equation 4-1

Ansourian (1975) recommendation –

$$\frac{b_{eff}}{T_{adj}/2} = 1.0 - 1.2\left(\frac{T_{adj}}{L_c}\right) \text{ when } \frac{T_{adj}}{L_c} \le 0.5 \text{ or; } b_{eff} = 0.1 L_c \text{ when } \frac{T_{adj}}{L_c} > 0.5$$

Equation 4-2

Figure 4-5 *Factors considered in determining effective width (Oehlers and Bradford, 1999).*

Figure 4-6 *Factors considered by Eurocode 4 (1994) in determining effective width (Oehlers and Bradford, 1999).*

Therefore, there are five different methods to determine the effective width considered in the calculation of moment of inertia. The first three methods, which include width = span, width = 0.4 * span and width = drop panel width, derive from RC slab analyses. The remaining two method of determining effective width derive from composite slab analysis and are summarised by Equation 4-1 and Equation 4-2.

The numerous column and middle strips at 151 Pirie contained equivalent cross sectional properties at certain locations. For example, column strip number 1 and column strip number 7 contained the same physical arrangements such as depths (of slab and drop panels), drop panel widths and adjacent span lengths. Due to these similarities it was found to be very beneficial to group together similar strips to reduce the number of strip analyses required for determining values of moment of inertia. It was found that for the strips located in the North – South (NS) direction there were 2 different types of strips. Strips numbered 1 and 7 were identical, and their values of moment of inertia were labelled "I_{NS1}". Strip number 4, which was the remaining NS strip, was labelled "I_{NS2}". All strips located in the EW direction were found to have identical properties and hence were all considered to have the same value of moment of inertial, labelled "I_{EW}".

Table 4-4 displays the values of moment of inertia for the three different categories of strips (I_{NS1}, I_{NS2} and I_{EW}). For each strip the five different methods of determining moment of inertia have been employed. Each strip contained drop panels which have higher local values of moment of inertia compared to the mid sections. Due to this difference in moment of inertia an average value of moment of inertia was determined based on a weighted average (of lengths) for each strip. This process was employed for each deformation prediction model which contains moment of inertia as a single valued input.

Table 4-4 *Comparison of Column Strip Moment of Inertias*

Sectional values of moment of inertia			Average values of moment of inertia		
	INS1			**INS1**	
	drop panel	middle			average
Weff = drop panel width	8.58E+09	1.60E+09		Weff = drop panel width	3.59E+09
Weff = 0.4 * span	1.07E+10	2.56E+09		Weff = 0.4 * span	4.89E+09
Weff = span	1.64E+10	6.40E+09		Weff = span	9.26E+09
Weff = Ansourian method	4.20E+09	7.84E+08		Weff = Ansourian method	1.76E+09
Weff = Eurocode 4 method	5.25E+09	9.80E+08		Weff = Eurocode 4 method	2.20E+09
	INS2			**INS2**	
	drop panel	middle			average
Weff = drop panel width	1.07E+10	2.00E+09		Weff = drop panel width	4.49E+09
Weff = 0.4 * span	1.21E+10	2.56E+09		Weff = 0.4 * span	5.29E+09
Weff = span	1.84E+10	6.40E+09		Weff = span	9.83E+09
Weff = Ansourian method	4.20E+09	7.84E+08		Weff = Ansourian method	1.76E+09
Weff = Eurocode 4 method	5.25E+09	9.80E+08		Weff = Eurocode 4 method	2.20E+09
	IEW			**IEW**	
	drop panel	middle			average
Weff = drop panel width	8.58E+09	1.60E+09		Weff = drop panel width	3.78E+09
Weff = 0.4 * span	1.01E+10	2.24E+09		Weff = 0.4 * span	4.70E+09
Weff = span	1.54E+10	5.60E+09		Weff = span	8.66E+09
Weff = Ansourian method	4.80E+09	8.96E+08		Weff = Ansourian method	2.12E+09
Weff = Eurocode 4 method	6.00E+09	1.12E+09		Weff = Eurocode 4 method	2.65E+09

I (mm^4)

Moment of inertia calculations were achieved for both the gross sectional properties as well as the transposed, or effective, sectional properties. A comparison was made to discover the effectiveness of the extra steps required to obtain transposed sectional properties for each deformation prediction calculation. A column strip analysis was performed on the 350 mm deep, 2400 mm wide, 9 strand section (including drop panel) where it was found that only a 0.6% difference was noticed between I_g and I_{trans}. Therefore, it was confirmed that minimal difference was evident between the two methods and gross sectional properties would retain adequate accuracy as well as ease of application. Tabulated results from this analysis have been presented in Table 4-5. It is worth noting that the change in concrete mix from N32 to N40, as well as prestress detailing, did slightly alter this outcome, but differences were insignificant. Therefore, it can be stated that gross sectional properties were adequate for all deformation prediction scenarios at 151 Pirie.

Table 4-5 *Example comparison of I_{gross} to I_{trans} for the PPS slab.*

	Gross Sectional Properties	Transposed Sectional Properties	Difference (%)
Cross Sectional Area (mm^2)	840000	844001	0.47
Moment of Inertia (mm^4)	8.58E+09	8.63E+09	0.58

The accurate inputs determined in this section are utilised in the following sections where the methods of deformation prediction are analysed. Assumptions, such as utilising the weighted average of moment of inertia to represent behaviour of the in situ member, are also examined.

4.3.   *Analysis of Slab Deformation Prediction Methods*

This section of the research investigates the application of a range of models of predicting both downward deflections and upward cambers. Accurate inputs for these models, and the associated level accuracy, have already been determined in earlier sections. The methods analysed in this section have been categorised into three categories. Firstly a simple numerical approach is analysed for both the design value inputs as well as the measured mean values obtained in the data analysis. In this comparison the design values refer to the inputs used in RAM Conce*pt* for the design of 151 Pirie, displayed in Table 4-3. Following this is a probabilistic approach to the same methods which utilises a Monte Carlo simulation to obtain a statistical prediction of deformations. Finally a detailed finite element approach is employed to reduce inaccuracies due to assumptions.

Each method of predicting a final deformation for a prestressed member contains the superimposed addition of predicted camber to predicted deflection. A final deformation value can then be compared to surveyed values on site. Logically individual predictions of camber and deflection can not be surveyed on site as they are naturally combined instantaneously on the same member. This unfortunately limits the ability to justify the accuracy of individual camber and deflection prediction models.

The range of deflection and camber prediction models analysed in this research, initially presented in Table 2-1 and Table 2-2, each contained slightly different values as inputs. For example, one model considers the value of slab depth (d) to be the entire depth of the slab whilst another model considers d to be the depth to the centre of the lower reinforcement. These slight differences have the ability to alter outcomes significantly. Hence, during the application of these models, a high degree of caution was taken to ensure that each of the inputs was utilised as the equation's developer(s) intended.

4.3.1. Numerical Approach to Slab Deformation Prediction

The array of deflection and camber prediction models available for use has been introduced and discussed previously in Section 2.3.2. From this list the most appropriate models for a numerical analysis at 151 Pirie were chosen. Reasons for excluding the remaining deformation prediction models were due to lack of directly applicable material property inputs for this numerical application. These models have been presented in Table 4-6 along with a brief description of their application.

To examine the application of these models, design values from 151 Pirie were utilised and applied to the models to observe the predicted deflections and cambers. The design values and models used have been displayed previously in Table 4-1. It is important to note that some equations were only applicable to mid panel deformations and hence can not be used to predict column strip deformations. For models which only predict column strip deformations, adjacent orthogonal column strip deformations were superimposed to obtain mid point deformations, as displayed previously in Figure 2-2. For this example analysis the moment of inertias from strips I_{EW} and I_{NS1} were utilised.

Table 4-6 *Expressions for predicting slab deflection and camber for use in numerical analysis*

Researcher	DEFLECTION CALCULATION	Comment
Chang and Hwang (1996)	$$\Delta_{b1} = \frac{1}{384}\frac{(wl_2){l_{n1}}^4}{EI_{b1}}$$ $$\Delta_{b2} = \frac{1}{384}\frac{(wl_2){l_{n2}}^4}{EI_{b2}}$$	- Sub scripts 1 & 2 denote the x & y direction. - Column strip deflection prediction, or combine to obtain mid panel deflection
Hwang and Chang (1996)	$$\Delta = \frac{0.00128wl^4}{D}$$ **where** $$D = \frac{E_c h^3}{12}\left(1 - v^2\right)$$	- Mid panel deflection prediction only. - Intended for use with continuous supports.
Collins and Mitchell (1997)	$$\Delta = \frac{2.60}{384}\frac{wl^4}{EI}$$	- Column strip deflection predictions only. - Use with continuous supports only.
Naaman (1983)	$$\Delta = \frac{5}{384}\frac{wl^4}{EI}$$	- Intended for use with column strip deflection predictions. - Intended for use with pinned supports.
Warner et al. (1998)	$$\Delta = K_1 K_2 \frac{(w + k_{cs}w_s)}{7E_c}L\left(\frac{L_n}{d}\right)^3$$	- K1 and K2 are constants that account for slab location. - Mid panel deflection prediction only.
Researcher	**CAMBER CALCULATIONS**	**Comment**
Collins and Mitchell (1997)	$$\Delta = \frac{5}{48}\frac{Pel^2}{EI}$$	- e is the difference between end and mid tendon drape height
Namaan (1983)	$$\Delta = \frac{Pl^2}{8EI}\left[e_2 + \frac{5}{6}(e_1 - e_2)\right]$$	- e1 is the distance from the centre line down to the mid drape height. - e2 is the distance from the centre line down to the end drape height.

A range of effective widths, which affects the moment of inertia, were incorporated into this analysis of camber and deflection models. Overall total slab movement (combined deflection and camber) was not calculated due to the numerous possibilities of pairing deflection and camber equations. For this comparison the design values of material properties was utilised. Both short term and long term loadings were included in this analysis. The outcomes of this comparison has been displayed in Table 4-7.

Table 4-7 *Initial comparison of Camber and Deflection equations for short and long term loading*

	SHORT TERM ANALYSIS					
	N32 design values			N40 design values		
	NS	EW	MID	NS	EW	MID
Camber	(mm)	(mm)	(mm)	(mm)	(mm)	(mm)
Collins and Mitchell (1997) (Weff = span)	9.7	15.1	24.8	8.5	13.4	21.9
Collins and Mitchell (1997) (Weff = drop panel width)	24.9	34.6	59.5	22.1	30.7	52.7
Collins and Mitchell (1997) (Weff = 0.4 x span)	18.3	27.8	46.1	16.2	24.7	40.8
Collins and Mitchell (1997) (Ansourians method)	50.8	61.7	112.5	45.0	54.7	99.6
Collins and Mitchell (1997) (Eurocode 4 method)	40.6	49.4	90.0	36.0	43.7	79.7
Naaman (1983) (Weff = span)	2.8	4.7	7.5	2.5	4.2	6.6
Naaman (1983) (Weff = drop panel width)	7.1	10.8	18.0	6.3	9.6	15.9
Naaman (1983) (Weff = 0.4 x span)	5.2	8.7	13.9	4.6	7.7	12.4
Naaman (1983) (Ansourians method)	14.6	19.3	33.9	12.9	17.1	30.0
Naaman (1983) (Eurocode 4 method)	11.6	15.4	27.1	10.3	13.7	24.0
Deflection						
Chang and Hwang (1996) (Weff = span)	-2.4	-3.9	-6.3	-2.1	-3.5	-5.6
Chang and Hwang (1996) (Weff = drop panel width)	-6.1	-9.0	-15.0	-5.4	-7.9	-13.3
Chang and Hwang (1996) (Weff = 0.4 x span)	-4.5	-7.2	-11.7	-3.9	-6.4	-10.3
Chang and Hwang (1996) (Ansourians method)	-12.4	-16.0	-28.4	-11.0	-14.2	-25.1
Chang and Hwang (1996) (Eurocode 4 method)	-9.9	-12.8	-22.7	-8.8	-11.3	-20.1
Hwang and Chang (1996) (using α[1])			-19.8			-17.5
Hwang and Chang (1996) (using α[2])			-9.1			-8.0
Hwang and Chang (1996) (using α[3])			-9.5			-8.4
Collins and Mitchell (1997) (Weff = span)	-8.3	-13.3	-21.7	-7.4	-11.8	-19.2
Collins and Mitchell (1997) (Weff = drop panel width)	-21.5	-30.5	-52.0	-19.1	-27.0	-46.1
Collins and Mitchell (1997) (Weff = 0.4 x span)	-15.8	-24.5	-40.3	-14.0	-21.7	-35.7
Collins and Mitchell (1997) (Ansourians method)	-43.9	-54.4	-98.3	-38.9	-48.2	-87.1
Collins and Mitchell (1997) (Eurocode 4 method)	-35.1	-43.5	-78.6	-31.1	-38.5	-69.6
Naaman (1983) (Weff = span)	-16.0	-25.6	-41.6	-14.2	-22.7	-36.9
Naaman (1983) (Weff = drop panel width)	-41.4	-58.7	-100.0	-36.7	-52.0	-88.6
Naaman (1983) (Weff = 0.4 x span)	-30.4	-47.2	-77.6	-26.9	-41.8	-68.7
Naaman (1983) (Ansourians method)	-84.4	-104.6	-189.0	-74.8	-92.6	-167.4
Naaman (1983) (Eurocode 4 method)	-67.5	-83.7	-151.2	-59.8	-74.1	-133.9
Warner et al. (1998)			-64.1			-56.8

	LONG TERM ANALYSIS					
	N32 design values			N40 design values		
	NS	EW	MID	NS	EW	MID
Camber	(mm)	(mm)	(mm)	(mm)	(mm)	(mm)
Collins and Mitchell (1997) (Weff = span)	28.9	45.2	74.0	27.2	42.6	69.8
Collins and Mitchell (1997) (Weff = drop panel width)	74.5	103.5	178.0	70.2	97.6	167.7
Collins and Mitchell (1997) (Weff = 0.4 x span)	54.7	83.2	137.9	51.5	78.5	130.0
Collins and Mitchell (1997) (Ansourians method)	151.9	184.6	336.4	143.2	174.0	317.1
Collins and Mitchell (1997) (Eurocode 4 method)	121.5	147.6	269.1	114.5	139.2	253.7
Naaman (1983) (Weff = span)	10.0	17.0	27.0	8.8	15.1	23.9
Naaman (1983) (Weff = drop panel width)	25.7	39.0	64.7	22.8	34.5	57.3
Naaman (1983) (Weff = 0.4 x span)	18.9	31.3	50.2	16.7	27.8	44.5
Naaman (1983) (Ansourians method)	52.4	69.5	121.9	46.4	61.5	108.0
Naaman (1983) (Eurocode 4 method)	41.9	55.6	97.5	37.1	49.2	86.4
Deflection						
Chang and Hwang (1996) (Weff = span)	-8.5	-14.1	-22.6	-7.5	-12.5	-20.0
Chang and Hwang (1996) (Weff = drop panel width)	-21.9	-32.3	-54.1	-19.4	-28.6	-47.9
Chang and Hwang (1996) (Weff = 0.4 x span)	-16.1	-26.0	-42.0	-14.2	-23.0	-37.2
Chang and Hwang (1996) (Ansourians method)	-44.6	-57.5	-102.1	-39.5	-51.0	-90.5
Chang and Hwang (1996) (Eurocode 4 method)	-35.7	-46.0	-81.7	-31.6	-40.8	-72.4
Hwang and Chang (1996) (using α[1])			-71.2			-63.1
Hwang and Chang (1996) (using α[2])			-32.7			-28.9
Hwang and Chang (1996) (using α[3])			-34.1			-30.2
Collins and Mitchell (1997) (Weff = span)	-30.0	-47.9	-78.0	-26.6	-42.5	-69.1
Collins and Mitchell (1997) (Weff = drop panel width)	-77.5	-109.8	-187.3	-68.6	-97.3	-165.9
Collins and Mitchell (1997) (Weff = 0.4 x span)	-56.9	-88.3	-145.2	-50.4	-78.2	-128.6
Collins and Mitchell (1997) (Ansourians method)	-158.0	-195.8	-353.8	-140.0	-173.4	-313.4
Collins and Mitchell (1997) (Eurocode 4 method)	-126.4	-156.7	-283.1	-112.0	-138.7	-250.7
Naaman (1983) (Weff = span)	-57.8	-92.2	-149.9	-51.2	-81.6	-132.8
Naaman (1983) (Weff = drop panel width)	-149.0	-211.2	-360.2	-131.9	-187.1	-319.0
Naaman (1983) (Weff = 0.4 x span)	-109.4	-169.9	-279.2	-96.9	-150.4	-247.3
Naaman (1983) (Ansourians method)	-303.9	-376.6	-680.4	-269.1	-333.5	-602.7
Naaman (1983) (Eurocode 4 method)	-243.1	-301.3	-544.3	-215.3	-266.8	-482.1
Warner et al. (1998)			-230.8			-204.4

note – positive results denote upward deformations for both camber and deflection. α[1], α[2] and α[3] relate to constants which effect the flexural rigidity of the slab.

A large number of conclusions can be drawn from reviewing the results in Table 4-7. Firstly it is clear that long term deflection and camber results were significantly higher than short term loadings, which was to be expected due to the effect creep has on E_c. Secondly it can be seen that the predicted deflections and cambers increase as the effective width or moment of inertia decreases. It can also be seen in the data displayed in Table 5.6 that increasing the concrete mix from N32 to N40 decreased the predicted camber or deflection by approximately 5 to 15%.

One of the main reasons for this initial numerical analysis was to determine the most appropriate deflection and camber prediction models for future use. Explained in the comments of Table 4-6 is that the deflection model produced by Naaman (1983) is intended to be used for pinned support conditions. This indicates a tendency for this model to over-predict values of deflections. The data produced from this model confirms this inaccurate tendency, with unrealistic deflections as high as 680.4 mm predicted. The model produced by Warner et al. (1998) also contains an over-predictive tendency with predicted deflections as high as 230.8 mm. This is expected to be due to the model being designed for use with RC slabs, rather than prestressed slabs. RC slab deflections are usually within the region of less than 40 mm so this model is operating outside of its designed parameters.

The deflection equation by Hwang and Chang (1996) contains limitations of application to only mid panel deflections. Due to this limitation this model was considered less favourable. The model proposed by Chang and Hwang (1996) is applicable to all sections of a slab. However, upon closer examination of the development of this model, it was also considered unfavourable due to the model being developed for usage with material properties which performed at significantly lower levels (28 day f_c of less than 20 MPa). Naaman (1983) proposes a camber model which contains eccentricity inputs that assume the level of prestressing does not extend higher than the centre line of the slab. This assumption is applicable to linear tendon profiles found in many slabs and other prestressed members, but is not the case for the PPS slabs at 151 Pirie. Due to this reason the remaining model derived by Collins and Mitchell (1997) is preferred.

In summary the preferred models of predicting deflections and camber for application in this research is the camber model proposed by Collins and Mitchell (1997) and the deflection model also proposed by Collins and Mitchell (1997). Reasons for these models being the preferred models include both of these models being developed for usage with PPS slabs as well as being developed for the material properties and prestress properties found onsite at 151 Pirie. These models are applicable for finding deformations at all required locations of the slab. These equations are also beneficial as they were developed for combined usage to determine accurate total deformations.

Collins and Mitchell (1997) do not specify, in either their deflection or camber prediction models, the most suitable value for effective width. Vanderbilt et al. (1963) discusses in great depth the usage of effective widths in flat slab. Vanderbilt et al. (1963) recommends the usage of 0.4 * span as the effective width for this specific scenario. Warner et al. (1998), who performed a comprehensive comparison of deflection prediction methods, refers to this method and draws focus to this method being widely accepted by flat slab designers. Due to the reasons stated above it can be summarised that the most appropriate method of predicting deformations at 151 Pirie includes the deformation prediction method by Collins and Mitchell (1997) combined with an effective width of 0.4 * span.

It is important to note that the data displayed in Table 4-7 does not include the effects of shrinkage. The predicted long term deformations and cambers include the effects of creep, as creep has a direct effect on the material properties and hence the predicted deformations. The effects of shrinkage are independent of other material properties or loadings, therefore shrinkage has been considered a separate form of deformation. For this comparative analysis, where individual values of deflection and camber are compared, shrinkage values are considered independent. Shrinkage will, however, be included in further calculations where final values of overall slab deformation are predicted.

The method of calculating deformations due to concrete shrinkage adopted by this research is the method proposed by Branson (1968). In this method concrete shrinkage strains are used to calculate an induced member curvature. This curvature can then be used to determine a member deflection. The shrinkage calculation is displayed in Equation 4-3.

$$\phi = 3.2 \times \frac{\varepsilon_{shrinkage} \, p^{0.33}}{D} \quad \text{where} \quad p = \frac{A_{st}}{bd} \qquad \textbf{Equation 4-3}$$

After establishing an appropriate method of numerical analysis, it was possible to establish a comparison between differing material property inputs. This comparison was used to determine the effect of utilising conservative design values of material properties to predict serviceability behaviour. Utilising experimentally recorded material properties minimises material property and prestressing inaccuracies and yields more accurate deformation predictions. For the initial application of exact material and prestressing properties it was assumed that the prestressing force in each strip was equal to the average prestressing force in that direction, for that bay. Prestressing quantities do differ slightly, as shown in Table 5.2, but not significantly enough to justify the extra time taken for multiple calculations in the initial calculation comparisons. Exact values of prestressing force are applied to the final statistical calculation methods chosen after this stage. Table 4-8 displays the outcomes of this analysis, where final slab deformations can now be

determined considering all influencing factors. The effects of shrinkage have been included in both the short and long term analysis as per the design specifications. An admixture was included in the concrete mix which helps induce high early age strength which induces early age shrinkage.

Table 4-8 *Comparison of deflection and camber predictions with altered material property inputs*

	N32 SHORT TERM ANALYSIS								
	Design values			Lab cured values			Site cured values		
	NS Strip	EW Strip	Midpoint	NS Strip	EW Strip	Midpoint	NS Strip	EW Strip	Midpoint
Camber (mm)	18.3	27.8	46.1	15.9	24.2	40.0	18.1	27.5	45.6
Deflection (mm)	-15.8	-24.5	-40.3	-13.7	-21.3	-35.0	-15.6	-24.3	-39.9
Shrinkage (mm)	-1.7	-1.3	-3.0	-1.7	-1.3	-3.0	-1.7	-1.3	-3.0
Total Deformation (mm)	**0.8**	**2.0**	**2.8**	**0.5**	**1.6**	**2.1**	**0.8**	**2.0**	**2.8**

	N32 LONG TERM ANALYSIS								
	Design values			Lab cured values			Site cured values		
	NS Strip	EW Strip	Midpoint	NS Strip	EW Strip	Midpoint	NS Strip	EW Strip	Midpoint
Camber (mm)	54.7	83.2	137.9	44.9	68.4	113.4	52.3	79.7	132.1
Deflection (mm)	-56.9	-88.3	-145.2	-49.4	-76.7	-126.1	-56.2	-87.4	-143.6
Shrinkage (mm)	-1.7	-1.3	-3.0	-1.7	-1.3	-3.0	-1.7	-1.3	-3.0
Total Deformation (mm)	**-3.9**	**-6.4**	**-10.2**	**-6.1**	**-9.5**	**-15.7**	**-5.6**	**-8.9**	**-14.5**

	N40 SHORT TERM ANALYSIS								
	Design values			Lab cured values			Site cured values		
	NS Strip	EW Strip	Midpoint	NS Strip	EW Strip	Midpoint	NS Strip	EW Strip	Midpoint
Camber (mm)	16.2	24.7	40.8	14.1	21.5	35.6	17.1	26.1	43.3
Deflection (mm)	-14.0	-21.7	-35.7	-12.2	-19.0	-31.2	-14.8	-23.0	-37.8
Shrinkage (mm)	-1.7	-1.3	-3.0	-1.7	-1.3	-3.0	-1.7	-1.3	-3.0
Total Deformation (mm)	**0.5**	**1.6**	**2.2**	**0.2**	**1.3**	**1.5**	**0.7**	**1.8**	**2.5**

	N40 LONG TERM ANALYSIS								
	Design values			Lab cured values			Site cured values		
	NS Strip	EW Strip	Midpoint	NS Strip	EW Strip	Midpoint	NS Strip	EW Strip	Midpoint
Camber (mm)	51.5	78.5	130.0	37.0	56.4	93.4	45.7	69.6	115.3
Deflection (mm)	-51.9	-80.5	-132.4	-44.0	-68.3	-112.2	-53.3	-82.8	-136.2
Shrinkage (mm)	-1.7	-1.3	-3.0	-1.7	-1.3	-3.0	-1.7	-1.3	-3.0
Total Deformation (mm)	**-2.0**	**-3.3**	**-5.3**	**-8.6**	**-13.1**	**-21.7**	**-9.3**	**-14.5**	**-23.8**

*note – positive results denote upward deformations for both camber and deflection.

The results produced in Table 4-8 indicate that for each location, as well as each set of material properties and mix of concrete, short term behaviour results in a final upward camber of up to 2.8 mm. Long term behaviour for each scenario then reveals a predicted final downward deformation of between 2.0 mm and 23.8 mm. Instantly it can be seen that these values are within the range of values measured on site. Typical short term behaviour of PPS slabs results in a relatively balanced deflection and camber scenario. Surveyed values of long term deformations (depending on span) are commonly in the order of 10 to 30 mm.

To discuss the results further it is useful to present this outcome graphically and this has been done in Figure 4-7. For the sake of this graphical comparison it has been assumed that short term is equivalent to 3 months and long term is equivalent to 3 years.
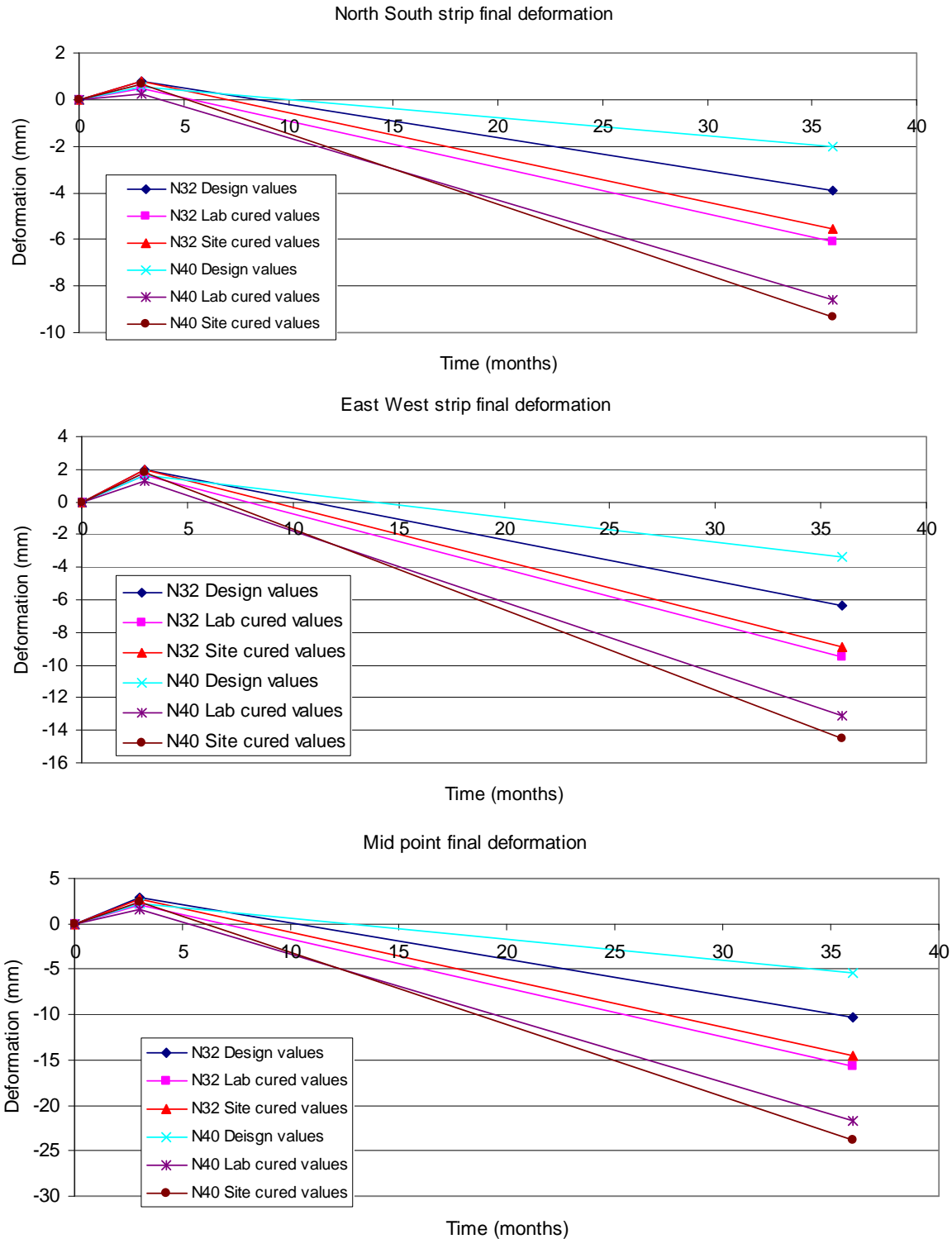

Figure 4-7 Graphical representation of the deformations predicted via numerical analysis

Examining the results in Figure 4-7 reveals a rather interesting outcome. It can be seen in each strip's long term results, within a certain concrete mix, that design values result in a lower overall predicted deformation. This trend hold true even though individual values of deflection and camber,

displayed in Table 4-8, often yield the highest predictions. When using conservative values of material properties the natural expectation is to over predict values of deformation. This does not appear to be the case, in fact the opposite appears to hold true for column strip deformations as well as mid point deformations. There also appears to be an unusual observation when comparing the results between the N32 mix and the N40 mix. Naturally a concrete mix with a higher value of E_{ci} and E_c should produce a lower value of long term deformation. Once again this expectation is not observed. Upon closer examination of the equations used to receive these results it becomes clear that it is not the magnitude of each material property that determines deformation predictions.

Camber prediction calculations require an input value of E_{ci} which is the modulus of elasticity which relates to the timing of prestress application (typically 7 days). Deflection prediction calculations require an input value of E_c which relates to the 28 day material property of E_c. Considering that deflections and cambers are negatively superimposed to obtain the deformation; it becomes clear that it is the ratio of E_{ci} to E_c which is of importance for predicting the magnitude of final deformation. Individual values of material properties have little meaning due to the cancellation effect of superimposing cambers and deflections to obtain overall deformation. Currently this ratio receives minimal consideration in typical design practise. This is evident in the values of E_{ci} and E_c chosen in the design stages of 151 Pirie. Table 5.1 shows that a constant value of E_{ci} is selected for both the N32 and N40 mixes. Data recorded from site reveals that this assumption may contain sufficient error. Data taken from 151 Pirie suggests that an increase in E_{ci} in the order of approximately 10% should be expected for this change in concrete mix. This lack of change of the value of E_{ci} when changing mixes gives reason for the inaccurate trends noticed in results in Figure 4-7.

In summary of this deterministic approach to serviceability behaviour it can be stated that the magnitudes of each deflection and camber equation are not of interest when considering overall deformations. It is the ratio of E_{ci} to E_c which effectively governs the magnitude of the final deformation. Further investigations into this ratio and the accurate determination of values of E_{ci} and E_c are covered in subsequent sections.

The next step in this analysis of slab deformation predictions incorporates the use of the natural variation in material properties experienced on site. For this stage of analysis, the material property data analysis is combined with a Monte Carlo simulation to investigate how much variation in deformations will be noticed for natural variations in material properties.

4.3.2. Monte Carlo Simulation of Slab Deformation Prediction

### 4.3.2.1.　Introduction of Monte Carlo Simulation Method

A Monte Carlo simulation is a useful and powerful tool which can be applied easily to complex engineering problems. In situations where inputs to single or multiple models are known to contain a specific statistical distribution, a Monte Carlo simulation is used to produce a statistical output. This is achieved by using number generators to create multiple individual values when combined represent the input's statistical distribution. These generated values are then each used individually in the model(s) to determine values of output. This process is then repeated multiple times, each time recording the value of output, until a clear statistical distribution of output is determined.

A Monte Carlo simulation is the ideal method for utilising the statistical distribution of material properties, which has been determined in earlier sections, and applying deformation prediction models. For this application it has been assumed that the array of material properties is normally distributed. It has also been assumed that the scatter of 7 day values and 28 day values are completely independent of each other and are each normally distributed. The accuracy of both of these assumptions is hard to determine, however, for this research these assumptions are considered to contain negligible effect on the final outcomes. These assumptions, as well as other factors which have the potential to limit accuracy are covered later in Section 4.5.

A comparison of the processes of the commonly used numerical method and the Monte Carlo simulations has been highlighted in Figure 4-8 and Figure 4-9 respectively. It should be noted that typical numerical processes utilise design values which are lower than the statistical mean values recorded. The numerical analysis in the previous section of this research incorporated both design and accurate mean values in its numerical analysis. However, it did not take into account the magnitude of the variation (or scatter) of each input. A Monte Carlo simulation will consider this magnitude of variation of each input. The numerical analysis in the previous section, which utilises the statistical mean values, also utilised the same models as this Monte Carlo simulation. Therefore, the mean outputs of the numerical analysis and the Monte Carlo simulation will be identical. The reason for application of the Monte Carlo simulation is to determine the effect of the scatter of the material properties on the scatter of the predicted deflections. Once the scatter of the output is determined, confidence limits of predicted deformations can be produced.

CONCRETE MATERIAL
PROPERTIES

Compressive strength (f'$_c$)
Modulus of Elasticity (E$_c$)
Tensile Strength (f'$_t$)
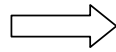
Single deterministic
deflection prediction
equations.
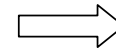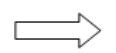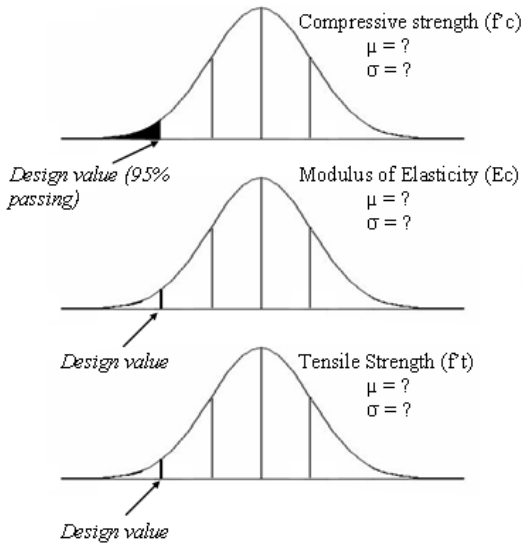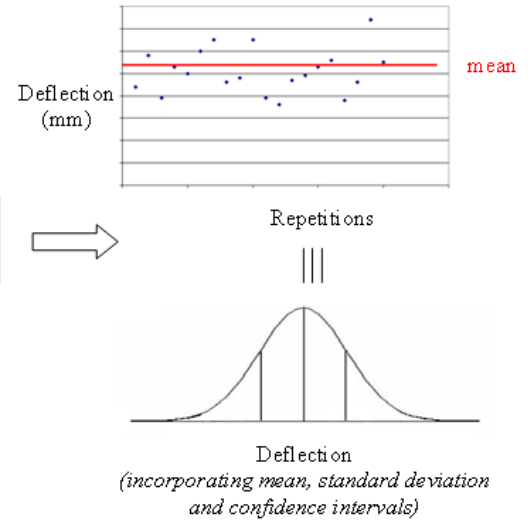
Deflection prediction
as a single value.

INPUT   **PROCESS**   **OUTPUT**

Figure 4-8 *Flow diagram of numerical serviceability behaviour prediction.*

CONCRETE MATERIAL PROPERTIES

Compressive strength (f'c)
μ = ?
σ = ?

Design value (95% passing)

Modulus of Elasticity (Ec)
μ = ?
σ = ?

Design value

Tensile Strength (f't)
μ = ?
σ = ?

Design value

Monte Carlo Simulation of Deflection prediction equations.

Deflection (mm)

mean

Repetitions

|||

Deflection
(incorporating mean, standard deviation and confidence intervals)

INPUT   **PROCESS**   **OUTPUT**

Figure 4-9 *Flow diagram of statistical approach to serviceability behaviour prediction.*

4.3.2.2. Explanation and Justification of Monte Carlo Simulation

The Monte Carlo simulation was created using Microsoft Excel. Inputs such as slab spans, loadings and prestressing details are variables inputted into the program by the user. The user then selects a specific concrete mix from one of the four following options; N32 lab, N32 site, N40 lab or N40 site. Each concrete mix, which relates to the mix type and curing conditions, has an associated mean and standard deviation for f$_{ci}$ and f$_c$. Once this combination of inputs has been selected, the program then runs a macro which creates a list of one thousand data points for both f$_{ci}$ and f$_c$ which relate to the realistic material properties experienced on site. Individual values of f$_{ci}$ and f$_c$ are then used to calculate E$_{ci}$ and E$_c$ based on the accurate model E$_c$=5850.6*$\sqrt{}$f$_c$. The scatter of E$_{ci}$ and E$_c$ is then applied to these values to ensure that an accurate statistical array of E$_c$ and E$_{ci}$ is produced. This method yields sufficient values which represent an accurate statistical array of f$_{ci}$, f$_c$, E$_{ci}$, and E$_c$ for each of the concrete mixes. The numerical deformation prediction method, explained in Section 4.3.1, is then applied individually to each set of the 7 and 28 day material properties to yield one

thousand corresponding deflection and camber predictions for each model. The one thousand predicted deflections and cambers are then combined to yield final deformations. The mean and standard deviations of the array of deflections, cambers and final deformations can then be determined. A flow diagram highlighting this process is presented in Figure 4-10.
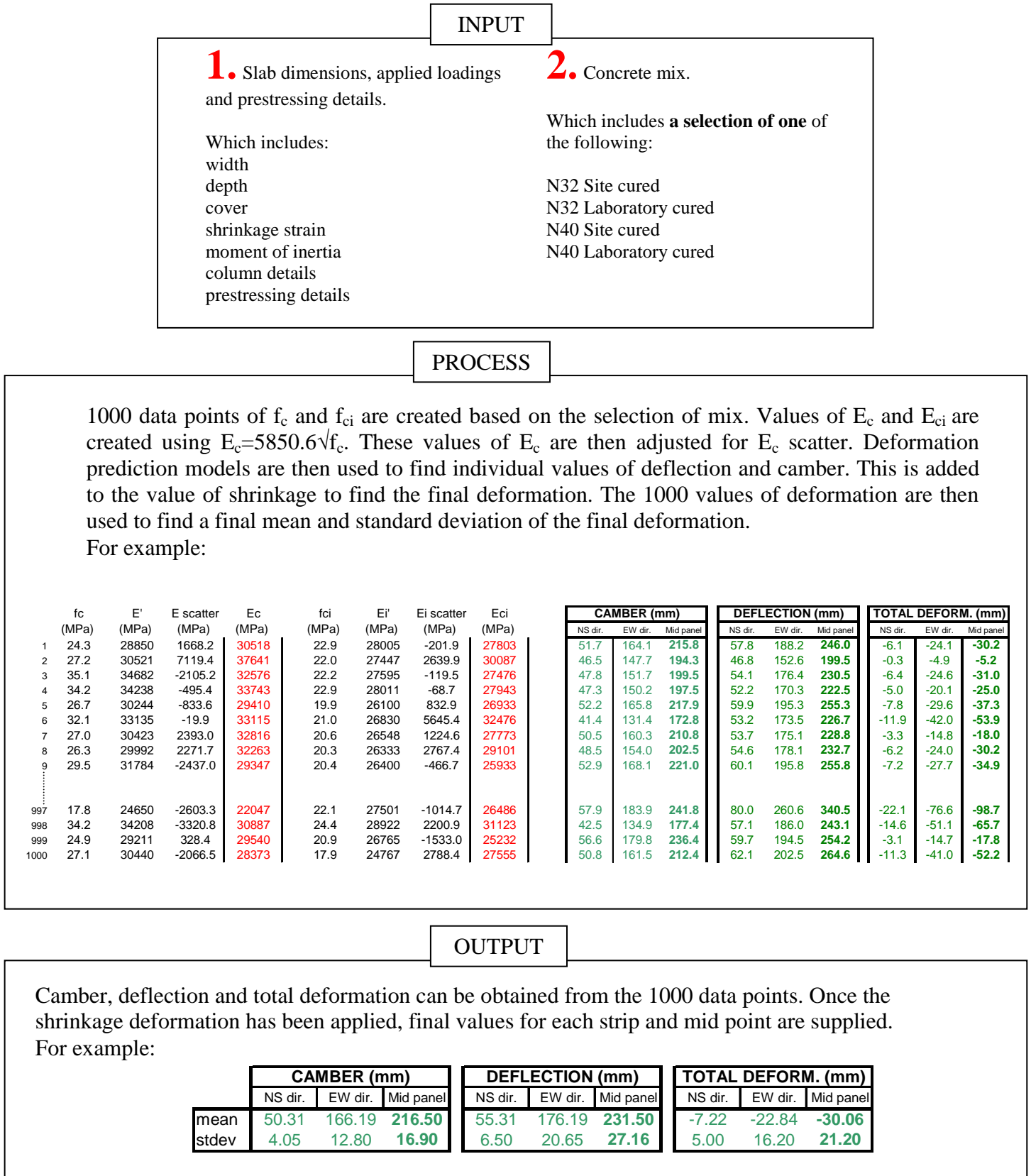
INPUT

1. Slab dimensions, applied loadings and prestressing details.

Which includes:
width
depth
cover
shrinkage strain
moment of inertia
column details
prestressing details

2. Concrete mix.

Which includes **a selection of one** of the following:

N32 Site cured
N32 Laboratory cured
N40 Site cured
N40 Laboratory cured

PROCESS

1000 data points of f_c and f_{ci} are created based on the selection of mix. Values of E_c and E_{ci} are created using $E_c=5850.6\sqrt{f_c}$. These values of E_c are then adjusted for E_c scatter. Deformation prediction models are then used to find individual values of deflection and camber. This is added to the value of shrinkage to find the final deformation. The 1000 values of deformation are then used to find a final mean and standard deviation of the final deformation.
For example:

	fc (MPa)	E' (MPa)	E scatter (MPa)	Ec (MPa)	fci (MPa)	Ei' (MPa)	Ei scatter (MPa)	Eci (MPa)	CAMBER (mm)			DEFLECTION (mm)			TOTAL DEFORM. (mm)		
									NS dir.	EW dir.	Mid panel	NS dir.	EW dir.	Mid panel	NS dir.	EW dir.	Mid panel
1	24.3	28850	1668.2	30518	22.9	28005	-201.9	27803	51.7	164.1	215.8	57.8	188.2	246.0	-6.1	-24.1	-30.2
2	27.2	30521	7119.4	37641	22.0	27447	2639.9	30087	46.5	147.7	194.3	46.8	152.6	199.5	-0.3	-4.9	-5.2
3	35.1	34682	-2105.2	32576	22.2	27595	-119.5	27476	47.8	151.7	199.5	54.1	176.4	230.5	-6.4	-24.6	-31.0
4	34.2	34238	-495.4	33743	22.9	28011	-68.7	27943	47.3	150.2	197.5	52.2	170.3	222.5	-5.0	-20.1	-25.0
5	26.7	30244	-833.6	29410	19.9	26100	832.9	26933	52.2	165.8	217.9	59.9	195.3	255.3	-7.8	-29.6	-37.3
6	32.1	33135	-19.9	33115	21.0	26830	5645.4	32476	41.4	131.4	172.8	53.2	173.5	226.7	-11.9	-42.0	-53.9
7	27.0	30423	2393.0	32816	20.6	26548	1224.6	27773	50.5	160.3	210.8	53.7	175.1	228.8	-3.3	-14.8	-18.0
8	26.3	29992	2271.7	32263	20.3	26333	2767.4	29101	48.5	154.0	202.5	54.6	178.1	232.7	-6.2	-24.0	-30.2
9	29.5	31784	-2437.0	29347	20.4	26400	-466.7	25933	52.9	168.1	221.0	60.1	195.8	255.8	-7.2	-27.7	-34.9
997	17.8	24650	-2603.3	22047	22.1	27501	-1014.7	26486	57.9	183.9	241.8	80.0	260.6	340.5	-22.1	-76.6	-98.7
998	34.2	34208	-3320.8	30887	24.4	28922	2200.9	31123	42.5	134.9	177.4	57.1	186.0	243.1	-14.6	-51.1	-65.7
999	24.9	29211	328.4	29540	20.9	26765	-1533.0	25232	56.6	179.8	236.4	59.7	194.5	254.2	-3.1	-14.7	-17.8
1000	27.1	30440	-2066.5	28373	17.9	24767	2788.4	27555	50.8	161.5	212.4	62.1	202.5	264.6	-11.3	-41.0	-52.2

OUTPUT

Camber, deflection and total deformation can be obtained from the 1000 data points. Once the shrinkage deformation has been applied, final values for each strip and mid point are supplied.
For example:

	CAMBER (mm)			DEFLECTION (mm)			TOTAL DEFORM. (mm)		
	NS dir.	EW dir.	Mid panel	NS dir.	EW dir.	Mid panel	NS dir.	EW dir.	Mid panel
mean	50.31	166.19	216.50	55.31	176.19	231.50	-7.22	-22.84	-30.06
stdev	4.05	12.80	16.90	6.50	20.65	27.16	5.00	16.20	21.20

***Figure 4-10** Flow diagram of the Monte Carlo Simulation.*

Justification of the accuracy of applying the Monte Carlo simulation can be achieved by graphing the experimentally measured material properties against the 1000 data points produced. This comparison allows an examination of the accuracy of the f_c values produced as well as the applied material property models. The graphs of the values of f_c and f_{ci} have been produced for the N40 lab cured mix and is displayed in Figure 4-11. The comparison of E_c to f_c as well as the comparison of E_{ci} to f_{ci} is displayed in Figure 4-12. For this comparison the corresponding experimentally measured values have been supplied.

N40 Lab cured		
	fci (MPa)	fc (MPa)
mean	32.27	47.01
stdev	3.56	3.94
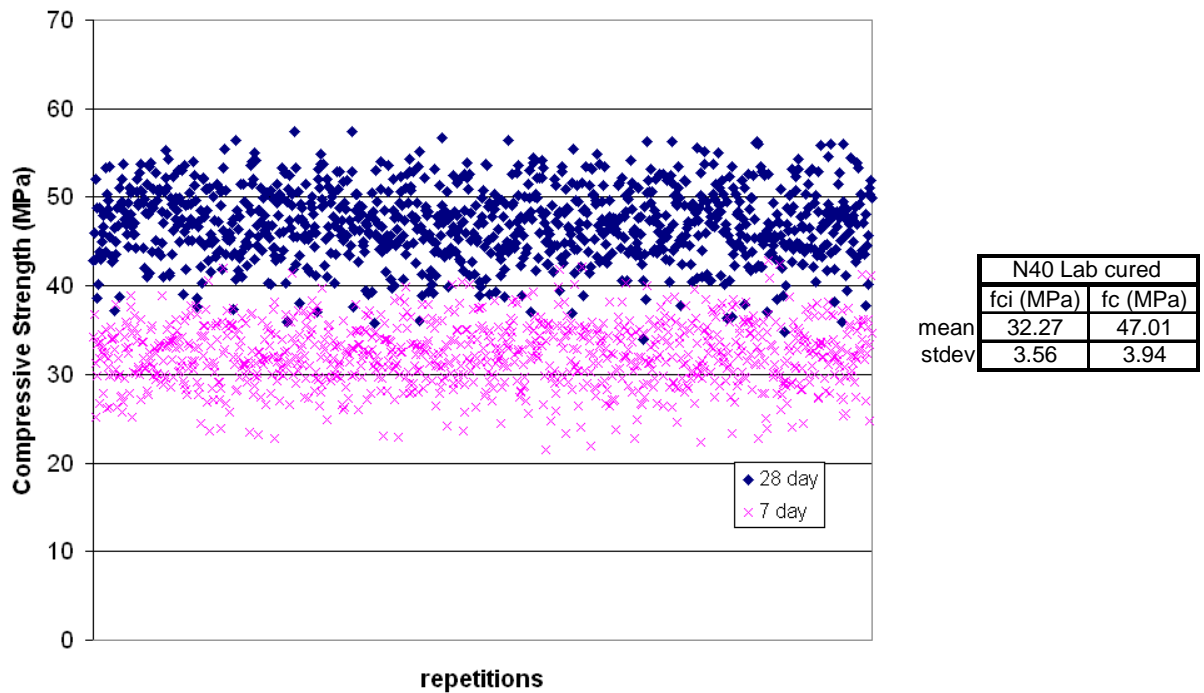
Figure 4-11 Justifying the accuracy of statistical array of compressive strengths
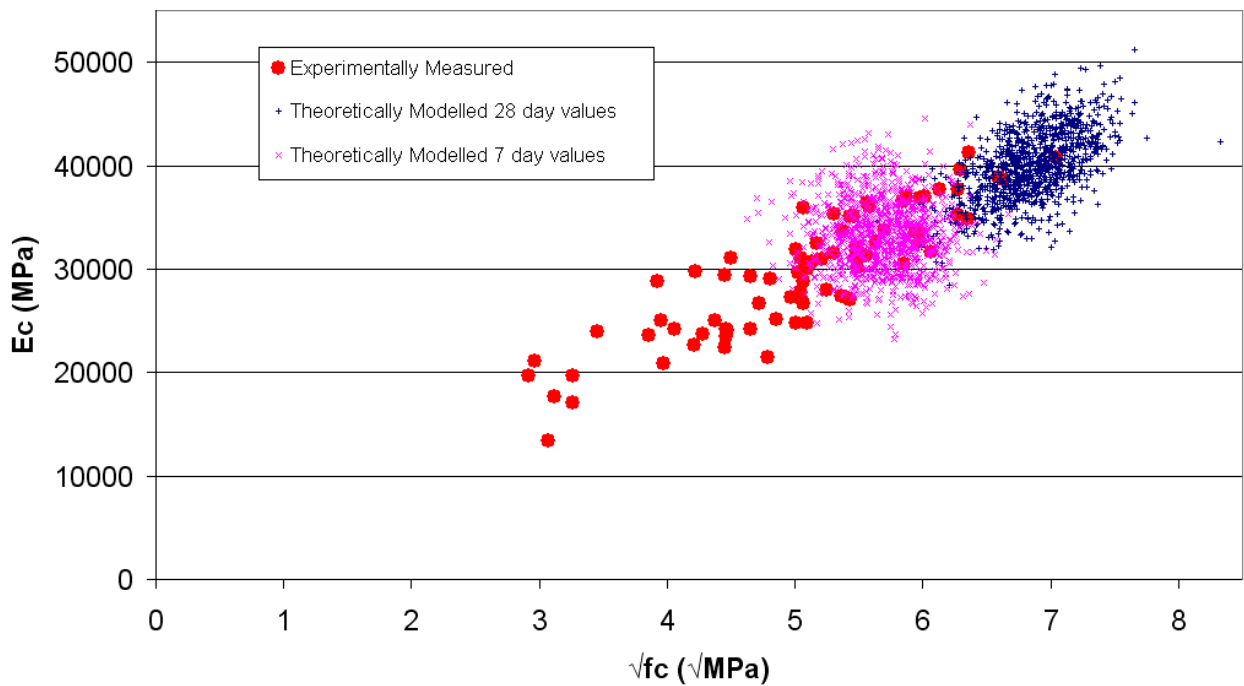
Figure 4-12 Justifying the accuracy of material property models

To complete the Monte Carlo justification of accuracy, the program was used to compare final outputs with a separate analysis. The separate analysis chosen was the well detailed explanation of deflection prediction supplied by Warner et al. (1998). Although this method was not selected as the most appropriate or accurate method for deformation prediction at 151 Pirie, the method can still be used to justify the accuracy of the Monte Carlo model. The main reason the example supplied by Warner et al. (1998) was chosen was due to the high level of detail of supplied inputs, this ensures that inaccuracies were not introduced due to incorrect inputs. The model produced by Warner et al. (1998) was applied to a continuous RC slab. The same inputs and models were utilised with the program to produce a single deflection value. As expected this single deflection prediction value (32 mm) was identical to the supplied answer. Following this, a Monte Carlo simulation was achieved with realistic statistical arrangement of the N32 concrete. This analysis yielded a deformation prediction of $\mu = 29.7$ mm and $\sigma = 2.6$ mm. This slight difference between supplied deformation, 32 mm, and the predicted deformation can be explained by the difference between using mean values of material properties and conservative design values. The standard deviation of final deformation was considered to be of a reasonable magnitude, however, there exists no benchmark for comparison.

In summary it can be stated that the Monte Carlo simulation is sufficiently accurate to be applied to the PPS slabs at 151 Pirie. Both the initial values of compressive strength as well as the material property models can be monitored for accuracy during the multiple simulations achieved.

4.3.2.3. Results of the Monte Carlo Simulation

The Monte Carlo simulation is applied to each of the column and middle strips at 151 Pirie. Unlike previous numerical analyses, exact values for each strip were utilised. Therefore, 9 different cambers and deflections were calculated based on the unique arrangement for each strip. For this analysis only the site cured material properties have been utilised. This choice has been made based on the necessity to reduce the quantity of outputs, combined with the previous conclusion that site cured cylinders contain a more accurate curing simulation of the thin PPS slabs.

The results of final deformations for each strip have been presented in Figure 4-13. Similar to previous displays of final deformations it was assumed that short term relates to 3 months whilst long term relates to 3 years. It is worth noting that although there are 11 different strips, only 9 deformations can be calculated due to strips doubling up for mid point calculations. The labelling of each of the points is the same in Chapter 4 and has been reproduced in Figure 4-13 for convenience. The effective widths for each of the Monte Carlo simulations have been entered as 0.4 * span and a weighted average of the moment of inertia of the drop panel and slab has been utilised.
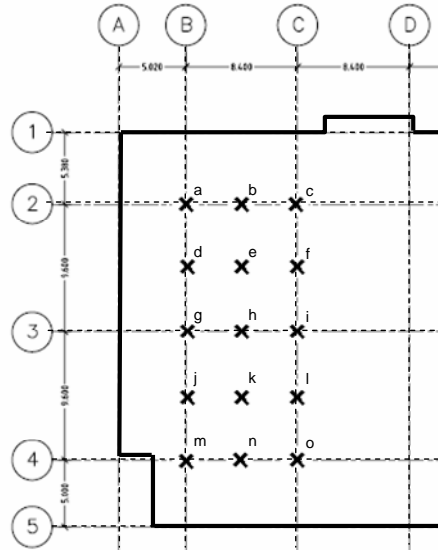
Labelling of points of interest in the column and middle strips of the slab at 151 Pirie
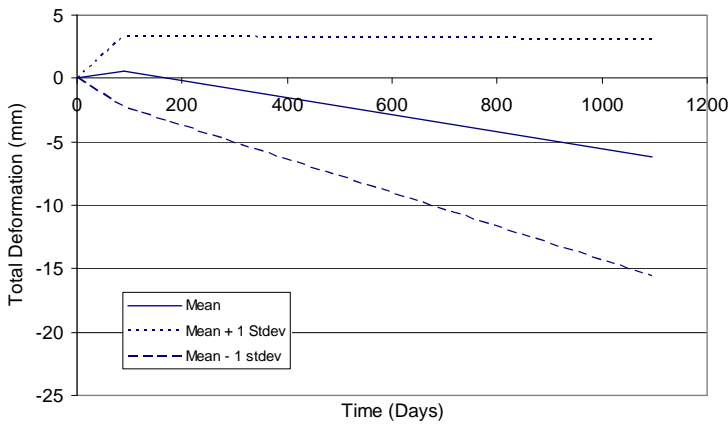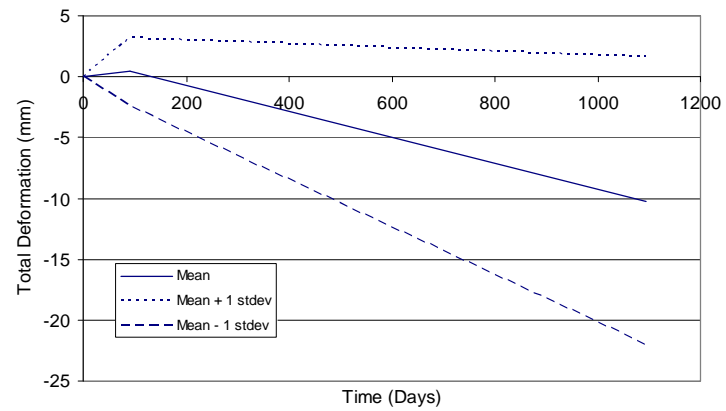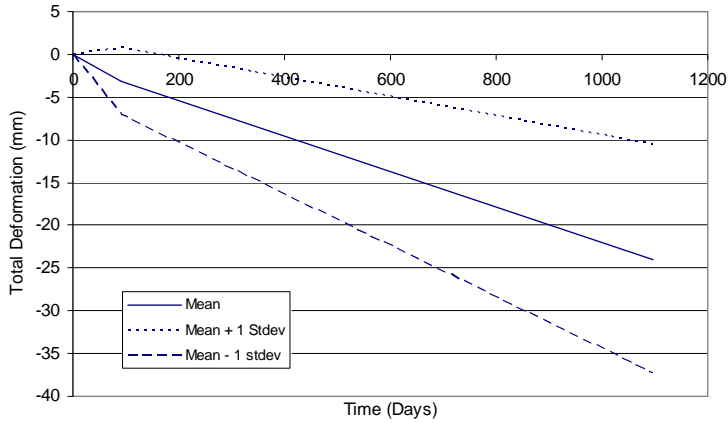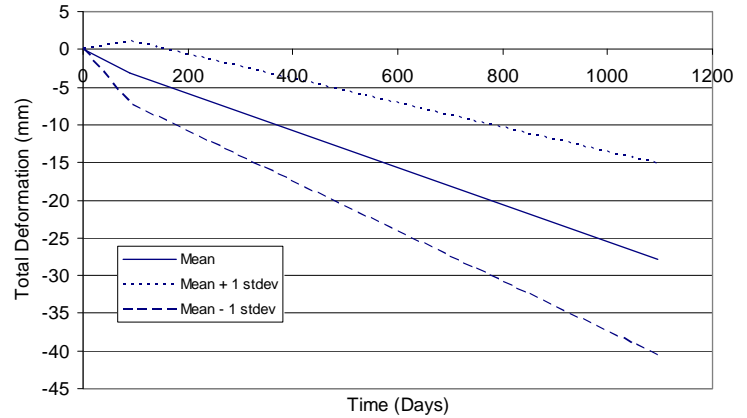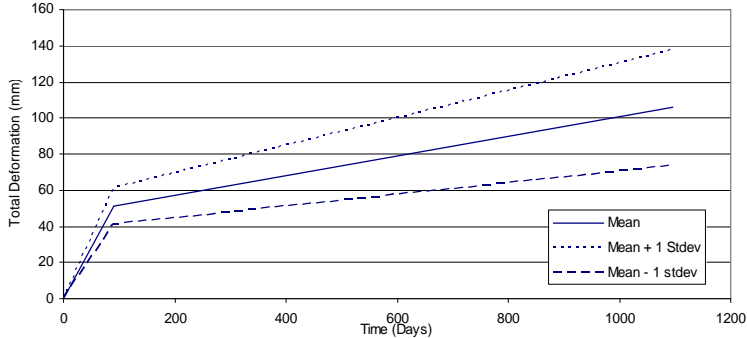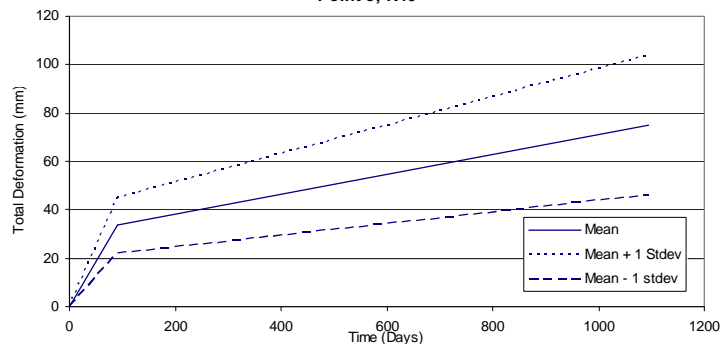
Figure 4-13 *Results of Monte Carlo simulation for predicting slab deformations*

Point f, N32
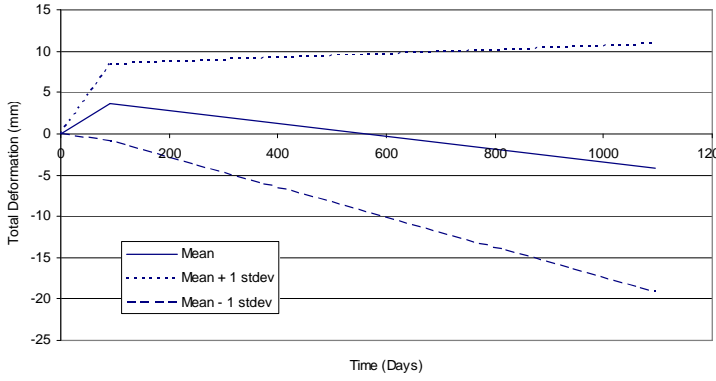
Point f, N40
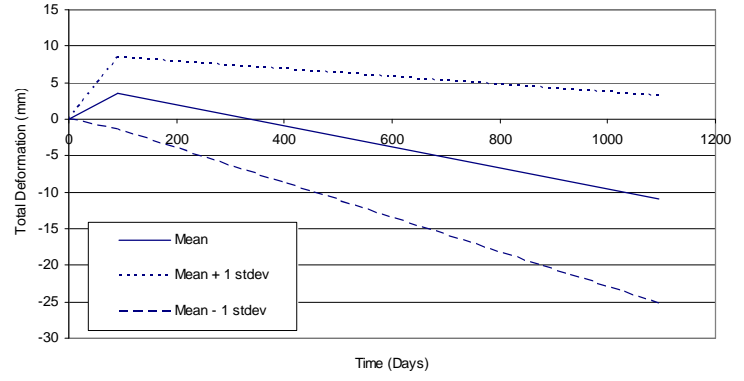
Point h, N32
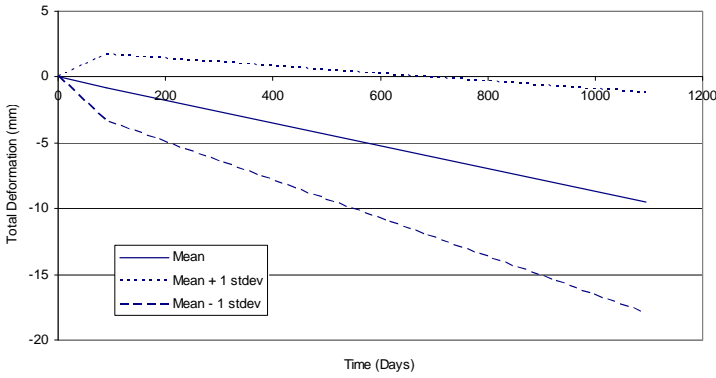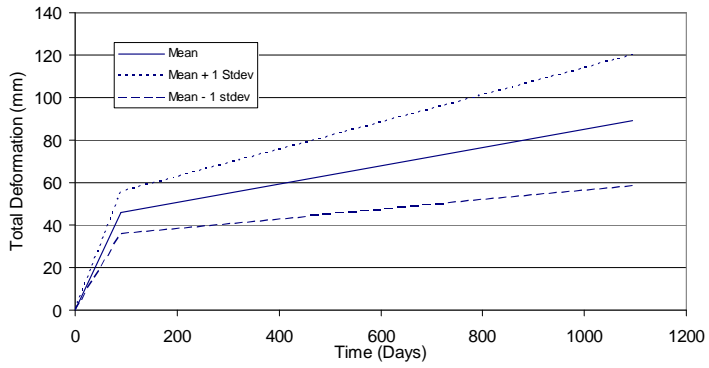

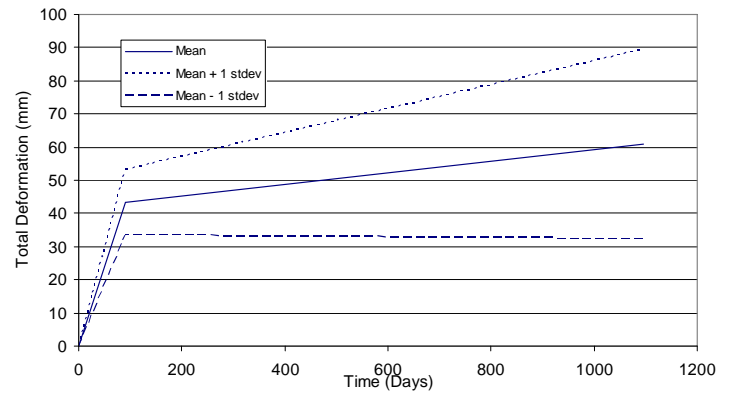### Point h, N40
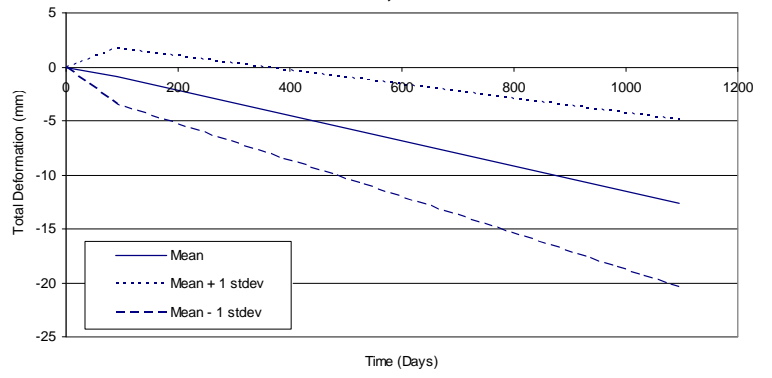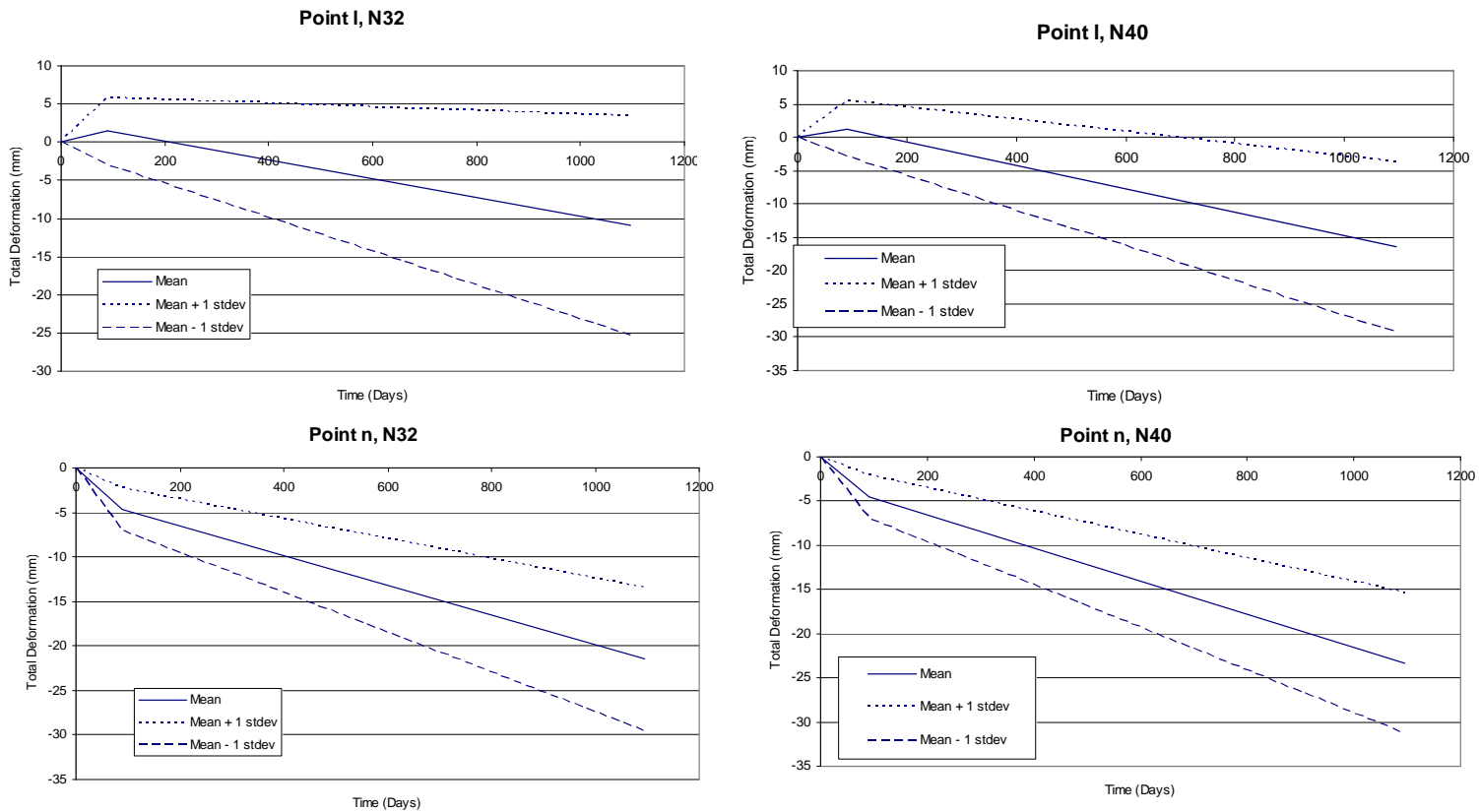

Point j, N32
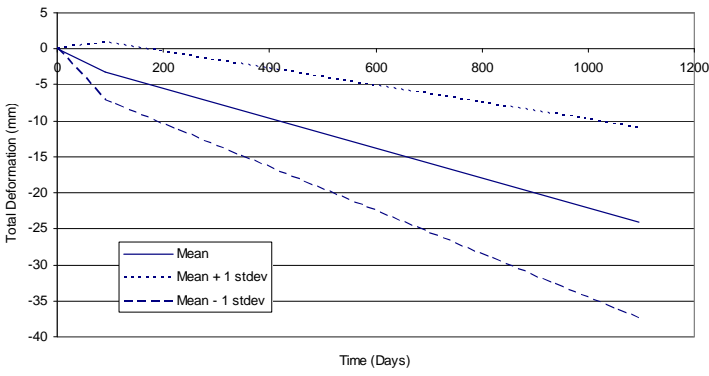
Point j, N40
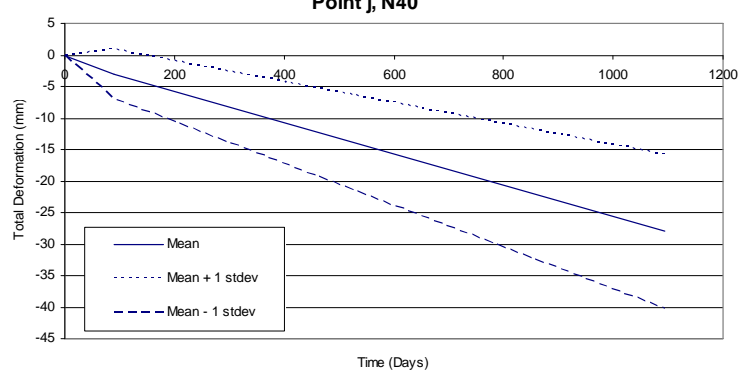
Point k, N32

Point k, N40

(Figure 5-13 continued)

(Figure 5-13 continued)

The results in Figure 4-13 include the final deformation prediction of each point over time, as well as plus and minus one standard deviation of the distribution of final deformation. It was immediately clear that the standard deviations predicted were relatively large and in some cases the magnitude of the standard deviation was larger then the magnitude of the mean total deformation. This magnitude of variation was a significant outcome proving that the natural variation experienced in concrete material properties has the potential to have significant impact on serviceability behaviour. It is worth mentioning that this impact of concrete material properties on serviceability behaviour is noticed for both the N32 and N40 mixes.

Comparing the outcomes from the N32 and the N40 concrete mixes reveals the same trend as previously noted. For each point it is found that the final deformation predicted is less for the N32 mix compared to the N40 mix. This outcome is the opposite of what was expected. A concrete mix that contains higher values of both E_{ci} and E_c is expected to yield lower values of deformations due to an increased rigidity of the slab. This continuing trend helps support the prediction made in the numerical analysis in Section 4.3.1, where it was stated that the magnitude of E_{ci} and E_c are not of interest, it is the ratio of these values that is of interest. For this set of site cured material properties the E_c/E_{ci} ratio favours the N32 mix where, $E_c/E_{ci} = 1.17$ for the N32 mix and $E_c/E_{ci} = 1.09$ for the N40 mix. The stronger ratio for the N32 mix gives reason to the higher values of total deformation observed in Figure 4-13.

The results in Figure 4-13 for the two mid panel points show unrealistic values of upwards deformations in the vicinity of 50 mm to 100 mm. The reason for these unexpected values was initially unclear. However, upon closer examination of the separate methods used to obtain column and mid strip values, the reason behind these unusual predictions became clear. Obtaining results for each column strip is relatively straightforward. These values are found by applying a single strip calculation to that strip. Mid panel deformations (point e and point k), however, are significantly more complicated due to multiple strips affecting the deformation at that point. To obtain the deformations for each mid panel point a logical approach is to combine a middle strip final deformation with a corresponding column strip final deformation. However, due to slight differences with each individual strip this yields inconsistent results when applied using different strip combinations. Therefore when considering the total deformations at the mid panel point, the average of all four surrounding column strips was determined. Following this, the average of the two central strip deflections was added. Finally the two central strip cambers were both combined to find the final total deformation. Following this method ensures that the applied sustained loads acting downwards is equally shared among the four column strips and two mid strips whilst the two upwards loads caused by the two independent prestressing directions are combined. To highlight this method Equation 4-4 has been displayed as the method of obtaining mid panel final deformations. The strips and slab points referred to in Equation 4-4 are the same strips that were introduced in Figure 4-1 and now recreated in Figure 4-14. The method of obtaining an associated standard deviation is by additions of the variances, as laws of algebra do not allow the direct addition of standard deviations. The method used to add the variances to obtain the final standard deviation is presented in Equation 4-5.
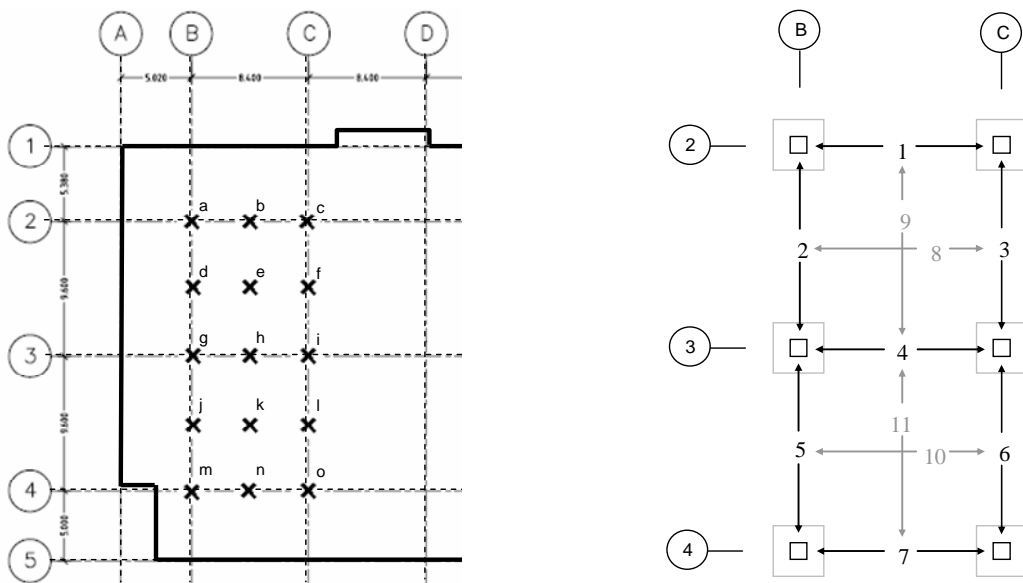
Figure 4-14 *Definition of slab strip and point labelling*

$$TD_e = \frac{\dfrac{TD_1 + TD_4}{2} + \dfrac{TD_2 + TD_3}{2}}{2} + \frac{\Delta_8 + \Delta_9}{2} + C_8 + C_9$$

<div align="right">**Equation 4-4**</div>

$$TD_e = \frac{TD_1 + TD_2 + TD_3 + TD_4}{4} + \frac{\Delta_8 + \Delta_9}{2} + C_8 + C_9$$

Where; TD denotes Total Deformation, C denotes Camber, Δ denotes deflection, subscript numbers refer to slab strip location and subscript letters refer to slab point locations.

Based upon the following algebraic laws;

$$If \quad y = ax_1 + bx_2$$

Where a and b are constants and x_1 and x_2 are independent variables.

$$\sigma_y^{\,2} = a^2 \sigma_{x_1}^{\,2} + b^2 \sigma_{x_2}^{\,2}$$

For this situation;

$$TD_e = \frac{TD_1 + TD_2 + TD_3 + TD_4}{4} + \frac{\Delta_8 + \Delta_9}{2} + C_8 + C_9$$

Therefore;

$$\sigma_{TD_e}^{\,2} = \left(\frac{1}{4}\right)^2 \sigma_{TD_1}^{\,2} + \left(\frac{1}{4}\right)^2 \sigma_{TD_2}^{\,2} + \left(\frac{1}{4}\right)^2 \sigma_{TD_3}^{\,2} + \left(\frac{1}{4}\right)^2 \sigma_{TD_4}^{\,2} + \left(\frac{1}{2}\right)^2 \sigma_{\Delta_8}^{\,2} + \left(\frac{1}{2}\right)^2 \sigma_{\Delta_9}^{\,2} + \sigma_{C_8}^{\,2} + \sigma_{C_9}^{\,2}$$

$$\sigma_{TD_e}^{\,2} = \frac{1}{16}\left(\sigma_{TD_1}^{\,2} + \sigma_{TD_2}^{\,2} + \sigma_{TD_3}^{\,2} + \sigma_{TD_4}^{\,2}\right) + \frac{1}{4}\left(\sigma_{\Delta_8}^{\,2} + \sigma_{\Delta_9}^{\,2}\right) + \sigma_{C_8}^{\,2} + \sigma_{C_9}^{\,2}$$

$$\sigma_{TD_e} = \sqrt{\frac{1}{16}\left(\sigma_{TD_1}^{\,2} + \sigma_{TD_2}^{\,2} + \sigma_{TD_3}^{\,2} + \sigma_{TD_4}^{\,2}\right) + \frac{1}{4}\left(\sigma_{\Delta_8}^{\,2} + \sigma_{\Delta_9}^{\,2}\right) + \sigma_{C_8}^{\,2} + \sigma_{C_9}^{\,2}}$$

<div align="right">**Equation 4-5**</div>

The method utilised by this research, which is outlined by Equation 4-4, is slightly different to the method utilised by Collins and Mitchell (1997). Close examination of examples displayed in Collins and Mitchell (1997) and their application of two way deformation prediction, reveals significant differences. Collins and Mitchell (1997) make the assumption that both orthogonal tendon profiles must each individually resist the dead load. The combined effect of both directions of prestressing was not addressed. When considering calculations to determine the final deformation, the assumption was made that upward camber resisted the sustained dead load, therefore only the live load contributed to overall deformation. This assumption was not considered to be accurate in this research and the assumption gives reason to the inaccurately predicted mid point deflections by this method.

If the assumption made by Collins and Mitchell (1997) was applied to the Monte Carlo simulation, the results displayed in Figure 4-15 were produced. These results have been produced by adjusting Equation 4-4 to consider an average of the effects of central strip cambers, as displayed in Equation 4-6. It can be seen that the assumption made by Collins and Mitchell (1997) yields more logically acceptable results, even though the application is fundamentally flawed due to inaccuracies in application of loads as previously explained. This assumption requires further attention and is done so in section 4.3.3 where a method of application is developed which reduces these assumptions.
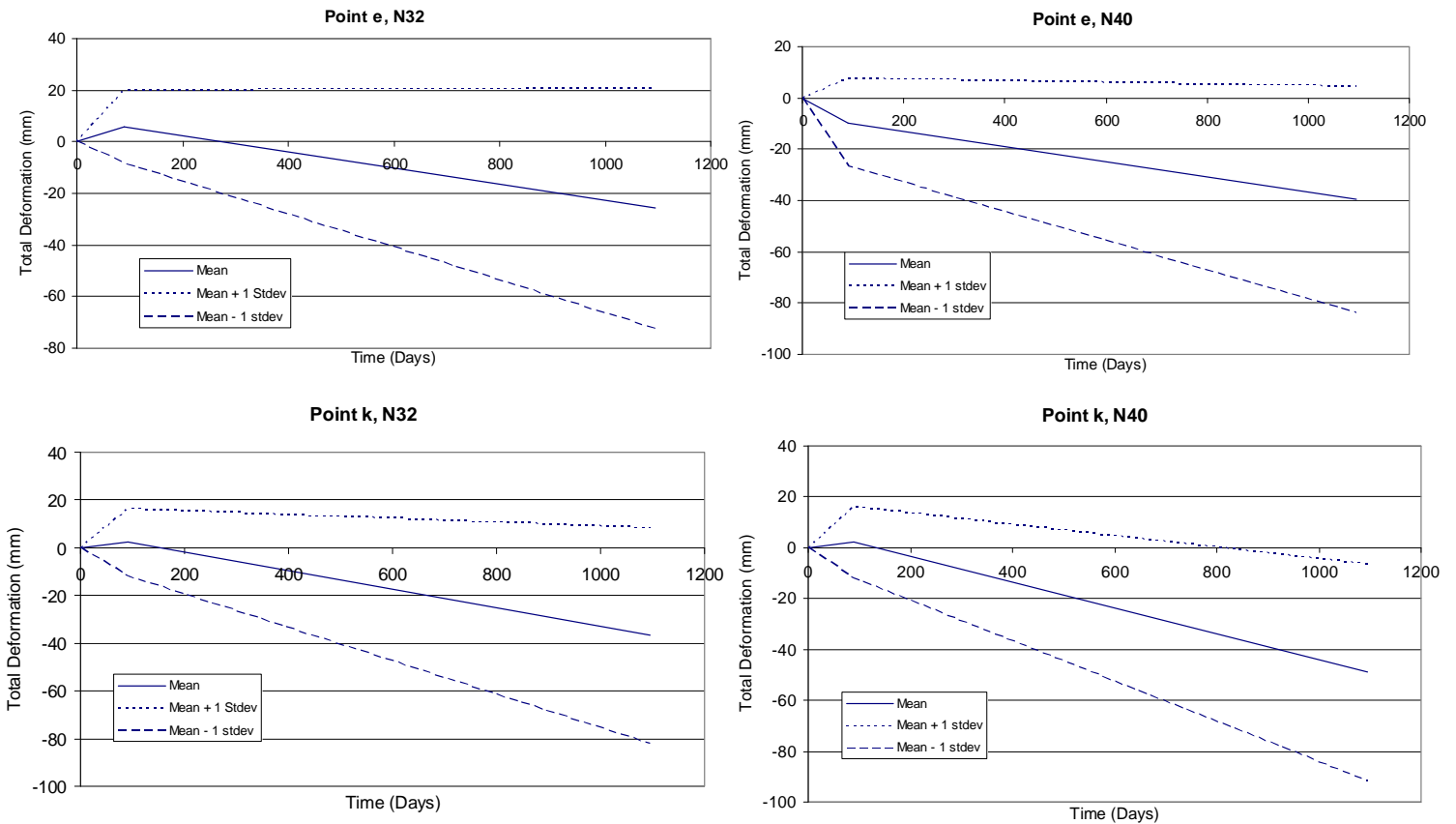
Figure 4-15 *Mid point deformations utilising the complete Collins and Mitchell (1997) method*

$$TD_e = \frac{TD_1 + TD_2 + TD_3 + TD_4}{4} + \frac{\Delta_8 + \Delta_9}{2} + \frac{C_8 + C_9}{2}$$

or,

Equation 4-6

$$TD_e = \frac{TD_1 + TD_2 + TD_3 + TD_4}{4} + \frac{TD_8 + TD_9}{2}$$

4.3.2.4. Summary of Monte Carlo Simulation

The Monte Carlo simulation created in this section reveals more detail about the behaviour of PPS slabs under serviceability loading. Not only were predicted mean deformations produced, but more importantly, the statistical distribution of the values of slab deformation was examined. This distribution in serviceability performance is directly due to the natural fluctuating distribution of concrete material properties. This statistical array of deformations allows designers to design slabs with a higher degree of understanding of the slabs potential variation in behaviour.

From the results produced in this section concrete slab designers can now apply confidence limits to the statistical prediction of deformations. Simple functions are commonly available in standard software, such as Microsoft Excel, which can calculate these cumulative distribution functions (CDF) easily and accurately. Using this method, designers can now provide a percentage probability of a slab deformation passing specific limits. Similar to what is applied to compressive strength requirements for structural strength. For example, it can be calculated that a slab has a 90% chance of not exceeding a certain deformation. Or alternatively a percentage chance can be determine for passing a particular level of deformation. Both methods become extremely useful for deformation predictions.

In summary, the process of applying variation in material properties to deformation predictions was achieved by the use of a Monte Carlo simulation. However, the processes and assumptions used in this Monte Carlo simulation contain questionable methods which affect the outputs. The justification of these assumptions can only be achieved with additional independent analyses that do not contain the same assumptions. The two main assumptions in this method which require further attention for justification include:

- Orthogonal prestressing tendons are designed to individually resist the dead load where combined effects are not considered.
- Weighted average, with respect to length, of moment of inertia represents realistic moment of inertia of slabs which contain drop panels.

The associated accuracy of both of these assumptions is investigated in the following section by applying a finite element style first principles approach to deformation prediction. This method of determining deflections and cambers is achieved with the intention of absolute minimal assumption in the deformation prediction method. In addition to these assumptions, a method of utilising values of modulus of elasticity which result in logical member behaviour is required.

4.3.3. Finite Element Method to Slab Deformation Prediction

4.3.3.1. Introduction to Finite Element Method

The finite element method developed in this section was created based on the need for a new deformation prediction method with minimal assumptions and accurate inputs. Prior to this method, each deflection and camber model contained certain assumptions which may or may not have a significant affect on the predicted results. These assumptions, such as constant moment of inertia for slabs with drop panels, are useful in design where it is necessary to trade small degrees of accuracy for speed and ease of calculation. For this research however, it was considered necessary to strive to produce a method of predicting deformations with the highest degree of accuracy.

To minimise the assumptions and increase the accuracy of the outputs it was decided to create a program based on the application of fundamental first principles. In previous sections it has been shown that the behaviour of the concrete slabs was observed to be linear elastic. Due to this finding it was considered appropriate to apply a deformation prediction method based on linear elastic behaviour. A finite element style sectional analysis was created and applied to the member where each segment along the member contained its own specific properties. Therefore segmented values of moment of inertia could be utilised to yield individual values of rotation and deformation for small increments along the member. The governing linear elastic equation relating these inputs to output is $\delta = \iint \Phi$, where $\Phi = M / E_c I_g$. For this relationship, δ = deformation, Φ = curvature, M = applied moment, E_c = modulus of elasticity of the concrete and I_g = gross moment of inertia. The number of segments used was one hundred, the accuracy of this is covered in section 4.5.

Increasing the accuracy of this deformation prediction method included a closer analysis of modulus of elasticity. In previous sections these values (E_c and E_{ci}) had proven to be pivotal values in determining deformations. Therefore in this section a new style of determining modulus of elasticity has been developed and applied. The following section introduces this new method of determining modulus of elasticity as well as the structure and application of the finite element program.

4.3.3.2. Explanation of Finite Element Method

The method of calculating deformations via fundamental first principles allows assumptions to be minimised and individual inputs to be specifically accurate. Therefore a higher degree of customisation can be achieved to ensure that the calculations are specifically applicable for the required scenario. Customising the first principles approach was achieved in this research by adjusting both the method of application as well as the inputs.

It is a common design procedure to calculate deflections and cambers at two time intervals, commonly referred to as short term and long term. The short term scenario contains typical 28 day member behaviour whilst long term loading accounts for long term effects such as creep and shrinkage. Theoretically these two separate scenarios are applied independently as though the concrete member has been loaded with short term loadings, then unloaded back to zero deformation, and then loaded again with long term loadings to adjusted material properties. Realistically this is not the case; progression of deformations is incremental, with each increment occurring due to the *differences* in load or member behaviour at each step. In other words; deformation at t_2 = deformation at t_1 + change in deformation between t_1 and t_2. This change in deformation between t_1 and t_2 occurs due to load and material property behaviour differences between t_1 and t_2.

This incremental time step approach considers load and material property changes to be paired together at a particular time interval. For example, at a certain time interval if there is no change in load application, but rigidity of the slab say doubles, this method considers that there would be no change in deformation at that time step. Compared to the numerical equations used in the previous sections, this method is considered to more precisely replicate member behaviour on site.

To apply this new method, accurate material properties and loadings are required for the time steps. Unfortunately it is not feasible to obtain realistic values for small time steps, hence the following times were decided upon;

$$t_1 = \text{Stress Transfer (7 days)}$$
$$t_2 = \text{Short Term 1 (28 days)}$$
$$t_3 = \text{Short Term 2 (3 months)}$$
$$t_4 = \text{Short Term 3 (1 year)}$$
$$t_5 = \text{Long Term 4 (3 years)}$$

Accurate material properties and loadings can be obtained for each of these times and hence differences in both material properties and loadings can be determined for each increment of time.

The data analysis performed in the previous chapter yielded accurate values of material properties for the first two time steps (t_1 and t_2). Values for the final three time steps have been obtained by using data provided by Kleiger (1957). Kleiger (1957) examined the gain in material properties beyond 28 days and concluded that on average an extra 10%, 20% and 30% of E_c is noticed at times of approximately 3 months, 1 year and 3 years respectively. This extra gain in material properties is due to slow perpetual hydration of the cement. This accurate correlation between E_c at 28 days and future values of E_c is applied in this finite element method.

Creep is a concrete phenomenon which affects concrete members under long term loading. Due to creep, concrete designers adjust long term values of modulus of elasticity by creep factors to yield the effective values of modulus of elasticity. However, creep strains measured in concrete samples prove that the effects of creep begin slowly progressing immediately after the application of the load. This known behaviour of creep was included in this research to obtain and apply partial effects of creep at all times of sustained loadings (t_2 to t_5).

Creep data from Eblen et al. (2004) was utilised to gain an appreciation of the percentage of creep that occurs at the listed time intervals. Creep data from Eblen et al. (2004) is relevant due to this data being obtained from two similar localised concrete batches. The measurements of creep strains over time can be seen in Figure 4-16 where a logarithmic extrapolation to the final creep strain has been made. It is worth noting that this extrapolation is slightly inaccurate for low ages, this is due to high fluctuations in maintaining consistent load at early ages. Hence creep strains lower than approximately 7 days can effectively be ignored. Exact values of creep strains are not of interest, an approximate ratio of interval values of creep to final values of creep will maintain accuracy when applied to predicting deformations.

For the time steps suggested above, the number of days under load required is each time interval minus the time of initial load application, as this time relates to sustained loading where creep occurs. Therefore, for prestressing that is applied at 7 days, times at 21, 69, 358 and 1088 days are of interest. However, due to the last point effectively denoting full long term effects, it was decided to let the 3 year point relate to full creep, as per standard design calculations (AS 1012.16, 1996). For this example the three remaining times and their corresponding magnitude and percentage of full creep have been highlighted in Figure 4-16 and been summarised in Table 4-9.

NOTE:
This figure is included on page 115 of the print copy of
the thesis held in the University of Adelaide Library.

Figure 4-16 *Creep data from Eblen et al. (2004)*

Table 4-9 *Percentage of full creep for application of prestress*

Time	% of full creep
7 days	**0**
28 days	220/400 = **55%**
3 months	280/400 = **70%**
1 year	300/400 = **75%**
Long term	**100%**

Accurate values of material properties have now been obtained for inputs into the first principle approach. To ensure that all inputs contained a high level of accuracy, accurate values of loading (timing and quantity) were also required. Loadings for this deformation prediction method included applying a Uniformly Distributed Load (UDL) vertically downwards for applied dead and live loads and upwards for applied prestressing. The magnitude of this loading as well as the timing of application is of key interest.

Loadings were separated into two categories; 1) loads which were sustained and therefore contributed to creep calculations and 2) loads which were temporary or instantaneous. For this scenario self weight, additional sustained dead load and the sustained proportion of the live load were combined and considered as the sustained slab loading. The temporary proportion of the live load was the only contributor to the temporary loading. Applied prestress was considered a sustained loading.

Due to the nature of the first principle calculations the above loadings were converted into equivalent Fixed End Moments (FEMs) and support reactions (or effectively end shear values). Table 4-10 tabulates each of these values for each of the time intervals. Also displayed in Table 4-10 is a summary of each applied loading and corresponding value of creep affected modulus of elasticity. Following this tabulated summary of inputs is an explanation of the complex nature of determining effective values of modulus of elasticity for each time step.

Table 4-10 *Summary of input for first principle style analysis*

| TIME | Loadings | | Modulus of Elasticity | | |
	Applied loads	Effective load due to prestress	Instantaneous	DEFLECTION calculations	CAMBER calculations
Transfer (7days)	**Sustained UDL** - Full self weight $\rightarrow$ (A) - 0.4*LL **FEMs** $= wL^2/12$ **End Shear** $= wL/2$	**UDL** (w) $= 8P(e_1+e_2)/L^2$ **FEMs** $= wL^2/12$ **End Shear** $= 4P(e_1+e_2)/L$	Eci (7days Mod of E)	Eci (7days Mod of E)	Eci (7days Mod of E)
Short Term 1 (28 days)	**Sustained UDL** - Full self weight - Extra DL (1.4kPa) $\rightarrow$ (B) - 0.4*LL **Instantaneous UDL** 0.3 LL **FEMs** $= wL^2/12$ **End Shear** $= wL/2$	**UDL** (w) $= 8P(e_1+e_2)/L^2$ **FEMs** $= wL^2/12$ **End Shear** $= 4P(e_1+e_2)/L$	Ec (28days Mod of E)	$\dfrac{A + (B - A)}{\dfrac{A}{\left[\dfrac{E_{ci}}{1 + 0.55\,\phi}\right]} + \dfrac{(B - A)}{E_c}}$	$\dfrac{E_{ci}}{1+0.55\phi}$
Short Term 2 (3 months)	**Sustained UDL** - Full self weight - Extra DL (1.4kPa) - 0.4*LL **Instantaneous UDL** 0.3 LL **FEMs** $= wL^2/12$ **End Shear** $= wL/2$	**UDL** (w) $= 8P(e_1+e_2)/L^2$ **FEMs** $= wL^2/12$ **End Shear** $= 4P(e_1+e_2)/L$	1.1*Ec	$\dfrac{A + (B - A)}{\dfrac{A}{\left[\dfrac{E_{ci}}{1 + 0.7\phi}\right]} + \dfrac{(B - A)}{\left[\dfrac{E_c}{1 + 0.6\phi}\right]}}$	$\dfrac{E_{ci}}{1+0.7\phi}$
Short Term 3 (1 year)	**Sustained UDL** - Full self weight - Extra DL (1.4kPa) - 0.4*LL **Instantaneous UDL** 0.3 LL **FEMs** $= wL^2/12$ **End Shear** $= wL/2$	**UDL** (w) $= 8P(e_1+e_2)/L^2$ *(P adjusted for HALF relaxation)* **FEMs** $= wL^2/12$ **End Shear** $= 4P(e_1+e_2)/L$	1.2*Ec	$\dfrac{A + (B - A)}{\dfrac{A}{\left[\dfrac{E_{ci}}{1 + 0.75\phi}\right]} + \dfrac{(B - A)}{\left[\dfrac{E_c}{1 + 0.75\phi}\right]}}$	$\dfrac{E_{ci}}{1+0.75\phi}$
Long Term (3yrs +)	**Sustained UDL** - Full self weight - Extra DL (1.4kPa) - 0.4*LL **Instantaneous UDL** 0.3 LL **FEMs** $= wL^2/12$ **End Shear** $= wL/2$	**UDL** (w) $= 8P(e_1+e_2)/L^2$ *(P adjusted for FULL relaxation)* **FEMs** $= wL^2/12$ **End Shear** $= 4P(e_1+e_2)/L$	1.3*Ec	$\dfrac{A + (B - A)}{\dfrac{A}{\left[\dfrac{E_{ci}}{1 + \phi}\right]} + \dfrac{(B - A)}{\left[\dfrac{E_c}{1 + \phi}\right]}}$	$\dfrac{E_{ci}}{1+\phi}$

Note: E_c in the above table relates to modulus of elasticity at 28 days only. The above loadings are based on the following arrangement. Applied loads act vertically down, whilst loads due to prestress act vertically upwards.
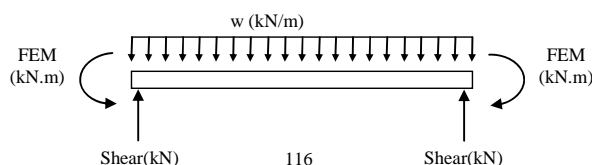
The method of obtaining an accurate effective value of E_c for each point of time was achieved by taking careful consideration of the gain of E_c with respect to time. This gain with respect to time, coupled with the appreciation of creep behaviour of concrete under sustained loadings, revealed an accurate method of utilising E_c and the loading history together. To help explain this method further a simplified example is presented. To help simplify this example and focus on the method of determining E_c, a concrete member is referred to in a simple axially loaded scenario.

In this simplified axially load scenario we consider two loading times (t_1 and t_2, due to loads A and B respectively), which occur when the E_c values of the sample are two different values (E_1 and E_2). For this loading scenario there are two methods of determining the expected final strain after full creep has occurred. The method detailed below to the left, is the method proposed by this research as the new method. This method takes into account the different loadings and their individual timing. The method detailed on the right is the current typically utilised method of determining long term effects (Collins and Mitchell, 1997 and Warner et al. 1998). Following this explanation is Figure 4-17 which displays a graphical representation of the calculation of each point.

Scenario details; t_1 = 7 days, t_2 = 28 days, E_1 = 15000 MPa, E_2 = 30000 MPa, Load A = 10 MPa, Load B = 25 MPa (separate loads, not additional) Creep factor = 2.6

New Approach	Current Method
At t_0 = 0 days, stress = 0 MPa, strain = 0	At t_0 = 0 days, stress = 0 MPa, strain = 0
At t_1 = 7 days, stress = 10 MPa, therefore strain = 10/15000 = 0.00067.	Stress at 7 and 28 days is combined in the short term analysis. Short term strain is considered to be total loading divided by 28day E_c.
At t_2, just before application of Load B, 55% of the creep has occurred due to Load A. Therefore strain $= 10 / \dfrac{15000}{1 + 0.55 \times 2.6} = 0.0016$.	Therefore;
	Short term strain = 25/30000=0.000833
After the load increase up to Load B (15 MPa) the change in strain is 15/30000 = 0.0005, therefore final strain at t_2 is 0.0016+0.0005=0.0021. Which relates to an effective E_c value of 25/.0021=11905 MPa.	Long term strain is considered to be the total loading divided by the long term value of E_c due to full creep effects.
	Therefore
Now if we consider t_3 to represent sufficient time so that full creep has occurred, effectively the final strain will correspond to a combination of the long term strain due to Load A (applied when E_1 was the current E_c) and long term strain due to Load B – Load A (applied when E_2 was the current E_c).	Long term strain = $25 / \dfrac{30000}{1 + 2.6} = 0.003$
Hence; Final long term strain = $10 / \dfrac{15000}{1 + 2.6} + 15 / \dfrac{30000}{1 + 2.6} = 0.0024+0.0018$ $= 0.0042$	
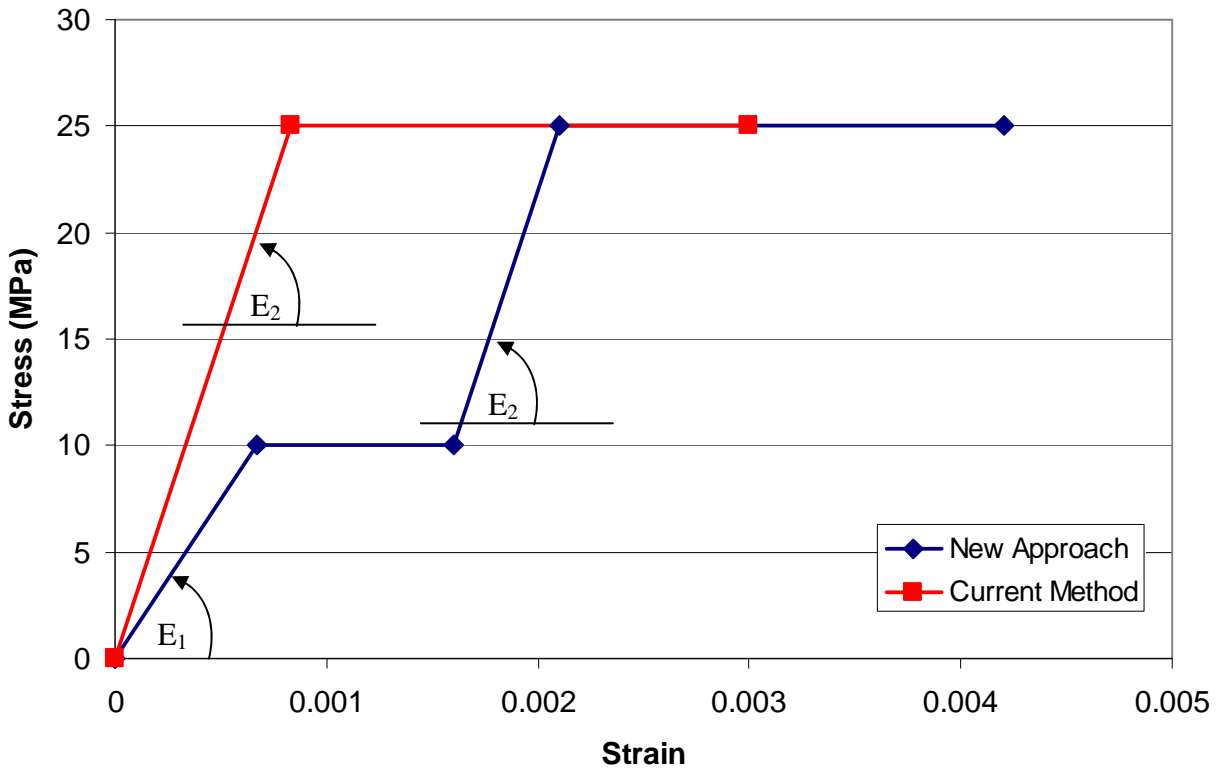
Figure 4-17 Graphical representation of accurate determination of E_c under sustained loads

The summary of this new approach, which has been displayed in Figure 4-17, is only intended to be utilised and associated with sustained loadings. Temporary loading behaviour is not affected by long term behaviour such as creep. In fact the strain or deformation experience by a temporary instantaneous loading is only resisted by the instantaneous value of E_c, which has been tabulated in Table 4-10.

It can be seen that there is a significant difference between the final predicted strains between the two methods (0.003 compared to 0.0042). This difference in strain directly relates to a difference in prediction of time effected E_c. This difference suggests that the current method of application of long term effects contains inaccuracies when predicting deformation behaviour. The methods of determining E_c highlighted in Table 4-10 were derived from this sample scenario where an effective E_c is determined as a weighted average of long term E_{ci} and E_c depending on magnitude of corresponding sustained loads.

To grasp a complete understanding of how to apply the simple axially loaded scenario to a scenario containing flexural behaviour, another example has been outlined. This example is conceptually identical to the previous scenario, however, the application has now changed to deformation prediction.

If a UDL load (A) is applied to a beam or slab then instantaneously there is an associated increase in deflection (Δ_1) at time t_1. This deformation is effectively resisted by the initial instantaneous modulus of elasticity (E_1). Then after a certain time period there is a load increase (to total load B) applied to the beam at time t_2. If a calculation of the deflection is required at t_2 then theoretically we have 3 deflections to determine;

- Δ_1 which is the initial deflection from load A, resisted by E_1, at t_1
- Δ_2 which is the instantaneous deflection from load B minus load A, resisted by E_2, at t_2
- Δ_3 which is the time dependant deflection due to creep. This creep is occurring due to load A over time period t_2-t_1.

To work out an effective value of modulus of elasticity for application of sustained loads at any point in time Equation 4-7 is used which simply works out a weighted average of E_2 and E_1 based on the magnitudes of loadings A and B.

$$\frac{A + (B - A)}{\dfrac{A}{E*} + \dfrac{(B - A)}{E**}}$$

Equation 4-7

where E* relates to time affected modulus of elasticity from sustained load A, and E** relates to the time affected modulus of elasticity from sustained load (B – A).

This method results in an application which considers values of E_c for deflection and camber, at a single point in time due to sustained loads, to be different values. Initially this appears incorrect but considering that the value of E_c is not for instantaneous loading it depends on load-time history, which are different for camber and deflection, it becomes logical. Figure 4-18 displays an example of the values of E_c for both camber and deflection for use with instantaneous and time dependent loadings. The instantaneous values of E_c were calculated separately to the sustained values of E_c. Calculated values of E_c have been displayed with their corresponding equations. It is worth mentioning that the deflection equations have been simplified by referencing the E_c values for camber instead of restating each method of obtaining E_c due to loadings at the time of stress transfer.

Applied Loads		
A =	60	kN/m²
B =	80	kN/m²

Modulus of Elasticity **for instantaneous loads** (MPa)			
Name	**Age**	**Value**	**Equation**
E1=	Ecurrent (7days)	25,000 MPa	
E2=	Ecurrent (28days)	36,000 MPa	
E3=	Ecurrent (3months)	39,600 MPa	*=1.1*E2*
E4=	Ecurrent (1yr)	43,200 MPa	*=1.2*E3*
E5=	Ecurrent (3yrs)	46,800 MPa	*=1.3*E4*

	Modulus of Elasticity **for sustained loads** (MPa)			
	Name	**Age**	**Value**	**Equation**
CAMBER	E6=	Stress transfer	25,000 MPa	*=E1*
	E7=	Short term1	10,288 MPa	*=E1/(1+0.55*2.6)*
	E8=	Short term2	8,865 MPa	*=E1/(1+0.7*2.6)*
	E9=	Short term3	8,475 MPa	*=E1/(1+0.75*2.6)*
	E10=	Long term	6,944 MPa	*=E1/(1+2.6)*
DEFLECTION	-	Stress transfer	25,000 MPa	*=E1*
	-	Short term1 initial	10,288 MPa	*=E1/(1+0.55*2.6)*
	-	Short term1 final	17,382 MPa	*=(A+B)/((A/E6)+(B/E2))*
	-	Short term2 final	15,573 MPa	*=(A+B)/((A/E8)+(B/(E2/1+0.6*2.6)))*
	-	Short term3 final	15,050 MPa	*=(A+B)/((A/E9)+(B/(E2/1+0.75*2.6)))*
	-	Long term final	12,889 MPa	*=(A+B)/((A/E10)+(B/(E2/1+2.6)))*

Figure 4-18 *An example of E_c values for camber and deflection*

The long term effects of shrinkage were accounted for by applying full shrinkage at 3 years and half shrinkage at 1 year. The progression of shrinkage strains in local concrete is unknown, therefore in an attempt to maintain logical progression of long term factors the above proportions of shrinkage were applied. The deflections due to shrinkage remain minimal, in the order of < 1 mm, therefore accurate percentages are not necessarily essential in final deformations predictions.

Deformations due to instantaneous loadings at each time, such as temporary daily applied live loads, are determined separately by using the instantaneous value of E_c (at the corresponding time). The instantaneous deformations are then superimposed on the time dependant deformations to reveal the final deformed shape.

The accurate methods and inputs explained in this section were combined together in a program created in Microsoft Excel. Similar to the Monte Carlo simulation, Excel was utilised to perform multiple calculations. The calculations for this program however, were not repetitions simulations (as used in the Monte Carlo simulation) to determine a statistical distribution of member deformation. The multiple calculations were incremental integration along the concrete member to determine the peak deflections and cambers.

A sample output of this program is displayed in Figure 4-19 where it can be seen that from the applied Bending Moment Diagram (BMD) a curvature profile can be created by dividing by E_cI_g. The integral of the curvature profile yields the member rotations and the final integration determines the deformation of the concrete member. End conditions, such as zero rotation, are used to adjust the graphs for accurate application.
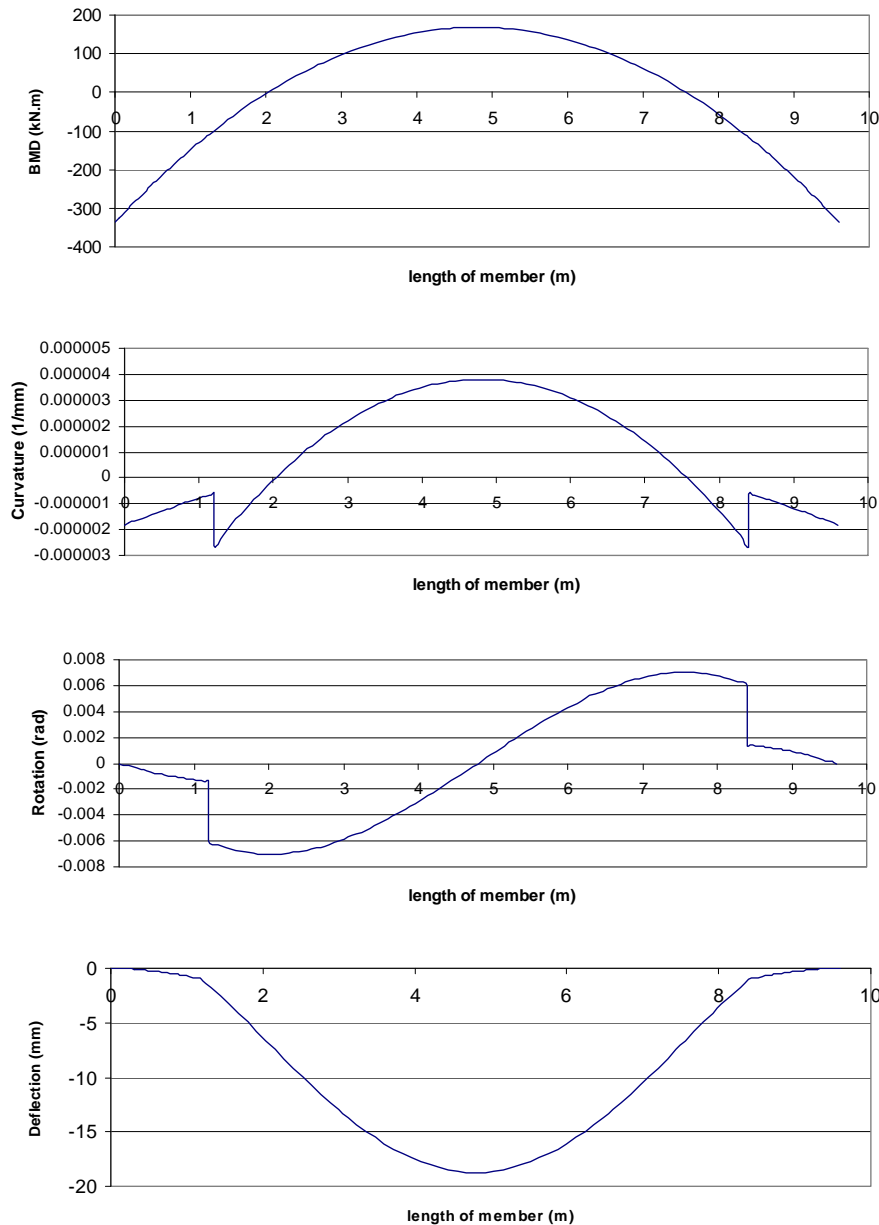
Figure 4-19 *Sample output from the First Principle Approach Program.*

It is clear in Figure 4-19 the effect of the change in I_g between the drop panels and the slab. This can be seen by the sharp changes in the curvature profile which translate to a step increase in rotation. This effect is also noticeable in the deformation profile. A comparison was made between using exact (or sectional) values of I_g, such as that presented in Figure 4-19, and utilising the weighted average value of I_g. This comparison is displayed in Figure 4-20 where a significant difference in predicted deformation is shown.
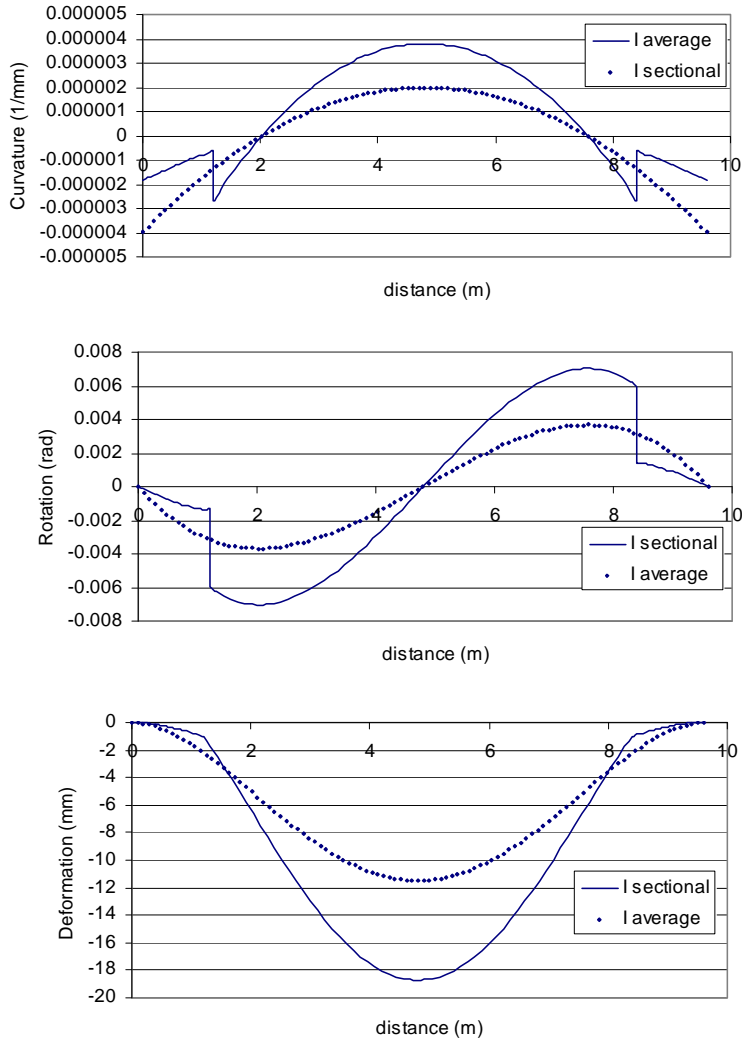
Figure 4-20 *Comparison of deformation profiles utilising I average and I sectional.*

It is clear in Figure 4-20 that there is a significant difference between the deformed shaped predicted using the different values of I_g. Ideally another Monte Carlo simulation would have been the best application for this method, however, due to the magnitude of calculations involved with this method, it was not considered feasible. A simple approach of individually altering each material property input by one standard deviation, and measuring the change in output, was utilised. In this method each value of E_c or E_{ci} was altered by either plus or minus one standard deviation whilst all remaining factors remain constant. The change in outcome was then measured and the process was repeated for each value until a full array of output for both deflection and camber was completed. This method supplied values of mean and standard deviation for camber and deflection due to changes in supplied values of E_{ci} and E_c. Values of standard deviations for total deformations for each strip were determined in the same method as the Monte Carlo simulation, and explained in Equation 4-5.

4.3.3.3.   Finite Element Method Results

Similar to the application of the Monte Carlo simulation, the Finite Element Method of determining slab deformations was applied to each of the column and middle strips at 151 Pirie. An accurate statistical variation of site cured material properties was utilised in the inputs. The effective widths for each of the calculations were entered as 0.4 * span, which is the same approach that was used for the analysis of the Monte Carlo simulation.

The deformation prediction method for slab mid points includes the addition of the centre strip cambers, as detailed in Equation 4-4. The results for each of the points have been displayed in Figure 4-21. For this method of deformation prediction more frequent time steps are used, with predictions achieved at 7 days, 28 days, 1 month, 3 months and 3 years. The labelling of each of the points is the same as previously referenced and has been included in Figure 4-21 for convenience.
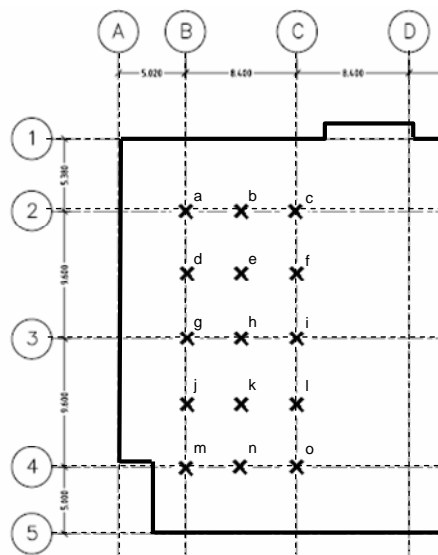
Labelling of points of interest in the column and middle strips of the slab at 151 Pirie
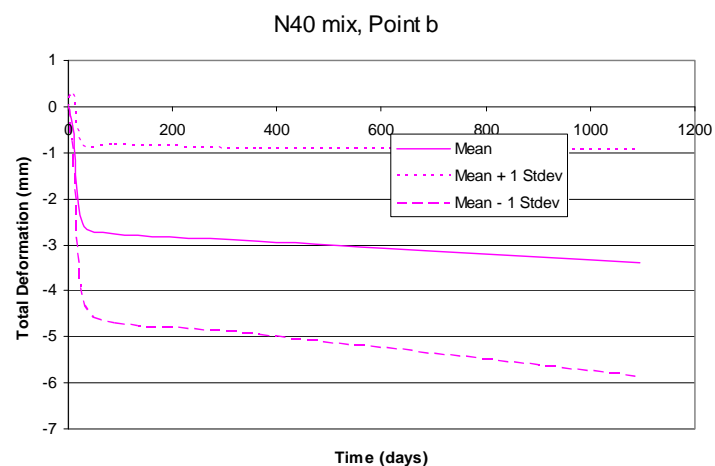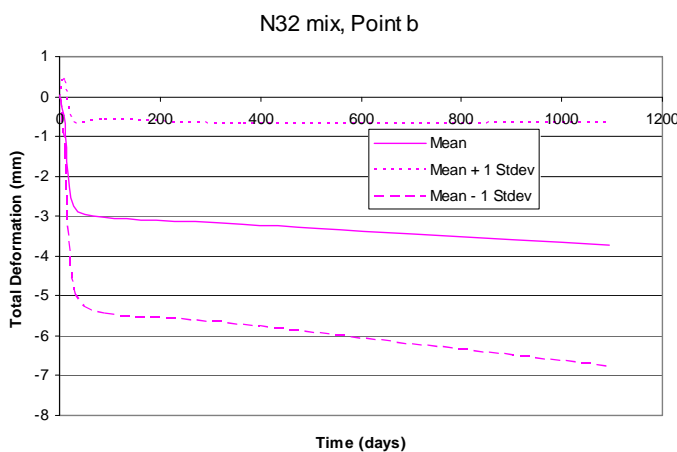
Figure 4-21 *Results of First Principles Approach for predicting slab deformations*

(Figure 5-21 continued)

N32 mix, point j.

N40 mix, point j

N32 mix, Point k

N40 mix, Point k

N32 mix, Point l

N40 mix, Point l.

N32 mix, Point n.

N40 mix, Point n.
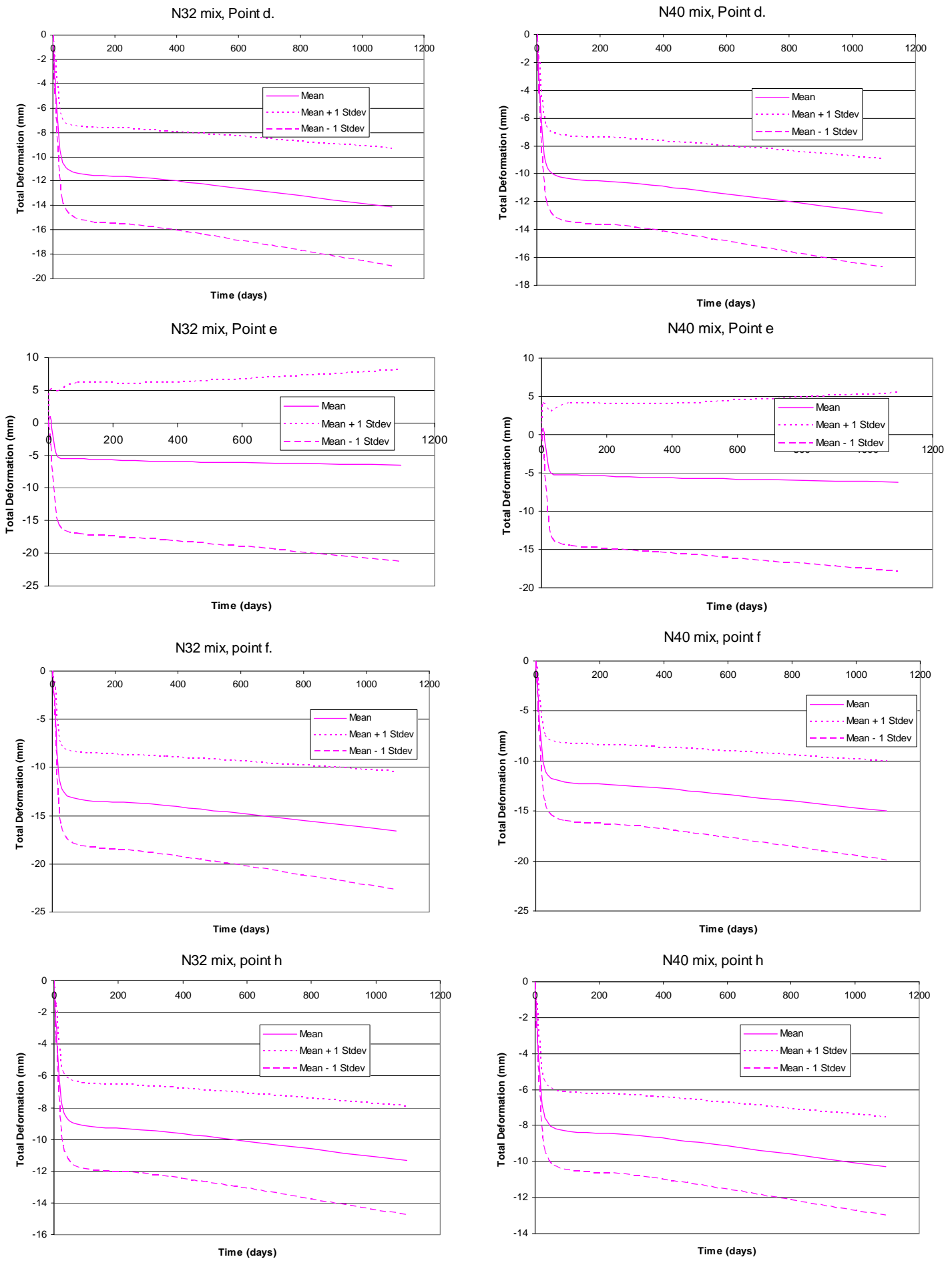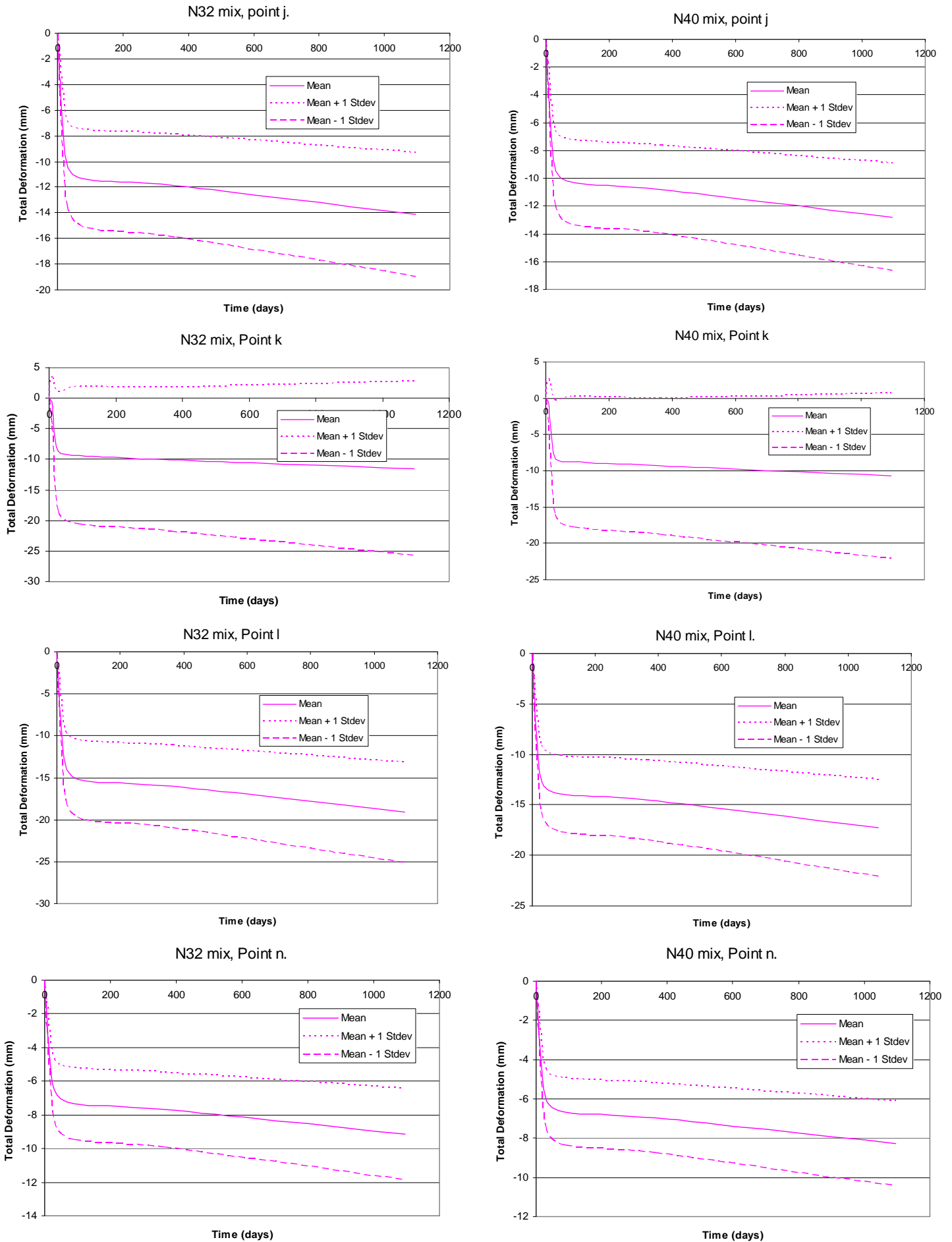
(Figure 5-21 continued)

The results displayed in Figure 4-21 are presented in the same manner as the results from the Monte Carlo simulation. The results include the final deformation prediction of each point over time, as well as plus and minus one standard deviation of the distribution of final deformation. It is evident in Figure 4-21 that all graphs have an expected progression of deformation over time. All graphs display a progressive increase in the magnitude of slab final deformation as time increases. It can also be seen that for each point on the two bay grid deformations predicted by the N32 concrete are all slightly lower than the deformations predicted by the N40 concrete. This outcome is the expected trend due to N32 concrete containing lower values of E_c at all times, compared to the N40 concrete mix. This trend was not observed in the previous deformation prediction methods and is a direct result of the new method of utilising E_{ci} and E_c, explained in section 4.3.3.2.

Due to the potential confusion with the nature of positive and negative labelling, it is worth reiterating that an upward final deformation is considered to be positive in this research. However, an increase in magnitude of final deformation refers to the magnitude of deformation becoming progressively negative, or progressively less.

It can be seen in Figure 4-21 that the standard deviation of the slab mid panel point deformations, points e and k, are much higher than the standard deviation of the column strip deformations. This trend appears to have occurred independent of the magnitude of the mean predicted deformation. The reason for this trend was considered to be due to the dependency of significantly more strips to obtain a standard deviation at this slab location. For example, the standard deviation of final deformation at each column strip is only affected by the standard deviation of the material properties within that strip. The standard deviation of final deformation at each mid panel point contains a statistical accumulation of the six surrounding strips, as outlined previously by Equation 4-5. For this two bay slab under analysis it results in long term standard deviations of approximately 3 to 5 mm for column strip deformations and over 10 mm for the two mid panel point deformations. In summary this indicates that mid panel point deformations for two-way prestressed slabs are not necessarily the location of greatest downward deformation, however they will naturally contain the highest amount of variation.

The true justification of accuracy of this finite element style model comes with the comparison of predicted deformations to the surveyed values. This comparison was performed for each of the deformation prediction methods in this chapter and is presented in section 4.4. Before this comparison is examined a comparative discussion between the three methods of deformation predictions is presented.

4.3.3.4. Summary of the Finite Element Method

The First Principles Approach to predicting PPS slab deformations was designed to reduce error trends associated with the Numerical Approach and the Monte Carlo simulation. These error trends, caused by inaccurate assumptions and highlighted in section 4.3.2.4, were not evident in the results produced by the First Principles Approach. This First Principles Approach maintained the ability to provide a statistical distribution of the final deformation of both the column strip mid points as well as the mid panel points.

The concept of partial application of creep for relatively young ages of concrete (< 3 years) was successfully applied to the deformation prediction method. This concept incorporated the pairing of applied loads and corresponding timing of load to determine an effective value of E_c which depended on time-load history. This resulted in separate values of effective E_c for downward deflection and upward camber for prestressed values (due to different time-load histories). The prediction of instantaneous deformations due to temporary short term loadings remained unchanged. Instantaneous deformations were determined with the use of instantaneous values of E_c. The First Principles Approach allowed the accurate inclusion of regions along a member of differing values of moment of inertia. This was a crucial step in the accurate representation of the slabs at 151 Pirie due to the inclusion of drop panels in their construction.

The results produced in this section contained an expected progression of deflection over time without any obvious assumption errors or result flaws. An in-depth comparison of the deformation predictions created in this section and the surveyed values is discussed in section 4.4. However, it can still be summarised in this section that mid panel point deformations for two-way prestressed slabs are not necessarily the location of greatest downward deformation as typically expected. However it was observed that they will contain the highest amount of variation in deformation prediction.

4.3.4. Summary of Deformation prediction methods

Three separate methods of determining slab deflections and cambers have been analysed and discussed in detail in this chapter. These three methods include the Numerical method, the Monte Carlo simulation method and the Finite Element method. Both the Numerical method and the Monte Carlo method contained multiple models within each method, the Finite Element method contained one single method. This summary of the deformation prediction methods summarises the advantages and disadvantages and suggests improvements to the application of these three methods.

The advantage of the Numerical method is the simplicity and ease of application. Each model in the Numerical method contains simple to use calculations which depend on easy to obtain factors such as span, I_g and E_c. However, due to the simplicity of this method only a single value of final deformation can be obtained from a given set of material property inputs. As proven in earlier sections, concrete material properties are not set values, they vary depending on their unique surroundings and placement. These variations in concrete performance can not be taken into consideration accurately in this method.

The Monte Carlo simulation method is based on the Numerical method, therefore application of each model within these two methods is the same. However, the Monte Carlo simulation contains the added benefit of being able to consider the variations of concrete material properties and provide a statistical distribution of member deformation. The disadvantage of the Monte Carlo simulation is the extra step required to obtain the statistical distribution of concrete material properties and to input this distribution in the simulation. An additional disadvantage of using either the Numerical method or the Monte Carlo simulation method is the inability to accurately incorporate members with multiple regions of differing values of I_g such as drop panels.

The Finite Element method is the method which is considered to contain the highest level of accuracy for determining PPS slab deformations. This method incorporates the variations of concrete material properties in determining a statistical distribution of member deformation. Due to its application the Finite Element method contains the fewest assumptions in predicting member deformations due to prestress or applied dead or live load. Unlike the two previous methods, this method allows for the load-time history of a member to influence the member deformation. This method also contains the benefit of determining member deformation at more frequent time steps than the other methods. The only disadvantage of this method is the complexity of this method. This method is not able to be applied as hand calculations. Utilising this method requires a computer program, such as the one developed in this research, to be applied.

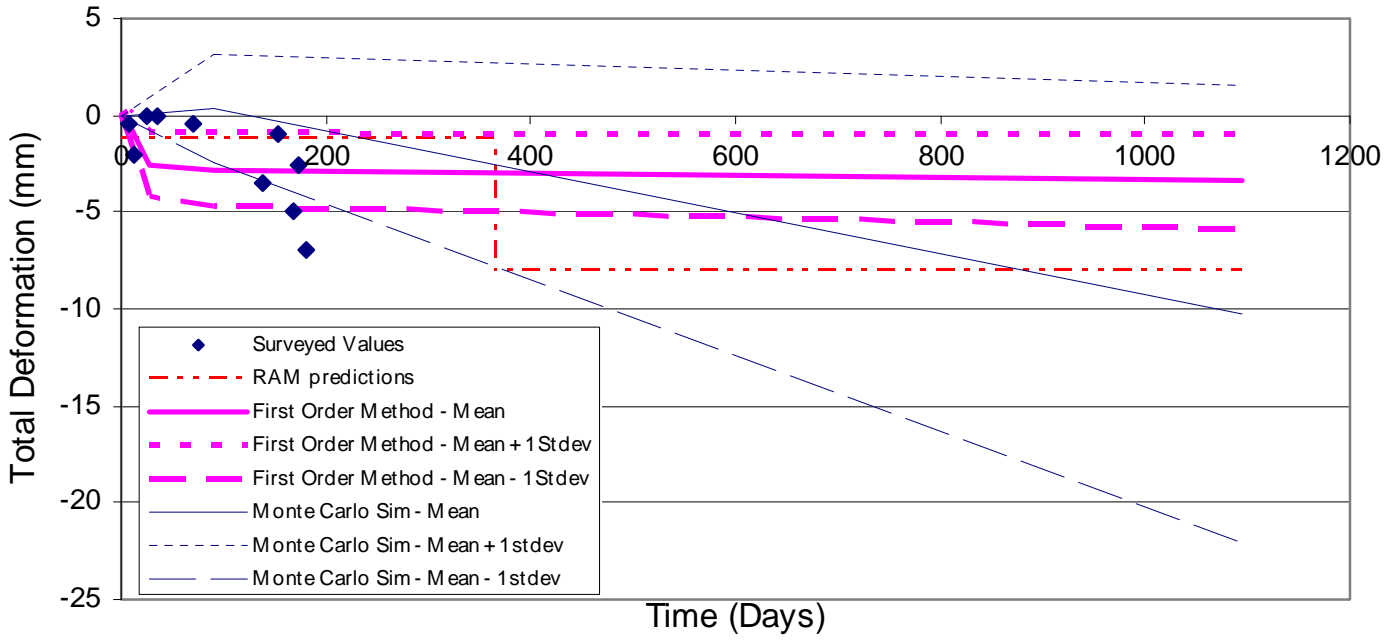## *4.4.   Comparison of Deformation Predictions to Surveyed Values*

A comparison has been made between the predicted slab deformations by the three deformation prediction methods and the surveyed data of the two bay grid. In addition to this, the predicted deformations by RAM Conce*pt* have also be included in this comparison. It should be noted in this comparison that the predicted deformations produced by the Numerical method and the mean of the Monte Carlo simulation will be identical. For presentation of the statistical results from the Monte Carlo simulation method and the Finite Element method, plus and minus one standard deviation have been included.

The comparison of surveyed data to prediction models is only achievable for the N40 concrete mix. This is due to the timing of the surveying of the two bay grid. Complete surveying data sets were only obtained for the third floor slab upwards. Due to the surveying grid being located on the southern side of the slab, only N40 concrete was used on slab number three. N40 concrete was the only concrete mix used in construction from that slab upwards.

The inputs utilised in each of the deformation prediction methods, except RAM Conce*pt*, are the inputs summarises in section 4.2. Due to RAM Conce*pt*'s intricate nature, each input could not be altered as required. This is partly the reason RAM Conce*pt*'s method was omitted in the comparison of deformation prediction methods. Therefore, when comparing the deformations from differing prediction methods it should be noted that RAM Conce*pt* contains the typical design inputs which have been explained and presented in section 4.2.

The date that surveying of the two bay grid started was after the pour of the second floor slab, so although monitoring of the second slab was achieved from day 23 onwards, the day 1 deformation (used as the crucial reference point) was not recorded. Therefore, although surveying data is presented for the second slab in the appendices it cannot be used in this comparison. The comparison of the predicted deformation to the surveyed values for each point on the two bay grid is presented in Figure 4-22.
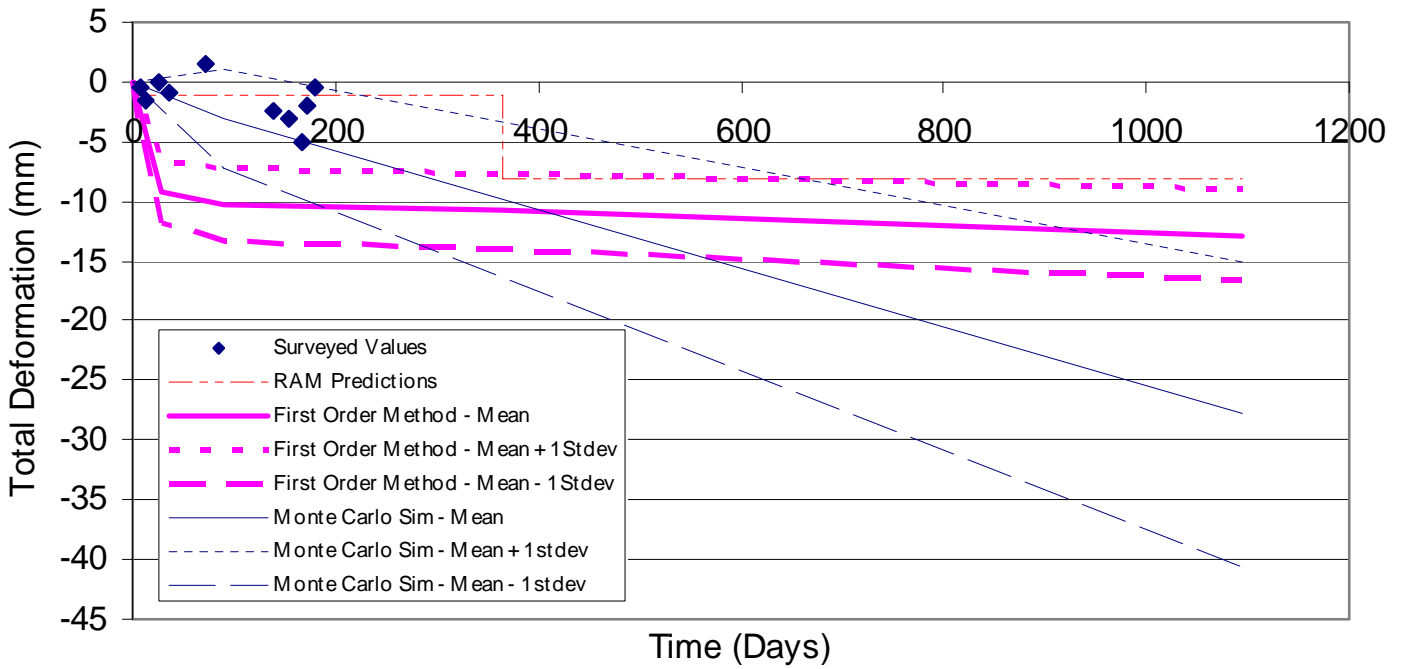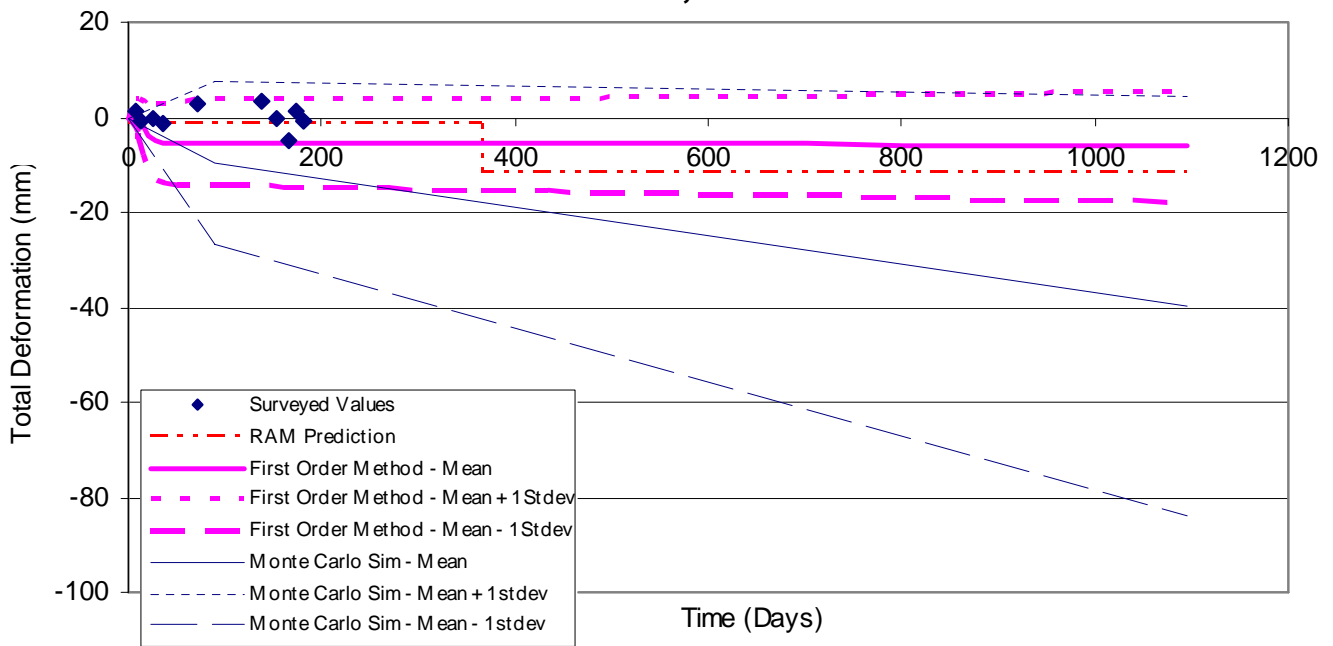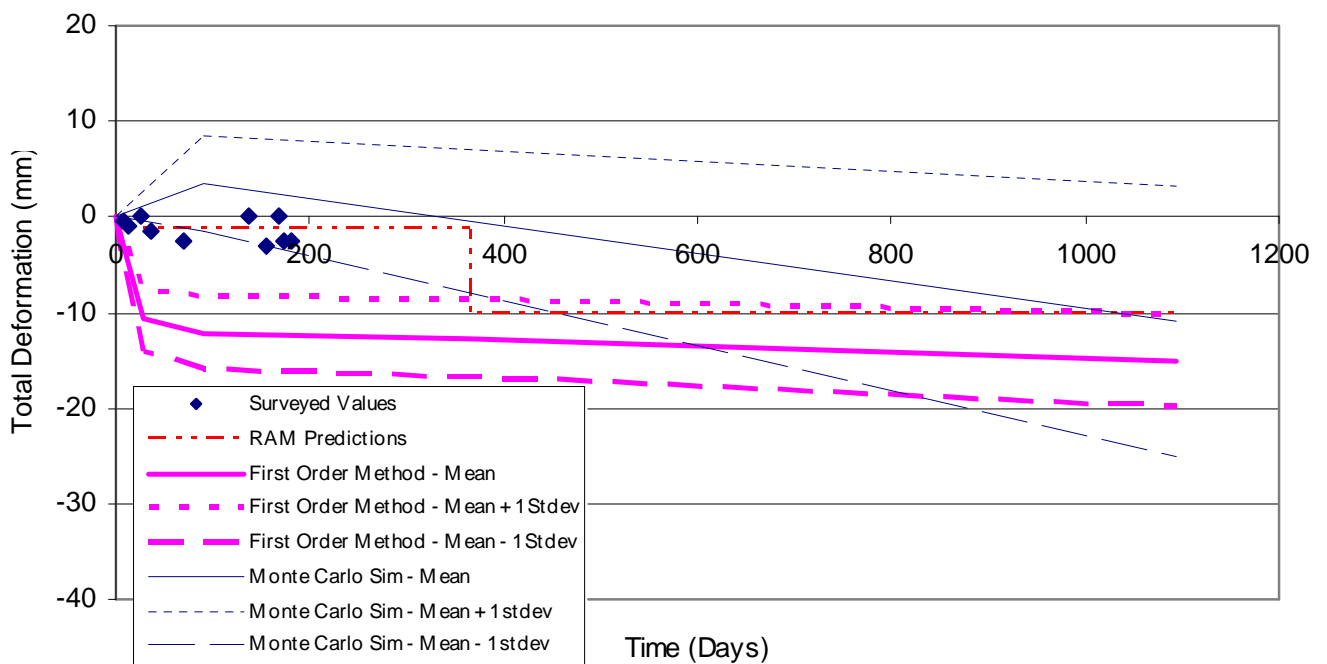
Point b, N40

Point d, N40

Figure 4-22 *Comparative summary of deformation predictions and surveyed values.*
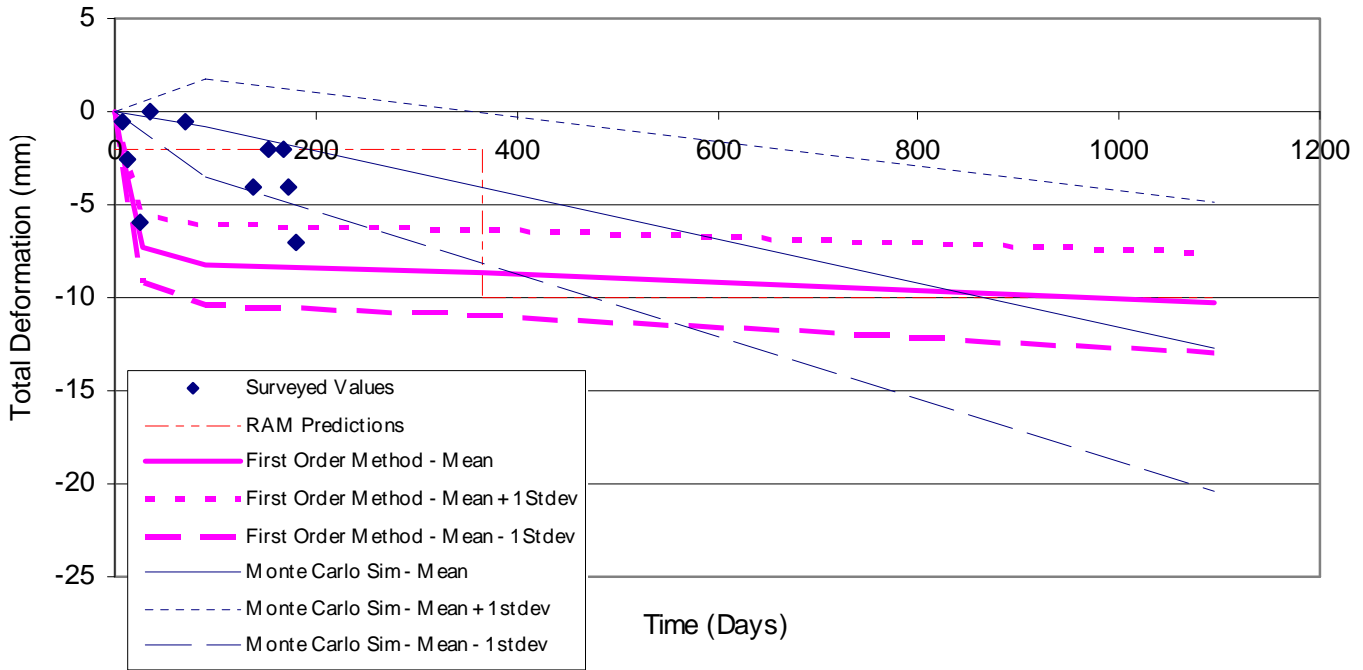
Point e, N40
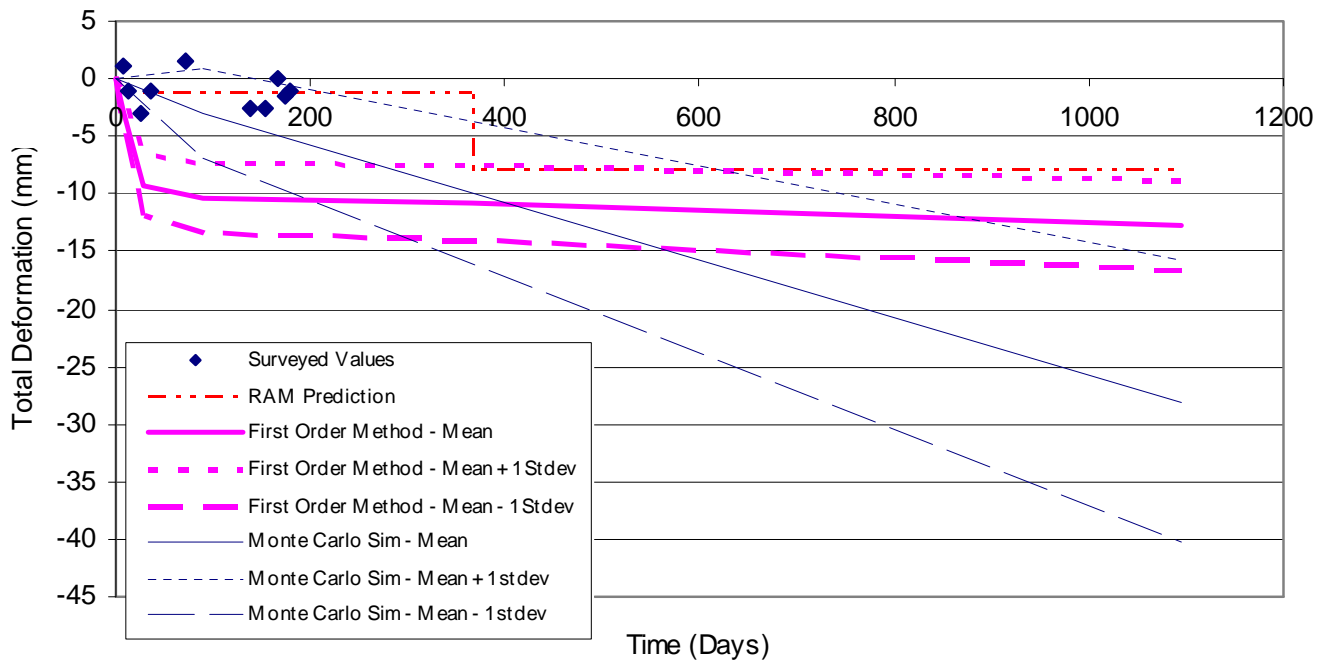

Point f, N40

(Figure 5-28 continued)

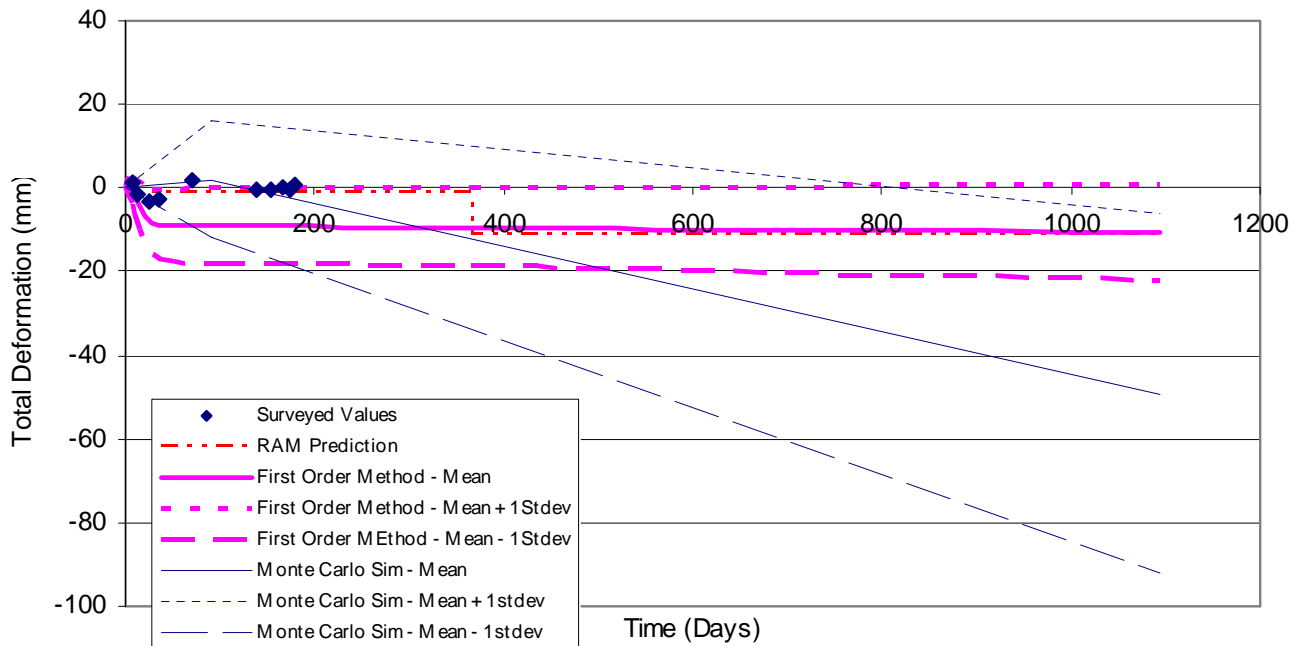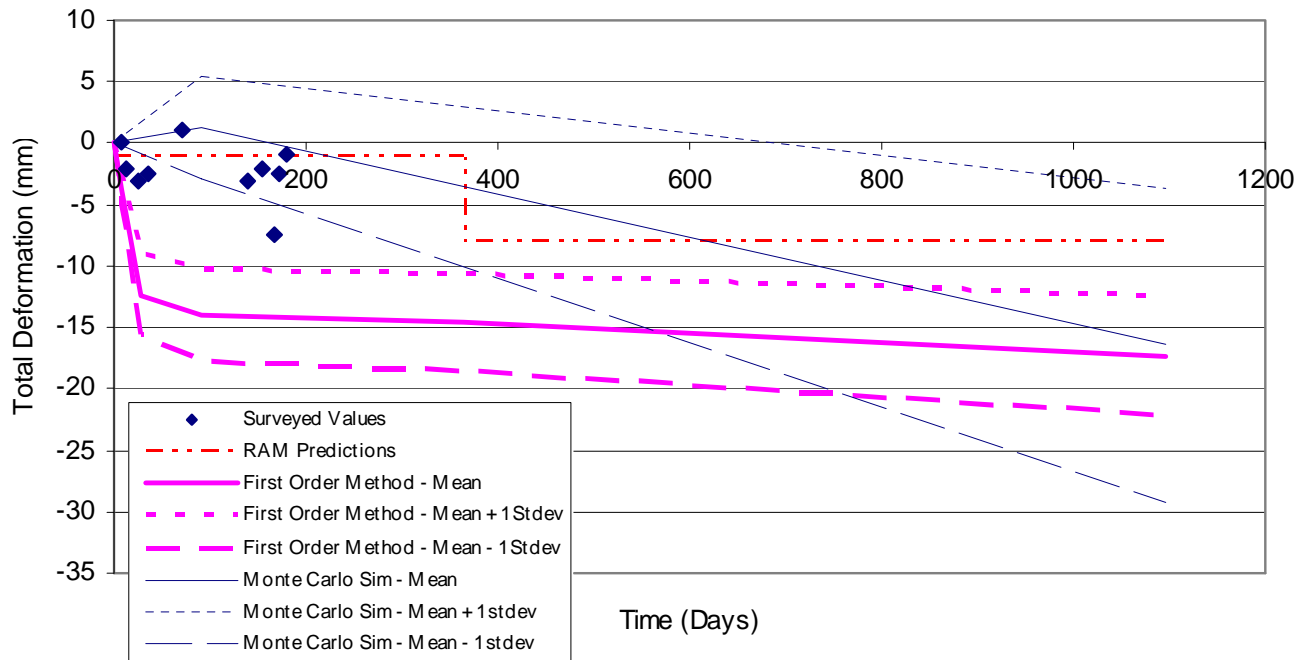## Point h, N40

Point j, N40
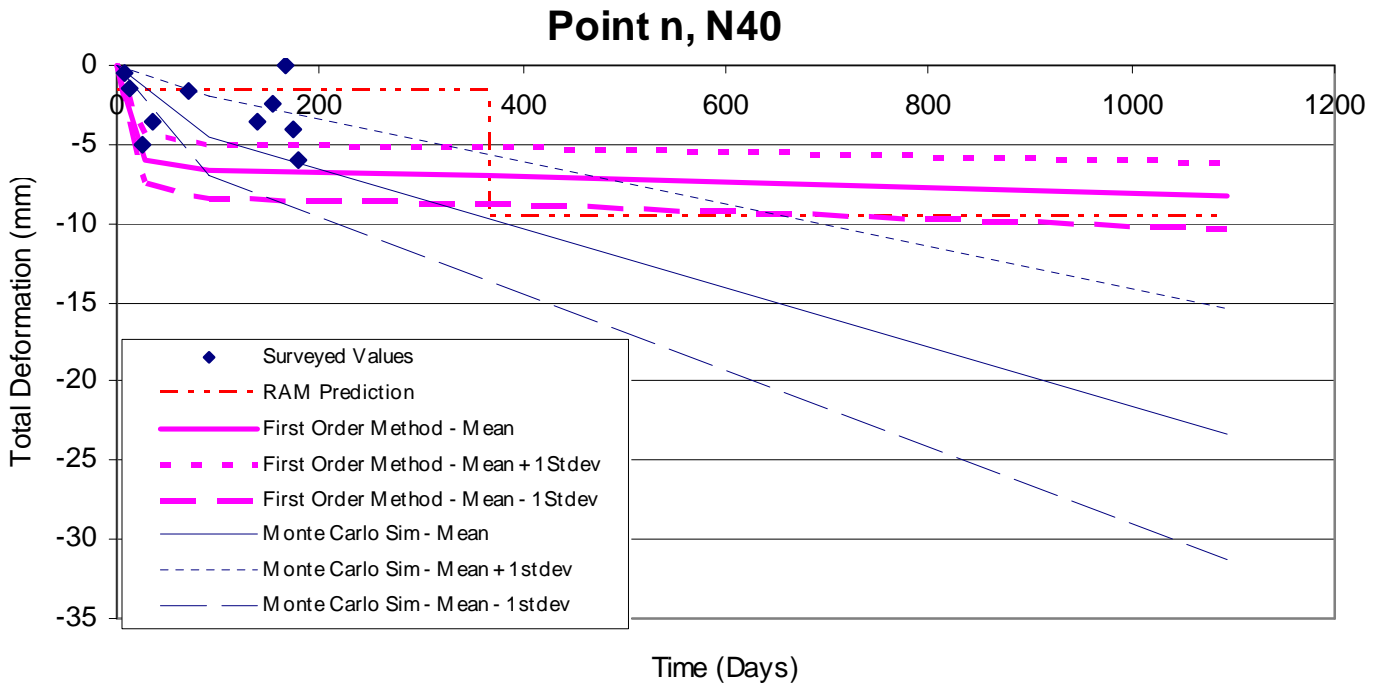

(Figure 5-28 continued)

Point k, N40

Point l, N40

(Figure 5-28 continued)

(Figure 5-28 continued)

The comparison presented in Figure 4-22 reveals that it is difficult to determine the method which contains the highest correlation to the surveyed deformations. Long term slab deformations, and corresponding surveying, is required for a complete comparison to be conducted. It can be concluded however that there is a significant difference between the predicted long term deformations for the different models. Surveying results of long term slab deformations were not available at the time of production of this thesis, once these results are obtained a more detailed comparison can be made.

It can be seen in Figure 4-22 that all points on the two bay grid appear to obtain surveyed deformations that contain a standard deviation of approximately 2 – 3 mm at an age of approximately 150 to 200 days. This conclusion suggests that column strips deformations and mid panel deformations may contain approximately the same standard deviation. This may be in conflict with the conclusion of section 4.3.3.3 where it is established that mid panel deformations contain higher values of standard deviation. For this to be proven long term deformations will need to be surveyed. This analysis will also need to be preformed on multiple slabs to obtain sufficient data points.

4.5.   *Limitations of Accuracy*

During the stages of data analysis and deformation predictions, this research utilised calculations and simulation processes that are subject to errors. Therefore the conclusions that are presented in this research need to be considered in light of these errors. The data obtained and presented in Chapter 3 was obtained from a limited number of concrete specimens. There was approximately 30 molds per concrete pour, which meant that only two test cylinders were tested for f_c, one test cylinder for multiple tests of E_c and one cylinder for testing f_t. Therefore, when presenting mean values of concrete material properties there remains a significant degree of uncertainty or error. Unfortunately this uncertainty or error is unavoidable, but still needs to be acknowledged in this research. The number of test cylinders selected for sampling concrete is considered adequate by Australian Standards and due reference has been made in the text.

The Monte Carlo simulation involved 1000 realisations from computation of member deformation. The standard error of the mean associated with this simulation, also referred to as the standard deviation of the mean (σ_μ), can be determined by the use of Equation 4-8.

$$\sigma_\mu = \frac{\sigma}{\sqrt{n}}$$

Equation 4-8

Where n = number of data points

Therefore, standard error of the mean camber and mean deflection determined using Equation 4-8, based on 1000 realisations is of the order of 3% of the standard deviation of the population. This is considered acceptable. The standard error of the variance associated with the Monte Carlo simulation, also referred to as the standard deviation of the variance (σ_σ), is determined by the use of Equation 4-9.

$$\sigma_\sigma = \frac{\sigma^2}{\sqrt{\dfrac{n-1}{2}}}$$

Equation 4-9

Where n = number of data points

Accordingly the standard deviation of the variance is of the order of 4.5% of the variance of the population. The statistical distribution of material properties, discussed in section 3.4, has been created with the assumption that each statistical distribution is normally distributed. To test the accuracy of application of the model, the profile of the frequency and cumulative ercentage are required to maintain a close resemblance. The Monte Carlo simulation utilised the material property model of E_c for both the 7 day values and the 28 day values. Therefore, this comparison presents the scatter analysis for the experimentally measured values as well as the 7 day and the 28 day modelled data. Figure 4-23 to Figure 4-25 display these three graphs. It can be seen in this visual comparison that there is a strong correlation between the experimentally measure scatter and both of the modelled scatter.
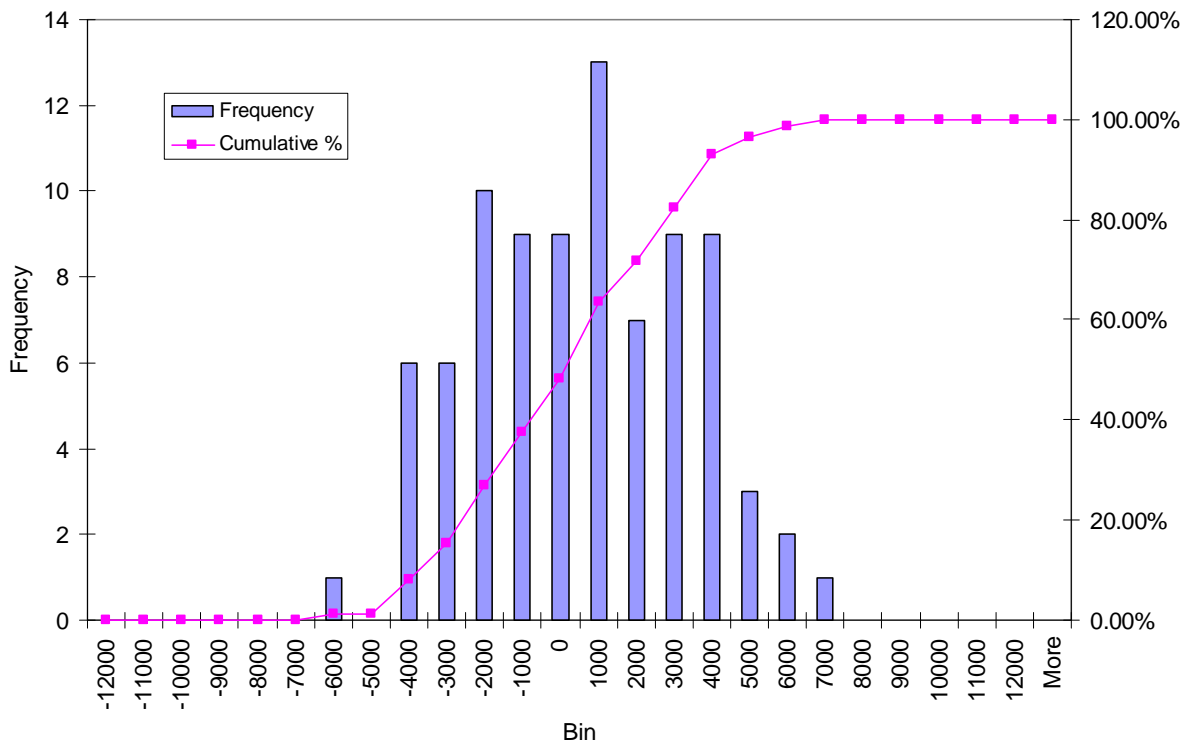

Figure 4-23 *Experimentally measured E_c scatter*

The Finite Element program created in excel is created with a sectional analysis which contains one hundred segments of equal length to represent the analysed member. The accuracy of selecting one hundred segments for this application is relatively unknown. A higher number of segments could be used, say five hundred or one thousand, which would naturally reduce the associated error. However, this increase in accuracy would be small and the amount of time to construct and apply the analysis would increase significantly.
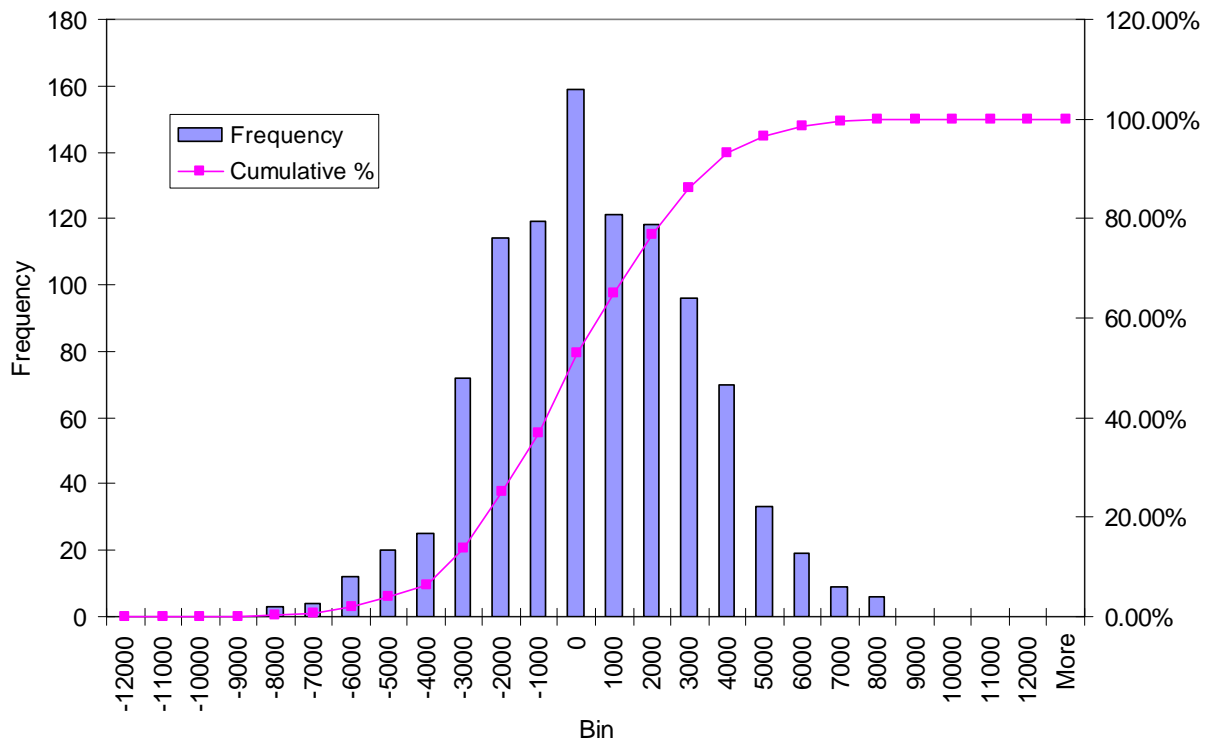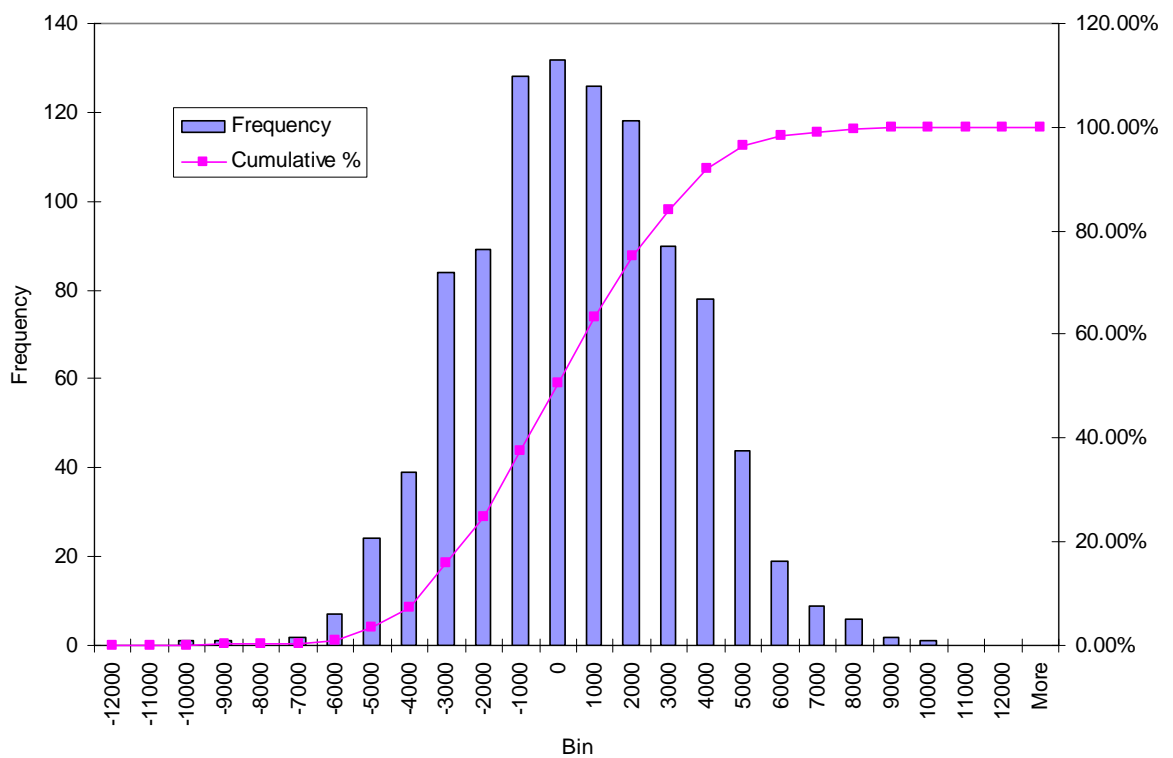
Figure 4-24 Simulated 28 day E_c scatter

Figure 4-25 Simulated 7 day E_c scatter

5. CONCLUSION AND RECOMMENDATIONS

5.1.   Research Conclusion

The experimental program performed in this research allowed detailed monitoring of the primary concrete material properties (f_c, E_c and f_t) at 151 Pirie over the time periods of 1, 3, 7, 14 and 28 days. This monitoring was performed for laboratory and site curing conditions for N32 and N40 concrete mixes. Secondary material properties were obtained from independent testing performed by Readymix. The database produced by the experimental program has produced a vital reference of onsite slab performance for future projects.

Cycle times at 151 Pirie ranged from between 7 and 11 days when using the N32 concrete mix and between 5 and 9 days when using the N40 concrete mix. No member damage, such as dead end pullouts, occurred during the prestressing stages of 151 Pirie.

A statistical analysis performed on the experimental data provided this research with a detailed understanding of the statistical distribution of primary material properties for Readymix's N32 and N40 concretes in Adelaide. This statistical analysis allowed this research to conclude that the variance of f_c, E_c and f_t does not depend on age. However it does depend on curing conditions, although only slightly. The variance of each material property does depend on concrete mix when a comparison was made between N32 and N40 mixes.

It was determined that the most appropriate current deformation prediction method was the deflection and camber prediction methods proposed by Collins and Mitchell (1997). However this numerical method does not consider the statistical distribution of concrete material properties. The Monte Carlo Simulation program produced in this research incorporates the statistical distribution of concrete material properties and produces an associated statistical distribution of member deformation.

Improvements to the Monte Carlo Simulation were performed and a Finite Element program was created. The improvements included allowing for a more accurate representation of I_g where multiple regions of I_g are present, such as drop panels. An improvement to the method of utilising E_c in determining member deformation has also been incorporate in the program.

5.2.   *Recommendations for future research*

The statistical analysis performed in this research was performed using Microsoft Excel. Although Excel has the benefit of being a simplistic program to use, it contains some programming limitations. A program such as MATLAB or Fortran for future research is expected to allow a more detailed statistical simulation to be performed without limitations such as only performing one thousand simulations.

An increase in the number of concrete cylinder samples taken on site is recommended for future research. An increase in the number of samples translates to a lower degree of statistical error in the data analysis. This would be beneficial to improve on the statistical distribution of tensile strength as this research only had access to minimal tensile strength data.

References

ACI (1992) 'State-of-the-art report on HSC', *ACI Manual of Concrete Practice,* pt 1, p.48.

ACI (1995) 'State-of-the-art report on HSC', *ACI Manual of Concrete Practice,* pt 1, p.46.

Ahmad, S. & Shah, S. (1985) 'Structural Properties of High Strength Concrete and its Implications for Precast Prestressed Concrete', *PCI Journal,* vol.304, pp.92-119.

Branson, D., (1966) 'Deflections of Reinforced Concrete Flexural Members', *ACI Committee 435*, June 1966, pp 637.

Chang, K. & Hwang, S., (1996) 'Practical Estimation of Two-Way Slab Deflections', *Journal of Structural Engineering,* February 1996, pp150.

Choong, J. 2003, Masters Thesis, *The University of Melbourne*, Melbourne, Australia.

Collins, M. & Mitchell, D. *Prestressed Concrete Structures*, Response Publications, Canada.

Comité Euro-International du Béton-Federation International du Betón (CEB-FIB). (1993). "Model Code 90" (final draft), *Bulletin 203*, Lausanne (CH), Switzerland.

Eblen et al., 2004, Honours Thesis – An Investigation into High Strength/Performance Concrete in Adelaide, *The University of Adelaide,* Adelaide, Australia.

Ghali, A. (1986) 'A Unified Approach for Serviceability Design of Prestressed and Nonprestressed Reinforced Concrete Structures', *PCI Journal*, March-April 1986, pp118.

Hwang, S & Chang, K., (1996) 'Deflection Control of Two-Way Reinforced Concrete Slabs' *Journal of Structural Engineering*, February 1996, pp160.

Iravani, S. (1996) 'Mechanical Properties of High Performance Concrete', *ACI Materials Journal*, vol.93, pp.416-426.

Klieger, P. (1957) 'Long-Time Study of Cement Performance in Concrete Chapter 10-Progress Report on Strength and Elastic Properties of Concrete', *ACI Journal Proceedings,* Vol. 54 No. 12, pp 481-504.

Kliszczewicz, A. & Ajdukiewicz, A. (2002) 'Differences in Instantaneous Deformability of HS/HPC according to the kind of coarse aggregate', *Cement and Concrete Composites*, Vol. 24, No. 2, pp.263-267.

Larrard, F. & Malier, Y. (1992) *High Performance Concrete: From Material to Structure*, E and FN Spon, London.

Naaman, A., (1983) 'Time-Dependent Deflection of Prestressed Beams by the Pressure-Line Method', *Journal of the Prestressed Concrete Institute*, Vol. 28, No. 2, March/April 1983, pp. 98-119.

Narrow, I. & Ullberg, E. (1963) 'Correlation Between Tensile Splitting Strength and Flexural Strength of Concrete', *ACI Journal Proceedings*, vol.60, iss.1, pp.27-38.

Nasser, G., (1969) 'A Look at Flat Plate Design and Construction', *PCI Journal*, December 1969, pp 62.

Neville, A. (1981) *Properties of Concrete*, Longman Scientific and Technical, England.

Norges, Standardiseringsforbund. (1992), *Concrete structures—Design rules,* NS 3473, Oslo.

Oehlers, D. & Bradford, M., (1999) *Elementary Behaviour of Composite Steel & Concrete Structural Members*, Butterworth- Heinemann, Oxford.

Prado, J.F.M.A et al., (2003) 'A New Procedure for the Analysis of Construction Loads in Multistory Reinforced Concrete Structures', *The Structural Design of Tall and Special Buildings,* July 2003, 12, pp 293-315.

Rashid, M, Mansur, M. & Paramasivam, P. (2002) 'Correlations Between Mechanical Properties of High – Strength Concrete', *Journal of Materials in Civil Engineering*, Vol.14, pp.230-237.

Saul A G A. (1951). "Principles Underlying the Steam Curing of Concrete at Atmospheric Pressure." *Magazine of Concrete Research,* 2(6), 127.

Standards Association of Australia 1985, *Methods of testing concrete - Determination of indirect tensile strength of concrete cylinders (Brasil or splitting test)* (AS 1012.10 – 1985), Standards Australia, Strathfield, NSW.

Standards Association of Australia 1987, *Steel tendons for prestressed concrete-7-wire stress-relieved steel strand for tendons in prestressed concrete* (AS 1311 – 1987), Standards Australia, Strathfield, NSW.

Standards Association of Australia 1996, *Methods of testing concrete – Method 16: Determination of creep of concrete cylinders in compression* (AS 1012.16 – 1996), Standards Australia, Strathfield, NSW.

Standards Association of Australia 1997, *Portland and blended cements* (AS 3972 – 1997), Standards Australia, Strathfield, NSW.

Standards Association of Australia 1997, *Specification and supply of concrete* (AS 1379 – 1997), Standards Australia, Strathfield, NSW.

Standards Association of Australia 1998, *Aggregates and rock for engineering purposes - Concrete aggregates* (AS 2758.1 – 1998), Standards Australia, Strathfield, NSW.

Standards Association of Australia 1998, *Methods of testing concrete – Method 3.1: Determination of properties related to the consistency of concrete – Slump test* (AS 1012.3.1 – 1998), Standards Australia, Strathfield, NSW.

Standards Association of Australia 1998, *Supplementary cementitious materials for use with portland and blended cement - Fly ash* (AS 3582.1 – 1998), Standards Australia, Strathfield, NSW.

Standards Association of Australia 1999, *Methods of testing concrete – Method 9: Determination of the compressive strength of concrete specimens* (AS 1012.9 – 1999), Standards Australia, Strathfield, NSW.

Standards Association of Australia 2000, *Chemical admixtures for concrete, mortar and grout - Admixtures for concrete* (AS 1478.1 – 2000), Standards Australia, Strathfield, NSW.

Standards Association of Australia 2000, *Methods of testing concrete – Method 8.1: Methods for making and curing concrete – Compression and indirect tensile test specimens* (AS 1012.8.1 – 2000), Standards Australia, Strathfield, NSW.

Standards Association of Australia 2001, *Concrete structures* (AS 3600 – 2002), Standards Australia, Strathfield, NSW.

Standards Association of Australia 1997, *Methods of testing concrete – Method 17: Determination of the static chord modulus of elasticity and Poisson's ratio of concrete specimens* (AS 1012.17 – 1997), Standards Australia, Strathfield, NSW.

Standards Association of Australia 2000, *Methods of testing concrete – Method 10: Determination of indirect tensile strength of concrete cylinders ('Brazil' or splitting test)* (AS 1012.10 – 1985), Standards Australia, Strathfield, NSW.

Standards Association of Australia 2002, *Structural design actions - Permanent, imposed and other actions* (AS 1170.1 – 2002), Standards Australia, Strathfield, NSW.

Stivaros, P., & Halvorsen, G., (1990) 'Shoring/Reshoring Operations for Multistory Buildings', *ACI Structural Journal*, September-October 1990, pp 589

Vanderbilt, M. D., Sozen, M. A. & Siess, C. P. 1963, *Deflections of Reinforced Concrete Floor Slabs,* Structural Research Series No 263, Dept of Civil Engg, University of Illinois.

Warner, R. Rangan, B. Hall, A. & Faulkes, K. (1998) *Concrete Structures,* Addison Wesley Longman Australia Pty Ltd, Melbourne.

Zain, M.F.M, Mahmud, H.B, Ilham, A. & Faizal, M. (2002) 'Prediction of splitting tensile strength of high-performance concrete', *Cement and Concrete Research*, vol.32, pp.1251-1258.